UNIVERSITAT POLITÈCNICA DE VALÈNCIA

DEPARTAMENTO DE INGENIERÍA MECÁNICA Y DE MATERIALES

DEVELOPMENT OF SHAPE-MEMORY COMPOSITES BASED ON A BIODEGRADABLE POLYESTER ELASTOMER

DOCTORAL THESIS

Águeda Sonseca Olalla

SUPERVISOR

Enrique Giménez Torres

Valencia, July 2015

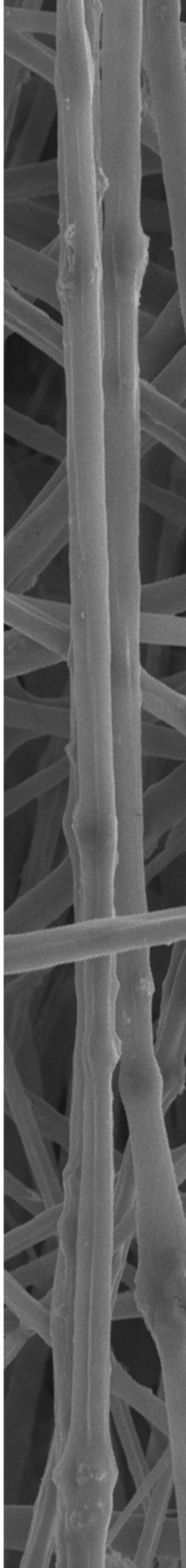

UNIVERSITAT POLITÈCNICA DE VALÈNCIA

DEPARTAMENTO DE INGENIERÍA MECÁNICA Y DE MATERIALES

TESIS DOCTORAL

DEVELOPMENT OF SHAPE-MEMORY COMPOSITES BASED ON A BIODEGRADABLE POLYESTER ELASTOMER

Memoria para optar al grado de doctor

Presentada por:

Águeda Sonseca Olalla

Director:

Enrique Giménez Torres

Valencia, Julio 2015

“I have notice that even people who claim everything is predestined, and that we can do nothing to change it, look before they cross the road”

Stephen Hawking

Als meus pares,
germans i nebots

Development of Shape-Memory Polymer Composites based on a Biodegradable Polyester Elastomer.

ABSTRACT

The current PhD thesis deals with the development and characterization of novel nanocomposites based on biodegradable poly(mannitol sebacate) (PMS) matrices with tailored properties and shape-memory capabilities for biomedical applications. Two types of fillers —cellulose nanocrystals (CNC) and electrospun poly(lactic acid) nanofibers (NF-PLA)— were used as reinforcement in order to induce and/or enhance the shape-memory properties of PMS matrices. Also, different crosslinking profiles and stoichiometric ratios between mannitol and sebacic acid (1:1 and 1:2) were studied and evaluated to obtain samples with low and high degrees of crosslinking. An appropriate combination of the crosslinking profile and the monomer ratio for PMS matrix, as well as the addition of low content of CNC, allowed the development of PMS/CNC nanocomposites with a wide range of mechanical properties and degradation profiles. On the other hand, highly oriented poly(lactic acid) (PLA) nanofiber mats obtained by electrospinning were embedded in the PMS matrices. An enhancement of up to 53-fold in the Young´s modulus was observed for PMS/NF-PLA nanocomposites filled with 15 wt% of PLA nanofibers. The incorporation of fillers (CNC and NF-PLA) allowed the development of thermally active shape-memory nanocomposites with an enhancement of parameters such as recovery stress and shape fixity. The electrospun PLA-reinforced nanocomposites, offered the best balance of mechanical and thermal properties, as well as a greater control of the transition temperature for switching the change of shape, within a useful range of temperatures. Owing to that, these materials may be of interest as smart responsive systems in long-term biomedical applications.

Desarrollo de Compuestos Poliméricos con Memoria de Forma basados en un Elastómero de Poliéster Biodegradable.

RESUMEN

La presente tesis doctoral, se centra en el desarrollo y caracterización de nuevos nanocompuestos biodegradables, a partir de matrices de poli(mannitol sebacato) (PMS) con propiedades a medida y capacidades de memoria de forma para aplicaciones biomédicas. Dos tipos de cargas —nanocristales de celulosa (CNC) y nanofibras de ácido poliláctico (NF-PLA) obtenidas mediante electrospinning— se han utilizado como refuerzo, con la finalidad de inducir y/o mejorar las propiedades de memoria de forma en matrices de PMS. Se han estudiado y evaluado diferentes tratamientos de curado y ratios de reacción entre el mannitol y ácido sebácico (1:1 y 1:2), con la finalidad de obtener muestras con bajo y alto grado de reticulación. Una combinación adecuada del tratamiento de curado y el ratio entre monómeros del PMS, así como la adición de bajos contenidos de CNC, permitió desarrollar nanocompuestos de PMS/CNC con un amplio rango de propiedades mecánicas y perfiles de degradación. Por otro lado, se han producido mats de nanofibras de ácido poliláctico (PLA) con alta orientación mediante la técnica de electrospinning, para embeberse en matrices de PMS, observándose una mejora de hasta 53 veces en el módulo de Young para nanocompuestos de PMS/NF-PLA con un 15% en peso de nanofibras. La incorporación de cargas (CNC y NF-PLA) permitió el desarrollo de nanocompuestos con memoria de forma activada térmicamente, con una mejora de parámetros tales como la fuerza de recuperación y la capacidad de fijación. Los nanocompuestos reforzados con NF-PLA obtenidas por electrospinning, ofrecieron el mejor balance de propiedades mecánicas y térmicas, así como un mayor control de la temperatura de transición para la activación del cambio de forma en un intervalo útil de temperaturas. Por todo ello, estos materiales pueden resultar de interés como sistemas activos en aplicaciones biomédicas de larga duración.

Desenvolupament de Compostos Polimèrics amb Memòria de Forma basats en un Elastòmer de Polièster Biodegradable.

RESUM

La present tesi doctoral se centra en el desenvolupament i caracterització de nous nanocompostos biodegradables a partir de matrius de poli(mannitol sebacato) (PMS) amb propietats a mesura i capacitats de memòria de forma per a aplicacions biomèdiques. Dos tipus de càrregues —nanocristals de cel·lulosa (CNC) i nanofibres d'àcid polilàctic (NF-PLA) obtingudes mitjançant electrospinning— s´han utilitzat com a reforç amb la finalitat d'induir i/o millorar les propietats de memòria de forma en matrius de PMS. S'han estudiat i avaluat diferents tractaments de curat i ràtios de reacció entre el mannitol i àcid sebàcic (1:1 i 1:2) amb la finalitat d'obtenir mostres amb baix i alt grau de reticulació. Una combinació adequada del tractament de curat i el ràtio entre monòmers del PMS, així com l´addició de baixos continguts de CNC, va permetre desenvolupar nanocompostos de PMS/CNC amb un ampli rang de propietats mecàniques i perfils de degradació. D'altra banda, s'han produït mats de nanofibres d'àcid polilàctic (PLA) amb alta orientació mitjançant la tècnica de electrospinning, per embeure's en matrius de PMS, observant-se una millora de fins a 53 vegades en el mòdul de Young per nanocompostos de PMS/NF-PLA amb un 15% en pes de nanofibres. La incorporació de càrregues (CNC i NF-PLA) va permetre el desenvolupament de nanocompostos amb memòria de forma activada tèrmicament, amb una millora de paràmetres tals com la força de recuperació i la capacitat de fixació. Els nanocompostos reforçats amb NF-PLA obtingudes per electrospinning, van oferir el millor balanç de propietats mecàniques i tèrmiques, així com un major control de la temperatura de transició per a l'activació del canvi de forma en un interval útil de temperatures. Per tot això, aquests materials poden resultar d´interés com a sistemes actius en aplicacions biomèdiques de llarga durada.

MOTIVATION

The development of biodegradable materials with tailored properties for potential clinical and biomedical applications is a current topic of significant interest in materials science. Due to that, main motivation of this thesis not only seeks the development of biodegradable materials, but also, the possibility of develop tailored materials “on demand”.

In the last few years, there is an increasing need towards the search and development of high performance biomaterials for specific medical applications which positively impact on patient´s quality of life. The main challenge is based to achieving less invasive medical treatments, more effective and with fewer secondary effects. Therefore, biodegradable polymers with the ability of returning to some previously defined shape under adequate thermal conditions, have received early recognition as materials of interest which can play an “active role” in this field. The international scientific community has therefore focused its attention on these new polymeric materials known as “shape-memory polymers” (SMPs). The main advantage of these polymers over shape-memory alloys (SMAs), is due to that the shape-memory performance can be controllable by different stimuli such as light or changes in the environmental, pH, etc.; and not only by thermal heating. Also, the biodegradability of these materials may result advantageous in reducing the number of invasive surgeries. However, although there are a large number of SMPs developed so far, very few of them show a “soft” elastomeric nature able to mimic the living human tissues. Some important limitations of these materials are associated with their mechanical behavior, which is more marked in those with biodegradable properties.

In this regard, the unique properties of biodegradable SMPs can broaden the spectrum of application of these smart materials, by providing unconventional functions for biodegradable implantable devices and minimally invasive surgery.

Although the demand for soft actuators is high, especially of polymers with improved mechanical properties which ensure a good shape-memory performance in the body's environment, more research is needed to develop materials that fulfil these requirements.

AIM AND THESIS OUTLINE

AIM AND THESIS OUTLINE

The scope of this thesis is focused in the development of new strategies for achieving shape-memory polymer composites (SMPCs) with biodegradability under physiological conditions, based on biodegradable soft matrices. More specifically, an ester-bonded crosslinked elastomer — Poly(mannitol sebacate) (PMS) — has been selected in this study as the matrix material. PMS is a member of the poly(polyol sebacate)s (PPS) family, which is obtained by melt polycondensation reaction between mannitol and sebacic acid, with relatively good mechanical properties, biodegradability and potential applications in biomedicine. However, its properties can be only slightly controlled by tuning the monomer ratio and by adjusting the curing conditions. In this regard, the addition of reinforcing fillers can be another strategy in order to tune and enhance the thermal and mechanical properties of the polymer matrices, as well as improve the shape-memory performance in the range of use for biomedical purposes.

In this regard, the aim or general objective of this thesis is to develop and characterize novel nanocomposites based on biodegradable poly(mannitol sebacate) (PMS) with tailored properties and shape-memory capabilities. This goal includes the study of two types of reinforcing fillers such as cellulose nanocrystals (CNC) and electrospun poly(lactic acid) nanofibers (NF-PLA).

This general objective will be pursed through the following specific objectives:

- Synthesize poly(mannitol sebacate) matrices with different stoichiometric ratios between mannitol and sebacic acid (initial monomers) obtained by applying different curing profiles in terms of time and temperature to obtain samples with different degrees of crosslinking.

- Isolation of cellulose nanocrystals through hydrolysis processes from cotton sources.
- Production of poly(lactic acid) (PLA) nanofibers by electrospinning process.
- Incorporation of different amounts of cellulose nanocrystals (CNC) into PMS networks through solvent casting process in order to obtain PMS/CNC nanocomposites.
- Infiltration of different amounts of electrospun PLA nanofibers into PMS networks to develop PMS nanocomposites reinforced with embedded electrospun PLA nanofibers.
- Characterization of relationship between structure-composition and properties of the all developed nanocomposites.
- Selection of the nanocomposite systems with better balances of mechanical properties and shape-memory performance.

OVERVIEW OF THE THESIS

This thesis is structured into seven chapters in order to clearly lay out the research carried out on the development of shape-memory polymer composites (SMPCs):

Firstly, two background chapters are focused on main concepts and a deep review of scientific literature necessary to understand the subsequent chapters as well as the materials and the analytical techniques used along the thesis. ***Chapter 1*** presents a brief introduction to shape-memory polymers and ***Chapter 2*** presents the materials, experimental procedures and characterization methods.

Chapters 3 to 6 are structured as four scientific articles. ***Chapter 3 (Contribution I)*** introduces the nanocomposites based on poly(mannitol sebacate) 1:1 and 1:2 ratio and cellulose nanocrystals. Mainly, mechanical properties and degradation studies in simulated body fluid of both systems (nanocomposites with cellulose nanocrystals from 1:1 and 1:2 mannitol:sebacic acid ratio) are compared. ***Chapter 4 (Contribution II)*** deals with the nanocomposites based on poly(mannitol sebacate) 1:1 ratio matrix and cellulose nanocrystals, with main emphasis on shape-memory properties.

Chapter 5 (Contribution III) contains information about the optimization of the processing conditions for obtaining highly-oriented poly(lactic acid) PLA nanofibers by electrospinning technique. Also, the incorporation of nano-sized hydroxyapatite filler into the nanofibers and their influence on the morphology and physical properties is discussed.

Chapter 6 (Contributions IV and V) contains presentation and discussion of the results obtained for PMS nanocomposites reinforced with electrospun PLA nanofibers. Mechanical and shape-memory properties as well as degradation issues are compared with the same matrix reinforced with cellulose nanocrystals.

The discrete scientific contributions are linked into the ***Chapter 7*** in which general conclusion and future works are presented.

LIST OF CONTRIBUTIONS OF THIS THESIS

I A. Sonseca, O. Sahuquillo, E. J. Foster, E. Giménez. *Mechanical properties and degradation studies of Poly(mannitol sebacate)/Cellulose nanocrystal nanocomposites*, *RSC Advances, 2015, **5***, 55879-55891.

II A. Sonseca, L. Peponi, O. Sahuquillo, J. M. Kenny, E. Giménez, *Electrospinning of biodegradable Polylactide/Hydroxyapatite Nanofibers: study on the morphology, crystalline structure and thermal stability*, *Polymer Degradation and Stability,* 2012, **97**, 2052-2059.

III A. Sonseca, S. Camarero-Espinosa, L. Peponi, C. Weder, E. J. Foster, J. M. Kenny, E. Giménez, *Mechanical and shape-memory properties of Poly(mannitol sebacate)/Cellulose nanocrystal nanocomposites, Journal of Polymer Science, Part A: Polymer Chemistry,* 2014, **52**, 3123-3133.

IV A. Sonseca, O. Sahuquillo, O. Menes, E. Giménez. *A comparative study of the mechanical, shape-memory, and degradation properties of fiber- and particulate- reinforced Poly(mannitol sebacate) nanocomposites*: *Manuscript.*

V Patent Application: *Compuesto no tejido elastomérico y bioabsorbible para su uso en prótesis y dispositivos quirúrgicos implantables. Método de fabricación.*

TABLE OF CONTENTS

CHAPTER 2. WORKFLOW, MATERIALS, METHODS AND EXPERIMENTAL TECHNIQUES

CHAPTER 7. CONCLUSIONS AND FUTURE RESEARCH LINES

GLOSSARIES

EPILOGUE

Chapter 1

Introduction to shape-memory polymers

1. SHAPE-MEMORY POLYMERS (SMPs)

1.1. GENERAL CONCEPT

Shape-memory polymers (**SMPs**) represent a class of smart materials which have the capability to change from a temporary shape (named A) to a memorized permanent shape (named B) upon the application of an external stimulus such as electric/magnetic field, temperature, light, pH, humidity, ions or enzymes, etc.[1-4] This property is known as shape-memory effect (**SME**) and is not intrinsic of the material, meaning that the combination of a determined polymer molecular structure and morphology and a specific tailored processing known as *"programming"* process is needed.[5, 6] Firstly, the material is formed into its initial permanent shape (B) by conventional processing methods such as extrusion or injection moulding. In the *"programming"* process the polymer is deformed to obtain and fix the temporary shape (A). Afterwards, a determined external stimulus is applied and the material is able to recover its initial permanent shape B, thus, the shape recovery takes place after a programming process as shown in **Figure 1.1**. *"Programming-recovery"* sequences can be repeated several times, even fixing two temporary shapes in each cycle for some polymers which possess the suitable network structure.[7, 8]

Certain metallic materials can undergo substantial plastic deformation and then be triggered into returning to its original shape by the application of heat. This phenomenon is called thermal shape-memory. The materials with such properties are known as shape-memory alloys (SMAs). Although shape-memory effect was first described on Gold-Cadmium (AuCd) alloys, these materials became popular in experimental works carried out on Nickel-Titanium alloys (Nitinol®).[6, 9] The shape-memory effect of Nitinol®, similarly to other metallic alloys, is based on a martensitic phase transition which takes place without diffusion (**Figure 1.2**).[10] The

material is cooled down from a phase with a cubic symmetry (austenitic phase) to a lower temperature phase with poor symmetry (martensitic phase).

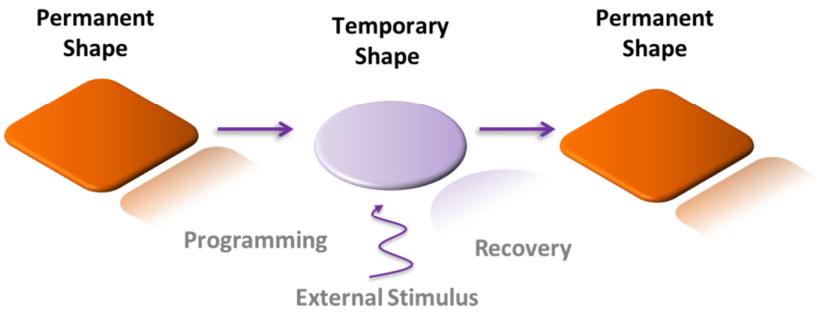

Figure 1.1. Schematic representation of the shape-memory effect (SME). The permanent shape is transformed to a temporary shape during the programming process. The recovery of the permanent shape takes place by applying an external stimulus.

The material adopts its temporary shape by deformation during the martensitic phase. Finally, the austenitic phase is recovered by heating the sample above the phase transition temperature. Up to date, a variety of SMAs have been developed; however, only three alloy systems, NiTi-based, Cu-based (CuAlNi and CuZnAl) and Fe-based, play an important place in the market. NiTi-based shape-memory alloy (Nitinol®) is commonly used for the manufacture of surgical devices and implants due to its high performance and good biocompatibility, which is essential in biomedical applications. On the other hand, Cu-Zn-Al alloys are often used for non-medical applications as a consequence of their low material cost and good workability during processing. In recent years, some progress has been made in the development of ferromagnetic SMAs, which are magneto-responsive. Even so, the thermo-responsive SMAs are a more mature technology and the number of commercial SMA materials and products is also greater.

In comparison with SMAs, the SMPs have advantages[6, 11-13] in terms of light weight, cost-effective (material and processing), easy processing (formability and workability) and high recoverable strains (see **Table 1.1**).

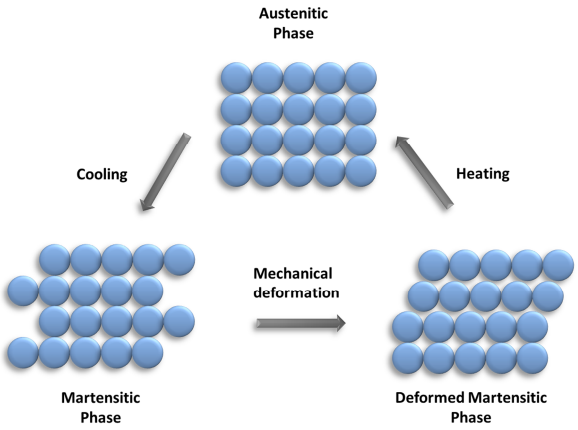

Figure 1.2. Schematic representation of the shape-memory effect (SME) in metallic alloys, where the programming is reached through a martensitic phase transformation.

Table 1.1. Comparison between different characteristics of SMPs and SMAs.

Material property	SMPs	SMAs
Density (g/cm^3)	0.9-1.1	6-7
Deformation extent (%)	30-600%	<8%
Young´s modulus at T<T$_{trans}$ (GPa)	0.01-3	83 (NiTi)
Young´s modulus at T>T$_{trans}$ (GPa)	0.1-10 x10^{-3}	28-41
Stress required for deformation (MPa)	1-3	50-200
Stress generated during recovery (MPa)	1-3	200-400
Recovery rate	<1 s. to several min.	<1 s.
Thermal conductivity (Wm^{-1}K^{-1})	0.15-0.30	18 (NiTi)
Biocompatibility and biodegradability	Can be biocompatible and/or biodegradable	Some are biocompatible (i.e. Nitinol), but not biodegradable
Processing conditions	<200 °C low pressure	High temperature (>1000 °C) and high pressure required
Shaping	Easy	Difficult
Corrosion performance	Excellent	Excellent
Cost	<20 € per Kg	~511 € per Kg

In addition, SMPs can be biocompatible and biodegradable and their shape-memory properties can be activated over a wide variety of stimuli which fit better the needs of a given application. Among all possible stimuli that can activate the

shape-memory effect, the thermal-induced response is the most studied[14, 15] and will be the focus of this thesis.

1.2. THERMALLY ACTIVATED SHAPE-MEMORY POLYMERS (SMPs)

Generally, the structure of the thermally activated SMPs is defined by means of crosslinks or net-points and temperature-sensitive molecular switches that connect them entropically. The net-points are capable of storing the permanent shape, while the dynamic chain domains act as molecular switches able to form strong reversible interactions (secondary crosslinks), which are triggered by a characteristic thermal transition temperature (T_{trans}). When the working temperature is above T_{trans} of the switching domains, the secondary interactions between polymer chains can be detached, allowing the system to be mechanically deformed when an external stress is applied (achieving certain orientation that increases with the length and flexibility of these chains). When the system is cooled below T_{trans} and the external stress is released, this deformation can be retained, and as a result, the system remains fixed in a temporary shape. The dynamic domains (switching domains) restore the initial conformation after heating up to T_{trans} by recoiling, releasing the internal stress previously stored and recovering the original shape determined by the net-points.[16, 17]

1.3. MOLECULAR MECHANISM OF THE SHAPE-MEMORY EFFECT AND THERMOMECHANICAL CHARACTERIZATION

According to J. Hu et al.[18] the molecular mechanism of SMPs consists of:

- Crosslinks or net points which determine the SMP permanent shape, as shape-memory polymer needs to maintain a stable network structure in order to allow the system to recover its original shape.
- Switchable segments which are used to create and maintain the temporary shape.

Macroscopically, a SMP is deformed at a temperature above a switching transition temperature (T_{trans}) and fixed into a temporary shape by being cooled down to a temperature below the T_{trans}.[6, 12, 19] Thus, the basis of the shape-memory effect of thermal responsive SMPs is associated with the large difference in Young´s modulus (E) of these materials which decreases significantly as the polymer is heated from below to above this temperature. Initially, the polymer chains of the switching segment are in a state of highest entropy and display a random coil conformation. When the polymer is heated above T_{trans} the softening of the switching domains occurs, and the orientation of polymer chains is initiated by applying tensile stress, thus, loosing entropy. At this point, if the external stress is released, the sample recovers its original length due to the entropy elasticity of the switching segments and gains back the entropy. To prevent this premature shape recovery in the material and fix the temporary shape, switching domains have to be frozen, and this effect is driven by the lack of micro-Brownian motion of the polymer chains at low temperatures. In this regard, the deformation obtained by applying load at high temperature can be retained when the polymer is cooled down below T_{trans}. Micro-Brownian motion of the switching segments is recovered when the sample is softened again at $T>T_{trans}$ which leads to a relaxation of fixed strain and to the recovery of the permanent shape of the material, as a consequence of the entropic gain that was lost when polymer chains were oriented.[2, 4, 20] In amorphous systems, the shape recovery depends on the entropic elasticity of the network chains when they return to a random coil state after been fixed in an oriented conformation. Moreover, when domains between covalently bonded structure are crystalline, shape recovery is triggered by the melting/crystallization of these crystallites. Thereby, the activation/deactivation of Brownian motion of the chains is the responsible for the shape-memory effect. By monitoring the strain in the samples during each step of the shape-memory cycle, a 3D plot of the strain versus temperature and versus force (stress) can be obtained. An example of the plot obtained is given in **Figure 1.3**.

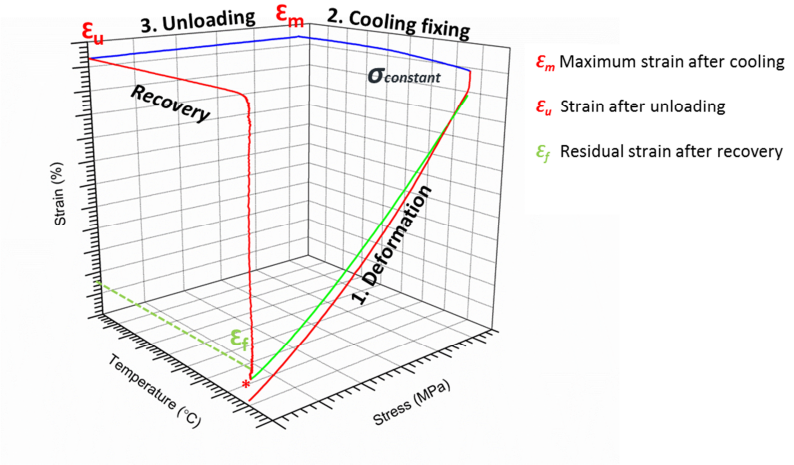

Figure 1.3. Schematic representation of a shape-memory cycle as measured by dynamic mechanical analysis (the asterisk indicates the beginning of the shape-memory cycle).

The ability to fix the temporary shape (**shape fixity ratio**, R_f) and the ability to recover the permanent shape (**shape recovery ratio**, R_r) could be quantified using the following equations:[2, 5, 21]

$$R_f(N) = \frac{\varepsilon_u(N)}{\varepsilon_m(N)} \times 100\% \tag{1.1}$$

$$R_r(N) = \frac{\varepsilon_m(N) - \varepsilon_f(N)}{\varepsilon_m(N) - \varepsilon_f(N-1)} \times 100\% \tag{1.2}$$

where ε_m is the maximum strain achieved in the *N*th cycle after cooling and before unloading, ε_u is the fixed strain after unloading the sample at T_{low} (below T_{trans}) in the same cycle, and ε_f is the residual strain of the sample after the recovery step at T_{high} (above T_{trans}). The values obtained from these equations are given in percentages.

1.4. TYPES OF SHAPE-MEMORY POLYMERS

The nature of the net-points responsible for the permanent shape can be both, chemical (covalent bonds) or physical (intermolecular interactions or non-covalent bonds). Typically, the chemical interactions are achieved through chemical

crosslinking, while physical interactions are present in polymers with at least two differentiated phases, usually crystalline and amorphous domains. In broad terms, the switching domains **in a covalent structure** are the chain segments between crosslinks, and the thermal transition for triggering the SME (T_{trans}) can be either the glass transition temperature (T_g) or the melting temperature (T_m). In the case of polymers with liquid crystalline domains, the thermal transition for SME is named isotropization temperature (T_i) and it is referred as the temperature at which liquid crystalline domains change to an isotropic state.[22-26] In case of **physical structure**, physical crosslinking is formed through interactions between the crystals, amorphous domains or other forms of entangled chains. Here, the highest thermal transition temperature domains (T_{perm}) are referenced as "hard domains" or "physical net-points" and act as net-points. The domains with the second highest thermal transition (T_{trans}) are denominated as "soft domains" or "switching segments". T_{trans} is the characteristic thermal transition above which, these "switching segments" are flexible and can be either T_g[27, 28], T_m[29-38] or T_i[39, 40] if the domain have amorphous, crystalline or liquid crystalline nature respectively.

The thermal responsive SMPs can be classified depending on the nature of their permanent net-points (chemical or physical) and the thermal transition associated to the switching domains (T_g, T_m or T_i) into:

I. SMPs with a Covalently crosslinked primary structure:

- **a.** Chemically crosslinked amorphous with $T_{trans}=T_g$
- **b.** Chemically crosslinked semi-crystalline with $T_{trans}=T_m$ or T_i

II. SMPs with a Physically crosslinked primary structure:

- **a.** Physically crosslinked thermoplastics with $T_{trans}=T_g$
- **b.** Physically crosslinked thermoplastics with $T_{trans}=T_m$ or T_i

Class I:

The covalently crosslinked SMPs exhibit a primary chemically interconnected structure that can be created during the synthesis from low molecular weight (co)monomers or by post-processing methods which determine the macroscopic shape. Chemical crosslinking by post-processing methods can be induced by the addition of radical initiators into the polymers or by high intensity irradiation techniques (e.g. electron beams or ultraviolet sources).[41-44] On the other hand, crosslinking during synthesis can be achieved from linear or branched polymers, as well as (co)polymerization/ poly(co)condensation of one or several low molecular weight (co)monomers, from which one has to be at least tri-functional in order to enable the creation of a covalently crosslinked SMP.[26, 45-49] These methods can be applied to obtain amorphous (***Class Ia.*** $T_{trans}=T_g$) and semi-crystalline (***Class Ib.*** $T_{trans}=T_m$) SMPs, whose T_{trans} corresponds to the characteristic thermal transition of the polymer segments between crosslinks and which are the shape-memory molecular switches. The simplest example of ***Class Ia*** is shown in **Figure 1.4a** for a crosslinked glassy polymer with a $T_{trans}=T_g$, comprising one kind of switching segments and net-points.[44, 50] Alternatively, in ***Class Ib*** the switching segments between covalent net-points are crystallisable or are liquid crystalline domains, and thus, the amorphous segments crystallizes when the material is in its temporary shape upon cooling below $T_{trans}=T_m$ or the shape-memory effect is triggered by the thermal transition of the liquid crystalline domains ($T_{trans}=T_i$) respectively.[22, 39, 43, 51, 52]

However, the polymer network architectures with covalent crosslinks as responsible for the permanent shape, can get more complex by combining the covalent networks with physical interactions. The main strategies are based on obtaining a biphasic polymer architecture by grafting side chains to the main covalent network (**Figure 1.4b**),[45, 47, 53] and on the incorporation of AB (**Figure 1.4c**)[7, 51, 54-56] or ABA[57] immiscible copolymers or triblock copolymer segments,

respectively (**Figure 1.4d**), into the covalently crosslinked structures. Generally, the segregated domains provide physical crosslinks and are used in the fixity of temporary shape by means of their characteristic temperature T_{trans} (that could be either T_g, T_m or T_i), while the main covalent crosslinks are responsible for the recovery of the permanent shape. Regarding the multi-material systems able of SME, the main types are the covalently crosslinked interpenetrating polymer networks (IPNs) in which the net-points of both polymer networks are responsible for the permanent shape, while the chains between these net-points act as switching segments (**Figure 1.4e**).[25, 58, 59]

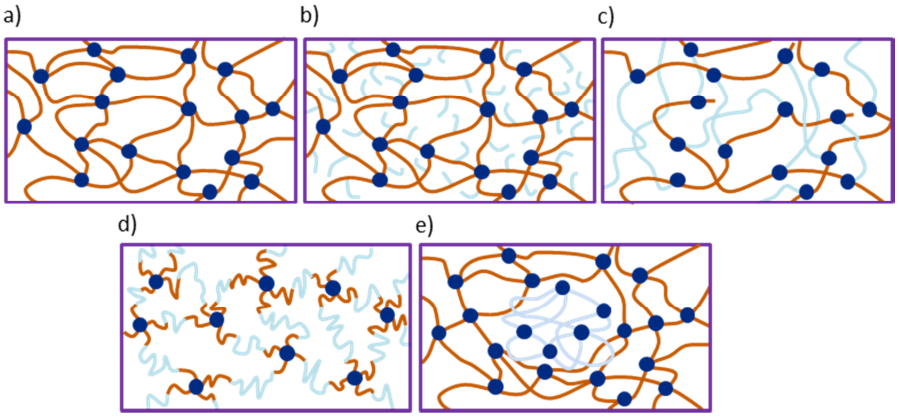

Figure 1.4. Schematic examples for polymer network architectures for Class I suitable to exhibit shape-memory effect. Molecular switches are represented in brown/light blue, and net-points in dark blue. The simplest polymer network consisting of switching segments linked by covalent net-points **(a)**. Polymer network having side chains as switching segments **(b)**. AB-polymer network **(c)**. Multiphase polymer network based on ABA triblock segments linked by covalent net-points **(d)**. Interpenetrating polymer network (IPN) **(e)**.

Class II:

The physically crosslinked SMPs are constituted of polymer chains interconnected by physical crosslinks which can be released in a thermal process. The main difference from covalently crosslinked SMPs is related to their permanent shape that can be altered by heating above T_{perm} which can be T_g, T_m or T_i. In order to achieve a good shape-memory behavior, a phase-segregated morphology is

required. Thermoplastic linear polymers, branched polymers and polymer complexes are the main members of this family. Among linear polymers, thermoplastic phase-segregated block copolymers are the most representative group of physically crosslinked SMPs, in which the blocks have to be immiscible and able to form microscopic phase-segregation. One of the phases consists in polymer chains interconnected by physical crosslinks which are stable at high temperature (T_{perm} well above the T_{trans}) and are able to retain the structure during the programming process, while the other phase acts as molecular switch at the desired T_{trans} for the SME. Generally the T_{trans} is the lowest thermal transition of the system and can be either T_g ***(Class IIa)***,[31, 60-64] T_m ***(Class IIb)***[65-67] or T_i ***(Class IIb)***,[67, 68] if the switching domains are amorphous, crystalline or liquid crystalline, respectively (**Figure 1.5**).

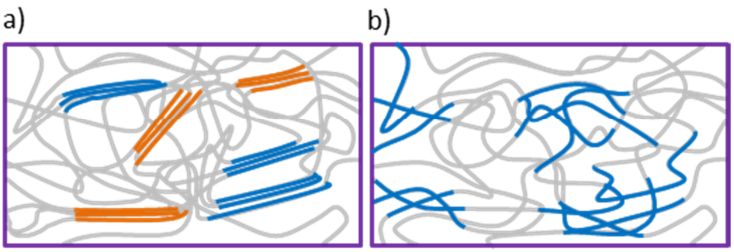

Figure 1.5. Schematic examples for thermoplastic polymer architectures of Class II suitable to exhibit shape-memory effect. With crystalline hard domains (blue) and crystalline switching domains (orange) **(a)**. With amorphous hard domains in grey and amorphous switching domains in blue **(b)**.

The synthesis strategies to achieve physically crosslinked SMPs are based on coupling pre-synthesized polymer blocks with low molecular weight units by pre-polymer method or melt blending. The pre-polymer method involves two-step polymerization stages and it is typically used to produce thermoplastic polyurethane elastomers.[67, 69] In a first step, the pre-polymers are obtained from the reaction of a macrodiol with a low molecular weight diisocianate. In a second step, a chain extender is added to couple these pre-polymers, thus obtaining linear phase-segregated PU block copolymers. Melt blending is used to obtain SME at a

cost-effective price by adjusting the T_{trans} of a certain SMP, or in the case of immiscible polymers, where one material can act as a molecular switch and the other as a fixed phase resulting in a multi-material shape-memory system.[70-72]

1.5. BIOMEDICAL APPLICATIONS OF SHAPE-MEMORY POLYMERS

Biomedical applications of shape-memory alloys (SMAs) have been extremely successful since 1990´s because of their usefulness in less-invasive surgeries.[73, 74] Since these pioneer works, the SMPs have been gaining widespread attention in the medical area as a research field focused on the development of active medical devices.[75, 76] An overview of medical devices in development that consist completely or partially of SMPs is given in **Table 1.2.** This information deals with configurations of shape-memory devices mainly based on non-degradable materials. Some of the potential applications have been briefly described in patent applications, and among the proposed materials, just a few ones are shown in the **Table 1.2**.

One of the major targets of SMPs for medical devices are **vascular applications** in which the materials are processed as embolic devices and stents.[77] SMP stents with tubular geometries are used to maintain the patency of the artery wall and they can compete with or replace the conventional stainless steel stents due to an increase in the compliance between the tissues and devices. These devices are programmed in a compact temporary shape for their introduction inside the human body and the recovery shape is produced at the physiological temperatures.[78-81]

An interesting case study is based on the substitution of the usually employed platinum coils to treat intracranial aneurysms and prevent strokes by a SMP composite made of tantalum and polyetherurethane (with $T_{trans}=T_g$, T_g=33 °C) with increased bio-activity.[77] Studies about stents based on commercial shape-memory

polyurethane (DIAPLEX®) have been also performed, demonstrating the potential application of SMPs in this field.[83]

Table 1.2. Potential applications of shape-memory polymer-based medical devices.

Application	Polymer	Principle	Ref.
Aneurysm treatment	Polyetherurethanes (CaloMER™) Polyurethanes (MP5510, Mitsubishi Heavy Industries Ltd.)	SMP devices (foams, fibers) fill distended balloon-like dilations (aneurysms) of blood vessels	77, 82
Stents	Polyurethanes (DIAPLEX®)	SMP hollow devices that are radially distensible	83
Clot removal	Polyurethanes (MP 4510 and MP5510, Mitsubishi Heavy Industries Ltd.)	Corkscrew-shape SMP or hybrid SMP-Nitinol® devices for endovascular removal of blood clots, devices of temporary straight shape are pierced through the clot and capture it upon recovery	84
Stomach fillers for obesity treatment	e.g.: block compolymers or possible commercially available materials such as Vicryl® (Ethicon)…	SMP device that unfolds in the stomach reducing the volume of the stomach, for weight reduction of overweight patients	85, 86
Arch-wires in orthodontics	Polynorbornene	SMP wire for correction of misaligned teeth, shape recovery creates forces that push the tooth in the desired position	87
Self-tightening suture/ Surgical fastener	e.g.: Polyurethanes, poly(styrene-butadiene) block compolymers, polynorbornenes…	SMP thread capable of forming a self-tightening knot, SMP needle that pierces implanted non-SMP devices By shape recovery, needle become a curved or helical shape which secures devices to the tissue	88
Fixation of damaged ligament or tendon	A copolymer of methyl methacrylate and poly(ethylene glycol) dimethacrylate (MMA-co-PEGDMA)…	SMP rod for replacement screw in surgical fixation of damaged ligament or tendon to bones, rod expands upon shape recovery and fixes the loose end of a ligament by defined pressure	89
Retrieval devices	e.g.: Copolymers of n-butylacrylate- hydroxyethyl methacrylate (HEMA) and ethyleneglycol-1-acrylate-2-CA (HEA-CA) crosslinked with poly(propylene glycol)-dimethacrylate)…	SMP devices of different permanent shapes (baskets, corkscrews) to capture stones in the cavities of kidney	90
Fertility control	e.g.: Polyurethanes, ethylene-vinyl acetate copolymers, poly(norbornyl-POSS) copolymers, polycyclooctenes…	SMP device inserted via catheter into fallopian tube and expanded upon application for permanent or temporary sterilization	91

Thermally activated SMP devices could be also used as devices to remove blood clots. These materials are designed to be delivered through a catheter in a narrow shape and subsequently take on the form of an umbrella- or a corkscrew-shaped device in order to grab and extract the clot.[82, 84] These materials have been also selected for cardiac valve repair in form of prosthetic rings which are implanted in a temporary shape with the diameter of patient´s malfunctioned mitral valve. Besides, the SMP ring diameter can be gradually reduced by resistive or inductive heating through inner resistances or magnetic particles reducing the mitral valve diameter to close properly.[92]

In addition to vascular applications, other studies cover specialized applications in different parts of the body by using different architectures of shape-memory devices. In this regard, intra-gastric shape-memory implants which inflate to make the patient feeling satiety by reduction of the stomach´s volume have been suggested to treat obesity in overweight patients.[85, 86] High strength shape-memory materials with T_{trans} in the range of 56-92 °C, and rubbery modulus values from 9.3-23 MPa based in a copolymer of methyl methacrylate and poly(ethylene glycol) dimethacrylate (MMA-co-PEGDMA) have been reported to be used as fixation devices to treat orthopaedics injuries. An example is given by the fixing method for ruptured tendons or ligaments to bones, in which a thin shape-memory rod recovers (shape recovery) to a more compact rod to fix both components.[89] In order to offer an aesthetical alternative to traditional orthodontic materials, polynorbornene-based SMP have been used as an arch in orthodontic braces with enough recovery force for aligning teeth.[87] Monofilaments of a SMP based on a thermoplastic block copolymer able to be stretched under heat and cooled to stabilize the temporary shape can be used as intelligent suture for wound closure in general surgical applications.[93] Shape-memory deployable devices to capture stones in the urinary tract or as contraception devices have been also considered as a potential application.[90, 91] Finally, there is a trend in studying the possible controlled drug-release capabilities of multifunctional SMP matrices through the

combination of controlled drug release, shape-memory capability, and in most of the cases, biodegradability.[94-96]

2. BIODEGRADABLE SHAPE-MEMORY POLYMERS

As discussed in the previous section, the possibility of tailoring the properties of SMPs systems for specific requirements of a wide variety of applications, makes them attractive materials which have recently gained attention in the medical field for their use as active medical devices. It is clear that there is a strong clinical trend towards minimally invasive surgical procedures that produce less trauma, limit the risk of infection and significantly reduce costs. In this regard, in the last 15 years, SMPs have been gaining attention and new products that offer new functionalities as compared with SMAs have been launched onto the market. The development of these new products based on polymers can be attributed to the possibility of combining shape-memory properties and **biodegradability**.

The first relevant application proposed for biodegradable SMPs was a smart suture for wound closure,[55, 93] in which the material was able to apply a defined stress to the wound lips. Although most of the SMPs associated to biomedical applications are still under development or in a conceptual stage, an overview of a biodegradable SMPs associated to biomedical applications is described in **Table 1.3**. This Table does not include the whole range of SMPs investigated, but introduces the most favourable configurations studied so far. As is evidenced in the **Table 1.3**, biodegradable polyesters play a key role in medical applications (as surgical sutures, catheters and stents) thanks to their biodegradable character and versatile synthesis which results in final adjustable properties promoting the conformation of shape-memory devices with adjusted T_{trans} to the physiological temperature.[97]

Elasticity is a major mechanical property of biological tissues, but is difficult to be provided by thermoplastic polymers. Some medical devices based on biodegradable poly(glycolic acid) (PGA) or poly(lactic acid) (PLA) are commercially available and have good mechanical properties.

Table 1.3. Biodegradable shape-memory polymers. Adapted from 5.

Polymer	Shape-memory properties	Properties at 50% of degradation mass loss	Ref.
Poly(ε-caprolactone) dimethacrylate and n-butyl acrylate	Third cycle Rf=93-98% Rr~95%	Phosphate buffer solution (pH 7.4, 37 °C) No mass loss after 140 days	55, 81
Star-shaped oligoesters of rac-dilactide and diglycolide	Fifth cycle Rf≥99% Rr≤97%	Aqueous buffer solution (pH 7, 37 °C) 80 days/150 days	23
Multiblock copolyesters from poly(ε-caprolactone) and PEG, and chain extender based on CA groups	Third cycle[a] Rf=100% Rr=88%	Phosphate buffer solution[a] (pH 7.2, 37 °C) 5% after 25 days	56
Oligo(ε-caprolactone) diols, oligo (*p*-dioxanone) diols, and diisocyanate	Third cycle Rf=98-99.5% Rr=98-99%	Aqueous buffer solution[b] (pH 7, 37°C) 270 days	93
Multiblock copolymers containing poly(L-lactide) and poly[glycolide-co-(ε-caprolactone)] segments	Third cycle Rf~99.0% Rr~99.6%	Phosphate buffer solution (pH 7.4, 37°C) 154 days	61

[a]75 wt% poly(ε-caprolactone) (M_n = 3000 $gmol^{-1}$), 25 wt% poly(ethylene glycol) (M_n = 3000 $gmol^{-1}$), total M_n = 28 700 $gmol^{-1}$, gel content 57%.
[b]42 wt% oligo(p-dioxanone).

However, the high stiffness (typically elastic modulus E = 10^1 to 10^3 MPa below T_{trans} in the fixed state)[98] and the lack of flexibility and elasticity because of their high glass transition temperature, results in failing to mimic the elastic nature of many soft tissues such as blood vessels, cartilage or ligaments. Indeed, one of the major drawbacks of these materials is their intrinsic difficulty to replicate the tissue elasticity, especially under variable loading situations. In order to overcome these shortcomings, the development of soft SMPs with elastic properties, low stiffness (E=10^{-2} to 10^{-1} MPa below T_{trans} in the fixed state), flexibility and recoverable deformation at physiological temperatures, (with T_g below or close to body temperature) is gaining attention.[99, 100] However, despite the apparent need for soft SMPs,[1] only few attempts can be found in the literature, including liquid crystalline elastomers,[39, 101] elastomeric ionomer blends with crystallisable fatty salts,[58] polyurethane-based polymer laminates[102] and blends of elastomers with

amorphous or semi-crystalline polymers such as PCL.[103] Most of these materials present some inherent challenges such as the possibility of obtaining complex shapes, custom chemical synthesis, or limited biodegradability under physiological conditions.[104]

2.1 SOFT BIODEGRADABLE POLYMERS (ELASTOMERS)

Huge efforts have been invested into the development of polymeric biomaterials that mimic natural tissues.[105] However, there are only few synthetic tissue engineering products able to substitute soft tissues such as muscle and connective tissue.[106]

In the late 1990s it started to emerge the use of degradable elastomeric biomaterials for medical devices, especially with applications in the field of tissue engineering. In this regard, the ability to synthesize biodegradable polymers with tuneable mechanical properties and degradation profiles is crucial. Recently, significantly research efforts have been carried out in order to synthesize biodegradable polyester-based soft materials with biocompatibility and controllable degradation profiles,[107-111] thus demonstrating their potential applications in tissue engineering[110] such as nerve-guidance,[112] vascular grafts,[113] drug delivery,[114] tissue adhesives[115] and scaffolds for cartilage,[116, 117] bladder,[118] blood vessels,[119] as well as for gene delivery.[120] Typically, all the reported systems have some key aspects in common: (1) the incorporation of ester bonds in polymer chains which allows the degradation by hydrolysis and enzymatic activity, (2) the mechanical properties can be tuned by processing conditions and (3) the use of non-toxic monomers which can be metabolized or excreted by the host.[107, 121]

Soft polymers or elastomers can be prepared as physically crosslinked elastomers or chemically crosslinked elastomers (also called just elastomers) which differ in the nature of links between chains that confer the elastic response to the material.[122] In general, interactions such as hydrogen bonding, dipolar forces,

crystalline regions or glassy domains are the responsible for holding together the chains in physically crosslinked elastomers. Conversely, the chains in chemically crosslinked elastomers are linked by covalent bonds introduced through UV or thermal curing processes.

2.1.1. PHYSICALLY CROSSLINKED (THERMOPLASTIC) ELASTOMERS

Thermoplastic elastomers are usually structured into hard and rigid segments alternated with soft and flexible segments. At ambient temperature the soft segments are responsible for the rubber elasticity while the hard segments can form rigid domains below T_g (amorphous) or T_m (semi-crystalline) by physical crosslinks.[123] In the particular case of the biodegradable thermoplastic elastomers, they are mainly based on polyurethanes (PUs), polyhydroxyalkanoates (PHAs) and copolymers of poly(ε-caprolactone) (PCL) with poly(glycolic acid) (PGA) or poly(lactic acid) (PLA).

Polyurethanes (PUs) are characterized by a wide diversity in chemical compositions and mechanical properties, being traditionally developed as long-term implant materials with slow biodegradation rate.[124] Recent attempts have been made towards the design of PUs with enhanced biodegradability in order to widen the applications for nerve guidance conduits,[125] cardiac tissue engineering[126-128] or drug delivery.[129] The strategy employed to enhance the biodegradation and achieve non-cytotoxic decomposition products *in vivo* of elastomeric PUs is frequently based on the incorporation of polyester macrodiols soft segments that are able to hydrolyse *in vivo* and *in vitro* conditions, such as poly(lactic acid) (PLA), poly(glycolic acid) (PGA), or poly(ε-caprolactone) (PCL).[130] Together with PUs, thermoplastic elastomers based on polyhydroxyalcanoates (PHAs) are the two dominant materials of this family, with P4HB and its copolymer with P3HB (P3HB-co-4HB) being the most representative of PHA-based polymers with elastomeric behavior. PHA-based polymers have been widely investigated to be used as cardiovascular

scaffolds due to the combination of proper mechanical properties and good elastic response when working under constant dynamic conditions.[108, 122, 131] Although some recent advances in porous PUs scaffolds have reported these materials to be resorbed or degraded in 8-12 weeks,[132-134] the PHAs and PUs have been traditionally developed for biomedical applications, such as tissue engineering, for tissues with slow healing times[125, 135-137] reparation of nerves,[125, 138-142] blood vessels,[143] intestines, load bearing tissue bone,[144-148] cartilage,[149] meniscus[150-152] and ligament tissues.[137]

On the other hand, the poly(ε-caprolactone) (PCL) copolymers with poly(glycolic acid) (PGACL) or poly(lactic acid) (PLACL) result in biocompatible and biodegradable rubber-like biomaterials.[153-156] The biodegradability of these PCL-based block copolymers varies as depending on the molecular weights and ratio of comonomers over a wide range of degradation rates and mechanical properties. In comparison to PUs or PHAs, these copolymers degrade faster; however, they have been successfully used in biodegradable scaffolds.[154, 155, 157, 158] One study carried out by Soo-Hong et. al[159] demonstrated that was possible to achieve a 50% of weight loss after 6 weeks of incubation for PGACL scaffolds.

2.1.1.1. TAILORING THE SHAPE-MEMORY EFFECT

Among all the different biodegradable thermoplastic elastomers with application in the medical field as SMPs, polyurethanes (PUs) have attracted the research efforts because of their versatile structure, mechanical properties and excellent biocompatibility.[160] Multiblock PUs networks architectures are preferred to produce shape-memory biodegradable devices. These materials are typically produced from two long-chain macrodiols, one with a lower thermal transition which acts as the switching segment and the other corresponding to the hard segments with a higher transition temperature. The diisocyanate is used only as the coupling agent. An intensively studied system for medical applications was a multiblock polyurethane composed of oligo(ε-caprolactone)diol (OCL) as precursor

for the switching, and a crystallisable oligo(*p*-dioxanone)diol (ODX) as hard segments, coupled with 2,2(4),4-trimethylhexanediisocyanate (TMDI). The T_{trans}, mass loss and shape-memory properties can be tailored for surgical sutures by adequate selection of the soft/hard segments ratio, which results in systems that exhibit a T_{trans} around 40 °C.[93] Likewise, Tri-arm polyurethanes based on ε-caprolactone and glycerol were obtained with T_{trans} of 36-39 °C,[161] and polyurethanes based on PCL (soft segments) and ethylene glycol (EG) (hard segments) coupled with 2,4-toluene diisocyanate (TDI) were prepared with T_{trans} in the range of 37-42 °C.[30]

Multiblock copolymers based on poly(glyclide-co-caprolactone)diol (PGC-diol) coupled with poly(L-lactide)diol (PLLA-diol) using 1,6-hexanediisocyanate to obtain PLLA hard segments and PGC soft segments have also been investigated.[61] Mechanical properties of these systems can be varied from soft to hard by adjusting the PLLA content. The mechanical behavior can be tailored from rubbery when PLLA is less than 60% to rigid when the PLLA content reaches 90%. Moreover, as depending on the composition, T_g can be varied between 41 °C and 49 °C, and T_m between 150 °C and 160 °C.

Copolymerization is also a strategy reported in the literature for decreasing the glass transition temperature of PLLA, and thereby to achieve soft shape-memory materials with appropriated thermal transitions for their use in human body applications. Some L-lactide-based copolymers which generally exhibit a phase-segregated morphology such as poly(L-lactide-co-ε-caprolactone) (PCL), poly(L-lactide-co-glycolide) (PLGA) and poly(L-lactide-co-p-dioxanone) (PLDON), show analogous shape-memory behavior to polyurethanes (PUs). The effect of chain flexibility of the different monomers copolymerized with L-lactide (glcolide (G), *p*-dioxanone (DON) and ε-caprolactone (CL)) on thermal, mechanical and shape-memory properties of the obtained copolymers was reported by Changchun et al.[162] The authors found that the ability of the studied monomers to reduce the T_g

and thereby to achieve softer materials at temperatures close to the body followed the trend CL>DON>G.

As example, the glass transitions (T_g) in the range of 46-34 °C were achieved by copolymerization of L-lactide with DON, while by using G instead of DON, the values obtained for the T_g were between 42 and 33 °C. A different approach to obtain PLLA-based shape-memory polymers with T_{trans} located in the neighbourhood of human body temperature was found in the poly(L-lactide-co-glycolide-co-trimethylene carbonate) (PLGTMC) terpolymer. The shape-memory effect in these materials is based on molecular chain entanglements, so that the switching temperature T_{trans} can be tuned in the range between 12 and 42 °C by changing the ratio between monomers.[163]

2.1.2. CHEMICALLY CROSSLINKED ELASTOMERS

The chemical bonds that link polymer chains to give rise to chemically crosslinked elastomers are usually achieved by reaction of multifunctional monomers, which contain two or more reactive groups capable of linking to other monomers.

2.1.2.1. POLY(POLYOL SEBACATE) FAMILY

Among all the chemically crosslinked elastomers, especial attention was focused onto poly(polyol sebacate) family (PPS) developed by Langer et al.[109, 164] The biocompatibility of these polymers has been reported to be similar to that of PLGA (with comparable response of the host tissue) even producing the formation of thinner fibrous capsules as well as lowering the inflammatory response.[107, 108, 165] The number of studies about possible applications in the biomedical field is increasing, demonstrating the potential of PPS elastomers as candidate materials for cardiovascular, cartilage and nerve tissue engineering,[112, 117, 119, 166, 167] among others.

A typical strategy to obtain these **biodegradable polyester elastomers** is *via* polycondensation reactions of multifunctional carboxylic acid and polyols.[168] The reactions between monomers are carried out in a two-stage synthesis. A low molecular weight pre-polymer is obtained in the first stage, and subsequently, the pre-polymer is post-polymerized under a temperature-time-vacuum profile to obtain an elastomeric material. The main advantage of this polycondensation method is that it can be applied to a wide variety of monomers without using any catalyst. However, the need of using long reaction times, high temperatures and vacuum conditions, can be a major limitation in some situations.[168] Networks of biodegradable polyester elastomers have been mainly prepared using glycerol condensed with adipic acid, sebacic acid, 1,10-didecanoic acid, or 1,12-didodecanoic acid.[109, 169] Elastomers from polyacids, such as citric acid, crosslinked with different polyols, such as 1,10-didecanediol or low molecular weight poly(ethylene glycol) (PEG), have been extensively investigated, as well.[110, 111, 170]

Great attention has recently been paid to the soft poly(glicerol sebacate) (PGS), a polyester elastomer based on monomers that are endogenous to the human metabolism. This material was firstly described as a tough biodegradable elastomer, obtained from polycondensation reaction of glycerol as polyol and sebacic acid as carboxylic acid.[109, 171] The superior elastomeric properties observed in this material were attributed to a low degree of crosslinking combined with hydrogen bonding interactions. In addition, PGS has been proved to possess better biocompatibility, *in vitro* and *in vivo,* compared to PLGA, as well as superior structural integrity and dimensional stability with the degradation time.[172, 173] In this regard, PGS has been used to fabricate micropatterned devices for contact guidance applications[167] and nerve tissue engineering.[112]

Other bioelastomer similar to PGS is the poly(diol citrate) (PDC), which uses citric acid instead of sebacic acid and is polymerized with diols of different chain lengths. These elastomers are able to degrade *in vitro* with better biocompatibility

compared to PLA and faster degradation than PGS, probably due to a catalytic effect of citric acid over the hydrolytic process.[110, 111]

Although the crosslinking density of PGS elastomers can be modified by changing the monomer stoichiometry or the polycondensation conditions, only a modest range of mechanical properties and degradation rates can be covered. Typically, PGS exhibits a Young´s modulus of 0.05-1.5 MPa and an ultimate tensile strength (UTS) of 0.4-0.7 MPa.[109, 174] In this regard, the variety of poly(polyol sebacate) (PPS) was recently investigated with the aim of broadening the PGS elastomers family. Instead of glycerol, other polyols such as mannitol, sorbitol, xylitol and maltitol were polycondensed with sebacic acid, to obtain poly(mannitol sebacate), poly(sorbitol sebacate), poly(xylitol sebacate) and poly(maltitol sebacate) polymers, respectively. It should be pointed out that these polyols were selected taking into account that they are (1) non-toxic, (2) multifunctional in order to allow the formation of randomly crosslinked networks as well as different crosslink densities, and (3) able to allow the formation of hydrolysable esters when are polycondensed with sebacic acid. All the monomers involved in the synthesis are endogenous to the mammalian organism, since sebacic acid is a metabolite derived from fatty acid oxidation and all the polyols are intermediates in carbohydrate metabolism. Following this strategy, a wide variety of mechanical properties and degradation rates were assessed.[107] As occurs with the PGS, the mechanical properties of PPS can be tuned by modifying the synthesis conditions of the polyol and the ratio between monomers, which allows to obtain values of Young´s modulus ranging from 0.4 to 400 MPa, UTS between 0.6-18 MPa and elongation at break from 11 to 200 %.[107] Among all the polymers in this family, poly(xylitol sebacate) (PXS) is the most studied member (aside from PGS) in order to overcome the rapid degradation kinetics of PGS which became one of the major drawbacks for its application in tissue engineering. In this way, the PXS can be as soft as PGS but its degradation is significantly slower.[165, 174]

As previously mentioned, the main limitation of PPS materials is represented by the need of harsh processing conditions during the thermal crosslinking. To overcome this shortcoming, several studies have been focused on the development of photo-crosslinkable systems. Nijst et al.[175] synthesized a poly(glycerol sebacate-co-acrylate) (PGSA) network able to be crosslinked under mild conditions and reaching similar mechanical properties to its thermally cured PGS counterpart. In this regard, new applications in tissue engineering arise for this PGSA photocurable elastomer, such as the encapsulation of temperature-sensitive factors and cells, due to the demonstrated potential *in vitro*[175] biocompatibility and mild to moderate *in vivo* inflammatory response.[176]

In chemically crosslinked elastomers, the shape-memory properties are strongly dependant on the crosslink density of the obtained network, which varies with the reaction conditions and curing times. In this case, the primary network is responsible for the permanent shape through the covalent crosslinked structure with switching segments between net-points. Switching segments could be either amorphous or crystalline and the T_{trans} is therefore related with the domains produced by amorphous/crystalline chains between net-points.

Poly(glycerol sebacate) (PGS) is one of the most representative chemically crosslinked elastomers obtained from polycondensation reactions. Although the shape-memory effect of PGS has been reported, it cannot be directly used as shape memory material for biomedical applications because of its low switching temperature.[177] However, many efforts have been made in order to increase the number of SMPs with similar chemistry to PGS and a T_{trans} around human body temperature. In this regard, Poly(glycol glycerol sebacate) (PGGS) and Poly(glycerol dodecanoate) (PGD) based elastomers were developed, expanding the list of shape memory biodegradable and biocompatible elastomers with recovery of the shape closer to the human body temperature (T_{trans}~39 °C).[178, 179] Another crosslinked SMP with covalently bonded network was the poly(propylene sebacate) (PPSe)

synthesized from polycondensation of 1,3,-propanediol (PDO), diethylene glycol (DEG) sebacic acid (SA) and itaconic acid (IA).[180] Different composition ratios as well as long curing times allowed to obtain materials ranging from rigid plastics to flexible elastomers at ambient temperature, and to achieve useful switching temperatures for biomedical applications of some systems.

Poly(diol citrate)s (PDC), were also reported as shape-memory polymers with tuneable mechanical properties and degradation profiles. A prominent example is Poly(1,12-dodecanediol-co-citrate), which has hydrophobic domains as physical crosslinks inside the elastomeric crosslinked network that are responsible from the shape-memory properties at clinically relevant temperatures (room to body temperature).[100]

2.2 LIMITATIONS OF SMPs FOR BIOMEDICAL APPLICATIONS

In the following sections, a review of the limitations of the physically and chemically soft biodegradable polymers as SMPs for biomedical purposes is presented.

As previously mentioned, is desirable from a medical point of view that an implantable polymeric device must be able to mimic soft tissue elasticity with the aim to avoid an adverse physiological response of the surrounding tissues and furthermore, it must withstand manipulation during implantation. In this regard, it is desirable the device to maintain a relatively rigid shape during implantation at room temperature in order to allow a better manipulation during its insertion in the proper position, while at a temperature close to the body, it is desirable the device to become soft and compliant with the soft human tissues. In addition, shape-memory properties are highly desirable for surgical implantation and minimal invasive applications so that the device can be inserted in a smaller shape, which allows passing through narrow places, and once in its final position, can

adopt the final functional shape. With this in mind, all the materials analysed in the above sections show the same limitations.

Physically crosslinked thermoplastic elastomers with potential applications as shape-memory polymers for biomedical purposes are mainly represented by PUs, PHAs, and PCL-based copolymers with PGA and PLA, due to their biocompatibility, biodegradability and tuneable mechanical properties. However, the main drawback in these biomaterials is related to the lack of mechanical compatibility between these implants and living tissues.

Regarding to the PHAs, some clear limitations are derived from its slower degradation and high degree of crystallinity which originates mechanical mismatch in medical applications due to the higher difference of stiffness in comparison with living tissues. To address these drawbacks, PHAs with softer and more flexible elastomeric behavior can be achieved by manipulating the length of the side chain and the distance between ester linkages in the polymer backbone.[181] The most promising candidates, in terms of biocompatibility, are the P4HB and P3HB-co-4HB grades. These materials have Young´s modulus values close to the living tissues (20 MPa); however longer degradation times are still required.[131, 135, 182] Moreover, the utilization of these materials in medicine has been hindered by the limited supply of medical grades, as well as their expensive production costs.

The biodegradable polyurethanes based on PCL show a recovery temperature that can be adjusted between 37-40 °C (close to human body temperature) by selecting the molecular weight of PCL and composition ratio between soft phase/hard phase. However most of these PCL-based PUs have too low shape-memory behavior, partly due to that the PCL phase does not have enough mechanical strength when it is incorporated in multiblock structure.[2] In contrast, PLA-based PUs, have been demonstrated to have better and faster shape-memory effect than PCL-based PUs.[183] In addition, when PGC-diol is introduced as soft segment, a faster

degradation than with PCL systems can be achieved (in particular a weight loss of 40-60% at 30 weeks was observed).

A major issue related to the development of such PUs-based SMPs is associated with a premature loss of mechanical strength after 5-7 weeks *in vitro*.[61] The reason for this, is because most of the studied PU systems possess crystalline regions that results in heterogeneous degradation rates as well as in non-linear loss of mechanical strength with time, which complicates a possible prediction of mechanical behavior under physiological conditions and results in mechanical failure of the device before that a large degradation occurs.[184-186]

Besides the incorporation of PCL and/or PLA as a polyurethane component, the copolymerization is another strategy followed in order to achieve satisfactory elastic properties and a better control over the degradation rate without sacrificing the biocompatibility.[156] PCL has been copolymerized or blended with PGA and PLA to produce elastomeric material, with good processability and wide range of degradation rates, through the adjustment of the molecular weights and the copolymerization ratios. However most of these materials undergo bulk erosion in contact with body fluids that can cause premature fails. In this sense, an abrupt release of the acidic degradation products can result in a strong inflammatory response.[187-189]

In summary, in order to achieve **shape-memory thermoplastic elastomers** with appropriate mechanical properties a minimum amount of hard segments have to be included in the molecular structure of the polymer. This fact usually results in high thermal transitions and heterogeneous and slow degradation. As a consequence, the thermoplastic elastomers require temperatures well above the physiological conditions to induce a shape-memory response, thus, thermal burns may occur when they are used in biomedical applications. Moreover, the physical nature of the crosslinks usually leads to insufficient shape fixity (R_f) and low shape

recovery ratio (R_r) due to the strong creep which occurs when is deformed or retained the strain at high temperatures.[6]

In comparison with the thermoplastic elastomers, the **chemically crosslinked shape-memory elastomers** (especially polyester-based), are attractive for biomedical applications, because they are able to provide mechanical stability and structural integrity, besides avoiding premature mechanical failure during their hydrolytic degradation.[116, 121] It is also clear that one of main advantage of these elastomers as novel shape-memory materials for biomedical applications, is their mild shape-memory transition temperature range that could avoid the need of applying excessive heat, which can be harmful to cells and tissues.

Physically and chemically crosslinked elastomers differ not only in their properties but also in their processing and programming procedures, that is to say, certain limitations arise from the molecular structure of both types of materials. In general, T_{trans} of most of physically crosslinked elastomers and in some of chemically crosslinked elastomers networks is the melting point. Here, the fixation of the temporary shape needs to be adjusted by the crystallization of the switching segments and detailed information about the crystallization process is necessary in order to optimize the programming of the shape-memory effect. In these networks, only the crystalline parts of the switching segments are contributing to the fixation of the temporary shape resulting in a worst cycling behavior. In this regard, T_g based shape-memory elastomers are preferred, since is not necessary to improve the crystallization during cooling to obtain good shape fixity rates. In addition, if the network is chemically crosslinked, the higher weight fraction or even the whole polymer network can act as switching segments resulting in good elasticity, higher shape stability during degradation and better behavior under repeated dynamic loading.[190]

Thereby, in general amorphous non-crystallisable shape-memory elastomers, based on chemical crosslinking networks with $T_{trans}=T_g$, is the favoured way to achieve SMPs, attending to better shape fixity, shape recovery over cycles (including recovery ratio of 98-100% in comparison with physically crosslinked systems which is around 90-95%), enhanced recovery stress, adjustable rubbery modulus and degradation profile, through the control of crosslinking degree. In this regard, **poly(polyol sebacate)** (PPS) family members, have been successfully reported as useful materials for many medical and soft tissue engineering applications. However, despite the biodegradable PPS possess interesting and desired properties for the medical field, they have poor intrinsic mechanical strength, stiffness and fracture toughness that could limit their biomedical application when the tissue involved is both stiff and elastic at the same time. Thus, these materials are not able to provide mechanical support to injured tissues or organs with high strength and flexibility as in the case of skin, nerves, cartilage, heart valves, tendons or trabecular bone. In addition, regarding to the development of a possible shape-memory medical device based in PPS, their low mechanical strength and stiffness, could produce low shape recovery stresses that could largely restrict their proper operation.

Hence, there is a need to improve their mechanical properties in order to develop PPS based shape-memory materials with better performance. In this regard, the combination with reinforcing fillers to obtain shape-memory composite materials could represent an effective approach to afford it.

3. ELECTROSPINNING

3.1. MECHANISM AND SET-UP

Electrospinning is a technique that provides a straightforward way to produce continuous polymer fibres with diameters in the range of 40–2000 nm[191] from a polymeric fluid stream (solution or melt) delivered through a millimeter-scale nozzle and using electrostatic forces.[192] The main advantage in reducing the diameters of fibers from microns to nanometers is that a large surface area to volume ratio is provided. This fact together with the interconnected porosity achieved in the nanofibers network, makes this technique an optimal candidate to produce polymer nanofibers for advanced applications, such as scaffolds for tissue engineering, drug release systems for biomedicine, membranes for filtering, optical sensors or textile parts for protective clothing. Typically, the electrospinning process is applicable to a wide range of polymers like those used in conventional spinning, i.e. polyolefines, polyamides, polyester and acrylics.

Figures 1.6 and 1.7 illustrate schematic diagrams of the electrospinning set-up. These figures show how a nanofiber mat can be easily obtained by applying a high voltage between a capillary filled with the polymer and an electrode. Regarding to the process, as the intensity of the electric field is increased the hemispherical surface of the fluid at the tip of the needle is elongated to form a conical shape known as the Taylor cone **(Figure 1.6)**. As the field increases, a critical value is achieved when the repulsive electrostatic force overcomes the surface tension and a charged jet of fluid is ejected from the tip of the Taylor cone. The discharged polymer solution jet undergoes a whipping process wherein the solvent evaporates, leaving behind a charged polymer fiber which is highly stretched and reduced in diameter as it travels towards the collector. Splaying occurs in a region where the radical forces from the electric charges carried by the jet become larger

than the cohesive forces within the jet. The single jet divides into many charged ones before landing on the collector. Although little is currently known about this splaying process of the primary jet into multiple filaments, it is thought to be responsible (together with the elongation due to the acceleration of the jet by electrical forces) for the unusually small diameter of the fibers (from 50 nm to few microns) produced by electrospinning. The electrospun nanofibers can even be aligned in a certain degree to provide extra strength to the obtained polymer mat. Despite the precise control of the alignment of spun fibers this still remains a challenge. The influence of different collector configurations on the nanofibers alignment has being studied.[193, 194] In fact, it has been seen that the nanofibers can be collected in a circumferential manner with higher alignment degree by using a rotating drum collector capable of rotate at high speeds.[195-197]

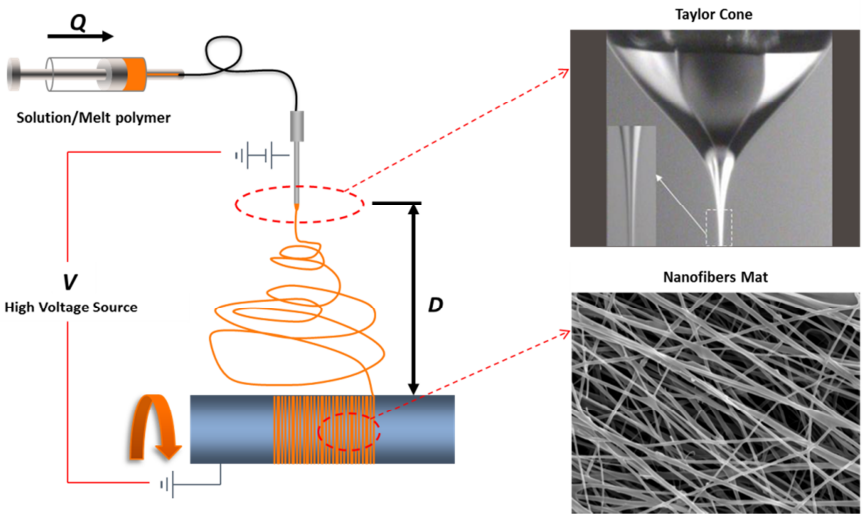

Figure 1.6. Schematic representation of electrospinning set-up and process. The three main process variables are represented as *Q* (flow rate of the polymer solution), *D* (distance between collector and needle tip) and *V* (applied voltage).[191]

Different electrospinning set-ups can be adopted depending on the fiber morphology desired, but main components have to be present; **(1)** a pump that makes the polymer solution flow through a syringe connected to a **(2)** metallic

needle or capillary, and a **(3)** high voltage source that connects the metallic needle to a **(4)** collector. These main components are usually mounted in horizontal or vertical configurations as is illustrated in **Figure 1.7**.

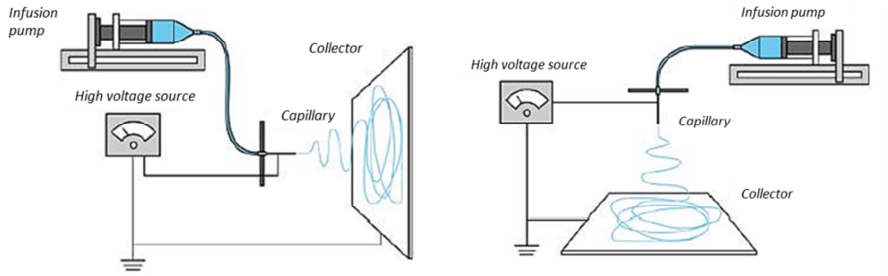

Figure 1.7. Schematic representation of horizontal (left) and vertical (right) electrospinning set-up.

In addition to the electrospinning **process parameters**, others variables related to the solution and ambient conditions are involved in the success of the process. Some of them, such as the viscosity of the solution, have been demonstrated to play an important role in the fiber morphology.

Figure 1.8 summarizes the large number of variables that affect the electrospinning process, while **Table 1.4** collects the most significant conclusions reported in the literature about the influence of the electrospinning parameters over the morphology and size of the obtained fibers.

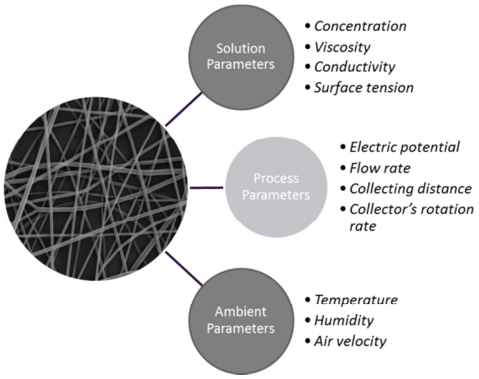

Figure 1.8. Summarizes the parameters and processing variables affecting the electrospinning process.

Table 1.4. Main electrospinning parameters and their influence over the fiber morphology.

Parameter	Effect on Fiber Morphology	References
	Solution parameters	
Viscosity	Low: Droplets formation High: Fiber diameter increases and droplet formation stops	198-201
Concentration	With an increasing polymer concentration, the fiber diameter increases as well	202-204
Molecular weight (polymer)	Droplets formation with low molecular weight	205-207
Conductivity	High conductivity reduces the fiber diameter	208-210
Surface Tension	Affects the Taylor cone stability	199, 210-212
	Process parameters	
Applied potential	High potential reduces the fiber diameter	202, 204, 207
Distance between needle and collector	Too short or too long distances induce droplet formation	199, 201, 205, 213, 214
Polymer flow	Low flows produce small diameter fibers High flows induce droplet formation	199, 212, 215
	Ambient Parameters	
Humidity	High humidity enhances fibers porosity	211, 216, 217
Temperature	High temperature reduces the polymer diameter	211, 218

3.2. ELECTROSPINNING OF BIODEGRADABLE NANOFIBERS

As previously mentioned, the electrospinning technique can be used to convert a wide variety of polymers into nanofibers. Many research efforts are aimed at finding the appropriate conditions for electrospinning of natural origin and synthetic biopolymers for medical applications, which include multifunctional membranes and biomedical structural elements (scaffolds used in tissue engineering, wound dressing, drug delivery, artificial organs, vascular grafts…) among others.[195, 219] Natural origin polymers commonly used in electrospinning include collagen, chitosan, gelatin, casein, cellulose acetate and silk protein among

others. However, synthetic biopolymers offer certain advantages over natural polymers, as they could be modified to provide the needed mechanical properties as well as degradation rates desired for biomedical applications.

Up to date, the most common synthetic biopolymers processed by electrospinning are biodegradable polyesters such as poly(glycolic acid) (PGA),[220-223] poly(lactic acid) (PLA),[202, 224-228] and poly (ε-caprolactone) (PCL),[229-232] mainly for their application as scaffolds. Some polyurethanes (PU) and poly(lactide-co-glycolide) (PLGA) copolymers have been electrospun and used as wound dressings or blood vessels replacements and vascular grafts.[233-241]

However, it should be pointed out that among all the biodegradable polymers mentioned, there is a growing interest parallel to the progress of this technology focused onto the electrospinning of poly(lactic acid) since it has been demonstrated to be easily processed by this process.[242] In addition, its degradation by simple hydrolysis of the ester backbone makes it a good candidate to be used as a biomaterial for temporary therapeutic applications, controlled drug release, support for cell culture and tissue engineering. Because of it, electrospinning technique has been extensively reported as an easy route to obtain PLA fibers membranes with large application in the biomedical field. Studies on the production of PLA nanofibers by means of electrospinning,[243-248] have demonstrated that this material can be successfully processed to obtain scaffolds for biomedical applications such as cardiac, neuronal, bone and blood vessels tissue regeneration.[249, 250, 250-252] In addition, several studies reported the use of electrospun PLA mats as carriers of bioactive agents such as antibiotics,[253] anticancer drugs,[254, 255] antibacterial silver nanoparticles[256] and enzymes.[257]

4. SHAPE-MEMORY POLYMER COMPOSITES (SMPCs)

Generally, despite the advantages of SMPs over SMAs, such as low density, large deformability, easy processability and low cost,[258] the major drawbacks are found into their poor mechanical properties (low strength and stiffness), more markedly in soft elastomeric systems, which directly affect the shape-memory behavior by means of a low recovery stress and slow recovery speed.[259] This fact affects their range of applications, limiting their incorporation within the biomedical field. These limitations have provided enough motivation for the development of new types of SMPs, more specifically of SMPCs. In this context, the development of shape-memory polymer composites (SMPCs) enables an improvement in mechanical properties, thus is, high recovery stress levels can be achieved to ensure an efficiently recovery of the permanent shape as well as to impart novel functions such as electrical conductivity, magnetism or biofunctionality.[2, 11, 21, 260] In shape-memory polymeric composites (SMPCs), the improvement of neat matrix properties and the capacity to create new functionalities are strongly related and can be controlled through the interfacial compatibility between the filler and the matrix, as well as with the micro/nano-structural parameters such as dimension, geometry, distribution, volume fraction, alignment and packing arrangement of fillers. Traditionally, the improvement of the mechanical properties in SMPCs has been achieved through the incorporation of micro sized fillers. However, their influence on improving the shape memory effect has not been entirely satisfactory. So, in many cases an increase in recovery stress is accompanied by a deterioration of shape memory performance with a significantly lowering in the recoverable strain rate of the initial shape, and even in the fixity rate during deformation.[261-263] Liang et al.[264, 265] and Gall et al.[264, 265] investigated glass and Kevlar fiber reinforced SMP composites. An improvement in stiffness was observed but on the contrary, a decrease in recoverable strain was obtained as a consequence of the filler incorporation. Ohki et al.[262] reported the changes in mechanical and shape

recovery properties with the addition of strand glass fiber to thermoplastic SMPC. An increase of 140% in the failure stress as well as a decrease 62% in the recovery rate was observed for composites with 50 wt% of glass fiber. Similar behavior was reported by using carbon fiber as reinforcement of SMPCs.[266]

To obtain SMPs that cover these needs, different types of **nano-sized** reinforcements have been introduced in the present thesis in order to improve the shape-memory properties of the neat matrices by modifying their thermal and mechanical properties. In comparison to micro scale, the incorporation of small amounts of compatible and well dispersed nano-sized fillers to reinforce SMPs, leads to an improvement in Young´s modulus and strength properties with a substantial enhancement in the overall material properties due to better interface properties between matrix and filler.[267, 268] These nano-fillers can be classified in three different categories both by their geometry or by their size, namely particles (such as silica, metal, POSS and other organic and inorganic particles), layered materials (graphite and layered silicates), and fibrous materials (nanofibers, single-walled and multi-walled nanotubes MWNTs). The major challenges in designing polymer composites are related to the complexity of the composite structure, dispersion of fillers, and the relationship between dispersion and properties. Uniform dispersion of nanoparticles against their agglomeration is the first step needed to process and understand the behavior of nanocomposites.[6, 25, 70] It is well known that the most desirable situation is to achieve a highly compatibility between the filler and polymer matrix. In this regard, several strategies such as solvent casting, with surface functionalization or sonication treatments, and in-situ polymerization results in better dispersion of fillers than direct melt processing of the nanocomposites.

In regards to the shape-memory properties of nanocomposites, the incorporation of carbon nanotubes or carbon nanofibers,[269] allows to obtain electrical conductive SMPCs, at the same time that an improvement in mechanical properties is obtained

without a markedly decrease in recovery strain. The authors reported that the incorporation of low carbon nanofiber contents (3.3 wt%) increased the recovery stresses by 200% with a shape recovery (R_f) higher than 90%. Koerner et al.[270] reported that through the incorporation of carbon nanotubes (CNT) into a SMPU matrices an increase in shape fixity was obtained with almost 100% of shape recovery. Other authors observed an improvement of both strain and recovery stress by using CNT into SMPU matrices.[271, 272] Similar behaviour was observed when adding fillers such as SiC nanoparticles in epoxy matrices. These fillers were found to enhance the Young´s modulus allowing the SMPC to generate higher recovery forces with good strain recoverability for strain levels of 30%.[267]

4.1. BIODEGRADABLE NANOCOMPOSITES WITH SHAPE-MEMORY EFFECT IN THE BIOMEDICAL FIELD

Recently, biodegradable SMPCs have been explored as an alternative to conventional biodegradable implants, due to the possibility to degrade either by hydrolytic or enzymatic processes without leaving any residue inside the body after a determined period of time.[26, 93, 273, 274]

Inorganic hydrophilic fillers such as Fe_3O_4 have been used to tune the degradation rates of SMPs based on poly(ε-caprolactone) PCL matrices, resulting in faster degradation rates for the composites compared with the neat matrix. Furthermore, the nanocomposites with 5 wt% of Fe_3O_4 showed an excellent shape recovery ratio before the degradation process, while an increase of 10 wt% filler content produced an accused decrease.[275] Zheng et al.[276] reported the improvement in the shape-memory recovery ratios of poly(D,L-lactide) (PDDLA) nanocomposites reinforced with hydroxyapatite, in comparation with neat PDDLA. In this regard, the addition of low contents of polyhedral oligosilsesquioxane (POOS) in poly(lactide-co-glycolide) (PLGA) matrices allowed to obtain versatile shape-memory properties while degradation rates decreased.[52, 277] Chitin nanocrystals as

a reinforcement of a biobased polyurethane matrix results in an enhancement of shape recovery ratios with increasing filler content while fixity of the shape is not affected for any loading content.[66]

Of main interest for the present work are the research efforts to improve the mechanical and functional properties of low modulus biodegradable matrices similar to poly(polyol-sebacates) that could found applications in the biomedical sector. The introduction of reinforcement fillers such as hydroxyapatite or Bohemite nanoplatelets in Poly(xylitol-co-dodecanedioate) (PXDD) and Poly(propylene sebacate) (PPSe) matrices respectively have been proved to be an effective way to enhance mechanical properties retaining good shape-memory properties with T_{trans} close to the body temperature in all the nanocomposites. The improvements obtained through the incorporation of nano-sized reinforcement fillers, positioned these materials as good candidates for biomedical materials with possible applications as high strength stents or hard tissue implantations devices.[180, 278, 279] PPSe/Bohemite nanocomposites showed an increase in the rubbery storage modulus (above T_{trans}) which favours a larger recovery stress during shape recovery.[280] This fact result in faster shape recovery speed and allows to possible shape memory devices to work properly under constrained environments.[281]

As could be seen, most usual nano-fillers geometries to reinforce SMPs are particles and layered materials. However, nowadays, there has been steady progress in the development of new polymeric fibers that can be potentially used as reinforcement for SMPCs. Significant progress has been made in the production of high performance fibers, elastic fibers and nanofibers from biodegradable polymers using different technologies, but the most promising one to obtain ultrafine diameters is the electrospinning process. This technique has been gaining popularity thanks to the unique nanometer architecture of the fiber mats obtained that confers considerable possibilities to be used in a wide variety of applications

including tissue engineering for wound healing and tissue regeneration, drug delivery, filtration devices or biosensors among others.[282, 283]

4.2. NANOFILLERS AS REINFORCEMENT OF BIODEGRADABLE ELASTOMERIC MATRICES

The present work is focused on improving the mechanical and functional properties of soft biodegradable matrices with especial interest in chemically crosslinked elastomers of PPS family. The PPS are limited for a variety of biomedical and clinical applications due to the low range of mechanical properties which can be enhanced without compromising their structural elasticity. Among the polymers of this family found in the literature with elongation to break of at least 10% (required for tissue engineering), the values for Young´s modulus (that ranging from 0.05 to 13 MPa)[107] are not useful when the tissue involved is at the same time elastic and stiffer (7-250 MPa).[284-286] Thus, their potential applications for biomedical purposes are limited when high strength and high flexibility are required, such as the case of ligating rubber bands for blood vessels, elastomeric sutures, flexible coatings for stents, surgical devices, vascular grafts, surgical wound dressings, catheters and small diameter tubes for drainage and cartilage tissue engineering among others.[287]

A first investigation of soft crosslinked biodegradable nanocomposites was performed on PGS matrix reinforced with bio-ceramic fillers.[285, 288] Most recently, PGS nanocomposites filled with halloysite or MWCNT have been also reported.[289, 290] By addition of 3 wt% of MWCNT filler to PGSC elastomeric matrices, higher Young´s modulus (close to 9 MPa) were achieved in comparison to neat matrix. In addition, the introduction of multi-walled carbon nanotubes (MWCNTs) allows the development of electronically active PGS based composite to be used as conducting biomaterial system in neural repair or nerve-tissue engineering. [290] As PGS, matrices of POC have been also combined with hydroxyapatite ceramic fillers to obtain elastomeric nanocomposites with Young´s modulus near to 10 MPa for contents of filler as high as 65 wt%. However, although the addition of nano-clays

and Bioglass® have been demonstrated to result in composites with simultaneously higher stiffness and degree of elasticity, still high contents of filler (10-20 wt%) are necessary to achieve a Young´s modulus close to 2 MPa.[285, 288, 289] Moreover in the case of PGS/Bioglass® nanocomposites a sudden drop in Young´s modulus after one day of immersion in tissue culture medium occurred, almost getting back to the strength level of neat PGS material. Thus, the main advantage of these nanocomposite systems lies in the improvement of biocompatibility but not in the enhancement of mechanical compliance for neat matrix. In comparison, the incorporation of halloysite nanotubes into PGS matrices allowed to more stable mechanical properties during incubation in tissue culture media.

4.2.1. CELLULOSE NANOCRYSTALS AS POTENTIAL FILLER FOR BIODEGRADABLE ELASTOMERIC MATRICES

As previously mentioned, biocompatible and bio-inert nanofillers such as hydroxyapatite, Bioglass®, nanoclays or other minerals have been used as potential reinforcing units for biodegradable elastomeric matrices. However, in the last decade, the cellulose components derived from plants such as cellulose whiskers and micro-fibrillated cellulose are emerging as promising fillers to improve thermal, mechanical and shape-memory properties of elastomeric biodegradable matrices. Recently, many efforts have been focused on the development of nanocomposite materials based on cellulose and its derivatives due to their, renewable nature, biodegradable character under certain conditions, abundance and low toxicity.[291, 292] Among the large varieties of cellulosic fibers, the cellulose nanocrystals (CNCs)[293-296] isolated from a diversity of renewable sources such as plants (e.g. wood or cotton) and bacterial or animal tissue sources (e.g. tunicates), have received considerable attention as reinforcement filler for low-modulus elastomeric matrices because of their high stiffness (Elastic modulus 143 GPa) and high aspect ratio (diameters from 5 to 50 nm, and lengths from 100 to 3000 nm depending on the source).[297-299] In this regard, has been reported a superior specific properties for cellulose-reinforced nanocomposites (specific Young´s Modulus ~100

GPa·cm^3/g)[291, 300] compared with nanoclays (specific Young´s Modulus ~55 GPa·cm^3/g)[301, 302] or Bioglass® (specific Young´s Modulus ~13 GPa·cm^3/g).[301-304]

The cellulose nanocrystals have been extensively used as reinforcement filler for mainly polyurethane based materials. In this regard, the addition of very low amount of CNCs (1 wt%) in elastomeric PU matrices revealed a remarkable improvement in mechanical properties (eight fold) and strain at break well above the improvements obtained for others inorganic fillers such as nano-clays or carbon nanotubes. These improvements were associated with the morphology of the CNCs as well as with the molecular interactions (hydrogen bonding or covalently interactions) between the filler and the polymeric chains.[305]

In this regard, the presence of abundant hydroxyl groups on the CNC surface have been demonstrate to be an advantage in order to promote the affinity between filler and polymeric matrices that contains polar groups or high hydroxyl functionality such as PLA, PEG or PU.[296, 306-305] The efficient interaction between matrix and filler through hydrogen bonding or chemical interactions, not only could be advantageous to remarkably improve the mechanical properties, but also to enhance the shape-memory performance directly related to recovery speed, recovery stress and recovery strain.

In addition, many reviews have been published focusing on shape memory PU/CNC reinforced materials with increased mechanical properties for low filler ratios, retaining the shape memory properties of the matrix or improving them[65, 307] and also combining thermally induced shape memory effect with water induced shape memory recovery through the disruption of hydrogen bonding percolation network of the fillers.[293, 308-310] Polyurethane-based nanocomposites filled with cellulose were studied by Navarro-Baena et al. and higher shape fixity ratios than the neat matrix were achieved. Also, the shape recovery ratio for all the nanocomposites was kept with switching temperatures close to the human body (35°C).[65]

As was discussed before, low mechanical strength and low mechanical output (recovery stresses) is still a challenge for soft biodegradable shape-memory polymeric matrices such as the PPS family. However, to our knowledge, there are very few reports on soft shape-memory polymers filled with CNCs that differ from polyurethane based.

Taking into account all the above mentioned properties for CNCs, it is expected that this filler can significantly improve the mechanical strength and shape-memory parameters of the biodegradable elastomeric matrix under study in the present PhD dissertation.

4.2.2. NANOFIBERS AS POTENTIAL FILLER FOR BIODEGRADABLE ELASTOMERIC MATRICES

Polymer nanofibers have been attractive materials for a wide range of applications thanks to their high aspect ratio (l/d), large surface area to volume ratio (until 10^3 times of micro-sized fiber), lightweight, flexibility and surface morphology, features that confers them unique geometry and properties. Polymeric nanofibers can be processed by a number of techniques such as drawing, template synthesis, phase separation, self-assembly and electrospinning.[311-314] Compared to the other techniques, electrospinning combine the ability to produce the thinner diameters, with the less complexity as well as the possibility to be used for a wide range of materials. Thus, among all the possible technologies from production of nanofibers, electrospinning is the most prominent, simplest, versatile and effective method for producing nanofibers with ultrafine diameters.

Nanofibers obtained by electrospinning, have found main applications on bioengineering. Although electrospun nanofibers have demonstrate even better mechanical properties than microfibers of same materials, they have been rarely used as fillers into polymeric matrices.[195, 196, 219] These few reported works demonstrate the possibility to achieve responsive materials using electrospun mats as fillers of soft and stiff matrices. Main advantage of use nanofibers as filler of

SMPCs respect other systems, is that provides much larger degree of design flexibility, since one can separately choose and modify the two functional components (matrix and fibers) to achieve optimum control of properties. In addition, this concept can be widely applicable to a large number of materials.

SMPU electrospun nonwoven nanofiber mats, compared to similar bulk polymers, have been found to exhibit better SME combined with higher tensile strength and tensile modulus.[315, 316]

First examples of nanocomposite materials containing electrospun nanofiber mats were based on nylon-4,6 and poly(benzimidazole) (PBI) mats into epoxide and rubber matrices.[317, 318] Epoxy was toughened by the PBI nanofibers (15% wt) with higher reinforcing effect than that obtained by using PBI fibroids (whisker like particles). Also, rubber matrix Young´s modulus was 10 times higher than unfilled rubber with the addition of PBI nanofibers.[318] Matrices of poly(vinil alcohol) (PVA) have been reinforced with electrospun cellulose acetate nanofiber mats obtaining an increase in mechanical strength by 50% and Young´s modulus by more than 600% for mass contents of nanofibers >10%.[319] Thus, nanocomposites reinforced with electrospun mats have been reported mainly for high-strength nanocomposites[317] or fuel membranes.[320]

Although there are reported works about how to obtain polymer nanofibers with shape memory properties by electrospinning,[315, 321, 322] very few of these works are based on the use of biodegradable polymers, and according to our knowledge, there are not any studies as reinforcing filler in SMPCs. [104] Recently is possible to find in the literature a couple of stimuli responsive polymer composites fabricated with electrospun mats as fillers of non-degradable matrices. Shape-memory was demonstrated for poly(ε-caprolactone)-reinforced silicon rubber (Sylgard 184)[104] with three different transitions; glass transition of silicon (T_g=-114.4 °C), glass transition of PCL mat (T_g=-49.5 °C) and melting transition of PCL mat (T_m=60.6 °C).

Shape-memory was achieved through melting the semicrystalline PCL nanofibers at 60 °C with almost completely shape fixity and recovery ratios (~100%). Another approach to obtain stimuli-responsive nanocomposites with electrical actuation capability has been developed by incorporation of carbon nanofibers electrospun mats into an epoxy matrix with enhancement of recovery stress by raising the rubbery modulus above T_g.[323] Using the same approach of electrospun PCL mat, triple-shape functionality can be achieved by selecting a higher T_g (15-33 °C) based SMP epoxy as a matrix. This allows introducing one more thermal transition, in addition to T_m of PCL, that can be used to fix a second temporary shape.[324] Despite of the good results obtained, to the best of our knowledge, although multitude of nanofibers with shape memory effect have been processed by electrospinning,[325] no more investigations have been published about thermally induced shape memory effect over composites involving nanofibers as a filler of soft biodegradable or non-biodegradable matrices.

With this background, we propose the use of PLA nanofibers obtained through electrospinning to improve shape-memory characteristics of a poly(mannitol-sebacate) matrix with T_g as switching temperature. Eventually, in this system proposed, both components (filler and matrix) have been reported to be biodegradable under physiological conditions that make them potentially useful for long term and high strength biomedical applications.

Moreover, the electrospinning method allows the introduction of components inside the fibers to increase the mechanical properties of the mats, as well as to generate new biological functionalities. Electrospun nanofibers have demonstrated to be promising as drug carriers for controlled delivery systems.[237, 253, 326] In this regard, nano-sized Ag nanoparticles have been incorporated into electrospun mats to achieve antimicrobial nano-filter applications[327] and hydroxyapatite nanoparticles have been potentially used in electrospun scaffolds to promote bone adhesion and regeneration.[252, 328]

5. REFERENCES IN THIS CHAPTER

1. P. T. Mather, *Nature Materials,* 2007, **6**, 93-94.
2. D. Ratna and J. Karger-Kocsis, *Journal of Materials Science,* 2008, **43**, 254-269.
3. M. Behl and A. Lendlein, *Journal of Materials Chemistry,* 2010, **20**, 3332-3334.
4. C. Liu, H. Qin and P. T. Mather, *Journal of Materials Chemistry,* 2007, **17**, 1543-1558.
5. M. Behl and A. Lendlein, *Materials Today,* 2007, **10**, 20-28.
6. A. Lendlein and S. Kelch, *Angewandte Chemie-International Edition,* 2002, **41**, 2034-2057.
7. M. Behl and A. Lendlein, *Journal of Materials Chemistry,* 2010, **20**, 3335-3345.
8. H. Meng, H. Mohamadian, M. Stubblefield, D. Jerro, S. Ibekwe, S. Pang and G. Li, *Smart Materials and Structures,* 2013, **22**, 093001.
9. W. J. Buehler, J. V. Gilfrich and R. C. Wiley, *Journal of Applied Physics,* 1963, **34**, 1475-1477.
10. K. Otsuka and C. M. Wayman, *Shape-Memory Materials*, ed. K. Otsuka and C.M. Wayman, Cambridge University Press, Cambridge, 1998, pp. 27-48.
11. Z. G. Wei, R. Sandstrom and S. Miyazaki, *Journal of Materials Science,* 1998, **33**, 3763-3783.
12. B. K. Kim, S. Y. Lee and M. Xu, *Polymer,* 1996, **37**, 5781-5793.
13. J. Leng, H. Lu, Y. Liu, W. M. Huang and S. Du, *MRS Bulletin,* 2009, **34**, 848-855.
14. V. Srivastava, S. A. Chester and L. Anand, *Journal of the Mechanics and Physics of Solids,* 2010, **58**, 1100-1124.
15. J. Xu and J. Song, *Biomedical engineering Frontiers and Challenges*, ed. R. Fazel-Rezai, Intech Scientific Publishers, 2011, pp. 125-142.
16. J. Hu and S. Chen, *Journal of Materials Chemistry,* 2010, **20**, 3346-3355.
17. M. Behl, J. Zotzmann and A. Lendlein, *Shape-Memory Polymers*, ed. A. Lendlein, Springer-Verlag, Berlin, 2010, pp. 1-40.

18. J. Hu, *Advances in Shape-Memory Polymers*, ed. J. Hu, Woodhead Publishing, Cambridge, 2013, pp. 1-22.
19. T. Takahashi, N. Hayashi and S. Hayashi, *Journal of Applied Polymer Science,* 1996, **60**, 1061-1069.
20. I. A. Rousseau, *Polymer Engineering & Science,* 2008, **48**, 2075-2089.
21. W. Wagermaier, K. Kratz, M. Heuchel and A. Lendlein, *Advances in Polymer Science,* 2010, **226**, 97-145.
22. A. Lendlein, A. M. Schmidt, M. Schroeter and R. Langer, *Journal of Polymer Science Part A: Polymer Chemistry,* 2005, **43**, 1369-1381.
23. A. Alteheld, Y. K. Feng, S. Kelch and A. Lendlein, *Angewandte Chemie-International Edition,* 2005, **44**, 1188-1192.
24. N. Choi and A. Lendlein, Soft Matter,**3**, 901-909.
25. S. Zhang, Y. Feng, L. Zhang, J. Sun, X. Xu and Y. Xu, *Journal of Polymer Science Part A: Polymer Chemistry,* 2007, **45**, 768-775.
26. A. Lendlein, J. Zotzmann, Y. Feng, A. Alteheld and S. Kelch, *Biomacromolecules,* 2009, **10**, 975-982.
27. S. Chen, J. Hu, Y. Liu, H. Liem, Y. Zhu and Q. Meng, *Polymer International,* 2007, **56**, 1128-1134.
28. H. Jeong, S. Lee and B. Kim, *Journal of Materials Science,* 2000, **35**, 1579-1583.
29. T. Chung, A. Romo-Uribe and P. T. Mather, *Macromolecules,* 2008, **41**, 184-192.
30. P. Ping, W. Wang, X. Chen and X. Jing, *Biomacromolecules,* 2005, **6**, 587-592.
31. B. S. Lee, B. C. Chun, Y. Chung, K. I. Sul and J. W. Cho, *Macromolecules,* 2001, **34**, 6431-6437.
32. S. Neuss, I. Blomenkamp, R. Stainforth, D. Boltersdorf, M. Jansen, N. Butz, A. Perez-Bouza and R. Knüchel, *Biomaterials,* 2009, **30**, 1697-1705.
33. X. Luo, X. Zhang, M. Wang, D. Ma, M. Xu and F. Li, *Journal of Applied Polymer Science,* 1997, **64**, 2433-2440.

34. M. Wang, X. Luo, X. Zhang and D. Ma, *Polymers for Advanced Technologies,* 1997, **8**, 136-139.
35. M. Wang and L. Zhang, *Journal of Polymer Science Part B: Polymer Physics,* 1999, **37**, 101-112.
36. K. Kim, Y. Akada, W. Kai, B. Kim and I. Kim, *Journal of Biomaterials and Nanobiotechnology,* 2011, **2**, 353-360.
37. F. Li, J. Hou, W. Zhu, X. Zhang, M. Xu, X. Luo, D. Ma and B. K. Kim, *Journal of Applied Polymer Science,* 1996, **62**, 631-638.
38. Z. Ma, W. Zhao, Y. Liu and J. Shi, *Journal of Applied Polymer Science,* 1997, **63**, 1511-1515.
39. I. Rousseau and P. Mather, *Journal of the American Chemical Society,* 2003, **125**, 15300-15301.
40. K. A. Burke and P. T. Mather, *Journal of Materials Chemistry,* 2010, **20**, 3449-3457.
41. G. Zhu, G. Liang, Q. Xu and Q. Yu, *Journal of Applied Polymer Science,* 2003, **90**, 1589-1595.
42. G. M. Zhu, S. G. Xu, J. H. Wang and L. B. Zhang, *Radiation Physics and Chemistry,* 2006, **75**, 443-448.
43. F. Li, W. Zhu, X. Zhang, C. Zhao and M. Xu, *Journal of Applied Polymer Science,* 1999, **71**, 1063-1070.
44. C. D. Liu, S. B. Chun, P. T. Mather, L. Zheng, E. H. Haley and E. B. Coughlin, *Macromolecules,* 2002, **35**, 9868-9874.
45. Y. Kagami, J. P. Gong and Y. Osada, *Macromolecular Rapid Communications,* 1996, **17**, 539-543.
46. E. J. Goethals, W. Reyntjens and S. Lievens, *Macromolecular Symposia,* 1998, **132**, 57-64.
47. W. G. Reyntjens, F. E. Du Prez and E. J. Goethals, *Macromolecular Rapid Communications,* 1999, **20**, 251-255.

48. N. J. Entwistle and E. R. Peterson, *International Journal of Educational Research,* 2004, **41**, 407-428.
49. S. Lee, J. Kim and B. Kim, *Smart Materials and Structures,* 2004, **13**, 1345-1350.
50. E. Wornyo, K. Gall, F. Yang and W. King, *Polymer,* 2007, **48**, 3213-3225.
51. S. Kelch, S. Steuer, A. M. Schmidt and A. Lendlein, *Biomacromolecules,* 2007, **8**, 1018-1027.
52. K. M. Lee, P. T. Knight, T. Chung and P. T. Mather, *Macromolecules,* 2008, **41**, 4730-4738.
53. I. Bellin, S. Kelch and A. Lendlein, *Journal of Materials Chemistry,* 2007, **17**, 2885-2891.
54. M. Behl, I. Bellin, S. Kelch, W. Wagermaier and A. Lendlein, *Advanced Functional Materials,* 2009, **19**, 102-108.
55. A. Lendlein, A. M. Schmidt and R. Langer, *Proceedings of the National Academy of Sciences U.S.A.,* 2001, **98**, 842-847.
56. M. Nagata and I. Kitazima, *Colloid & Polymer Science,* 2006, **284**, 380-386.
57. N. Choi, S. Kelch and A. Lendlein, *Advanced Engineering Materials,* 2006, **8**, 439-445.
58. R. A. Weiss, E. Izzo and S. Mandelbaum, *Macromolecules,* 2008, **41**, 2978-2980.
59. Y. Wu, J. Hu, J. Han, Y. Zhu, H. Huang, J. Li and B. Tang, *Journal of Materials Chemistry A,* 2014, **2**, 18816-18822.
60. R. Mohr, K. Kratz, T. Weigel, M. Lucka-Gabor, M. Moneke and A. Lendlein, *Proceedings of the National Academy of Sciences U.S.A.,* 2006, **103**, 3540-3545.
61. C. C. Min, W. J. Cui, J. Z. Bei and S. G. Wang, *Polymers for Advanced Technologies,* 2005, **16**, 608-615.
62. H. Jeon, P. Mather and T. Haddad, *Polymer International,* 2000, **49**, 453-457.

63. D. Pérez-Foullerat, S. Hild, A. Mücke and B. Rieger, *Macromolecular Chemistry and Physics,* 2004, **205**, 374-382.
64. B. C. Chun, T. K. Cho and Y. Chung, *European Polymer Journal,* 2006, **42**, 3367-3373.
65. I. Navarro-Baena, J. M. Kenny and L. Peponi, *Cellulose,* 2014, **21**, 4231-4246.
66. A. Saralegi, S. C. M. Fernandes, A. Alonso-Varona, T. Palomares, E. J. Foster, C. Weder, A. Eceiza and M. A. Corcuera, *Biomacromolecules,* 2013, **14**, 4475-4482.
67. Y. Feng, M. Behl, S. Kelch and A. Lendlein, *Macromolecular Bioscience,* 2009, **9**, 45-54.
68. H. M. Jeong, B. K. Kim and Y. J. Choi, *Polymer,* 2000, **41**, 1849-1855.
69. S. Xu and M. Zhang, *Journal of Applied Polymer Science,* 2007, **104**, 3818-3826.
70. M. Behl, U. Ridder, Y. Feng, S. Kelch and A. Lendlein, *Soft Matter,* 2009, **5**, 676-684.
71. M. Behl, U. Ridder, W. Wagermaier, S. Kelch and A. Lendlein, *Active Polymers,* 2009, **1190**, 25-30.
72. H. M. Jeong, B. K. Ahn and B. K. Kim, *European Polymer Journal,* 2001, **37**, 2245-2252.
73. D. Mantovani, *JOM,* 2000, **52**, 36-44.
74. L. G. A. S. Machado M.A., *Brazilian Journal of Medical and Biological Research,* 2003, **36**, 683.
75. C. M. Yakacki and K. Gall, *Shape-Memory Polymers*, ed. A. Lendlein, Springer-Verlag, Berlin, 2010, pp.147-175.
76. R. Langer and D. A. Tirrell, *Nature,* 2004, **428**, 487-492.
77. J. M. Hampikian, B. C. Heaton, F. C. Tong, Z. Zhang and C. P. Wong, *Materials Science and Engineering: C,* 2006, **26**, 1373-1379.
78. H. M. Wache, D. J. Tartakowska, A. Hentrich and M. H. Wagner, *Journal of Materials Science: Materials in Medicine,* 2003, **14**, 109-112.

79. K. Gall, C. M. Yakacki, Y. Liu, R. Shandas, N. Willett and K. S. Anseth, *Journal of Biomedical Materials Research Part A,* 2005, **73A**, 339-348.
80. C. M. Yakacki, R. Shandas, C. Lanning, B. Rech, A. Eckstein and K. Gall, *Biomaterials,* 2007, **28**, 2255-2263.
81. D. Rickert, A. Lendlein, A. M. Schmidt, S. Kelch, W. Roehlke, R. Fuhrmann and R. P. Franke, *Journal of Biomedical Materials Research Part B: Applied Biomaterials,* 2003, **67B**, 722-731.
82. D. J. Maitland, M. F. Metzger, D. Schumann, A. Lee and T. S. Wilson, *Lasers in Surgery and Medicine,* 2002, **30**, 1-11.
83. G. Baer, W. Small, T. Wilson, W. Benett, D. Matthews, J. Hartman and D. Maitland, *Biomedical Engineering Online,* 2007, **6**, 43.
84. M. Metzger, T. Wilson, D. Schumann, D. Matthews and D. Maitland, *Biomedical Microdevices,* 2002, **4**, 89-96.
85. A. Lendlein and R. Langer, S*elf-expanding device for the gastrointestinal or urogenital area,* Patent 2004.
86. D. Marco, Biodegradable s*elf-inflating intragastric implants and method of curbing appetite by the same*, Patent 2008.
87. A. Nakasima, H. J. FAU, M. F. Ichinose and H. Shimada, *European Journal of Orthodontics,* 1991, **13**, 179-86.
88. M. Bettuchi and R. Heinrich, *Novel surgical fastener*, Patent 2009.
89. C. M. Yakacki, R. Shandas, D. Safranski, A. M. Ortega, K. Sassaman and K. Gall, *Advanced Functional Materials,* 2008, **18**, 2428-2435.
90. J. A. Teague, *Light responsive medical retrieval devices*, Patent 2008.
91. K. Gall, M. Lyons, D. P. Nair, R. Shandas and C. M. Yakacki, *Shape memory polymer-based transcervical device for permanent or temporary sterilization*, Patent 2008.
92. A. Díaz Lantada, P. Lafont, I. Rada, A. Jiménez, J. Hernández, H. Lorenzo-Yustos and J. Muñoz-García, *Biomedical Engineering Systems and Technologies,* ed. A. Fred, J. Filipe and H. Gamboa, Springer-Verlag*,* Berlin, 2009, pp. 59-72.

93. A. Lendlein and R. Langer, *Science and Technology of Advanced Materials,* 2002, **296**, 1673-1676.
94. A. T. Neffe, B. D. Hanh, S. Steuer and A. Lendlein, *Advanced Materials,* 2009, **21**, 3394-3398.
95. C. Wischke, A. T. Neffe, S. Steuer and A. Lendlein, *Journal of controlled Release*, 2009, **138**, 243-250.
96. K. Nagahama, Y. Ueda, T. Ouchi and Y. Ohya, *Biomacromolecules,* 2009, **10**, 1789-1794.
97. J. Karger-Kocsis and S. Keki, *Express polymer Letters,* 2014, **8**, 397-412.
98. K. Ishida, R. Hortensius, X. Luo and P. T. Mather, *Journal of Polymer Science Part B: Polymer Physics,* 2012, **50**, 387-393.
99. J. Li, J. A. Viveros, M. H. Wrue and M. Anthamatten, *Advanced Materials,* 2007, **19**, 2851-2855.
100. M. C. Serrano, L. Carbajal and G. A. Ameer, *Advanced Materials,* 2011, **23**, 2211-2855.
101. S. Dey, D. M. Agra-Kooijman, W. Ren, P. J. McMullan, A. C. Griffin and S. Kumar, *Crystals,* 2013, **3**, 363-390.
102. S. Chen, J. Hu, H. Zhuo and Y. Zhu, *Materials Letters,* 2008, **62**, 4088-4090.
103. H. Zhang, H. Wang, W. Zhong and Q. Du, *Polymer,* 2009, **50**, 1596-1601.
104. X. Luo and P. T. Mather, *Macromolecules,* 2009, **42**, 7251-7253.
105. L. S. Nair and C. T. Laurencin, *Progress in Polymer Science,* 2007, **32**, 762-798.
106. L. E. Freed, G. C. Engelmayr, J. T. Borenstein, F. T. Moutos and F. Guilak, *Advanced Materials,* 2009, **21**, 3410-3418.
107. J. P. Bruggeman, B. de Bruin, C. J. Bettinger and R. Langer, *Biomaterials,* 2008, **29**, 4726-4735.
108. Y. Li, G. A. Thouas and Q. Chen, *RSC Advances*, 2012, **2**, 8229-8242.
109. Y. Wang, G. Ameer, B. Sheppard and R. Langer, *Nature Biotechnology,* 2002, **20**, 602-606.
110. J. Yang, A. Webb and G. Ameer, *Advanced Materials*, 2004, **16**, 511-516.

111. J. Yang, A. Webb, S. Pickerill, G. Hageman and G. Ameer, *Biomaterials,* 2006, **27**, 1889-1898.
112. C. Sundback, J. Shyu, Y. Wang, W. Faquin, R. Langer, J. Vacanti and T. Hadlock, *Biomaterials,* 2005, **26**, 5454-5464.
113. J. B. Allen, S. Khan, K. A. Lapidos and G. A. Ameer, *Stem Cells,* 2010, **28**, 318-328.
114. Z. Sun, C. Chen, M. Sun, C. Ai, X. Lu, Y. Zheng, B. Yang and D. Dong, *Biomaterials,* 2009, **30**, 5209-5214.
115. A. Mahdavi, L. Ferreira, C. Sundback, J. W. Nichol, E. P. Chan, D. J. D. Carter, C. J. Bettinger, S. Patanavanich, L. Chignozha, E. Ben-Joseph, A. Galakatos, H. Pryor, I. Pomerantseva, P. T. Masiakos, W. Faquin, A. Zumbuehl, S. Hong, J. Borenstein, J. Vacanti, R. Langer and J. M. Karp, *Proceedings of the National Academy of Sciences U.S.A.,* 2008, **105**, 2307-2312.
116. D. G. Barrett and M. N. Yousaf, *Molecules,* 2009, **14**, 4022-4050.
117. Y. Kang, J. Yang, S. Khan, L. Anissian and G. Ameer, *Journal of Biomedical Materials Research Part A,* 2006, **77A**, 331-339.
118. A. K. Sharma, P. V. Hota, D. J. Matoka, N. J. Fuller, D. Jandali, H. Thaker, G. A. Ameer and E. Y. Cheng, *Biomaterials,* 2010, **31**, 6207-6217.
119. D. Motlagh, J. Yang, K. Lui, A. Webb and G. Ameer, *Biomaterials,* 2006, **27**, 4315-4324.
120. X. Zhang, H. Tang, R. Hoshi, L. De Laporte, H. Qiu, X. Xu, L. D. Shea and G. A. Ameer, *Biomaterials,* 2009, **30**, 2632-2641.
121. C. J. Bettinger, *Macromolecular Bioscience,* 2011, **11**, 467-482.
122. Q. Chen, S. Liang and G. A. Thouas, *Progress in Polymer Science,* 2013, **38**, 584-671.
123. S. Hiki, M. Miyamoto and Y. Kimura, *Polymer,* 2000, **41**, 7369-7379.
124. J. P. Santerre, K. Woodhouse, G. Laroche and R. S. Labow, *Biomaterials,* 2005, **26**, 7457-7470.

125. M. Borkenhagen, R. C. Stoll, P. Neuenschwander, U. W. Suter and P. Aebischer, *Biomaterials,* 1998, **19**, 2155-2165.
126. K. L. Fujimoto, K. Tobita, W. D. Merryman, J. Guan, N. Momoi, D. B. Stolz, M. S. Sacks, B. B. Keller and W. R. Wagner,*Journal of the American College of Cardiology,* 2007, **49**, 2292-2300.
127. T. C. McDevitt, K. A. Woodhouse, S. D. Hauschka, C. E. Murry and P. S. Stayton, *Journal of Biomedical Materials Research Part A,* 2003, **66A**, 586-595.
128. C. Alperin, P. W. Zandstra and K. A. Woodhouse, *Biomaterials,* 2005, **26**, 7377-7386.
129. J. Y. Cherng, T. Y. Hou, M. F. Shih, H. Talsma and W. E. Hennink, *International Journal of Pharmaceutics,* 2013, **450**, 145-162.
130. P. Bruin, G. J. Veenstra, A. J. Nijenhuis and A. J. Pennings, *Makromolekulare Chemie-Rapid Communications,* 1988, **9**, 589-594.
131. D. P. Martin and S. F. Williams, *Biochemical Engineering Journal,* 2003, **16**, 97-105.
132. K. L. Fujimoto, J. Guan, H. Oshima, T. Sakai and W. R. Wagner, *The Annals of Thoracic Surgery,* 2007, **83**, 648-654.
133. Y. Hong, J. Guan, K. L. Fujimoto, R. Hashizume, A. L. Pelinescu and W. R. Wagner, *Biomaterials,* 2010, **31**, 4249-4258.
134. A. E. Hafeman, K. J. Zienkiewicz, A. L. Zachman, H. Sung, L. B. Nanney, J. M. Davidson and S. A. Guelcher, *Biomaterials,* 2011, **32**, 419-429.
135. U. A. Stock, T. Sakamoto, S. Hatsuoka, D. P. Martin, M. Nagashima, A. M. Moran, M. A. Moses, P. N. Khalil, F. J. Schoen, J. P. Vacanti and J. E. Mayer Jr, *The Journal of Thoracic and Cardiovascular Surgery,* 2000, **120**, 1158-1167.
136. B. Saad, T. D. Hirt, M. Welti, G. K. Uhlschmid, P. Neuenschwander and U. W. Suter, *Journal of Biomedical Materials Research ,* 1997, **36**, 65-74.
137. E. Liljensten, K. GisselfÃ¤lt, B. Edberg, H. Bertilsson, P. Flodin, A. Nilsson, A. Lindahl and L. Peterson, *Journal of Materials Science: Materials in Medicine,* 2002, **13**, 351-359.

138. V. Chiono, S. Sartori, A. Rechichi, C. Tonda-Turo, G. Vozzi, F. Vozzi, M. D'Acunto, C. Salvadori, F. Dini, G. Barsotti, F. Carlucci, S. Burchielli, S. Nicolino, C. Audisio, I. Perroteau, P. Giusti and G. Ciardelli, *Macromolecular Bioscience,* 2011, **11**, 245-256.
139. L. A. Pfister, M. Papaloïzos, H. P. Merkle and B. Gander, *Journal of the Peripheral Nervous System,* 2007, **12**, 65-82.
140. G. Soldani, G. Varelli, A. Minnocci and P. Dario, *Biomaterials,* 1998, **19**, 1919-1924.
141. A. Hazari, M. Wiberg, G. Johansson-Rudén, C. Green and G. Terenghi, *British Journal of Plastic surgery,* 1999, **52**, 653-657.
142. C. Ljungberg, G. Johansson-Ruden, K. J. Boström, L. Novikov and M. Wiberg, *Microsurgery,* 1999, **19**, 259-264.
143. L. Soletti, A. Nieponice, Y. Hong, S. Ye, J. J. Stankus, W. R. Wagner and D. A. Vorp, *Journal of Biomedical Materials Research Part A,* 2011, **96A**, 436-448.
144. C. Schlickewei, S. Verrier, S. Lippross, S. Pearce, M. Alini and S. Gogolewski, *Macromolecular Symposia,* 2007, **253**, 162-171.
145. C. M. Hill, Y. H. An, Q. K. Kang, L. A. Hartsock, S. Gogolewski and K. Gorna, *Macromolecular Symposia,* 2007, **253**, 94-97.
146. S. Gogolewski and K. Gorna, *Journal of Biomedical Materials Research Part A,* 2007, **80A**, 94-101.
147. S. Gogolewski, K. Gorna and A. S. Turner, *Journal of Biomedical Materials Research Part A,* 2006, **77A**, 802-810.
148. N. Galego, C. Rozsa, R. Sánchez, J. Fung, Analía Vázquez and J. Santo Tomás, *Polymer Testing,* 2000, **19**, 485-492.
149. D. Eglin, S. Grad, S. Gogolewski and M. Alini, *Journal of Biomedical Materials Research Part A,* 2010, **92A**, 393-408.
150. J. Klompmaker, R. P. H. Veth, H. W. B. Jansen, H. K. L. Nielsen, J. H. de Groot, A. J. Pennings and R. Kuijer, *Biomaterials,* 1996, **17**, 1685-1691.

151. J. Klompmaker, R. P. H. Veth, H. W. B. Jansen, H. K. L. Nielsen, J. H. De Groot and A. J. Pennings, *Biomaterials,* 1996, **17**, 1169-1175.
152. J. H. de Groot, R. de Vrijer, A. J. Pennings, J. Klompmaker, R. P. H. Veth and H. W. B. Jansen, *Biomaterials,* 1996, **17**, 163-173.
153. O. Jeon, S. Lee, S. H. Kim, Y. M. Lee and Y. H. Kim, *Macromolecules,* 2003, **36**, 5585-5592.
154. D. Cohn and A. Hotovely Salomon, *Biomaterials,* 2005, **26**, 2297-2305.
155. L. Wang, Z. Zhang, H. Chen, S. Zhang and C. Xiong, *Journal of Polymer Research,* 2010, **17**, 77-82.
156. B. L. Seal, T. C. Otero and A. Panitch, *Materials Science and Engineering: R: Reports,* 2001, **34**, 147-230.
157. G. Matsumura, S. Miyagawa-Tomita, T. Shin'oka, Y. Ikada and H. Kurosawa, *Circulation,* 2003, **108**, 1729-1734.
158. G. Matsumura, N. Hibino, Y. Ikada, H. Kurosawa and T. Shin'oka, *Biomaterials,* 2003, **24**, 2303-2308.
159. S. Lee, B. Kim, S. H. Kim, S. W. Choi, S. I. Jeong, I. K. Kwon, S. W. Kang, J. Nikolovski, D. J. Mooney, Y. Han and Y. H. Kim, *Journal of Biomedical Materials Research Part A,* 2003, **66A**, 29-37.
160. A. Metcalfe, A. Desfaits, I. Salazkin, L. Yahia, W. M. Sokolowski and J. Raymond, *Biomaterials,* 2003, **24**, 491-497.
161. L. Xue, S. Dai and Z. Li, *Macromolecules,* 2009, **42**, 964-972.
162. C. Min, W. Cui, J. Bei and S. Wang, *Polymers for Advanced Technologies,* 2007, **18**, 299-305.
163. E. Zini, M. Scandola, P. Dobrzynski, J. Kasperczyk and M. Bero, *Biomacromolecules,* 2007, **8**, 3661-3667.
164. C. Bettinger, E. Weinberg, K. Kulig, J. Vacanti, Y. Wang, J. Borenstein and R. Langer, *Advanced Materials,* 2006, **18**, 165-169.
165. J. P. Bruggeman, C. J. Bettinger, C. L. E. Nijst, D. S. Kohane and R. Langer, *Advanced Materials,* 2008, **20**, 1922-1927.

166. G. C. Engelmayr , M. Cheng, C. J. Bettinger, J. T. Borenstein, R. Langer and L. E. Freed, *Nature Materials,* 2008, **7**, 1003-1010.
167. C. J. Bettinger, B. Orrick, A. Misra, R. Langer and J. T. Borenstein, *Biomaterials,* 2006, **27**, 2558-2565.
168. M. Okada, *Progress in Polymer Science,* 2002, **27**, 87-133.
169. T. Kiyotsukuri, M. Kanaboshi and N. Tsutsumi, *Polymer International,* 1994, **33**.
170. T. Ding, Q. Liu, R. Shi, M. Tian, J. Yang and L. Zhang, *Polymer Degradation and Stability,* 2006, **91**, 733-739.
171. M. Nagata, T. Machida, W. Sakai and N. Tsutsumi, *Journal of Polymer Science Part A: Polymer Chemistry,* 1999, **37**, 2005-2011.
172. Y. Wang, Y. Kim and R. Langer, *Journal of Biomedical Materials Research Part A,* 2003, **66A**, 192-197.
173. I. Pomerantseva, N. Krebs, A. Hart, C. M. Neville, A. Y. Huang and C. A. Sundback, *Journal of Biomedical Materials Research Part A,* 2009, **91A**, 1038-1047.
174. Q. Chen, X. Yang and Y. Li, *RSC Advances,* 2012, **2**, 4125-4134.
175. C. L. E. Nijst, J. P. Bruggeman, J. M. Karp, L. Ferreira, A. Zumbuehl, C. J. Bettinger and R. Langer, *Biomacromolecules,* 2007, **8**, 3067-3073.
176. J. L. Ifkovits, P. R. FAU and J. A. Burdick, *Biomedical Materials*, 2008, **3**, 034104-034111.
177. W. Cai and L. Liu, *Materials Letters,* 2008, **62**, 2171-2173.
178. L. Liu and W. Cai, *Materials Letters,* 2009, **63**, 1656-1658.
179. F. Migneco, Y. Huang, R. K. Birla and S. J. Hollister, *Biomaterials,* 2009, **30**, 6479-6484.
180. B. Guo, Y. Chen, Y. Lei, L. Zhang, W. Y. Zhou, A. B. Rabie and J. Zhao, *Biomacromolecules,* 2011, **12**, 1312-1321.
181. Z. Spitalsky and T. Bleha, *Macromolecular Bioscience,* 2004, **4**, 601-609.
182. U. Rao, R. Kumar, S. Balaji and P. K. Sehgal, *Journal of Bioactive and Compatible Polymers,* 2010, **25**, 419-436.

183. W. S. Wang, P. Ping, X. S. Chen and X. B. Jing, *European Polymer Journal,* 2006, **42**, 1240-1249.
184. J. Yang, F. Liu, L. Yang and S. M. Li, *European Polymer Journal,* 2010, **46**, 783-791.
185. R. Storey and T. Hickey, *Polymer,* 1994, **35**, 830-838.
186. B. Amsden, *Soft Matter*,2007, **3**, 1335-1348.
187. J. Tams, F. Rozema, R. Bos, J. Roodenburg, P. Nikkels and A. Vermey, *IInternational Journal of Oral and Maxillofacial Surgery,* 1996, **25**, 20-24.
188. C. Martin, H. Winet and J. Y. Bao, *Biomaterials,* 1996, **17**, 2373-2380.
189. R. Suuronen, T. Pohjonen, J. Hietanen and C. Lindqvist, *Journal of Oral and Maxillofacial Surgery,* 1998, **56**, 604-614.
190. A. Lendlein, M. Behl and S. Kamlage, *NATO Science for Peace and Security Series A: Chemistry and Biology,* 2010, 131-156.
191. P. P. Quynh, S. Upma and G. M. Dr. Antonios, *Tissue Engineering,* 2006, **12**, 1197-1211.
192. A. Frenot and I. Chronakis, *Current Opinion in Colloid & Interface Science,* 2003, **8**, 64-75.
193. H. Liu and Y. Hsieh, *Journal of Polymer Science Part B: Polymer Physics,* 2002, **40**, 2119-2129.
194. H. S. Kim, K. Kim, H. J. Jin and I. Chin, *Macromolecular Symposia,* 2005, **224**, 145-154.
195. Z. M. Huang, Y. Z. Zhang, M. Kotaki and S. Ramakrishna, *Composites Science and Technology,* 2003, **63**, 2223-2253.
196. S. F. Fennessey and R. J. Farris, *Polymer,* 2004, **45**, 4217-4225.
197. B. Sundaray, V. Subramanian, T. Natarajan, R. Xiang, C. Chang and W. Fann, *Applied Physics Letters,* 2004, **84**, 1222-1224.
198. L. Huang, K. Nagapudi, R. P. Apkarian and E. L. Chaikof, *Journal of Biomaterials Science-Polymer Edition,* 2001, **12**, 979-993.

199. C. Zhang, X. Yuan, L. Wu, Y. Han and J. Sheng, *European Polymer Journal,* 2005, **41**, 423-432.
200. H. L. Jiang, D. F. Fang, B. S. Hsiao, B. Chu and W. L. Chen, *Biomacromolecules,* 2004, **5**, 326-333.
201. Z. Z. Zhao, J. Q. Li, X. Y. Yuan, X. Li, Y. Y. Zhang and J. Sheng, *Journal of Applied Polymer Science,* 2005, **97**, 466-474.
202. Z. Jun, H. Q. Hou, A. Schaper, J. H. Wendorff and A. Greiner, *E-Polymers,* 2003,**3**, 1-9.
203. W. Son, J. Youk, T. Lee and W. Park, *Polymer,* 2004, **45**, 2959-2966.
204. B. Kim, H. Park, S. Lee and W. Sigmund, *Materials Letters,* 2005, **59**, 829-832.
205. C. Buchko, L. Chen, Y. Shen and D. Martin, *Polymer,* 1999, **40**, 7397-7407.
206. V. Chen and P. Ma, *Biomaterials,* 2004, **25**, 2065-2073.
207. M. M. Demir, I. Yilgor, E. Yilgor and B. Erman, *Polymer,* 2002, **43**, 3303-3309.
208. A. K. Haghi and M. Akbari, *Physica Status Solidi A-Applications and Materials*, 2007, **204**, pp 1830-1834.
209. A. Koski, K. Yim and S. Shivkumar, *Materials Letters,* 2004, **58**, 493-497.
210. M. M. Hohman, M. Shin, G. Rutledge and M. P. Brenner, *Physics of Fluids,* 2001, **13**, 2221-2236.
211. C. Mit-uppatham, M. Nithitanakul and P. Supaphol, *Macromolecular Chemistry and Physics,* 2004, **205**, 2327-2338.
212. W. W. Zuo, M. F. Zhu, W. Yang, H. Yu, Y. M. Chen and Y. Zhang, *Polymer Engineering & Science,* 2005, **45**, 704-709.
213. C. S. Ki, D. H. Baek, K. D. Gang, K. H. Lee, I. C. Um and Y. H. Park, *Polymer,* 2005, **46**, 5094-5102.
214. X. Geng, O. Kwon and J. Jang, *Biomaterials,* 2005, **26**, 5427-5432.
215. T. J. Sill and H. A. von Recum, *Biomaterials,* 2008, **29**, 1989-2006.
216. D. Li and Y. N. Xia, *Nano Letters,* 2004, **4**, 933-938.
217. C. L. Casper, J. S. Stephens, N. G. Tassi, D. B. Chase and J. F. Rabolt, *Macromolecules,* 2004, **37**, 573-578.

218. Darrell H Reneker and,Iksoo Chun, *Nanotechnology,* 1996, **7**, 216-223.
219. I. S. Chronakis, *Journal of Materials Processing Technology,* 2005, **167**, 283-293.
220. X. Fang and D. H. Reneker, *Journal of Macromolecular Science, Part B,* 1997, **36**, 169-173.
221. E. D. Boland, G. E. Wnek, D. G. Simpson, K. J. Pawlowski and G. L. Bowlin, *Journal of Macromolecular Science, Part A,* 2001, **38**, 1231-1243.
222. E. D. Boland, T. T. FAU, S. D. FAU, W. G. FAU and G. L. Bowlin, *Journal of biomedical Materials Research Part B Applied Biomaterials*, 2004, **71B**, 144-152.
223. G. L. Bowlin, E. D. Boland and P. G. Espy, *Encyclopedia of Biomaterials and Biomedical Engineering*, ed. G. E. Wnek and G.L. Bowlin, Taylor & Francis, 2014, pp. 2828-2837.
224. M. Bognitzki, T. Frese, J. H. Wendorff and A. Greiner, *Abstracts of Papers of the American Chemical Society,* 2000, **219**, U491-U491.
225. J. Zeng, X. Chen, X. Xu, Q. Liang, X. Bian, L. Yang and X. Jing, *Journal of Applied Polymer Science,* 2003, **89**, 1085-1092.
226. Z. Jing, X. Xu, X. Chen, Q. Liang, X. Bian, L. Yang and X. Jing, *Journal of Controlled Release,* 2003, **92**, 227-231.
227. F. Yang, R. F. Murugan, S. F. Ramakrishna, X. F. Wang, M. Y. FAU and S. Wang, *Biomaterials*,2004, **25**, 1891-1900.
228. D. R. Nisbet, L.M. Lu, T. Zahir, J.S. Forsythe, and M. S. Shoichet, *Journal of Biomaterials Science Polymer Edition*, 2008, **19**, 623-634.
229. C. Hsu and S. Shivkumar, *Macromolecular Materials and Engineering,* 2004, **289**, 334-340.
230. C. Hsu and S. Shivkumar, *Journal of Materials Science,* 2004, **39**, 3003-3013.
231. K. Ohkawa, H. Kim and K. Lee, *Journal of Polymers and the Environment,* 2004, **12**, 211-218.
232. E. P. S. Tan, S. Y. Ng and C. T. Lim, *Biomaterials,* 2005, **26**, 1453-1456.

233. J. Kim and D. S. Lee, *Polymer Journal,* 2000, **32**, 616-618.
234. H. Yoshimoto, Y. M. Shin, H. Terai and J. P. Vacanti, *Biomaterials,* 2003, **24**, 2077-2082.
235. M. S. Khil, C. D. FAU, K. H. FAU, K. I. FAU and N. Bhattarai, *Journal of Biomedical Materials Research Part B*, 2003, **67**, 675-679.
236. S. R. Bhattarai, N. Bhattarai, H. K. Yi, P. H. Hwang, D. I. Cha and H. Y. Kim, *Biomaterials,* 2004, **25**, 2595-2602.
237. D. S. Katti, K. W. Robinson, F. K. Ko and C. T. Laurencin, *Journal of Biomedical Materials Research Part B: Applied Biomaterials,* 2004, **70B**, 286-296.
238. M. Shin, O. F. Ishii, T. Sueda and J. P. Vacanti, *Biomaterials*, 2004, 25, 3717-3723.
239. M. Shin, H. Yoshimoto and J. P. Vacanti, *Tissue Engineering,* 2004*,* **10**, 33-41.
240. X. M. Mo, C. Y. Xu, M. Kotaki and S. Ramakrishna, *Biomaterials,* 2004, **25**, 1883-1890.
241. C. Y. Xu, R. F. Inai, M. F. Kotaki and S. Ramakrishna, *Biomaterials*, 2004, **25**, 877-886.
242. B. Gupta, N. Revagade and J. Hilborn, *Progress in Polymer Science,* 2007, **32**, 455-482.
243. R.K. Kulkarni, K.C. Pani, C.C. Neuman, F.F. Leonard, *Archives of Surgery,* 1966, **93**, 839-843.
244. R. K. Kulkarni, E. G. Moore, A. F. Hegyeli and F. Leonard, *Journal of Biomedical Materials Research ,* 1971, **5**, 169-181.
245. B. Kalb and A. J. Pennings, *Polymer,* 1980, **21**, 607-612.
246. S. Hyon, K. Jamshidi and Y. Ikada, *Polymers as Biomaterials,* ed. S.W. Shalaby, A.S. Hoffmann, B.D. Ratner and T. A. Horbett, Plenum Press, New York, 1984, pp. 51-65.
247. B. Eling, S. Gogolewski and A. J. Pennings, *Polymer,* 1982, **23**, 1587-1593.
248. C. Migliaresi and L. Fambri, *Macromolecular Symposia,* 1997, **123**, 155-161.

249. X. H. Zong, H. Bien, C. Y. Chung, L. H. Yin, D. F. Fang, B. S. Hsiao, B. Chu and E. Entcheva, *Biomaterials,* 2005, **26**, 5330-5338.
250. F. Yang, R. Murugan, S. Wang and S. Ramakrishna, *Biomaterials,* 2005, **26**, 2603-2610.
251. C. M. Vaz, S. van Tuijl, C. V. C. Bouten and F. P. T. Baaijens, *Acta Biomaterialia,* 2005, **1**, 575-582.
252. H. Kim, H. Lee and J. C. Knowles, *Journal of Biomedical Materials Research Part A,* 2006, **79A**, 643-649.
253. E. Kenawy, G. L. Bowlin, K. Mansfield, J. Layman, D. G. Simpson, E. H. Sanders and G. E. Wnek, *Journal of Controlled Release,* 2002, **81**, 57-64.
254. X. L. Xu, L. X. Yang, X. Y. Xu, X. Wang, X. S. Chen, Q. Z. Liang, J. Zeng and X. B. Jing, *Journal of Controlled Release,* 2005, **108**, 33-42.
255. M. Song, C. Pan, J. Li, X. Wang and Z. Gu, *Electroanalysis,* 2006, **18**, 1995-2000.
256. X. Xu, Q. Yang, Y. Wang, H. Yu, X. Chen and X. Jing, *European Polymer Journal,* 2006, **42**, 2081-2087.
257. Y. Zhou and L. Lim, *Journal of Food Science,* 2009, **74**, C170-C176.
258. J. Leng, X. Lan, Y. Liu and S. Du, *Progress in Materials Science,* 2011, **56**, 1077-1135.
259. Y. Pan, T. Liu, J. Li, Z. Zheng, X. Ding and Y. Peng, *Journal of Polymer Science Part B: Polymer Physics,* 2011, **49**, 1241-1245.
260. M. Behl, M. Y. Razzaq and A. Lendlein, *Advanced Materials,* 2010, **22**, 3388-3410.
261. F. Li, L. Qi, J. Yang, M. Xu, X. Luo and D. Ma, *Journal of Applied Polymer Science,* 2000, **75**, 68-77.
262. T. Ohki, Q. Q. Ni, N. Ohsako and M. Iwamoto, *Composites Part A-Applied Science and Manufacturing,* 2004, **35**, 1065-1073.
263. X. Lan, Y. Liu, L.V. Haibao, X. Wang, J. Leng,S. Du, *Smart Materials and Structures,* 2009, **18**, 024002.

264. C. Liang, C. A. Rogers and E. Malafeew, *Journal of Intelligent Material Systems and Structures,* 1997, **8**, 380-386.
265. K. Gall, M. Mikulas, N. A. Munshi, F. Beavers and M. Tupper, *Journal of Intelligent Material Systems and Structures,* 2000, **11**, 877-886.
266. C. Zhang and Q. Ni, *Composite Structures,* 2007, **78**, 153-161.
267. Y. Liu, K. Gall, M. L. Dunn and P. McCluskey, *Mechanics of Materials,* 2004, **36**, 929-940.
268. K. Gall, M. L. Dunn, Y. Liu, D. Finch, M. Lake and N. A. Munshi, *Acta Materialia,* 2002, **50**, 5115-5126.
269. N. G. Sahoo, Y. C. Jung, N. S. Goo and J. W. Cho, *Macromolecular Materials and Engineering,* 2005, **290**, 1049-1055.
270. H. Koerner, G. Price, N. Pearce, M. Alexander and R. Vaia, *Nature Materials,* 2004, **3**, 115-120.
271. S. Mondal and J. Hu, *Iranian Polymer Journal,* 2006, **15**, 135-142.
272. I. S. Gunes, F. Cao and S. C. Jana, *Polymer,* 2008, **49**, 2223-2234.
273. M. Bertmer, A. Buda, I. Blomenkamp-Höfges, S. Kelch and A. Lendlein, *Macromolecules,* 2005, **38**, 3793-3799.
274. A. Lendlein and S. Kelch, *Clinical Hemorheology and Microcirculation,* 2005, **32**, 105-116.
275. X. Yu, S. Zhou, X. Zheng, Y. Xiao and T. Guo,*The Journal of Physical Chemistry C,* 2009, **113**, 17630-17635.
276. X. T. Zheng, S. B. Zhou, X. H. Li and H. Weng, *Biomaterials,* 2006, **27**, 4288-4295.
277. P. T. Knight, K. M. Lee, T. Chung and P. T. Mather, *Macromolecules,* 2009, **42**, 6596-6605.
278. T. W. Wong, M. U. Wahit, M. R. Abdul Kadir, M. Soheilmoghaddam and H. Balakrishnan, *Materials Letters,* 2014, **126**, 105-108.
279. W. Guo, H. Kang, Y. Chen, B. Guo and L. Zhang, *ACS Applied Materials & Interfaces,* 2012, **4**, 4006-4014.

280. B. Chun, T. Cho, M. Chong and Y. Chung, *Journal of Materials Science,* 2007, **42**, 9045-9056.
281. J. Xu, W. Shi and W. Pang, *Polymer,* 2006, **47**, 457-465.
282. A. Greiner, J. H. Wendorff, S. Ramakrishna and S. Agarwal, *Electrospinning: Materials, Processing, and Applications*, John Wiley & Sons, Germany, 2012.
283. N. Bhardwaj and S. C. Kundu, *Biotechnology Advances,* 2010, **28**, 325-347.
284. Q. Chen, A. Bismarck, U. Hansen, S. Junaid, M. Q. Tran, S. E. Harding, N. N. Ali and A. R. Boccaccini, *Biomaterials,* 2008, **29**, 47-57.
285. S. Liang, W. D. Cook, G. A. Thouas and Q. Chen, *Biomaterials,* 2010, **31**, 8516-8529.
286. M. A. Meyers, P. Chen, A. Y. Lin and Y. Seki, *Progress in Materials Science,* 2008, **53**, 1-206.
287. V. R. Sastri, *Plastics in Medical Devices, properties, requirements, and applications*, ed. V.R. Sastri, William Andrew Publishing, Boston, 2010, pp. 217-262.
288. Q. Chen, L. Jin, W. D. Cook, D. Mohn, E. L. Lagerqvist, D. A. Elliott, J. M. Haynes, N. Boyd, W. J. Stark, C. W. Pouton, E. G. Stanley and A. G. Elefanty, *Soft Matter,* 2010, **6**, 4715-4726.
289. Q. Chen, S. Liang, J. Wang and G. P. Simon, *Journal of the Mechanical Behavior of Biomedical Materials,* 2011, **4**, 1805-1818.
290. Q. Liu, J. Wu, T. Tan, L. Zhang, D. Chen and W. Tian, *Polymer Degradation and Stability,* 2009, **94**, 1427-1435.
291. S. J. Eichhorn, A. Dufresne, M. Aranguren, N. E. Marcovich, J. R. Capadona, S. J. Rowan, C. Weder, W. Thielemans, M. Roman, S. Renneckar, W. Gindl, S. Veigel, J. Keckes, H. Yano, K. Abe, M. Nogi, A. N. Nakagaito, A. Mangalam, J. Simonsen, A. S. Benight, A. Bismarck, L. A. Berglund and T. Peijs, *Journal of Materials Science,* 2010, **45**, 1-33.
292. M. J. D. Clift, E. J. Foster, D. Vanhecke, D. Studer, P. Wick, P. Gehr, B. Rothen-Rutishauser and C. Weder, *Biomacromolecules,* 2011, **12**, 3666-3673.

293. J. Mendez, P. K. Annamalai, S. J. Eichhorn, R. Rusli, S. J. Rowan, E. J. Foster and C. Weder, *Macromolecules,* 2011, **44**, 6827-6835.
294. L. Hsu, C. Weder and S. J. Rowan, *Journal of Materials Chemistry,* 2011, **21**, 2812-2822.
295. M. Samir, F. Alloin, J. Sanchez and A. Dufresne, *Macromolecules,* 2004, **37**, 4839-4844.
296. L. Goetz, M. Foston, A. P. Mathew, K. Oksman and A. J. Ragauskas, *Biomacromolecules,* 2010, **11**, 2660-2666.
297. R. Rusli and S. J. Eichhorn, *Applied Physics Letters,* 2008, **93**, 033111.
298. A. Sturcova, G. Davies and S. Eichhorn, *Biomacromolecules,* 2005, **6**, 1055-1061.
299. A. Lima, J. Wong, M. Paillet, R. Borsali and R. Pecora, *Langmuir,* 2003, **19**, 24-29.
300. C. Sun, *Journal of Pharmaceutical Sciences,* 2005, **94**, 2132-2134.
301. B Lecouvet and J Horion and C D'Haese and C Bailly and,B.Nysten, *Nanotechnology,* 2013, **24**, 105704.
302. K. Prashantha, M. F. Lacrampe and P. Krawczak, *Express polymer Letters,* 2011, **5**, 295-307.
303. T. Kokubo, H. Kim and M. Kawashita, *Biomaterials,* 2003, **24**, 2161-2175.
304. M. Bellantone, H. Williams and L. Hench, *Antimicrobial Agents and Chemotherapy,* 2002, **46**, 1940-1945.
305. A. Pei, J. Malho, J. Ruokolainen, Q. Zhou and L. A. Berglund, *Macromolecules,* 2011, **44**, 4422-4427.
306. P. Qu, Y. Gao, G. Wu and L. Zhang, *BioResources,* 2010, **5**, 1811-1823.
307. J. Han, Y. Zhu, J. Hu, H. Luo, L. Yeung, W. Li, Q. Meng, G. Ye, S. Zhang and Y. Fan, *Journal of Applied Polymer Science,* 2012, **123**, 749-762.
308. H. Luo, J. Hu and Y. Zhu, *Macromolecular Chemistry and Physics,* 2011, **212**, 1981-1986.
309. H. Luo, J. Hu and Y. Zhu, *Materials Letters,* 2011, **65**, 3583-3585.

310. Y. Zhu, J. Hu, H. Luo, R. J. Young, L. Deng, S. Zhang, Y. Fan and G. Ye, *Soft Matter,* 2012, **8**, 2509-2517.
311. L. A. Smith and P. X. Ma, *Colloids and Surfaces B: Biointerfaces,* 2004, **39**, 125-131.
312. S. Ramakrishna, K. Fujihara, W. E. Teo, T. C. Lim and Z. Ma, *An Introduction to Electrospinning and Nanofibers*, World Scientific, Singapur, 2005.
313. Z. Ma, M. F. Kotaki, R. F. Inai and S. Ramakrishna, *Tissue Engineering*, 2005, **11**, 101-109.
314. C. P. Barnes, S. A. Sell, E. D. Boland, D. G. Simpson and G. L. Bowlin, *Advanced Drug Delivery Reviews,* 2007, **59**, 1413-1433.
315. H. T. Zhuo, J. L. Hu and S. J. Chen, *Materials Letters,* 2008, **62**, 2074-2076.
316. S. Chen, J. Hu, Y. Liu, H. Liem, Y. Zhu and Y. Liu, *Journal of Polymer Science Part B: Polymer Physics,* 2007, **45**, 444-454.
317. M. M. Bergshoef and G. J. Vancso, *Advanced Materials,* 1999, **11**, 1362-1365.
318. J. Kim and D. H. Reneker, *Polymer Composites,* 1999, **20**, 124-131.
319. C. Tang and H. Liu, *Composites Part A: Applied Science and Manufacturing,* 2008, **39**, 1638-1643.
320. J. Choi, K. M. Lee, R. Wycisk, P. N. Pintauro and P. T. Mather, *Macromolecules,* 2008, **41**, 4569-4572.
321. H. Zhuo, J. Hu, S. Chen and L. Yeung, *Journal of Applied Polymer Science,* 2008, **109**, 406-411.
322. J. Hu, *Shape Memory Polymers and Textiles*, Woodhead Publishing, 2007.
323. X. Luo and P. T. Mather, *Soft Matter,* 2010, **6**, 2146-2149.
324. X. Luo and P. T. Mather, *Advanced Functional Materials,* 2010, **20**, 2649-2656.
325. T. Gong, W. Li, H. Chen, L. Wang, S. Shao and S. Zhou, *Acta Biomaterialia,* 2012, **8**, 1248-1259.
326. X. Luo, C. Xie, H. Wang, C. Liu, S. Yan and X. Li, *International Journal of Pharmaceutics,* 2012, **425**, 19-28.

327. H. J. Jeon, J. S. Kim, T. G. Kim, J. H. Kim, W. Yu and J. H. Youk, *Applied Surface Science,* 2008, **254**, 5886-5890.
328. X. Xu, X. Chen, A. Liu, Z. Hong and X. Jing, *European Polymer Journal,* 2007, **43**, 3187-3196.

Chapter 2

Experimental Workflow, materials, methods and experimental techniques

1. EXPERIMENTAL WORKFLOW

Figure 2.1 below shows the experimental workflow in this thesis.

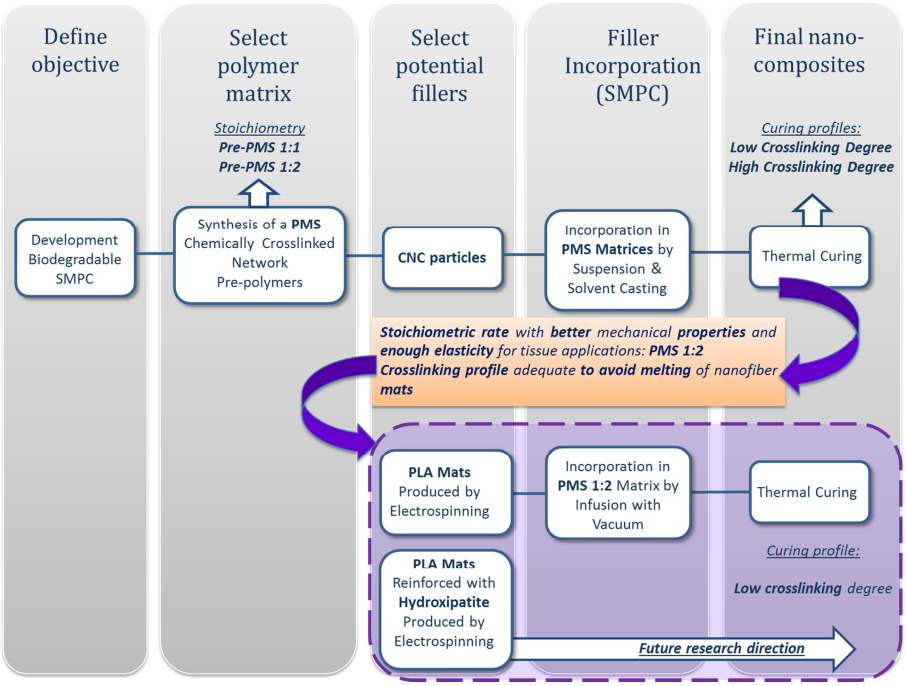

Figure 2.1. Schematic diagram of the experimental workflow.

This thesis is mainly focused on the design, synthesis, and characterization of novel shape-memory nanocomposites whose chemical and physical structure, biodegradability under physiological conditions as well as mechanical properties can be tailored to meet the requirements of soft-tissue engineering applications. The most important challenge of material development is not related to a singular parameter, but rather to a combination of all desired properties within an appropriate filler-matrix system. Newly developed material nanocomposites have to be biocompatible and exhibit tunable elasticity and adjustable degradation rate.

1.1. SELECTION OF THE POLYMER MATRIX

Poly(polyol sebacate)s (PPS) comprise a family of crosslinked polyester elastomers with demonstrated potential as soft-tissue engineering materials. From this polyester family, the poly(mannitol sebacate) (PMS) will be selected as matrix for the development of the nanocomposites. In order to find the best stoichiometry during synthesis and post-processing conditions of the PMS matrix required for an appropriate balance of mechanical and shape-memory properties as well as biodegradation rate of the final samples, two different stoichiometric ratios will be studied, defined as 1:1 PMS and 1:2 PMS, in reference to the mannitol:sebacic acid ratio used.

Taking into account that crosslinking degree is known to be a determinant factor in the final properties of these materials, two different crosslinking profiles in terms of temperature and time will be studied: one named low crosslinking degree profile (LCD) defined for samples with low crosslinking degree and another one named high crosslinking degree profile (HCD) defined for samples with high crosslinking degree. The study of different crosslinking conditions is considered highly attractive in order to obtain shape-memory devices with adjusted T_{trans} to the physiological temperature.

1.2. SELECTION OF FILLERS

The development of nanocomposite materials in such way as to achieve higher modulus without significantly lowering or compromising the elongation at break will be selected as the best strategy. Two different filler morphologies will be used:

- Cellulose nanocrystals with superior specific properties (low density and high modulus) will be incorporated in order to achieve high mechanical properties and to improve the shape-memory characteristics with respect to the PMS matrix. In addition, the high hydroxyl functional groups will be beneficial to promote affinity with the matrix.

- The electrospinning technique will be used for obtaining nanofiber mats to be subsequently used as reinforcing filler. Among all the possible polymers that can be formed as nanofibers, a biodegradable thermoplastic polymer of low melting point, namely, poly(lactic acid) PLA, will be selected. Other properties such as moderate stiffness at physiological temperature and long-term biodegradable character will be considered. In order to enhance or impart shape-memory properties to the neat matrix, a glass transition temperature above physiological one will be considered, as it is beneficial for enhancing the shape retention of the temporal shape during the fixing and recovery stages of low modulus matrix.

- Additionally, a study on the possible incorporation of hydroxyapatite (HAp) as filler into the nanofibers will be carried out in order to explore the effect on the shape-memory behaviour given its potential in promoting the bone adhesion and regeneration and opening new possibilities of future research based on the development of new biofunctionalities.

1.3. FILLER INCORPORATION

As depending on the intrinsic properties of the fillers, different strategies will be followed to incorporate them to the PMS pre-polymers obtained after the first polycondensation step. In this regard, CNC-reinforced nanocomposites will be obtained by solvent casting processes, while electrospun PLA-reinforced nanocomposites will be infiltrated with the aid of vacuum. Further, all the materials will be crosslinked following the selected curing profiles explained above.

1.4. CHARACTERIZATION OF NANOCOMPOSITES

Once the samples are prepared, several characterization techniques will be used in order to corroborate the polymer structure and study its morphology, mechanical, thermomechanical behaviour and shape-memory properties, among others. Preliminary studies on degradability tests in simulated body fluid will be initiated in the final stage of the workplan. It is to be mentioned that biocompatibility tests are outside the focus of this thesis, therefore they will be performed elsewhere. Detailed information on the selected experimental characterization techniques is given in section 3 of this chapter.

2. MATERIALS AND METHODS

The second part of this chapter presents the main characteristics of the materials employed in the research, as well as detailed information on the protocols followed during the synthesis of poly(mannitol sebacate) polymers and processing of their cellulose nanocrystal and poly(lactic acid) nanofiber nanocomposites. The isolation of cellulose nanocrystals as well as the electrospinning of poly(lactic acid) and poly(lactic acid)/hydroxyapatite nanofibers mats is also covered.

2.1. MATERIALS

Synthesis of polymer matrices

Sebacic acid (SA) (99% purity) and D-mannitol (MA) (99% purity) were purchased from Sigma Aldrich (**Figure 2.2**). The monomers (MA and SA) were used without further purification. N,N-dimethylformamide (DMF, ACS reagent grade) solvent used to dissolve the pre-polymers, deuterated dimethylsulfoxide (DMSO-d_6) (deuteration degree 99.96%) used in NMR studies, and tetrahydrofuran (Chromasolv® Plus grade, ≥99.9% purity) for chromatography were purchased from Sigma Aldrich. Ultrapure water used in precipitation steps was obtained from a Sartorius Stedim Arium 611 VF® water purification system (ρ=18.2 mΩ cm).

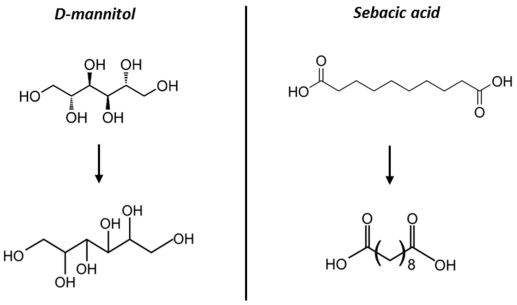

Figure 2.2. Chemical structures of D-mannitol and sebacic acid (above), and the schematic representations (below).

Isolation of cellulose nanocrystals (CNCs)

Whatman No 1 filter paper was used as a cotton source for the extraction of cellulose nanocrystals (**Figure 2.3**) by hydrolysis with sulfuric acid (H_2SO_4) (95-98% ACS reagent grade) according to a protocol[3] developed from a method originally described by Dong et al.[4] This protocol introduces a small concentration of sulfate ester groups on the surface of cellulose nanocrystals to help in the formation of stable suspensions in polar solvents.[5] Conductometric titration with hydrochloric acid (HCl) (37% ACS reagent grade) and sodium hydroxide (NaOH, 98% ACS reagent grade) was employed in order to calculate the concentration of surface charges present as sulfate groups on the surface of the CNC. All the reagents were purchased from Scharlau while the ultrapure water used for hydrolysis was obtained from a Sartorius Stedim Arium 611 VF® water purification system (ρ =18.2 mΩ cm).

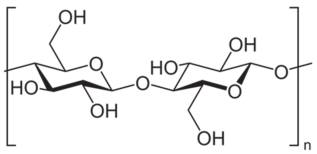

Figure 2.3. Schematic representation of the structure of cellulose molecule.

Nanofibers production

Poly(lactic acid) (PLA) with 3% of D-lactic (**Figure 2.4**) acid monomer was supplied by NatureWorks® (USA) under the trade name PLA3051D (M_n ca. 142 x 10^4 g/mol, density 1.24 g/cm^3). The main properties of commercial PLA are shown in **Table 2.1**. Dichloromethane (DCM) and N,N-dimethylformamide (DMF) ACS reagent grade solvents, and sodium dodecyl sulphate (SDS) (>99% purity) were purchased from Sigma Aldrich. Nano-sized hydroxyapatite (HA) (Calcium-Phosphorous (Ca/P) molar ratio of 1.67) synthesized by chemical precipitation from calcium and phosphorous precursors in solutions and 30 g/L commercial gelatin (Dr Otker) was

supplied by Chemistry Department of State University of Ponta Grossa (UEPG, PR, Brazil) (see **Figure 2.5**).

Figure 2.4. Stereoisomers of lactic acid. (left): L(+), right: D(-).

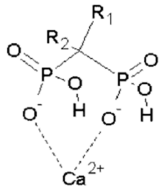

Figure 2.5. Crystal structure of hydroxyapatite.

Table 2.1. Main properties of PLA 3051D from NatureWorks®.

Material property	Value
Crystalline Melt Temperature (°C)	145-155
Glass Transition Temperature (°C)	55-65
Tensile Yield Strength (MPa)	48
Elongation at break (%)	2.5
Flexural Strength (MPa)	83
Flexural Modulus (MPa)	3828

2.2. SAMPLE PREPARATION METHODS

2.2.1. SYNTHESIS OF POLY(MANNITOL SEBACATE) PRE-POLYMERS

Poly(mannitol sebacate) (PMS) polymers were synthesized by a well established solvent-free **two-step** polycondensation method as previously reported, after slight modifications.[1] Melt polycondensation is a low cost manufacturing process effectuated at relatively high temperatures. During the **first step**, low molecular

weight pre-polymers are formed (**Figure 2.6**). Ideally, in this first stage, the esterification is dominated by the reaction of the primary hydroxyl groups of polyol (mannitol, MA), with carboxylic acid groups from diacid (sebacic acid, SA). During the **second step**, chemical crosslinking takes place.[6-8]

Figure 2.6. Waxy aspect of the low molecular weight PMS pre-polymer obtained.

For the first step, the starting materials (MA and SA, where MA:SA stoichiometric ratio was 1:1 and 1:2) were mixed into a 250 mL three-necked round bottom flask equipped with a stirrer and a condenser in order to obtain the PMS pre-polymers. Briefly, the flask was charged with appropriate amounts of monomers depending on the reaction ratio, then, it was purged with inert gas for 0.5 h and placed in a silicon heating bath. The temperature was slowly increased to 150 °C (above melting temperature of SA) under continuous stirring and nitrogen flow to produce approximately 20 g of each pre-polymer. Although the general protocol is similar for both stoichiometric ratios, slight differences were introduced to achieve the two mentioned pre-polymers as specified below:

- ***For PMS 1:1 pre-polymer:*** Equimolar amounts (0.068 mol) of SA (13.79 g) and MA (12.42 g) were used, and the reaction was stopped after 13 h (before gelation occurs).
- ***For PMS 1:2 pre-polymer:*** Molar amounts 0.034:0.069 mol of MA (6.21 g) and SA (13.79 g) were used respectively. The reaction was stopped after 5 h (before gelation occurs).

After reaction, both pre-polymers were dissolved in DMF (150 mg/mL), filtered and purified by dropwise precipitation into a four-fold excess of cold ultrapure water under continuous stirring. Once precipitated, PMS pre-polymers were collected and dried under vacuum until no more solvent was detected in the infrared spectra. Experimental set-up and procedure are schematically shown in **Figure 2.7**.

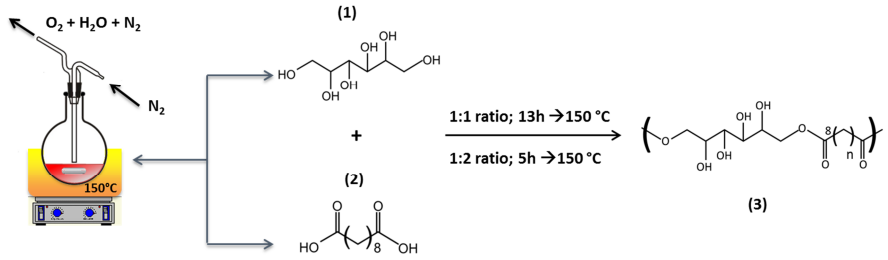

Figure 2.7. Schematic representation of the general synthetic procedure to obtain poly(mannitol sebacate) pre-polymers. D-mannitol (1) was polymerized with sebacic acid (2) in different stoichiometries, yielding poly(mannitol sebacate) pre-polymers (pre-PMS) (3) with ratio 1:1 and 1:2. *Note: simplified chemical representations are shown*.

2.2.2. ISOLATION OF CELLULOSE NANOCRYSTALS (CNCs)

Cellulose nanocrystals were isolated from cotton (Whatman No. 1 filter paper) by controlled hydrolysis with sulphuric acid according to a protocol[3] based on the method originally described by Dong et al.[4] The protocol introduces a small concentration of sulfate ester groups on the surface of the CNC, to help the formation of stable suspensions in polar solvents **(Figure 2.8)**.[5] Briefly, Whatman No 1 filter paper (5g) was soaked in ultrapure water (250 mL, ρ =18.2 mΩ cm) for 15 min, and vigorously blended in a regular kitchen blender until a pulp-like slurry was formed. The resulting slurry was placed in a beaker and cooled down in an ice bath under continuous stirring for 15 min. Sulfuric acid (140 mL) was dropped slowly as to maintain the temperature below 30 °C. Further, the reaction vessel was placed in a silicon bath preheated to 50 °C and stirred for 4 h. The reaction mixture was subsequently cooled to room temperature by using an ice bath. The CNCs were separated by centrifugation at 3600 r.p.m. for 20 min. The supernatant

was decanted and the same amount of ultrapure water was added to centrifuge again in the same conditions. This process was repeated at least three times. The resulting CNCs dispersion was dialyzed against ultrapure water for 3-5 days, exchanging the water daily, until the pH reached value 5. The final dispersion was subsequently sonicated for 15 min using a horn sonicator (Q500 sonicator, QSonica, 20 kHz/500 Watts, fitted with a 1=4" microtip probe), then frozen in liquid nitrogen and lyophilized (VirTis BenchTop 2K XL lyophilizer) for 3 days.

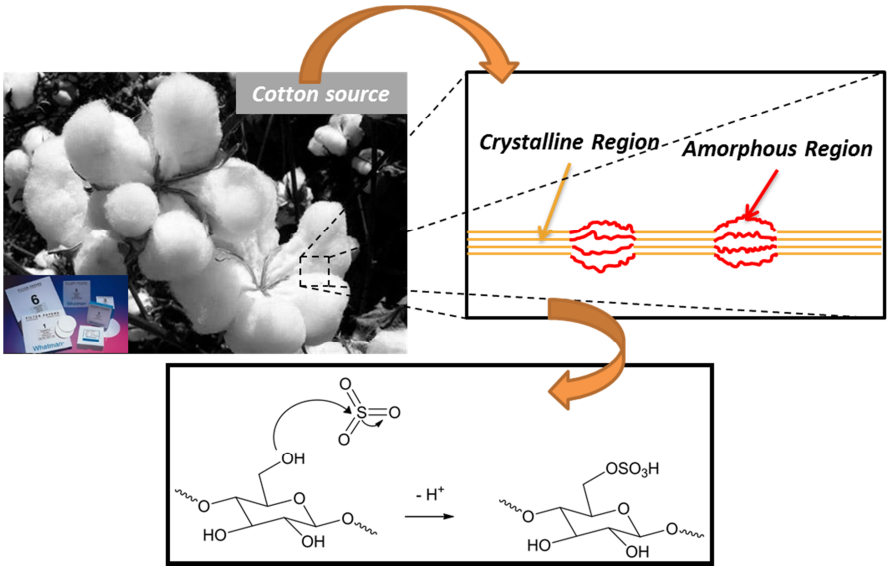

Figure 2.8. Acid hydrolysis breaks down disordered regions and isolates nanocrystals. Sulfate ester groups are likely formed on the cellulose surface.

2.2.3. PRODUCTION OF NANOFIBER MATS

2.2.3.1. IMPLEMENTATION OF SOLUTION, ELECTROSPINNING PARAMETERS AND PLA:HA RATIOS TO OBTAIN NEAT PLA AND PLA:HA MATS.

PLA fibers were produced by varying the electrospinning conditions to obtain an organized network of polymer fibers. The first step of the process relied on the adequate selection of the solvent and the process parameters in order to successfully generate fiber mats. Based on related literature, **Table 2.2** lists the

solvents and main parameters used to successfully produce fibers from PLA with several L/D ratios.

Table 2.2. Most common solvents and processing conditions used in PLA electrospinning systems, as reported in the literature. Where $CHCl_3$ is chloroform, C_3H_7NO is N,N-dimethilformamide, $C_3H_2F_6O$ is 1,1,1,3,3,3-hexafluoro-2-propanol, CH_2Cl_2 is dichloromethane and CF_3CH_2OH is 2,2,2-trifluoroethanol.

Polymer	Concentration	Needle diameter (mm)	Distance collector-needle (cm)	Potential (kV)	Flow (mL/h)	Fiber diameter (μm)	Ref.
PLA	20% (w/v) in $CHCl_3$	-	15	25	0.1	1.0-2.0	9
PLA	14 % (w/v) in 15:3 $CHCl_3$:C_3H_7NO	-	20	13	1.5	0.8-3.0	10
PLA	10 wt% in 9:1 $CHCl_3$: C_3H_7NO	0.6	16	10	1.0	0.6-2.0	11
5% D-Lactide	10 wt% in $C_3H_2F_6O$	-	15	30	6	0.9-1.0	12
5% D-Lactide	20-35 wt% in 1.5:1 (w/w) in CH_2Cl_2:C_3H_7NO	0.7	15	20-30	1.2	0.2-1.0	13
PLLA	1-5 wt% in 70:30 CH_2Cl_2:C_3H_7NO	0.7-1.2	10	12	1.0	0.1-3.0	14
PLLA	14%(w/v) in $CHCl_3$	-	30	15	18-21	3.0-6.0	15
PLA	12%(w/v) in $C_3H_2F_6O$ or 11%(w/v) CF_3CH_2OH	0.5	20	11	0.3	0.1-2.2	16
PLLA	5.5 to 6 wt% in $CHCl_3$	0.4	18	45-50.4	3.0-4.2	0.3-1.0	17
PLLA/PDLA	4g/dL $CHCl_3$	0.5	10	12-25	6	0.4-2.7	18

A number of useful observations can be derived from **Table 2.2**. In particular:

- Solutions of PLA from 5.5 to 10 wt% in solvent mixtures of chloroform:dimethylformamide or dichloromethane:dimethylformamide are useful to produce fibers with average diameters in the nanometer range (0.3 to 2 μm).
- By using dichlorometane, porous surfaces are induced due to the rapid evaporation of the solvent.[19] Therefore, the use of some organic solvents

such as dichloromethane or chloroform may result in electrospun fibers with undesirable morphology, because of their volatility. This problem can be overcome by adding a second solvent, such as dimethylformamide, thanks to the vapor pressure reduction.

- Defects in the morphology of the PLA electrospun fibers related with the presence of "beads", can be overcome by incorporating small amounts of salts such as pyridinium formate ($C_6H_7NO_2$), monopotassium phosphate (KH_2PO_4), monosodium phosphate (NaH_2PO_4), sodium chloride (NaCl) and sodium dodecyl sulfate ($NaC_{12}H_{25}SO_4$).[13, 20]

Among these possibilities found in the literature, chloroform, N,N-dimethylformamide (DMF), dichloromethane (DCM) and a combination of DCM:DMF (70:30) mixtures were proved in the electrospinning equipment. Based on the reported literature as well as the characteristics of the available electrospinning set-up (a horizontal configuration with a rotating mandrel as collector connected directly to a high voltage power supply and a syringe infusion pump), the PLA concentration was varied from 2-15 wt%. The starting processing parameters were also varied in order to obtain nano-sized fibers and a stable Taylor cone: the applied voltage ranged from 8 to 15 kV, the distance from the collector to the needle tip was varied from 10 to 15 cm and the flow rate was varied in the range of 0.6 to 1.3 mL/h. The morphology of the obtained mats was studied by scanning electron microscopy (SEM) to adjust the parameters and concentrations following these rules:

- When drops were obtained instead of fibers, the polymer concentration was increased.
- When electrospun fibers were obtained with high diameters (μm), polymer concentration and flow rate were decreased while voltage was increased.

The experimental tests indicated the best results were obtained for the "PLA 7 wt% in DCM:DMF (70:30)" system where 7 wt% poly(lactic acid) was dissolved in a mixture solvent (70 parts of dichlorometane (DMF) and 30 parts of dimethylformamide (DMF)) (**Table 2.4.**):

Table 2.3. Selected values in the electrospinning set-up for obtaining PLA nanofibers.

Solution	Voltage (kV)	Distance (cm)	Flow rate (mL/h)	Size
PLA 7 wt% in DCM:DMF (70:30)	14	13	0.6	Nanometric

Once the electrospinning conditions were implemented to obtain neat PLA nanofiber mats, the next step was to prepare different samples with nano-hydroxyapatite (HA) as filler. Based on the available literature,[9, 21-23] and considering the change in the solution characteristics and hence the electrospinning process due to the addition of HA particles, the PLA:HA ratios were set to ensure continuous electrospinning without varying the process parameters set for neat PLA. Therefore, PLA:HA mats were prepared by dissolving 7 %wt PLA in 70:30 DCM:DMF (solvent system that allowed us to obtain nanofibers), and adding HA particles with the following ratios: PLA: HA 9:1, 5:1 and 3:1. A salt (sodium dodecyl sulphate, SDS) was used in all the solutions (neat PLA and PLA:HA) to increase the surface tension and ensure good morphology of the fibers produced.

2.2.3.2. EXPERIMENTAL PROCEDURE

Five different solutions were prepared for the electrospinning experiment: one of 7 wt% of PLA (3051D) for the neat PLA and other four of PLA/HA mixtures (9:1, 5:1 and 3:1 PLA:HA ratios) used for PLA:HA mats. The solvent system used for the preparation of all solutions was DCM:DMF 70:30. For nano-composite solutions, proper amounts of HA were added to the polymer solutions and thoroughly mixed during 0.5 h by sonication using a horn sonicator (Q500 sonicator, QSonica, 20 kHz/500 Watts, fitted with a 1=4" microtip probe). A 0.5 wt% SDS salt (calculated

from the weight of added PLA) was added to all the solutions. A summary of the sample preparation is shown in **Table 2.4**.

Table 2.4. PLA, and PLA/HA solutions.

Sample Code	PLA Concentration (wt%)	Ratio PLA:HA	Solvent System	Sonication time (h)
HCR PLA/HA (3:1)	7 wt%	3:1	DCM:DMF 70:30	0.5
HCR PLA/HA (5:1)	7 wt%	5:1	DCM:DMF 70:30	0.5
HCR PLA/HA (9:1)	7 wt%	9:1	DCM:DMF 70:30	0.5
HCR PLA	7 wt%	1:0	DCM:DMF 70:30	0
LCR PLA/HA (3:1)	7 wt%	3:1	DCM:DMF 70:30	0.5
LCR PLA/HA (5:1)	7 wt%	5:1	DCM:DMF 70:30	0.5
LCR PLA/HA (9:1)	7 wt%	9:1	DCM:DMF 70:30	0.5
LCR PLA	7 wt%	1:0	DCM:DMF 70:30	0

A standard horizontal electrospinning set-up directly connected to a high voltage power supply and a syringe infusion pump was used to produce electrospun nanofiber mats. In order to promote fiber orientation, the set-up was provided with a rotating mandrel as a collector. The polymer solutions were injected using a 10 mL disposable syringe with a 22-G needle connected to the positive terminal of the high voltage supply. All air bubbles were purged prior to electrospinning, the applied voltage was set to 14kV, the distance between the charged capillary tip and the collector mandrel was set to 13 cm, and the flow rate of the solution was maintained at 0.6 mL/h (**Table 2.3**). The collector mandrel was covered with aluminium foil, and two different take up velocities (rotation speeds) were used: 300 r.p.m were applied to obtain randomly oriented fibers (low collecting rate fibers, **LCR**), while 1100 r.p.m. were employed to obtain high oriented mats (high collecting rate fibers, **HCR**).

2.2.4. PREPARATION OF NANOPARTICULATE REINFORCED COMPOSITES (PMS/CNC)

PMS/CNC nanocomposites were obtained by using the pre-polymers (1:1 and 1:2 MA:SA ratio) previously dissolved in DMF (100 mg/mL) for 4 h under continuous stirring. Suspensions of CNC (10 mg/mL) were prepared at appropriate ratio in DMF (designed to combine with 1.5 g of dry pre-polymers and form 1 wt%, 5 wt% and 10 wt% of PMS/CNC nanocomposites) by 40 min of ultrasonic treatment in a horn sonicator with 1 sec on/off pulse conditions at a 20% of amplitude. CNC suspensions were stirred with PMS pre-polymer/DMF solution for 30 min and cast into aluminium Petri dishes (93 x 7 mm) and allowed to dry in an oven at 70 °C.

Films consisting in the neat pre-polymers (without CNCs), were prepared for reference purposes under the same conditions. The resulting pre-polymer/nanocomposites and the neat pre-polymer films were placed in a vacuum oven for further reaction.

Two different curing profiles named as **LCD** (low crosslinking curing profile) and **HCD** (high crosslinking curing profile) were applied to both pre-polymer/nanocomposites series (1:1 and 1:2 MA:SA reaction ratios), in which temperature and duration of the thermal treatment were varied to obtain samples with low and high degree of crosslinking and reaction ratios 1:1 and 1:2. Samples with low degree of crosslinking were maintained at 120 °C for 72 hours under vacuum (60 cm Hg). Samples with high degree of crosslinking were obtained by using the same protocol and subsequently increasing the temperature to 170 °C while maintaining the vacuum (60 cm Hg) for further 24 hours. Both procedures afforded eight different samples with ~ 150-200 μm thickness for each reaction ratio of PMS, four with low degree of crosslinking and four with high degree of crosslinking. The employed methodology is schematically shown in **Figure 2.9**.

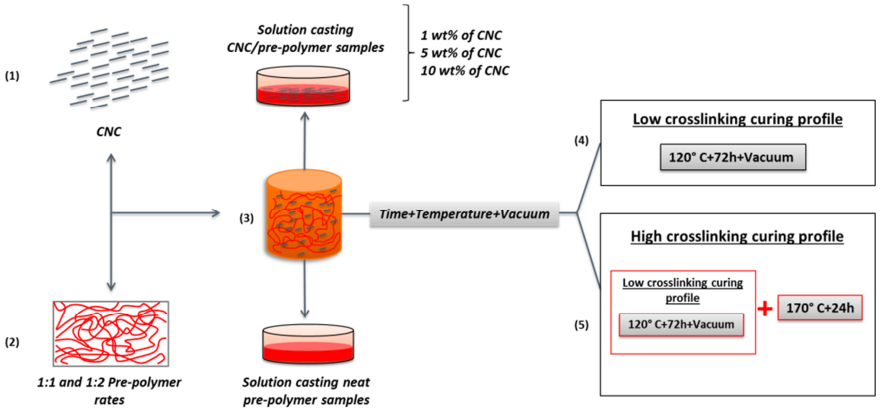

Figure 2.9. Schematic representation of the methodology followed to obtain all the PMS/CNC nanocomposites. Solutions of pre-polymers in DMF **(1)** were mixed with CNC suspensions also in DMF **(2)**. Mixtures obtained and neat pre-polymer solutions were casted **(3)** and after evaporation of the solvent, samples were crosslinked through further polycondensation steps under two different curing profiles designed to obtain samples with low **(4)** and high **(5)** crosslinking degree.

2.2.5. PREPARATION OF ELECTROSPUN NANOFIBER REINFORCED COMPOSITES

Selection of the appropriate matrix and curing conditions for nanofiber based nanocomposites

In order to develop fibrous nanocomposites based on PMS matrices and PLA nanofibers, the limitation of the curing profiles by the T_m of the electrospun mats must be taken into account. Thus, only low crosslinking curing profile (120 °C) could be used to achieve the final nanocomposites, as PLA nanofiber mats melt at temperatures close to 150 °C. In addition, it should be pointed out that nanofiller reinforced systems (CNCs reinforced) were the first developed and studied in this thesis. Because of it, the two different matrices (stoichiometric ratio between mannitol and sebacic acid 1:1 and 1:2) as well as the two crosslinking profiles (low and high crosslinking degree profiles) were tested with this filler. Considering the results obtained with this first developed system, decisions over the nanofibers reinforced system were taken in order to continue with the research. The use of poly(lactic acid) nanofibers as reinforcement followed the main considerations

based on the results obtained for CNC particulate reinforced systems, as presented below:

- Selection of the stoichiometric mannitol:sebacic acid ratio that will allow to develop fibrous nanocomposites with the best possible shape-memory properties. In these regards, matrix selection for this system was based on the following requirements:

  - Higher mechanical properties of the matrix can better assist in the nano-composites shape recovery and shape retention capability; thus, they can result in better shape-memory behaviour thanks to higher tensile strength and tensile modulus as well.
  - In general, regarding the dynamo-mechanical properties, higher rubbery modulus of the polymer networks results in better shape-memory properties.[24] By increasing the rubbery modulus above T_g, an increase in the stored energy is observed which could lead to higher recovery stresses when the SMPs are deformed at temperature of interest.[25]
  - Matrix selected has at least to ensure 10% of elongation to be useful in tissue engineering applications.

Table 2.5 shows values of storage modulus for the two PMS matrices developed that aid in the decisions about the selection of the best matrix for the PLA nanofibers system. In addition to tensile results, dynamo-mechanical results evidenced that low crosslinking degree PMS 1:2 matrix also resulted in higher Young´s modulus (E; 7.2±0.1 Mpa) and ultimate tensile strength (UTS; 4.5±0.7 MPa) than its PMS 1:1 counterpart (E; 1.8±0.3 MPa, UTS; 1.2±0.7 MPa).

Considering all the previously mentioned characteristics, the nanofiber nanocomposites were developed by using PMS 1:2 as a matrix and low crosslinking degree curing profile.

Table 2.5. Storage modulus at different temperatures of interest for PMS neat matrices with 1:1 and 1:2 stoichiometric ratios cured with low crosslinking degree profile. Storage modulus measured at 25 °C is indicative of properties at room temperature, at 40 °C is important for possible medical applications and at 100 °C is when the samples achieve the rubbery plateau.

Sample	E´ at 25 °C (MPa)	E´ at 40 °C (MPa)	E´ at 100 °C (MPa)
PMS 1:1 LCD	8.0	2.0	2.0
PMS 1:2 LCD	24.4	3.6	3.0

Experimental procedure for fabrication of the samples

In order to prepare PMS-based composites with PLA nanofiber content varied up to 15 wt%, layers of 4 x 8 cm from PLA nanofiber mat (~150 µm of thickness) were infiltrated with PMS pre-polymer, as schematically shown in **Figure 2.10**.

Briefly, 0.6 g pre-polymer and 1, 2 and 3 layers of PLA nanofiber mat were used to obtain composites with increasing PLA weight (%) with respect to the neat matrix. The pre-polymer (1:2 MA:SA ratio) was heated at 40 °C (pre-polymer starts to be a viscous clear liquid losing the waxy aspect at this temperature) and spread onto a Teflon® surface, appropriate amounts of previously cut PLA mat fragments were then immersed under vacuum (30 cm Hg) for 20 min to ensure complete infiltration of PMS into the PLA nanofiber mats. To avoid mat displacement during infiltration, adhesive tape was used to hold the mats together and fix them to the Teflon® surface. Finally, the pre-PMS/PLA composites were placed in a vacuum oven for further reaction of the matrix at 120 °C for 72 hours under vacuum (60 cm Hg).

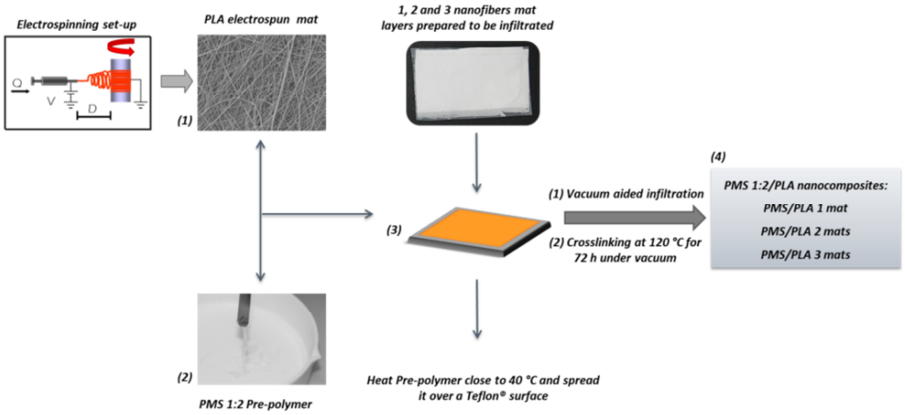

Figure 2.10. Schematic representation of the methodology followed to obtain electrospun nanofiber reinforced composites based on PMS. Electrospun PLA mats (1) were infiltrated into spread pre-polymer PMS 1:2 (2) over a Teflon® surface (3) with the help of vacuum. After infiltration, further polycondensation step under low curing designed profile was carried out (4).

Table 2.6 presents the content of PLA nanofibers (wt%) equivalent to the infiltration of 1, 2 and 3 mats into the PMS matrix. "PMS/NF-PLA x" abbreviation indicates the poly(mannitol sebacate) matrix (pre-polymer with 1:2 ratio) with specific poly(lactic acid) nanofiber mat layers incorporated during the infiltration process.

Table 2.6. Weight % of infiltrated PLA mats into PMS 1:2 matrix, and dimensions of the final samples.

Sample	*Weight % PLA measured by weighting
PMS/NF-PLA 1 mat	4
PMS/NF-PLA 2 mat	10
PMS/NF-PLA 3 mat	15

* Determined as the relation between the weights of the pre-polymer matrix and nanofibers previously to infiltration and the weight of the obtained nanocomposite after apply the crosslinking profile.

3. EXPERIMENTAL TECHNIQUES

This section presents a short description of the fundamentals of each analytical technique, along with the experimental parameters and calculation methods employed in this thesis. The analytical techniques were chosen to offer a complete analysis of morphological, structural, mechanical, thermal, viscoelastic, shape-memory and degradation properties of the developed materials. **Figure 2.11** shows the main analytical techniques used in the characterization of the samples. The experiments were carried out at the laboratories of the Technological Institute of Materials (ITM) (Polytechnic University of Valencia) and the Adolphe Merkle Institute in Switzerland.

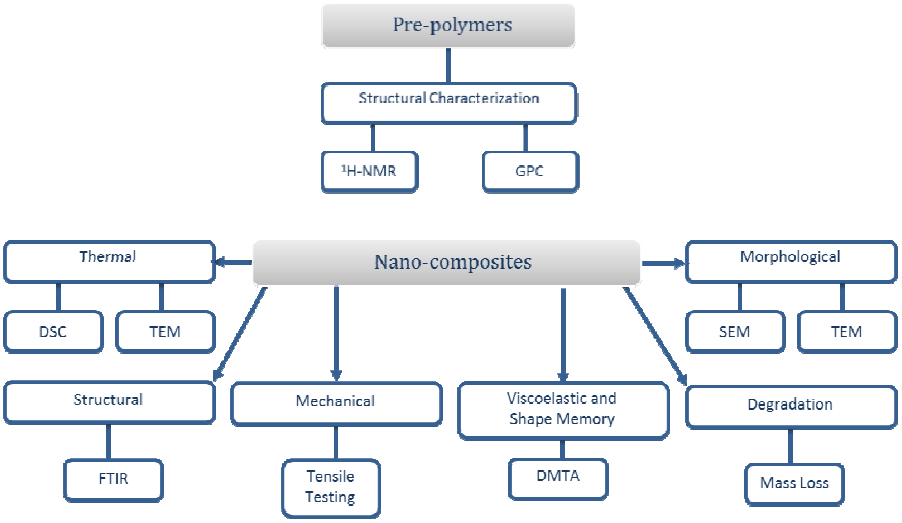

Figure 2.11. Summary of the experimental techniques applied, in connection with the analyzed properties.

3.1. GEL PERMEATION CHROMATOGRAPHY (GPC)

3.1.1. FUNDAMENTALS[26]

Chromatography uses the chemical and physical properties of sample molecules and mobile phases to detect their presence as they elute from a column, and so different detectors have been developed that make use of the different characteristics of compounds.

It is well known that polymers are molecules composed of many repeating units joined together. The chemical basis for the formation of polymers is the ability of the single, or 'monomer', units to form long chains through polymerization chemical reactions. In practice, a sample of polymer will contain a distribution of molecules of different lengths.

Gel permeation/size exclusion chromatography (GPC/SEC) allows to separate out the different lengths of polymer chain in a sample, and measure their relative abundance. Basically, the measurement of chain lengths is achieved by separating them on the basis of their size. The instrument consists of a pump to push the solvent through the instrument, an injection port to introduce the test sample onto the column, a column to hold the stationary phase, one or more detectors to detect the components as they leave the column and software to control the different parts of the instrument, and calculate and display the results. Thus, GPC/SEC is purely a physical partitioning of the sample on the basis of size.

The polymer sample is first dissolved in a solvent. When dissolved, the molecules coil up on themselves to form a coil conformation, so when the sample is analysed by GPC/SEC it behaves like tiny spheres with size dependent on the molecular weight (higher molecular weight polymers coil up to form larger spheres). The sample is then introduced into the mobile phase and flows into the GPC/SEC column. The dissolved polymer molecules move past the beads as the mobile phase

carries them down the column. As the polymer coils move past each bead, they can either, skip the pores in the column being carried straight past by the mobile phase, or they can enter the pores occupying some or potentially all of the available stationary phase, as depending on their size. As the molecules enter the column, this partitioning occurs repeatedly, with diffusion acting to bring the molecules into and back out of any pores they pass, as they travel down the column. As a result, the **small polymer coils** can enter into many pores in the beads taking a long time to pass through the column and therefore they **exit the column slowly**. Conversely, the **large polymer coils** cannot enter the pores requiring **less time to leave the column**, and polymer coils of **intermediate size exit** the column somewhere in **between**. Thus, the way in which the samples elute from the column depends greatly on the size of the pores in the beads, but always the larger molecules get to the exit first.

The separating mechanism is shown in **Figure 2.12**. This diagram shows how different sized sample molecules can be excluded completely, partially, or not at all from entering the pores in the particles, depending on the size of the pores and of the sample molecules.

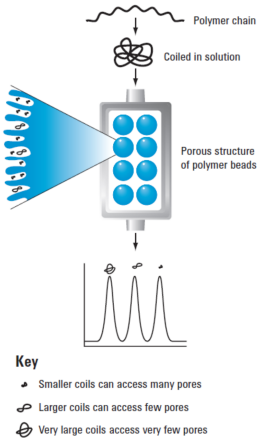

Figure 2.12. How GPC/SEC separates molecules of different sizes. Adapted from 26.

As the components exit the column they are detected in various ways, and the elution behaviour of the sample is displayed in a graph, or **chromatogram** that shows how much material exit the column with time. The higher molecular weight, thus larger polymer chains, eluting first, followed by successively lower molecular weight, smaller polymer chains, eluting later. The primary separation is according to **elution volume**, and this is **converted to time** for ease of measurement, on the assumption that there is a constant flow rate. The time it takes for a group of molecules of the same size (a fraction) to emerge from the column is called the **retention time**. The final determination of the molecular weight of the components of a polymer sample depends on the configuration of the instrument.

3.1.1.1. DETECTION SYSTEM[27]

Detectors may respond to a change in the mobile phase due to the presence of the sample, or to a property of the sample alone. Different types have been developed that make use of the different characteristics of compounds. The ability of the compounds to scatter light, molecular viscosity and the adsorption of ultraviolet (UV) or infrared (IR) are all used as measurement parameters, thus detectors can be divided into two main categories:

- Those that measure concentration alone, such as differential refractive index (DRI), UV and evaporative light scattering (ELS) detectors.
- Those whose response is proportional to concentration and other properties of the polymer molecules, such as static light scattering detectors or viscometers.

The most common GPC detector is the differential refractive index detector (DRI) that is based on the principle of refractive index, and works by assessing the difference in refractive index between the mobile phase and the pure solvent. Viscosity detectors also compare the mobile phase with the pure solvent, but using

viscosity, or resistance to flow, as the measurement parameter. Static light scattering detectors use the fact that a beam of light will be scattered when it strikes a polymer molecule. There are various types, including low angle laser light scattering (LALLS), multi angle laser light scattering (MALLS) and right angle laser light scattering (RALLS). The advantage of these detectors is that they give a response directly proportional to the molecular weight of the polymer molecules, and can provide size information too. Depending on how many detectors are used, two most important types of GPC instruments can be found.

Refractive index increment dn/dc:[28]

A light scattering detector comprises a sample cell, a laser beam, and one or more detectors set at some angle to the incident beam to collect the scattered laser light. During operation, the laser beam irradiates the sample and the detector collects the resulting scattered light from relaxation of the molecule. When polarized monochromatic light passes through the solvent containing macromolecules, the excess light scattered by the molecule (sample) and solvent combination through an angle to the incident beam over the scattered light by the solvent alone, is directly proportional to the molecular mass. Thus, the weight average molecular weight *(M_w)* and the z-average mean square radius $< r_g >^2$ can be calculated through the **Rayleigh-Gans-Debye** approximation:

$$\frac{K \cdot c}{R_\theta} = \frac{1}{M_w \cdot P_\theta} + 2A_2 \cdot c \tag{2.1}$$

, where the physical constant K for vertically polarized incident light is given by:

$$K = \frac{4\pi^2 n_0 (dn/dc)^2}{N_A {\lambda_0}^4} \tag{2.2}$$

, where c is the concentration of the molecules in the solvent, M_w is the weight average molecular weight of the molecules present in the solution, $2A_2$ is the

second virial coefficient (from the virial expansion or equation of state, that is a function of temperature), n_0 is the refractive index of the solvent, N_A is Avogadro´s number, λ_0 is the wavelength of incident light in a vacuum, and dn/dc is the refractive index change in the solution with respect to a change in concentration of the solute (refractive index increment). R_θ is the excess Rayleigh scattering at angle θ, and P_θ is the form factor of the light scattered at angle θ as alternating power series in $sin^2(\theta/2)$. Thus:

$$P_\theta = 1 - \alpha_1 sin^2(\theta/2) + \alpha_2 sin^4(\theta/2) - \alpha_3 sin^6(\theta/2) + \ \ldots\ldots \tag{2.3}$$

For molecules smaller than $\lambda/20$, where λ is the wavelength of the scattered light in solution, P_θ can be expressed as:

$$P_\theta = 1 - \frac{16\pi^2}{3\lambda^2} < r_g >^2 sin^2(\theta/2) \tag{2.4}$$

, where $< r_g >^2$ is the mean square radius of the molecules.

The **Rayleigh ratio** is directly proportional to the molecular weight of the solute molecule scattering the light, and its main advantage is that it is independent of the incident light intensity and the distance to the scattered light detector. As it could be seen, the equation that relates R_θ to M_w is really complex but a simplified form can be made following some assumptions: **(1)** For any polymer and solvent combination the refractive index increment (dn/dc) is considered a constant. **(2)** The virial expansion related to intermolecular interactions and under the dilute conditions of GPC can be considered zero. **(3)** P_θ, the scattering function is equal to one, if the molecule is below a certain fundamental size of around 10 nm. Under these conditions the equation simplifies to:[28]

$$R_\theta = M_w \cdot K \cdot \left(\frac{dn}{dc}\right)^2 \cdot c \tag{2.5}$$

, where K is a system constant determined before measurement that depends on the solvent properties, on wavelength of light (λ) and on the angle of collection (θ). M_w is the weight average molecular weight and c is the concentration of the polymer. dn/dc is a material constant for a given polymer in a given solvent, named as specific refractive index increment, and means how much the refractive index of a solution varies for a given increment in concentration. Usually these constants are available for several polymers and can be found in several databases and books. However, sometimes it is unavailable, and as every light scattering experiment requires this constant, its impact on the determination of the molecular weight is far from negligible. From the previous equation, it results that M_w is inversely proportional to the square of dn/dc, so this value is the vital importance in light scattering calculations, and that the response from the detector is directly proportional to M_w, K and c. When measuring an unknown sample by light scattering, the molecular weight can be calculated from the R_θ, if the previously mentioned values are known, as it is shown in **Figure 2.13.**

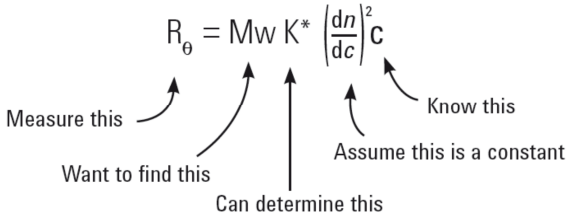

Figure 2.13. Relation between Rayleigh ratio, molecular weight, a constant K and concentration.

3.1.2. CALCULATION METHODS AND EXPERIMENTAL PROCEDURE

When the dn/dc is not known, as in the case of PMS pre-polymers synthesized in this thesis, it is possible to be determined experimentally by using appropriate multi-detector combination and software. Typical configurations involve using

three detection systems based on UV and DRI detectors combined with a LS detector (SEC-UV/LS/RI).[28-30]

The number average molecular weight (M_n), weight average molecular weight (M_w), and the polydispersity (PDI=M_w/M_n) of the PMS pre-polymers, were determined by gel permeation chromatography (GPC). Experiments were conducted on a series 1200 HPLC system (Agilent Technologies instrumentation) equipped with a Polymer Laboratories PLgel 5 µm mixed-C column and multi-detector system with a multi-angle laser light scattering (MALLS, miniDawn^{TM} TREOS laser photometer) (λ = 658 nm, 25 °C) and refractive index (RI, Optilab REX interferometric refractometer) (λ = 658 nm, 40 °C) detectors. The chromatograms were processed using Wyatt Technology software (ASTRA). THF was used as the mobile phase (eluent) at a flow rate of 1.0 mL/min at 40 °C, and samples were prepared at concentrations of 2 mg/mL.

ASTRA software has an "Online measurement" of the incremental refractive index (dn/dc) estimated by a single-injection method that works assuming that 100 % of the injected mass reaches the refractive index detector, that is, assumes 100% mass recovery from the columns. The steps below were followed to ensure a proper calculation of the M_w from the dn/dc of the system. **Table 2.7** summarizes the results obtained from each pre-polymer by analysis of the chromatograms using ASTRA.

- *Sample Preparation*: PMS pre-polymers were prepared with a concentration of 2 mg/mL in THF (from the same batch that the one used during the GPC analysis) using small volumetric flasks. The samples were perfectly dissolved and filtered with a syringe filter (0.2 µm pore size, PTFE) previous to injection.

- *Analysis of the results with ASTRA software*: After running the samples, the system automatically calculates the dn/dc from the peaks and recalculates the M_w and M_n considering the newly obtained values.[31]

Table 2.7. Gel Permeation Chromatography (GPC) results from each synthesized pre-polymer, where M_w is the weight average molar mass and M_n is the number average molar mass.

Sample	M_w (g/mol)	M_n (g/mol)
Pre-PMS 1:1	7501	6180
Pre-PMS 1:2	9360	8341

3.2. NUCLEAR MAGNETIC RESONANCE SPECTROSCOPY

3.2.1. FUNDAMENTALS

Nuclear Magnetic Resonance (NMR) spectroscopy is one of the most useful and versatile instrumental techniques for characterizing polymeric materials to provide valuable information regarding their structure. It exploits the magnetic properties of a certain atomic nuclei to obtain spectra that assist to a greater understanding of the detailed chain structure of polymers and copolymers, morphology, molecular motions and transitions in the solid state, as well as to allow the identification of intermediate structures formed during polymerization reactions. The main components of equipment for nuclear magnetic resonance measurements (**Figure 2.14**) are: a stable magnet with a controller to produce an accurate magnetic field, a radio frequency transmitter capable of emitting precise frequencies, a detector for measuring the absorption of radiofrequency energy from the sample, and a computer with a recorder for constituting the NMR plot spectrum.

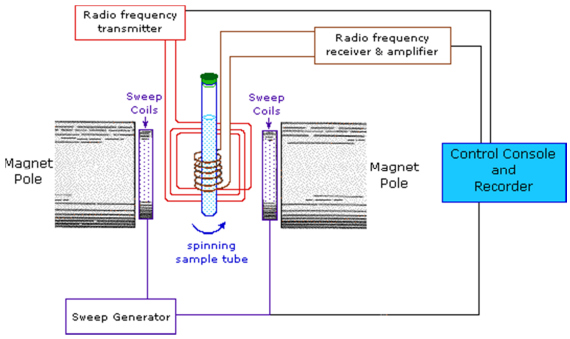

Figure 2.14. Basic arrangement of NMR spectrometer. The sample is positioned in the magnetic field and excited via pulsations in the radio frequency input circuit. The realigned magnetic fields induce a radio signal in the output circuit which is used to generate the output signal. Fourier analysis of the complex output produces the actual spectrum. The pulse is repeated as many times as necessary to allow the signals to be identified from the background noise.

Nuclear Magnetic Resonance (NMR) arises from the interaction (absorption or emission) of an applied electromagnetic radiation with nuclear spins when the energy levels in the latter are split by an external magnetic field.

Thus, the intramolecular magnetic field around an atom in a molecule changes the resonance frequency, thereby giving access to details of the electronic structure of a molecule. This technique can be used only for studying atomic nuclei with an odd number of protons or neutrons (or both). This situation occurs in the atoms of ^{1}H, ^{13}C, ^{19}F and ^{31}P. However more recently ^{14}N and ^{2}H are also being studied. For the vast majority of polymeric materials ^{1}H exists in high concentration and has been the subject of most of applications of NMR. The NMR of ^{13}C which occurs naturally in low abundance has been also widely studied.

These nuclei are magnetically active, i.e. possess spin (like the electrons), as the nuclei have positive charge and a rotation movement about an axis, them behave as small magnets. In the absence of magnetic field, the nuclear spins are randomly oriented. When a sample is placed in a magnetic field, the nuclei with positive spin are oriented in the field direction, in a minimum energy state (α spin state), while

nuclei with negative spin are oriented opposite to magnetic field in a higher energy state (β spin state), as it is shown in **Figure 2.15**.

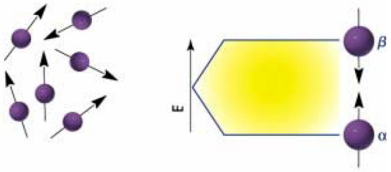

Figure 2.15. The energy difference between the two states α and β depends on the strength of the applied magnetic field H_0.

When a sample containing an organic compound is irradiated by an intense radiation pulse (rf, radio frequency), the nuclei in the α spin state moves towards the β spin state (is in resonance with the radiation). When nuclei return to their initial state emit signals with frequency dependant on the energy difference (ΔE) between α and β state. The NMR spectrometer detects these signals and records them as a plot of intensity versus frequency, which is called NMR spectrum. The dependence between frequency signal and the strength of magnetic field (H_0 in Teslas) can be expressed as:

$$\Delta E = h\upsilon = h\frac{\gamma}{2\pi}H_0 \tag{2.6}$$

, where γ is giromagetic radius which value depends on the nature of nuclei that is irradiated.

At the end, to obtain an NMR spectrum, a small amount of the organic compound dissolved in organic solvent onto a glass tube is charged within the magnetic field of the instrument. While the glass tube with the sample is rotated around its vertical axis, the magnetic field is kept constant and a short pulse of radio-frequency (rf) radiation excites all nuclei simultaneously. Like the short radio frequency pulse covers a wide frequency range, protons individually absorb the radiation frequency necessary to enter in resonance (change the spin state). As

such nuclei return to their initial position, they emit radiation of frequency equal to the energy difference between spin states. The intensity of this frequency decreases with time as all the nuclei return to their initial state. A computer collects the intensity versus time and converts the **data to intensity versus frequency (Figure 2.16)**, known as Fourier transform (FT-NMR).

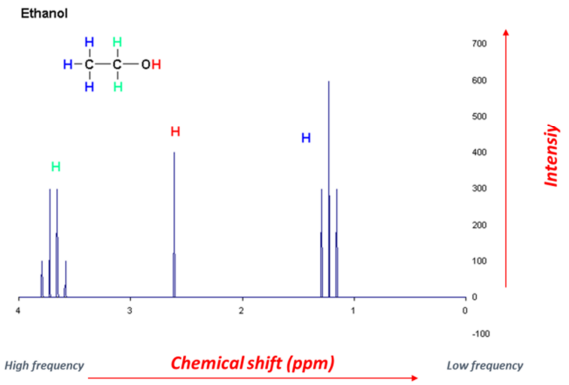

Figure 2.16. Example of ^{1}H-NMR spectrum of ethanol plotted as signal intensity vs. chemical shift (frequency δ).

3.2.1.1. STRUCTURAL DETERMINATION

As was mentioned before, NMR spectrum is used for structural determination of molecules, by taking into account several phenomena. First, the protons (atoms) forming organic molecules are surrounded by electrons which orbit the nucleus, thus, the resonance frequency of these protons depends on the electronic environment. That means the small induced magnetic field (opposite to the external field) produced by the electrons will slightly change the magnetic field experienced by the nucleus causing changes in the energy levels. The fact that nuclei experience different magnetic fields due to the local electronic interactions will cause that same nuclei resonate at different frequency (creates a new peak in the NMR spectrum) depending on the surrounding environment. This phenomenon is known as **nuclear shielding (Figure 2.17)**, as the magnetic field that reaches the

proton (H_{ef}) is weaker than the external field, it means that it is protected or shielded, and therefore, the external magnetic field have to be higher, to make the nuclei resonate:

$$H_{ef} = H_0 - H_{loc} \tag{2.7}$$

If all protons (^{1}H) of an organic molecule were shielded, the same combination of frequency and magnetic field will make them resonate. However, protons are within different electronic environments and therefore are differently shielded.

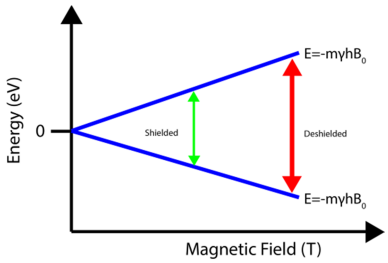

Figure 2.17. The effect that shielding from electrons has on the splitting of the nuclear energy levels. Electrons impart their own magnetic field which shields the nucleus from the externally applied magnetic field. Note that this effect is greatly exaggerated in this illustration.

Variations in the absorption frequencies due to the different shielding of nuclei are known as chemical shifts (δ units or ppm). Usually, these small changes or chemical shifts values are expressed accurately with respect to a reference compound with a single strong absorption at lower fields (most commonly used is tetramethylsilane (TMS, $(CH_3)_4Si$) added into the sample. Chemical shifts response then to:

$$\delta(ppm) = \frac{\upsilon_{sample} - \upsilon_{reference}}{\upsilon_{reference}} x10^6 \tag{2.8}$$

Taking into account that the NMR signal intensities are directly proportional to the number of nuclei causing the signal, is possible to know stoichiometric ratios of polymerization reactions by **integrating NMR** spectra. Thus, the area under the NMR resonance is proportional to the number of hydrogens (in case of ^{1}H-NMR

spectra) which that resonance represents. In this way, by measuring or integrating the different NMR resonances, information regarding the relative numbers of chemically distinct hydrogens can be found. Thereby, the chemical composition of a sample can be determined by calculating the ratios of the signal integrals.

3.2.2. EXPERIMENTAL PROCEDURE

In order to verify the chemical structures of the synthesized PMS pre-polymers, ^{1}H-NMR characterizations were performed on a Varian Mercury VX-300 MHz NMR spectrometer. The samples were prepared dissolving each pre-polymer in 750 μL of deuterated dimethylsulfoxide (DMSO-d_6) at room temperature in a glass tube, with tetramethylsilane (TMS) added as an internal standard.

Figure 2.18 shows an integrated ^{1}H-NMR spectra, for 1:2 ratio pre-PMS, as example.[1, 32] As could be seen, five different hydrogens groups that give a resonance in the NMR spectra are distinguished. Peaks from the mannitol appeared at 3.5-5.5 ppm due to central and terminal methylene units identified by hydrogens on the carbons “a” and “b”. The protons from the methylene units of sebacic acid showed peaks at 1.3, 1.6 and 2.3 ppm identified by hydrogens on the carbons “c”, “d” and “e” respectively. The peak at 2.5 is due to the solvent used (deuterated dimethylsulfoxide, DMSO- d_6), and the peak at 3.3 was due to residual water.[33]

The composition (stoichiometric ratio) of the pre-polymers was then determined from the ratio of the integrals of the signals associated with the mannitol and sebacic acid peaks, based on previously reported works.[1]

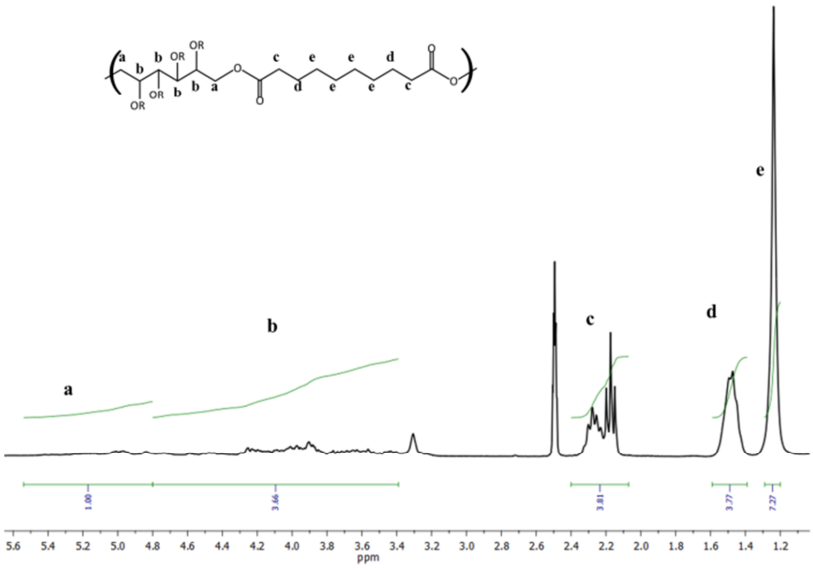

Figure 2.18. Integrated ^{1}H NMR spectrum for PMS 1:2 purified pre-polymer.

3.3. FOURIER TRANSFORM INFRARED ANALYSIS

3.3.1. FUNDAMENTALS[34-36]

As one of the few techniques that can provide information about the chemical bonding of an extremely wide variety of materials, it is particularly useful for the non-destructive analysis of solids and thin films, for which there are few alternative methods. Liquids and gases are also commonly studied, more often in conjunction with other techniques. Chemical bonds vary widely in their sensitivity to probing by infrared techniques.

As it is shown in **Figure 2.19** the term infrared refers to that part of the electromagnetic spectrum between the visible and microwave regions. Electromagnetic spectrum refers to the seemingly diverse collection of radiant energy, from cosmic rays to X-rays to visible light to microwaves, each of which can be considered as a wave or particle traveling at the speed of light.

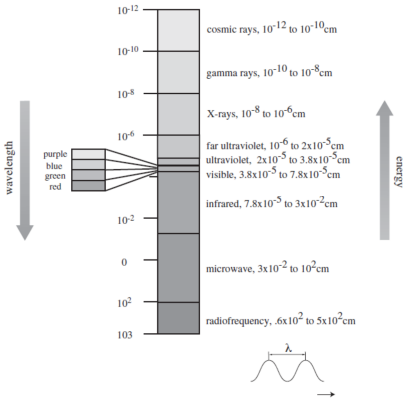

Figure 2.19. The electromagnetic spectrum. Adapted from 36.

These waves differ from each other in the length λ (wavelength measured in *cm*) and frequency ν (measured in $Hz = s^{-1}$) that are inversely related:

$$\nu = c \cdot \lambda^{-1} \tag{2.9}$$

At the same time both terms are associated to the energy, which is directly proportional to frequency and inversely proportional to wavelength by means of:

$$E = h \cdot \nu \tag{2.10}$$

, where h is the Planck´s constant (6.6×10^{-34} J·s^{-1}).

As it is shown in **Figure 2.20**, in wavenumbers the mid IR range is 4000-400 cm^{-1} (3-30 μm wavelength) an increase in wavenumber corresponds to an increase in energy. Infrared radiation is absorbed by organic molecules and converted into energy of molecular vibration, thus, a transition occurs from a ground vibrational state to an excited vibrational state. In FTIR spectroscopy, an organic molecule is exposed to infrared radiation. When the radiant energy matches the energy of a specific molecular vibration, absorption occurs.

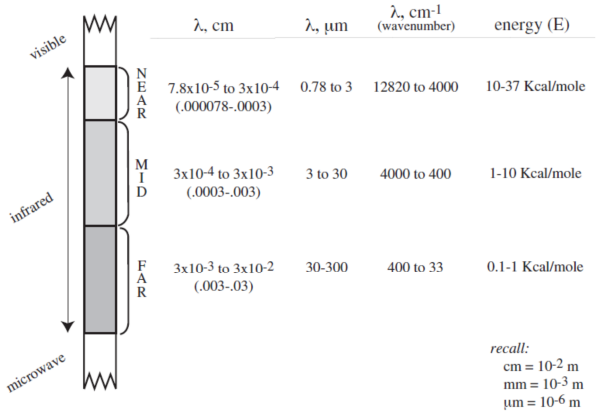

Figure 2.20. The IR regions of the electromagnetic spectrum. Adapted from 36.

The wavenumbers (sometimes referred to as *frequencies*) at which an organic molecule absorbs radiation give information on functional groups present in the molecule allowing gathering information about the structure of a sample. Certain groups of atoms absorb energy and therefore, give rise to bands at approximately the same frequencies in an infrared spectrum. The potential utility is that FTIR spectrum is like a molecular fingerprint which means that different molecular structures produce different infrared spectra.

The goal of the basic infrared experiment is to determine changes in the intensity of a beam of infrared radiation (typically *y*-axis in a plot) as a function of wavelength or frequency (typically *x*-axis in a plot) after it interacts with the sample.

Defining I_o as the intensity of the light incident upon the sample and I as the intensity of the beam after it has interacted with the sample, an infrared experiment determine the intensity ratio I/I_o as a function of the frequency of the light (ν). A plot of this ratio versus the frequency is the infrared spectrum. The infrared spectrum is commonly plotted in one of three formats: as transmittance,

reflectance, or absorbance. First format (transmittance) measures the fraction of light transmitted through the sample, and this ratio is defined as:

$$T_\nu = \left(\frac{I_T}{I_o}\right)_\nu \tag{2.11}$$

, where T_ν is the transmittance of the sample at frequency ν, and I_T is the intensity of the transmitted light. Similarly, if the light reflected from the surface of the sample is measured (second plot format, reflectance), then the ratio is equated to the reflectance of the spectrum (R_ν), thus I_T is replaced with the intensity of the reflected light I_R. Absorbance (the third format), is related to transmittance by the Beer-Lambert Law:

$$A_\nu = -\log(T_\nu) = \varepsilon_\nu \cdot b \cdot c \tag{2.12}$$

, where c is the concentration of chemical bonds responsible for the absorption of infrared radiation, b is the sample thickness (optical path), and ε_ν is the frequency-dependent absorptivity, a proportionality constant that must be experimentally determined at each ν by measuring the absorbance of samples with known values of $b \cdot c$. Beer-Lambert Law provides a simple foundation for quantitating FTlR spectra being easier to obtain quantitative results when collecting an absorbance spectrum, however, main goal of FTIR experiment is to obtain qualitative information more than quantitative, but still, absorbance format dominates because to first order it is a linear function of concentration.

In addition, different accessories have been developed to allow the measurement of different sample geometries. By using a configuration with an Attenuated Total Reflection (ATR) crystal (typically of diamond, germanium or an alloy of zinc and selenium), the infrared beam is directed into the crystal (**Figure 2.21**). Exploiting the principles of a waveguide, the change in refractive index at the crystal surface causes the beam to be back-reflected several times as it propagates down the

length of the crystal before it finally exits to the detector. If the sample is put into contact with the crystal surface, the beam will interact weakly with the sample at several points.

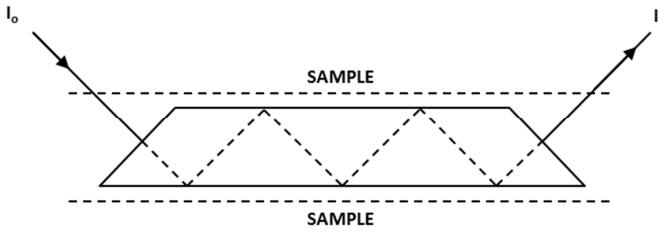

Figure 2.21. Typical beam path configuration for FTIR spectrum using an ATR accessory.

As was mentioned before, certain atoms absorb energy and give rise to bands in an infrared spectrum. The molecular vibrations behind this are of two fundamental types, stretching and bending. **Figure 2.22** shows them in a simple case of water molecule.

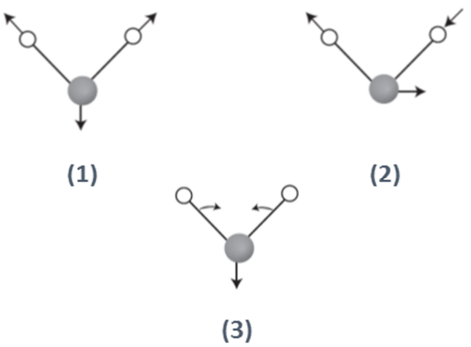

Figure 2.22. Stretching and bending fundamental vibrational modes. (1) Symmetrical stretching (2) anti symmetrical stretching (3) Bending (scissoring). Adapted from 36.

As vibration modes depends on the linearity or non-linearity of the molecule as well as the surrounding scenario, these fundamental modes can combine and

multiply to give rise to numerous other modes of vibration, such as the in-plane and out-of plane alternatives.

3.3.2. EXPERIMENTAL PROCEDURE

The FTIR spectra of all the samples were collected in a Thermo Nicolet 5700 spectrometer (Thermo Fisher Corporation, MA, USA) equipped with Attenuated Total Reflection (ATR) cell, in the 500 to 4500 cm^{-1} region with a 4 cm^{-1} resolution. All samples were vacuum dried before measurement and in order to obtain accurate results, 32 scans were performed to complete each spectrum in at least 4 locations on the sample. Furthermore, background was acquired before every 3rd sample measurement and the effect of atmospheric CO_2 was corrected and subtracted from each spectra. Baselines, refractive indexes and incident angles corrections were also applied.

Qualitative identification of functional groups in the samples was performed by identifying the characteristic wavenumber of vibration, thus, examining peak position in the obtained spectra, the formation of polyesters and the presence of nanofillers (CNC nanoparticles and PLA nanofibers) were verified. Also, the extent of curing (crosslinking) in the materials was evidenced by changes in intensity of –OH and –COOH peaks and appearance of new peaks concerning creation of new ester bonds (C=O and C–O). All the spectra were normalized with respect to the 2926 cm^{-1} peak, as it is a characteristic band in the skeleton of the polymer that doesn't change with the extent of curing. Also, it is commonly used for normalization in the literature as it does not participate in the esterification reaction. This approach is useful to correct possible variations arisen from defects in surface quality or sample positioning. Same protocol was followed to obtain infrared spectra of all degraded samples (after 150 days of immersion in SBF) in order to analyse possible new peaks that evidence degradation processes.

3.4. X-RAY DIFFRACTION (XRD)

3.4.1. FUNDAMENTALS[37, 38]

X-ray diffraction is the most widely used technique to determine the arrangement of atoms of a crystalline solid in a three dimensional space. In comparison with other diffraction techniques, XRD do not directly identify the atoms involved, but give long-range order information on atomic positions from diffraction patterns. Owing to the huge data bank available covering practically every phase of every known material (powder diffraction patterns), it is routinely possible to identify phases in poly-crystalline bulk materials, measure their structural properties (average unit cell dimensions, symmetries, orientations) and determine their relative amounts from diffraction peak intensities. It is also used to determine the thickness of thin films and multilayers, and atomic arrangements in amorphous materials including polymers.

X-ray diffraction is based on constructive interference of monochromatic X-rays and a crystalline sample. The X-ray wavelength λ is typically 0.7-2 Å (wavelength in between UV and γ rays), which corresponds to X-ray energies (E = 12.4 keV/λ) of 6-17 keV. These X-rays are generated by a cathode ray tube, filtered to produce monochromatic radiation, collimated to concentrate, and directed toward the sample. As the sample and detector are rotated, the intensity of the reflected X-rays is recorded. The interaction of the incident rays with the sample produces constructive interference (and a diffracted ray) when conditions satisfy Bragg's Law, resulting in a peak in intensity (**Figure 2.23**). A detector records and processes this X-ray signal and converts the signal to a count rate which is then output to a device such as a printer or computer monitor.

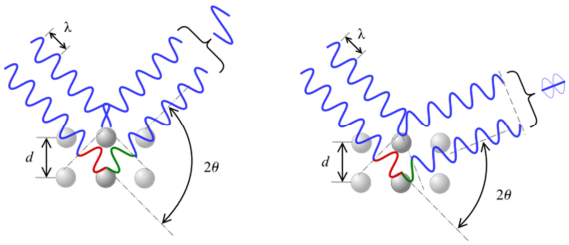

Figure 2.23. According to the 2θ deviation, the phase shift causes constructive (left figure) or destructive (right figure) interferences.

Bragg´s law relates the wavelength of electromagnetic radiation to the diffraction angle and the lattice spacing in a crystalline sample:

$$n\lambda = 2d_{dkl}\sin\theta \tag{2.13}$$

, where d_{hkl} is the spacing between Miller planes (layers of atoms), θ is the angle between the incident/scatter rays and the surface of the specimen, n is an integer that indicates the order of diffraction and λ is the wavelength of the X-rays. Therefore, Bragg´s law is a simple model that defines the geometric conditions that must be met for the phenomenon of diffraction to occur. To explain the diffraction phenomenon in crystals, it is assumed that parallel planes of atoms act as "mirrors" for incident beam, so each family of planes reflects (diffracts) a fraction of the incident radiation and transmit the rest. These diffracted X-rays are then detected, processed and counted. By scanning the sample through a range of 2θ angles, all possible diffraction directions of the lattice should be attained. Conversion of the diffraction peaks to d-spacings allows the identification of the sample. Typically, this is achieved by comparing the d-spacings with standard reference patterns.

Figure 2.24 shows the basic features of an XRD experiment where X-rays are generated in an X-ray tube. These X-rays are directed at the sample and the diffracted rays are collected, where the diffraction angle 2θ is the angle between the incident and diffracted X-rays. In a typical experiment, the diffracted intensity is

measured as a function of 2θ and the orientation of the specimen, which yields the diffraction pattern and arrangement of their atoms in space by Fourier analysis.

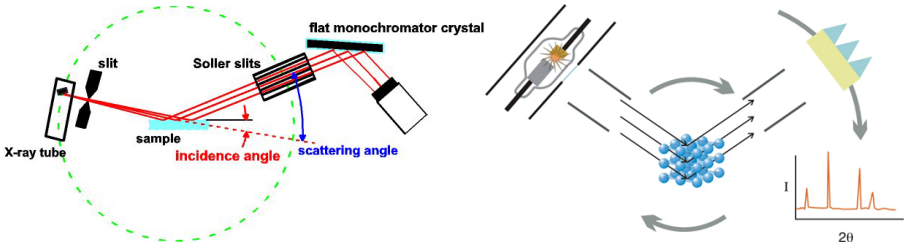

Fig 2.24. Schematic representation of how crystalline structure (shown diagrammatically in the left figure as a latticework of atoms) may be determined through X-ray diffraction. As the crystal and detector rotate, X-rays diffract at specific angles. The detector reports the intensity (I) of X-ray photons as it moves. Angles of diffraction (where the Bragg equation is satisfied) are marked by peaks. The peak height is a function of the interaction of the X-rays with the crystal and the intensity of the source. With respect to the Bragg equation, we are looking for d as we change theta (lambda λ, is constant).

Although this technique is applicable to solid, liquid or gaseous samples, in the field of polymers its use is restricted almost entirely to the determination of the atomic arrangement in the solid crystalline part.

3.4.2. CALCULATION METHODS

Main applications of this technic are related to the identification of unknown crystalline materials (i.e. minerals, inorganic compounds). Other applications include the characterization of the percentage of apparent crystallinity in semicrystalline polymers or crystalline materials. As was explained above, the intensity of diffracted X-rays is continuously recorded as the sample and detector rotate through their respective angles. A peak in intensity occurs when the mineral contains lattice planes with d-spacings appropriate to diffract X-rays at that value of θ. Thus, results are commonly presented as peak positions at 2θ and X-ray counts (intensity) in the form of an x-y plot. From this plot, determination of **percentage of apparent crystallinity** is possible based on the relative intensity of specific peaks, by the following equation:

$$A.C = 100\ \frac{I_c}{I_c + I_{(non\ crystalline)}}\ [\%] \tag{2.14}$$

, where $A.C$ means apparent crystallinity, I_c is the total area under the crystalline peaks and $I_{(non\ crystalline)}$ is the total area under the non-crystalline peak region.

3.4.3. EXPERIMENTAL PROCEDURE

In the present thesis, X-Ray diffractograms were obtained by wide-angle X-ray diffraction (WAXS, RX Siemens D5000, Germany) equipped with a Cu Kα source (λ = 1540 A) operating at 40 kV. The scanning range was from 2 to 40°, step-size and count time per step were 0.02° and 8 seconds respectively. This technique has been used to confirm the structure of hydroxyapatite (HA) and cellulose nanocrystals (CNCs) according to ICDD (International Centre for Diffraction Data)[39, 40] and previously reported literature.[41, 42] CNCs sample was dispersed in water and dried in oven at 100 °C for 0.5h. After drying, the obtained compact powder was re-grounded and transferred to a quartz holder. HA sample was directly compacted into the quartz holder.

Percentage of apparent crystallinity was also estimated from the ratio of the crystalline area peaks to the total area including the non-crystalline peaks for hydrolysed CNCs and electrospun mats of PLA and PLA/HA following the previous mentioned equation. Electrospun samples were directly cut from the middle regions of mats with the dimensions of quartz holders. The percentages of crystallinity were calculated by a fitting process using a deconvolution method of the peaks. A peak fitting program (PeakFit; www.systat.com) was used and Gaussian shaped peaks were assumed and let free for intensity, position and FWMH after background subtraction while non-crystalline peak was fixed at position.

3.5. SCANNING ELECTRON MICROSCOPY

3.5.1. FUNDAMENTALS[43, 44]

Basically, in scanning electron microscopy (SEM) (**Figure 2.25**) a beam of high-energy electrons (keV energy) is focused (in vacuum) to generate a variety of signals when scanning the surface of the solid specimens. As the electrons hits the surface, the signals that derive from electron-sample interactions result in the emission of electrons or photons from (or through) the surface revealing information about external morphology (tophography), chemical composition, and crystalline structure and orientation. At the end, the main role in this thesis is to produce images that are good representations of three-dimensional shape of the sample.

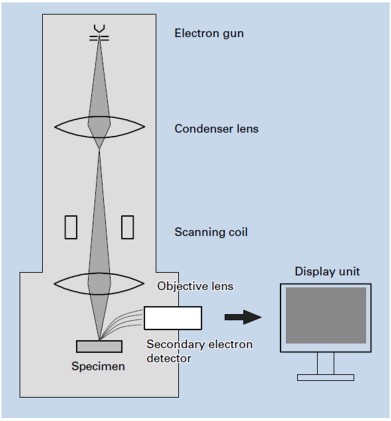

Figure 2.25. Basic construction of a SEM, adapted from 44.

When the high-energy primary electron beam interacts with an atom, some amount of energy can exit from the solid mainly as an emitted electron and electromagnetic waves. Main signals derived from electron-sample interactions define three principle “images” that can be produced by SEM:

- **Secondary electron images (SE):** Electrons involved in this process, leave the specimen with an upper energy limit of 50 eV. Typically, secondary electrons able to be detected are produced within the first few nm of the surface, there are much more produced much deeper in the material but due to their lower energy cannot escape from the solid been quickly absorbed by the specimen. These electrons are commonly used for imaging samples and are the most valuable for showing morphology and topography of the surface with excellent contrast.
- **Backscattered electron images (BSE):** Electrons involved in this process leave the specimen with an amount of energy comparable to the energy of the primary electron beam. They are sometimes called reflected electrons, and by convention they are referred to have energy greater than 50 eV. Since they possess higher energy than secondary electrons, they can offer information from a relatively deep region. Thanks to their sensitivity to the specimen composition, they are commonly used for imaging samples by illustrating contrasts in composition in multiphase samples (e.g. for rapid phase discrimination).
- **Elemental X-ray maps:** Electrons involved in this process result when the primary electron beam hits and ejects an inner-core electron from an atom in the sample. The vacancy left by the ejected electron is filled with an outer-core electron and the substance emits a characteristic X-ray photon whose energy (wavelength) is characteristic of the element. Thus, the characteristic X-rays are used for elemental analysis. Some other different X-rays can be emitted such as “continuous X-rays”, “white X-rays” or “background X-rays”. Importantly, these interactions are especially useful in qualitatively or semi-qualitatively analysis, to identify the elements present in a specimen, thus, its chemical composition.

3.5.2. EXPERIMENTAL PROCEDURE

Morphological investigation of the obtained samples, was carried out by means of a JEOL JSM6030 Scanning Electron Microscope (Tokyo, Japan). Nanofiber mats samples were prepared by cutting square pieces from randomly chosen parts of the processed specimen, while nanocomposites were cryo-fractured under liquid nitrogen (at least three different parts of each specimen were analysed). These pieces were mounted on metal studs and sputter-coated with ~ 2nm gold layer using a LEICA EM MED020 sputter coater (Wetzlar, Germany), to prevent the accumulation of static electric fields in the specimen due to electron irradiation, as well as to confer enough conductivity to the sample. Operating conditions were set at 10 kV accelerating voltage, 10-15 mm working distance and vacuum conditions (pressure below 10^{-4} Torr).

ImageJ software (National Institute of Health in USA) was used to evaluate the diameters and the alignment of the PLA and PLA/HA nanofiber mats from the SEM micrographs obtained (x5000). Diameters and fiber orientation angle were calculated as an average of 30 randomly measures, angle was measured between the long axes of the fibers and the vertical axis of the image.

3.6. TRANSMISION ELECTRON MICROSCOPY

3.6.1. FUNDAMENTALS[45]

In transmission electron microscopy (TEM) (**Figure 2.26**) as in SEM, a focused electron beam is used, but in this case, the beam is **transmitted** through an ultra-thin specimen (preferable less than 200 nm of thickness), interacting with the specimen as it passes through. For most materials this insures the retention of high coherency of the incident source as well as relatively few scattering events as each electron traverses the sample. The signal to form the image is obtained from both, **non-scattered and scattered** electrons that penetrate the sample thickness. A

series of magnetic lenses, at and below the sample position, deliver the signal to a detector such a fluorescent screen, a photographic film or a video camera where the image is focused and magnified. Accompanying this signal, transmission is a magnification of the spatial information in the signal by as little as 50 times to as much as a factor of 10^6. This remarkable magnification range is facilitated by the small wavelength of the incident electrons, and it is the key to the unique capabilities associated with TEM analysis.

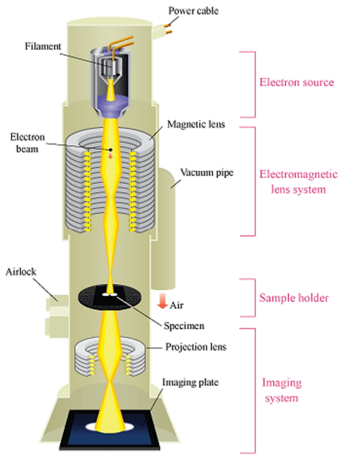

Figure 2.26. Basic construction of a TEM.

TEM is capable of imaging at a significantly high resolution. The high lateral spatial resolution in a TEM instrument is a consequence of the use of a highly focused electron beam as a probe. This probe focuses on the specimen in a small spot, often 1 μm or less in diameter. The probe's source is an electron gun designed to emit a highly coherent beam of monoenergetic electrons of exceedingly small wavelength. The wavelength (λ) of 100 keV electrons is only 0.0037 nm, much smaller than that of light, X-rays, or neutrons used in other analytical techniques. Having such small wavelengths, since electrons in a TEM probe are in phase as they enter the specimen, their phase relationships at exit are correlated with spatial associations between scattering centres (atoms) within the material. This enables

the examination in fine detail, even as small as a single column of atoms. One of TEM applications is the study through the images of the size, shape and dispersion of small particles whether incorporated or not in a matrix. A second application is the identification of crystal structure of crystalline particles by electron diffraction. Although TEM has no inherent ability to distinguish atomic species, nonetheless, electron scattering is exceedingly sensitive to the target element.

A TEM image is made up of non-scattered electrons (which strike the screen) and scattered electrons which do not, and therefore appear as a dark area on the screen. Heavy atoms, having large positively charged nuclei, scatter electrons more effectively and to higher angles of deflection than do light atoms. Thus, the heavier the interacting atom, the darker the spot on the screen.

Main imaging modes operated in TEM are (**Figure 2.27**):

- **Bright field mode:** In this mode the contrast formation is formed directly by occlusion and **absorption** of electrons in the sample. Thicker regions of the sample or regions with a higher atomic number will appear dark, whilst regions with no sample in the beam path will appear bright. This is the most common mode of operation in which the image is a simple two dimensional projection of the sample down the optic axis.
- **Diffraction contrast or dark field mode:** In this mode, the samples exhibit **diffraction** contrast, whereby the electron beam undergoes Bragg scattering. The desired Bragg reflections can be selected or excluded thus only parts of the sample that are causing the electrons to scatter to the selected reflections will end up projected onto the imaging apparatus. If the reflections that are selected do not include the non-scattered beam, the image will appear dark wherever no sample scattering to the selected peak is present. Thus, a region without a specimen will appear dark.

Typical applications are grain size determination and detection of second-phase particles.

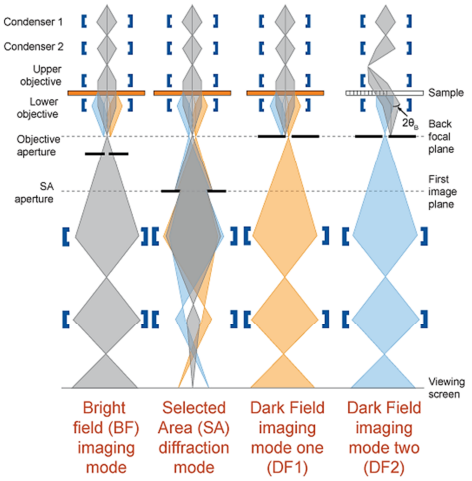

Figure 2.27. Diagram showing beam paths for the different imaging modes.

3.6.2. EXPERIMENTAL PROCEDURE

A FEI/Philips CM10 Transmission Electron Microscope (Oregon, USA) was used to analyse PLA/HA nanofibers morphology as well as to verify if the HA nanoparticles were inside the fibers. A few fibers were electrospun onto a carbon-coated copper grid (Electron Microscopy Sciences) and observed at 100kV. This analytical technique was also employed to evaluate the dispersion of the CNCs into PMS nanocomposites. In this regards, thin cross sections (thickness 3–10 mm) were cut from nanocomposites under cryogenic conditions using a Leica CM1950 cryostat; they were stained with 2% aqueous uranyl acetate on carbon-coated copper grids and observed at accelerating voltage of 80kV. At least two cut slides from different parts of each sample were analysed to verify the dispersion and incorporation of the CNCs into the composite. Visual control of all the samples was also carried out to confirm the dispersion of the CNCs along the matrix.

Dimensions and aspect ratio of CNCs obtained from hydrolysis process were calculated as an average of randomly measures in TEM (80 kV) images at different magnifications. Several samples were prepared by drying a drop of dilute whiskers suspension in distilled H_2O (0.1 mg/mL) onto a carbon-coated copper grid (Electron Microscopy Sciences) and subsequently dried under a lamp for 1h. ImageJ software (National Institute of Health in USA) was used to evaluate the length and width of the CNCs.

3.7. DIFFERENTIAL SCANNING CALORIMETRY

3.7.1. FUNDAMENTALS[46]

Differential Scanning Calorimetry (DSC) is a thermal analytical tool for characterizing physical properties of a sample as changes in its heat capacity (Cp) by temperature. Briefly, a sample of known mass is heated or cooled and the changes in its heat capacity are tracked as changes in the heat flow. This technique allows the determination of transitions such as melting, crystallization, and glass transition temperatures, as well as the corresponding enthalpy and entropy changes. Because of this flexibility, simplicity and ease of use, is widely applied in polymer science.

Commonly, DSC contains two pans isolated from the ambient environment in a chamber, one pan has the sample to be analysed, and the other pan is empty or filled with an inert material that acts as a reference sample (**Figure 2.28**). The essential feature is then the record of differential measurements, thus it is the measure of the different amounts of heat required to equalize the temperature of the sample and the reference to follow the same temperature program.

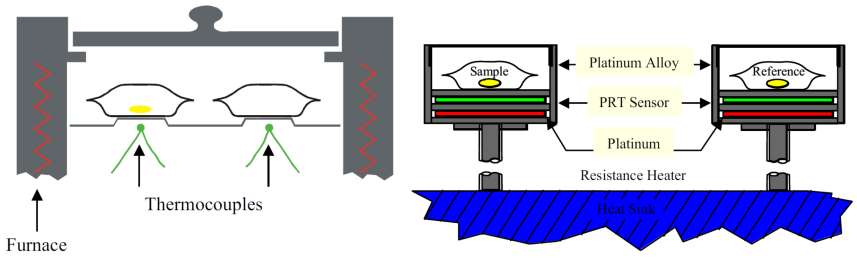

Figure 2.28. Different configurations of DSC with differences into disposal sample and reference.

There are several DSC configurations, but the most common is based on a set of heaters under both pans at a constant rate ($\Delta T/\Delta t$), thus, the same power is supplied to both microfurnaces during heating through the control circuit. If there is thermal symmetry, the temperature in both microfurnaces is equal (thus, there is null balance). But when an asymmetry occurs (i.e. a chemical or physical transition involves the release or absorption of heat), a temperature difference is registered between both microfurnaces containing sample and reference due to their different heat capacity. Then, this temperature difference is compensated electronically by proportional control, either increasing or decreasing the heat flow, which is the rate at which thermal energy ($\Delta Q/\Delta t$), is supplied to the pans.

Thus, the differential measurements will be proportional to heat flow between the reference and sample, which at the end is the heat flow for the sample.

3.7.2. CALCULATION METHODS

As was mentioned, DSC experiments display heat flow as a function of the temperature or time, which are denoting different thermal transitions of the sample under study. **Figure 2.29** shows a DSC trace for neat PLA nanofibers mat collected at low speed (LCR), corresponding to first and second heating and intermediate cooling. This graph exemplifies the observation of the glass transition, melting and crystallization transitions that can be detected by DSC.

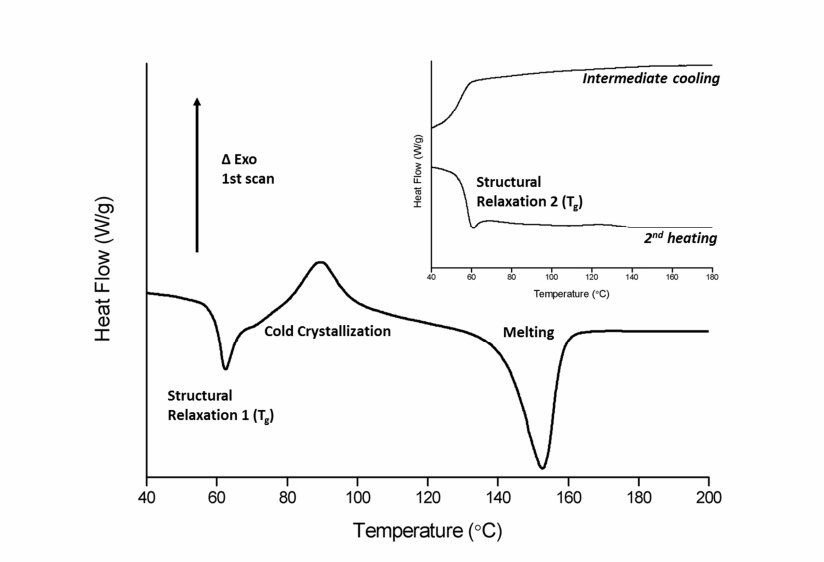

Figure 2.29. DSC trace showing a first heating, an intermediate cooling and a second heating, exemplifying main transitions detected.

Characterization of DSC curves depends on which phenomenon is analysed:

Direct parameters

- **Glass transition** has no latent heat associated with it, and such transitions are referred to as second order transitions. The glass transition temperature is usually measured as the midpoint of the jump in change of heat capacity. In this work, the ISO-11357-2 was followed.
- The **crystallization** and **melting** are first order transitions as latent heat is associated with them. Crystallization is an exothermic process that releases energy, while melting is an endothermic process that absorbs energy. Any material that melts must first crystallize, if crystallization was produced during the heating ramp, and it is known as glass or cold-crystallization. In the same way when the melt is cooled, crystallization from the melt is visible in the cooling ramp. Both transitions are measured or characterized by the onset temperature of the process and peak

temperatures. Area under the thermal phenomenon in relation to a baseline may be used to find the latent heat of melting or crystallization.

Amorphous and crystalline fractions

This technique also allows the measurement of the crystalline percentage (X_c%) in semicrystalline polymers, and it is calculated as follows:

$$X_c\% = \frac{\Delta h_m - \Delta h_c}{\Delta h_m^0} \tag{2.15}$$

, where Δh_m and Δh_c represent the specific melting and cold-crystallization enthalpies ($J \cdot g^{-1}$) and Δh_m^0 the melting enthalpy of the fully crystalline polymer under study. Enthalpies were measured through the area under the corresponding peaks.

3.7.3. EXPERIMENTAL PROCEDURE

DSC analysis for all the developed samples in this thesis were carried out by a Mettler-Toledo DSC 800 instrument (Columbus, OH) calibrated with indium standards. Approximately 5 mg of sample were placed in 40 µL aluminium sealed pans. The pans were pierced to allow the N_2 gas flow over the sample (50 $mL \cdot min^{-1}$). Samples were programed to be analysed over a heating/cooling/heating program at 10 °C·min^{-1} heating rate, with the temperature ranging from 30 to 220 °C for nanofibers of PLA and PLA/HA, and -60 to 180 °C for PMS and all its CNC nanocomposites. The samples were characterized at least by duplicate.

Glass transition temperatures (T_g) were calculated for all the developed samples, melting (T_m) and cold crystallization (T_{cc}) transitions, as well as crystalline percentages (X_c%) were also studied and calculated for all the electrospun mats following the calculation methods previously mentioned.

3.8. THERMOGRAVIMETRY (TGA)

3.8.1. FUNDAMENTALS[47]

Thermogravimetry or Thermogravimetric Analysis (TGA) is usually employed to complement DSC analysis by studying the thermal stability and the fraction of volatile components in a sample by monitoring mass changes as a function of temperature or time in an instrument with the configuration showed in **Figure 2.30**. The analysis can be done dynamically by employing a temperature-controlled program that heats at constant speed or in isothermal conditions as a function of time. In both cases, weight loss or weight loss rate for each temperature or time is determined, directly associated either to the elimination of volatile or to a chemical process.

The results from a thermogravimetric analysis are presented in a thermogram or thermogravimetric curve (TG) where *X*-axis usually displays temperature and *Y*-axis the weight (mg) or weight percent (%). Individual processes of mass loss correspond to sigmoidal stages in the TG curve. The number of steps depends on the chemical nature of the components, composition of the sample or the gas atmosphere. The amount of mass remaining at the end of the experiment is assigned to the residue or non-degraded part of the sample. It is also common to analyse the first derivative (DTG) of the thermogravimetric curve whose maximum peak corresponds to the maximum falling slope of the thermogravimetric curve. By using an inert gas such as Ar, an inert environment is simulated aiming to determine the thermal stability as only effect of temperature; more realistic scenarios can be performed by using reactive gases, such as O_2. In this sense, TGA can be used for testing thermo-oxidative decomposition behaviour of the samples.

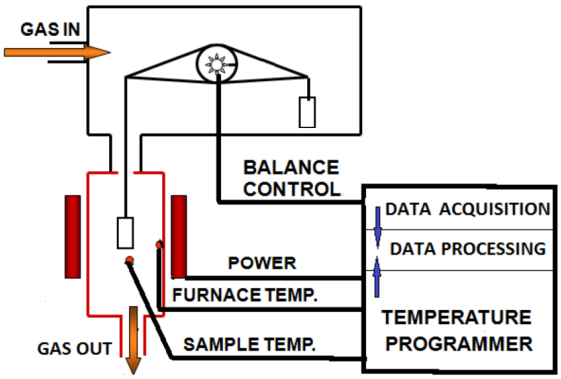

Figure 2.30. TGA instrument configuration. Adapted from 47.

Physical and chemical processes occurring during thermal degradation of a polymer depend on the nature of the material. However, in general, thermal decomposition processes of a polymeric material, regarding to mass loss as a function of temperature, measured in a thermo-balance follow a similar basic pattern consisting on the following main steps:

- Weight losses at moderate temperatures, typically T < 150 °C, corresponds to a loss of highly volatile matter such water, organic solvents or low molecular weight gases absorbed.
- In the range of 150-250 °C, matter of medium volatility is lost, such as additives, water of crystallization and plasticizers. Even, first decomposition products can be detected.
- At temperatures above 225-250 °C, thermal degradation is normally initiated, which evolution depends on the type of atmosphere used during the test (inert or oxidative).
- At T>500 °C charring occurs for hydrocarbon compounds which thermal degradation does not lead to the formation of volatile fragments. Waste is left after their oxidative decomposition along with ashes of inorganic fillers or additives which are not degradable.

3.8.2. EXPERIMENTAL PROCEDURE

Non-isothermal thermogravimetric experiments in this thesis were carried out in a Mettler-Toledo TGA/STDA 851[e] (Columbus, OH, USA). Samples weighing ~5 mg were heated in alumina holders with 70 µL of capacity. Experiments were performed in O_2 atmosphere (50 mL·min^{-1}) from 25 to 700 °C, at heating rate of 10 °C·min^{-1}, for assessing the thermo-oxidative decomposition processes. Experiments were repeated at least two times. Thermal stability temperatures were obtained as onset temperatures (T_o), obtained by a tangential intercept method onto the TG curve.

3.9. TENSILE TESTING

3.9.1. FUNDAMENTALS[48]

In materials science, tensile properties of a material are often used to predict the behaviour under loads. In this regards, the strength of a material is measured as the ability to withstand an applied stress without failure. Most common conformations of the applied stress are as a tensile, compressive, bending or shear.

In a tensile test, by applying a force on a material using a uniaxial load, internal forces (stresses) that cause deformations (strain) are induced over it until failure, while the reaction of the material can be readily recorded and analysed. Thus, stress and strain are the two basic magnitudes in a mechanical experiment that are determined from measuring the load and deformations using the original specimen cross-sectional area and length. When the stress is plotted against the strain, the result is the stress-strain curve, as shown in **Figure 2.31**. As the material is typically stretched until it breaks, analytical methods are applied to define the strength of the material based in concepts of stiffness and stability that are thoroughly explained in the ISO 527-1. The results obtained by analysing the stress-strain plot are commonly used to material selection or quality control.

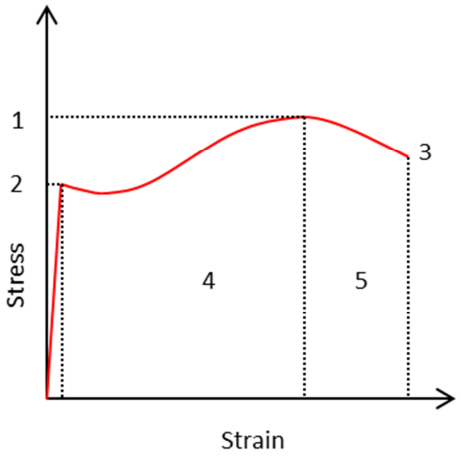

Figure 2.31. Typical stress-strain curve for a ductile material. (1) Ultimate strength, (2) yield strength, (3) rupture, (4) strain hardening region and (5) necking region.

The main properties obtained from a tensile test relative to the characterization of mechanical behaviour performed in this thesis are the **Young´s modulus, ultimate tensile stress, strain at break and toughness:**

- **Young´s modulus** is a constant of proportionality that correlates strain and stress in a tensile test in the linear part of the curve where materials obey Hooke´s law. The knowledge of the elastic properties describing the reversible deformation behaviour is a fundamental requirement for the design of dynamically loaded components such as biomaterials inside the body. As strain is increased many materials deviate from this linear proportionality that is usually associated with stress-induced "plastic" flow in the specimen due to a rearrangement of the internal molecular structure. Young´s modulus (E), can be calculated using the following equation:

$$E = \frac{\sigma}{\varepsilon} \tag{2.16}$$

- **Ultimate tensile strength (UTS),** is the maximum stress that a material can withstand while being stretched or pulled before failing or breaking.
- **Strain at break,** also known as elongation at break, refers to the elongation achieved at breaking point.
- **Toughness,** is referred to the ability of the material to absorb energy up to fracture, and is approximated by the area under the stress-strain curve.

Data obtained is processed to be in function of the geometry of the sample. The elongation is converted to engineering strain (ε), by the following equation:

$$\varepsilon = \frac{\Delta L}{L_0} = \frac{L - L_0}{L_0} \tag{2.17}$$

, where ΔL is the change in gage length, L_0 is the initial gage length, and L is the final length. The force measurement is converted to stress (σ), by the following equation:

$$\sigma = \frac{F}{A} \tag{2.18}$$

, where F is the force and A is the cross-section area of the sample.

The most common testing machine used in tensile testing is the universal testing machine. However, for small dimensions non-commercial polymeric samples such as the samples developed in this thesis, **micro-tensile testing machine** is usually employed. Dimensions of the samples are usually no more than 4 cm in length and 0.6 cm in width.

3.9.2. EXPERIMENTAL PROCEDURE

Tensile testing was carried out on a DEBEN microtester equipped with a 150 N load cell and operated at a crosshead speed of 0.4 mm/min at room temperature with

length between clamps (gage length) of 10 mm. Tensile tests were performed on specimens with typical dimensions length x width of 15-20 x 4 mm. The analysis was repeated at least 5 times per sample.

The mechanical properties of the samples subjected to degradation studies were also evaluated in order to investigate the changes in macroscopic mechanical properties over immersion time. The elongation to break (strain at break), Young´s modulus, toughness and ultimate tensile strength were analysed for samples at initial stage (day 0 of degradation), Young´s modulus of degraded samples was also analysed at different degradation stages (immersion in SBF at 37 °C for 1, 28 and 150 days).

3.10. DYNAMICAL-MECHANICAL-THERMAL ANALYSIS

3.10.1. FUNDAMENTALS[49]

Dynamic Mechanical Thermal Analysis (DMTA) is a technique used to study and characterize the **viscoelastic nature of polymers**.[50] An actuator imposes an oscillatory displacement, and a sinusoidal stress (σ) and strain (ε) are measured to finally determine the storage modulus (E'), loss modulus (E'') and loss factor ($tan\delta = E''/E'$) that is indicative of the released energy as heat during deformation. Storage and loss moduli are indicative of material stiffness and can be measured in shear, tensile or flexural configurations depending on the instrumentation. The sample is vibrated in tension, compression and shear or bending, whereby the frequency for the oscillating mechanical stimulation and the temperature can be varied. This approach performed over a range of temperatures at a set heating or cooling rate can be used to detect thermal transitions of the polymer such as glass-rubber relaxation (glass transition temperature, T_g) as well as to identify transitions corresponding to other molecular motions.

The dynamic tests compared to other mechanical tests have some advantages, such as being able to perform a test on a wide range of temperatures or frequencies in a relatively short time, also, from the results is possible to predict material behaviour and to estimate other mechanical properties. A deep understanding of the physical-chemical structure of polymers and variation of their properties could be achieved by knowing $E^{'}$ and $E^{''}$ moduli, as well as $tan\delta$ loss factor. Thus, these dynamic parameters are commonly used to determine phenomena such as glass transition regions, relaxation spectrums, crystallinity and crosslinking degrees, molecular orientations, phase separation and structural alterations in polymers, polymers blends or copolymers and composites.

Dynamic viscoelastic moduli of a polymer

In order to determine the dynamic mechanical properties, such as dynamic storage modulus $E^{'}$, loss modulus $E^{''}$, and the internal friction loss factor ($tan\delta = E^{''}/E^{'}$), different methods can be used. These methods, measure the response of a material under periodic forces, thus, vibrational parameters (amplitude, frequency, oscillation type and propagation of the wave) become important variables. Vibrations commonly used in dynamic mechanical analysis are free vibrations, resonance vibrations, wave propagation and sinusoidal excitation and response. The method based on sinusoidal excitation is used in viscoelastic studies of polymeric materials, and is the one applied in this thesis by means of DMTA instrumentation. In this case, the applied forces (stresses) and resulting deformations (strains) vary sinusoidally with time. The relationship is usually specified by the frequency in cycles/sec.

When a sinusoidal force (stress, σ) is applied in a perfectly elastic solid, the resulting strain and the stress will be perfectly in phase. For a purely viscous fluid, there will be a 90 degree phase lag of strain with respect to stress. For a linear viscoelastic behaviour as occurs with polymers, something in between happens. As

part of the provided energy is stored and recovered in each cycle, and part is released as heat some phase lag will occur (**Figure 2.32**). The deformation (strain, ε) will vary sinusoidally but not in phase with force (stress, σ). This phase lag is the time required for a molecular rearrangement and is associated with relaxation phenomena.

If both strain and rate of strain rate are infinitesimal, and the stress-strain relationship (with dependence of time) can be described by linear differential equations with constant coefficients, we have a **linear viscoelastic behaviour**. Then, for a given experiment, the ratio of stress to strain (modulus) will be a function of time (or frequency) and temperature, but not a function to the amount of stress or strain. Thus, stress and strain are defined as:

$$\sigma(t) = \sigma_0 \cdot \cos(\omega \cdot t + \delta) \tag{2.19}$$

$$\varepsilon(t) = \varepsilon_0 \cdot \cos(\omega \cdot t) \tag{2.20}$$

, where ω is frequency of strain oscillation, t is time, and δ is the phase lag between stress and strain.

The stress can be then expressed as a sum of two contributions or components:

$$\sigma = \sigma_0 \cdot \sin(\omega t) \cdot cos\delta + \sigma_0 \cdot \cos(\omega t) \cdot sin\delta \tag{2.21}$$

The component $\sigma_0 \cdot \cos(\delta)$, is in phase with the strain, while the component $\sigma_0 \cdot \sin(\delta)$, is $\pi/2$ out of phase. Dividing both component by the deformation amplitude component ε_0, the previous equation becomes:

$$\sigma(t) = \varepsilon_0 \cdot E' \cdot \cos(\omega \cdot t) + \varepsilon_0 \cdot E'' \cdot \sin(\omega \cdot t) \tag{2.22}$$

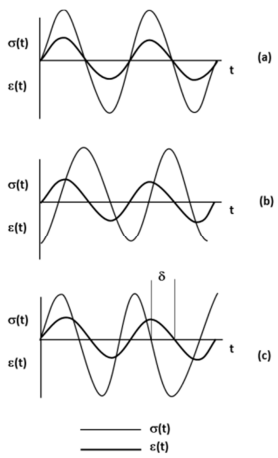

Figure 2.32. Schematic representation of the relationship between stress and strain for a sinusoidal excitation, (a) pure elastic behaviour, (b) pure viscous behaviour, (c) viscoelastic behaviour.

It is then possible to define two dynamic moduli: $E^{'}$, in phase with the strain (real), and $E^{''}$, $\pi/2$ degrees out of phase with the strain (imaginary). Stress-strain relation can be expressed through these moduli defined as:

Storage modulus **($E^{'}$)** which measures the stored energy in each cycle when the material is deformed, representing the elastic portion is:

$$E^{'} = \frac{\sigma_0}{\varepsilon_0} \cdot \cos(\delta) \tag{2.23}$$

Loss modulus **($E^{''}$)** which measures the energy dissipated as heat in each cycle when the material is deformed, representing the viscous portion is:

$$E^{''} = \frac{\sigma_0}{\varepsilon_0} \cdot \sin(\delta) \tag{2.24}$$

Then, $E^{'}$ is the relation between the amplitude of stress component in phase with the amplitude of strain (deformation) and $E^{''}$ is the relation between the amplitude

of the stress component with a lag of phase with the amplitude of strain (deformation).

Since these are orthogonal contributions, the mathematic treatment of cyclic loads, in most of the cases can be simplified by using the complex notation for the representation of the dynamic mechanical properties of viscoelastic materials, achieving:

$$\sigma^* = \sigma_0 \cdot e^{i(\omega \cdot t + \delta)} \tag{2.25}$$

$$\varepsilon^* = \varepsilon_0 \cdot e^{i(\omega \cdot t)} \tag{2.26}$$

, where $i = \sqrt{(-1)}$. The overall complex modulus E^* is given by (**Figure 2.33**):

$$E^* = \frac{\sigma^*}{\varepsilon^*} = \frac{\sigma_0}{\varepsilon_0} \cdot e^{i \cdot \delta} = \frac{\sigma_0}{\varepsilon_0} \cdot (cos\delta + i \cdot sin\delta) = E' + i \cdot E'' \tag{2.27}$$

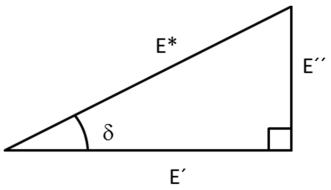

Figure 2.33. Complex modulus decomposition in real and imaginary parts as a function of lag phase.

In most of the cases, E'' is much lower than E', and then $|E^*| \approx E'$. Consequently, the dynamical mechanical behaviour of the polymers is usually defined in E' and $\tan(\delta)$, being:

$$tan(\delta) = \frac{E''}{E'} \approx \frac{\Delta}{\pi} \tag{2.28}$$

This last relationship is known as **Loss tangent (tan Delta)** and is the relationship between the released energy and the maximum potential energy stored in each cycle, thus is, a relation between loss modulus and storage modulus. Instead of

$tan(\delta)$ sometimes, the mechanical damping is used, depending on the DMTA instrument:

$$\Delta = \pi \cdot \tan(\delta) \tag{2.29}$$

3.10.2. DMTA INSTRUMENTATION

Typically, a DMTA consists of a linear variable differential transformer (LVDT) that acts as a displacement sensor which measures a change in voltage as a result of the instrument probe moving through a magnetic core, a temperature control system or furnace, a drive motor (a linear motor for probe loading which provides load for the applied force), a drive shaft support and guidance system to act as a guide for the force from the motor to the sample, and clamps to hold the sample. **Figure 2.34** shows a schematic representation of the main components of a DMTA instrument.

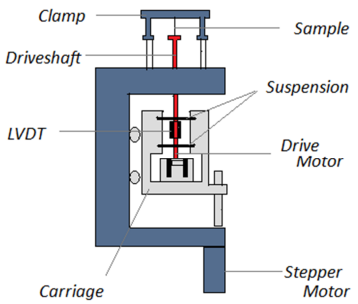

Figure 2.34. Schematic representation of a DMTA instrument.

Stress (force) and strain (displacement) controls are possible:

- In strain control, the probe is displaced and the resulting stress of the sample is measured by implementing a force balance transducer, which utilizes different shafts. The advantages of strain control include a better

short time response for materials of low viscosity and experiments of stress relaxation are done with relative ease.

- In stress control, a set force is applied to the same and several other experimental conditions (temperature, frequency, or time) can be varied. Stress control is typically less expensive than strain control because only one shaft is needed, but this also makes it harder to use. Some advantages of stress control include the fact that the structure of the sample is less likely to be destroyed and longer relaxation times/longer creep studies can be done with much more ease.

Two major kinds **of test modes** in tension, compression, shear or bending can be used to probe the viscoelastic properties of polymers: temperature sweep and frequency sweep tests. A third, less commonly studied test mode is dynamic stress-strain testing.

3.10.3. EXPERIMENTAL PROCEDURE

Dynamic mechanical analysis of all the samples were assessed by means of a TA Q800 instrument (TA instruments, New Castle, USA) in order to analyse their glass transitions regions as well as other possible relaxation processes. The results obtained from the analysis of the dynamic mechanical properties provide valuable insight into the structure, the morphology, and the viscoelastic behaviour of the samples, that have been employed to perform and define the shape-memory tests explained in the next section (**3.10.3.1**). Samples were cut into 30 x 4 mm rectangular shapes and tested in tensile mode with a temperature ramp method (temperature sweep) at a heating rate of 3 °C·min^{-1}. Frequency and strain amplitude were kept constant at 1 Hz and 15 µm, respectively. Experiments for PLA nanofiber mats were carried out from 30 °C to 130 °C, while for neat PMS matrices and their CNC nanocomposites, temperature range was set from -50 to 150 °C as glass transition of PMS occurs at lower temperatures than for PLA. The analysis was

performed at least twice per sample. Glass transition temperatures were calculated as the maximum in tangent delta peak.

3.10.3.1. DMTA SET-UP FOR SHAPE-MEMORY CHARACTERIZATION

In order to characterize the shape-memory behaviour of developed composites, the same dynamic mechanical analyser employed to characterize the viscoelastic properties (TA Q800 from TA instruments) was used in a somewhat unconventional manner.

Shape-memory properties of the samples were quantified by cyclic, thermomechanical tensile tests. Typically, shape-memory tests involve the creation and fixation of a temporary shape in a programming mode, and subsequently a free stress recovery step of the permanent shape. In the present thesis, the programming mode was performed under strain-controlled conditions in three steps: **(1)** the sample was equilibrated at T_{high} (45 °C) for 10 min (under a preload of 0.01 N as required by the instrument) before a force ramp of 3 $N \cdot min^{-1}$ was applied until a desired strain (30%) was reached. This step is referred to as the deformation step. **(2)** While the stress was kept constant, the sample was subsequently cooled to T_{low} (10 °C·min^{-1} to 15°C). **(3)** The sample was unloaded to zero stress (to preload of 0.01 N) and the temperature was maintained at T_{low} for 5 min to ensure the fixation of the temporary shape, allowing the determination of the sample shape fixing ability. At this point, the recovery step was initiated by increasing the temperature to T_{high} (5 °C·min^{-1} to 45 °C), which was then maintained for 20 min. All samples were cut into rectangular strips of 30 x 4 mm and tested for three or four cycles. Thus, by monitoring the strain exhibited by the samples in each step of the shape-memory cycle, a 3D plot of the strain versus temperature and versus force is obtained.

Should be pointed out that the temperature profiles used for the shape-memory tests were selected taking in account the results obtained in the previous DMTA analyses and to fulfil the requirements for future biomedical applications. Shape-memory biomedical devices are recommended to be activated in the range of 36 to 55 °C (T_{high}).[51] Some of the samples with the lowest recovery values were also tested at T_{high} of 60 °C to corroborate if higher recovery values were able to be achieved as temperatures close to 60 °C could be still useful in biomedical applications.

3.11. SWELLING AND DEGRADATION STUDIES IN SIMULATED BODY FLUID (SBF)

As it was pointed out before, although degradation studies are not the central aim of the present thesis, a preliminary study has been carried out as a first step in future research direction, as it could provide valuable information of the behaviour and applicability of the developed systems as biomedical materials. Polymer degradation assays can be performed by hydrolytic or biodegradation by biological degradation systems. Usually, in the first research investigations, degradation studies are usually carried out in simulated body fluids (SBF) at physiological temperature, while once the research is more advanced, in order to simulate *in vivo* conditions enzyme can also be added to SBF. In both cases, a known weight of material is incubated in degradation media and changes in morphology, mechanical strength and weight changes are followed at different time intervals to determine extent of degradation. The ultimate performance of degradation studies is carried out using suitable *in vitro* cell culture conditions or *in vivo* animal model.

In the present thesis, preliminary hydrolytic degradation tests under physiological conditions in simulated body fluid were carried out. Simulated body fluid (SBF) used as a buffer solution for degradation and swelling studies, was prepared following a previously reported protocol[52] to achieve ionic concentration nearly similar to human blood plasma (**Table 2.8**).

Table 2.8. Ionic concentration (mmol/dm^3) in SBF and Human blood plasma.

Ion	Simnulated Body Fluid(SBF)	Human blood plasma
Na^+	142.0	142.0
K^+	5.0	5.0
Mg^+	1.5	1.5
Ca^+	2.5	2.5
Cl^-	147.8	103.0
HCO_3^-	4.2	27.0
HPO_4^-	1.0	1.0
SO_4^-	0.5	0.5

Sodium Chloride (NaCl, ACS 99.5%), sodium hydrogencarbonate ($NaHCO_3$, ACS 99.7%), potassium chloride (KCl, ACS 99.5%), di-potassium hydrogen phosphate trihydrate ($K_2HPO_4 \cdot 3H_2O$, ACS 98%), magnesium chloride hexahydrate ($MgCl_2 \cdot 6H_2O$, ACS 99%), hydrochloric acid 1mol/l (HCl, ACS 1N), calcium chloride anhydrous ($CaCl_2$, ACS 96%), sodium sulfate anhydrous (Na_2SO_4, ACS 99%) and tris(hydroxymethyl)aminomethane buffer substance ($(CH_2OH)3CNH_2$, ACS buffer substance) reagents, were all purchased from Scharlau. Ultrapure water used to dissolve all the salts, was directly taken from a Sartorius Stedim Arium 611 VF® water purification system (ρ =18.2 mΩ cm). One SBF was prepared, films of 5 x 5 mm (n=4) were cut from each sample and incubated in 15 mL of the buffer solution at pH 7.4±0.5 at temperature of 37 °C. The degradation behaviour was determined by monitoring the weight loss at different times. Samples were removed from SBF at 14 days, 28 days, 42 days, 56 days and 150 days thoroughly washed with distilled H_2O and dried under vacuum at 37 °C until constant weight was reached. Two longer degradation time intervals at 210 days (7 months) and 240 days (8 months) were incorporated to the degradation study of PLA nanocomposites. The polymer degradation degree in SBF was calculated averaging the values of 4 samples by

comparing the mass at each time interval (M_t) with the initial mass (M_o) using following equation:

$$Mass\ Loss\ (\%) = \frac{M_o - M_t}{M_o} \tag{2.30}$$

For **swelling studies**, samples were collected after a 24 hour hydration period in SBF, blotted with a filter paper to remove excess surface water, and weighed (swelled weight: W_S). The swelling percentage of the materials after 24 h was determined comparing the swelled weight (W_S) with the initial weight (W_O) using the equation:

$$Swelling\ degree(\%) = \frac{W_S - W_O}{W_o}\ x\ 100 \tag{2.31}$$

3.12. CONDUCTOMETRIC TITRATION

In order to determine the surface charge density of the cellulose nanocrystals (CNCs) a conductometric titration method was applied in accordance with the literature.[53, 54] Briefly ~50 mg of CNCs were dispersed via 10 min sonication in a horn sonicator (Q500 sonicator, QSonica, 20 kHz/500 Watts, fitted with a 1=4" microtip probe) in a mixture of 10mL of 10mM aqueous hydrochloric acid and 25 mL of ultrapure H_2O in a glass beaker. The dispersion was subsequently titrated with aliquots of 10 mM aqueous NaOH recording the conductivity after the addition of each aliquot. In order to increase the accuracy of the titration, the neat medium (mixture of 10 mL H_2O which had also been sonicated), was also titrated with 10 mM aqueous NaOH. The titration volume was determined by plotting the data and fitting it to three lines; the first one corresponding to the titration of the HCl, the second one corresponding to the sample or acidity of the medium, and the third one to the excess of base. The three different series of data were separated by evaluating the slope. Intersection of the line fitted to the sample titration series

with the other two series was calculated and the volume comprised between the two intersecting points was calculated. The volume required for titration as well as concentrations are an average of three titration measurements. Thus, an average volume required for titration of the neat medium was then subtracted to the volume required to titrate each of the samples. The net volume required for sample titration was employed to calculate the concentration of sulfate groups on CNCs.[55] The concentration of sulfate groups was calculated following the equation:

$$\frac{mmol\ SO_4^-}{kg\ cellulose} = \frac{C_{NaOH} \cdot V_{NaOH}}{W_{CNC}} \cdot 10^6 \tag{2.32}$$

, where C_{NaOH} is the concentration of the base used for titration (M), V_{NaOH} is the volume (L) required to titrate one proton, and W_{CNC} is the weight of CNCs employed for the measurement (g).

4. REFERENCES IN THIS CHAPTER

1. J. P. Bruggeman, B. de Bruin, C. J. Bettinger and R. Langer, *Biomaterials,* 2008, **29**, 4726-4735.
2. B. Gupta, N. Revagade and J. Hilborn, *Progress in Polymer Science,* 2007, **32**, 455-482.
3. J. R. Capadona, O. Van Den Berg, L. A. Capadona, M. Schroeter, S. J. Rowan, D. J. Tyler and C. Weder, *Nature Nanotechnology,* 2007, **2**, 765-769.
4. X. Dong, T. Kimura, J. Revol and D. Gray, *Langmuir,* 1996, **12**, 2076-2082.
5. B. Braun and J. R. Dorgan, *Biomacromolecules,* 2009, **10**, 334-341.
6. R. Maliger, P. J. Halley and J. J. Cooper-White, *Journal of Applied Polymer Science,* 2013, **127**, 3980-3986.
7. Q. Chen, *Biomedical Materials and Diagnostic Devices*, ed. A. Tiwari, M. Ramalingam, H. Kobayashi and A. P. F. Turner, John Wiley & Sons, Inc., MA, USA, 2012, pp. 529-560.
8. G. Odian, *Principles of Polymerization*, ed. G. Odian, John Wiley & Sons, Inc., New Jersey, 2004, pp. 39-197.
9. H. Kim, H. Lee and J. C. Knowles, *Journal of Biomedical Materials Research Part A,* 2006, **79A**, 643-649.
10. C. M. Vaz, S. van Tuijl, C. V. C. Bouten and F. P. T. Baaijens, *Acta Biomaterialia,* 2005, **1**, 575-582.
11. Y. Zhou and L.T. Lim, *Journal of Food Science,* 2009, **74**, C170-C176.
12. X. H. Zong, H. Bien, C. Y. Chung, L. H. Yin, D. F. Fang, B. S. Hsiao, B. Chu and E. Entcheva, *Biomaterials,* 2005, **26**, 5330-5338.
13. X. H. Zong, K. Kim, D. F. Fang, S. F. Ran, B. S. Hsiao and B. Chu, *Polymer,* 2002, **43**, 4403-4412.
14. F. Yang, R. Murugan, S. Wang and S. Ramakrishna, *Biomaterials,* 2005, **26**, 2603-2610.

15. E. Kenawy, G. L. Bowlin, K. Mansfield, J. Layman, D. G. Simpson, E. H. Sanders and G. E. Wnek, *Journal of Controlled Release,* 2002, **81**, 57-64.
16. E. S. Medeiros, L. H. C. Mattoso, R. D. Offeman, D. F. Wood and W. J. Orts, *Canadian Journal of Chemistry,* 2008, **86**, 590-599.
17. X. L. Xu, L. X. Yang, X. Y. Xu, X. Wang, X. S. Chen, Q. Z. Liang, J. Zeng and X. B. Jing, *Journal of Controlled Release,* 2005, **108**, 33-42.
18. H. Tsuji, M. Nakano, M. Hashimoto, K. Takashima, S. Katsura and A. Mizuno, *Biomacromolecules,* 2006, **7**, 3316-3320.
19. M. Bognitzki, W. Czado, T. Frese, A. Schaper, M. Hellwig, M. Steinhart, A. Greiner and J. H. Wendorff, *Advanced Materials,* 2001, **13**, 70-72.
20. Z. Jun, H. Q. Hou, A. Schaper, J. H. Wendorff and A. Greiner, *E-Polymers,* 2003, **3** , 1-9.
21. S. I. Jeong, E. K. Ko, J. Yum, C. H. Jung, Y. M. Lee and H. Shin, *Macromolecular Bioscience,* 2008, **8**, 328-338.
22. G. Sui, X. Yang, F. Mei, X. Hu, G. Chen, X. Deng and S. Ryu, *Journal of Biomedical Materials Research Part a,* 2007, **82A**, 445-454.
23. X. Xu, X. Chen, A. Liu, Z. Hong and X. Jing, *Eur. Polym. J.,* 2007, **43**, 3187-3196.
24. Y. Pan, T. Liu, J. Li, Z. Zheng, X. Ding and Y. Peng, *Journal of Polymer Science Part B: Polymer Physics,* 2011, **49**, 1241-1245.
25. X. Luo and P. T. Mather, *Soft Matter,* 2010, **6**, 2146-2149.
26. *An Introduction to Gel Permeation Chromatography and Size Exclusion Chromatography*, Agilent Technologies, 2014.
27. *A guide to multi-detector gel permeation chromatography*, Agilent technologies, 2012.
28. P. Debye, The Journal of Physical and Colloid Chemistry, 1947, **51**, 18-32.
29. B. S. Kendrick, B. A. Kerwin, B. S. Chang and J. S. Philo, *Analytical Biochemistry,* 2001, **299**, 136-146.
30. R. Mhatre and I. S. Krull, *Analytical Chemistry,* 1993, **65**, 283-286.

31. C.S.Y. Shann, T. A. Meyer, C. E. Nelson, *Shimadzu GPC/Wyatt miniDAWN Treos User's Guide/Protocol*, 2010.
32. J. P. Bruggeman, C. J. Bettinger, C. L. E. Nijst, D. S. Kohane and R. Langer, *Advanced Materials,* 2008, **20**, 1922-1927.
33. H. Gottlieb, V. Kotlyar and A. Nudelman, *Journal of Organic Chemistry,* 1997, **62**, 7512-7515.
34. C. R. Brundle, C. A. Evans and S. Wilson, *Encyclopedia of Materials Characterization: surfaces, interfaces, thin films*, ed. C. R. Brundle, C. A. Evans and S. Wilson, Butterworth-Heinemann, Boston, 1992, pp. 413-415.
35. J. Neal Cox, *Encyclopedia of Materials Characterization: surfaces, interfaces, thin films*, ed. C. R. Brundle, C. A. Evans and S. Wilson, Butterworth-Heinemann, Boston, 1992, pp. 416-427.
36. Department of Chemistry and Biochemistry. University of Colorado, *Infrared Spectroscopy: Theory*, Online edition for organic chemistry lab courses, 2002.
37. Department of Earth and Environmental Science. Rensselaer Polythechnic Institute, *X-ray Diffraction*, Online edition, 2015.
38. B.D. Cullity, *Elements of X-ray Diffraction*, Addison-Wesley Publishing Company, University of Minnesota, 1956.
39. A. Bigi, B. Bracci and S. Panzavolta, *Biomaterials,* 2004, **25**, 2893-2899.
40. M. Sadat-Shojai, *Journal of the Iranian Chemical Society,* 2009, **6**, 386-392.
41. E. N. J. Ford, S. K. Mendon, S. F. Thames and J. W. Rawlins, *Journal of Engineered Fibers and Fabrics,* 2010, **5**, 10-20.
42. N. Terinte, R. Ibbett and C. K. Schuster, *Lenzinger Berichte,* 2011, **89**, 118-131.
43. J. F. Bindell, *Encyclopedia of Materials Characterization*, *surfaces, interfaces, thin films*, ed. C. R. Brundle, C. A. Evans and S. Wilson, Butterworth-Heinemann, Boston, 1992, pp.70-84.
44. Jeol Ltd., *Scanning Electron Microscope A to Z, Basic Knowledge For Using The SEM*.

45. K. E. Sickafus, *Encyclopedia of Materials Characterization*, *surfaces, interfaces, thin films*, ed. C. R. Brundle, C. A. Evans and S. Wilson, Butterworth-Heinemann, Boston, 1992, pp.99-116.
46. C. Schick, *Analytical and Bioanalytical Chemistry,* 2009, **395**, 1589-1611.
47. T.C. Vaimakis, Department of Chemistry. University of Ioanmina, *Thermogravimetry (TG) or Thermogravimetric Analysis (TGA)*, Online edition for thermal analysis courses, 2014.
48. J.R. Davis, *Tensile Testing*, ASM International, USA, 2004, pp 1-8.
49. R. Artiaga and A. Garcia, in *Thermal analysis. Fundamentals and applications to material characterization*, ed. Universidade da Coruña Servicio de Publicaciones, España, 2005, p. 183-205.
50. I. M. Ward and J. Sweeney, *An introduction to the mechanical properties of solid polymers*, ed. I.M. Ward and J. Sweeney, J. Wiley & Sons, Chichester; New York, 1993.
51. C. M. Yakacki and K. Gall, *Shape-Memory Polymers,* ed. A. Lendlein, Springer-Verlag, Berlin, 2010, pp. 147-175.
52. T. Kokubo, H. Kushitani, S. Sakka, T. Kitsugi and T. Yamamuro, *Journal of Biomedical Materials Research,* 1990, **24**, 721-734.
53. M. Jorfi, M. N. Roberts, E. J. Foster and C. Weder, *ACS Applied Materials & Interfaces,* 2013, **5**, 1517-1526.
54. A. C. Correa, E. d. M. Teixeira, L. A. Pessan and L. H. Capparelli Mattoso, *Cellulose,* 2010, **17**, 1183-1192.
55. S. Camarero Espinosa, T. Kuhnt, E. J. Foster and C. Weder, *Biomacromolecules,* 2013, **14**, 1223-1230.

Chapter 3

Mechanical properties and degradation studies of Poly(mannitol sebacate)/Cellulose Nanocrystal nanocomposites

Águeda Sonseca, Oscar Sahuquillo, E. Johan Foster, Enrique Giménez

RSC Advances 5 (2015) 55879-55891

DOI: 10.1039/C5RA06768E

MECHANICAL PROPERTIES AND DEGRADATION STUDIES OF POLY(MANNITOL SEBACATE)/CELLULOSE NANOCRYSTAL NANOCOMPOSITES

Águeda Sonseca[1*], Oscar Sahuquillo[1], E. Johan Foster[2] and Enrique Giménez[1]

[1]Instituto de Tecnología de Materiales, Universitat Politècnica de València (UPV), Camino de Vera s/nº, 46022 Valencia (Spain)

[2]Virginia Tech, Department of Materials Science & Engineering, 445 Old Turner Street, 213 Holden Hall, Blacksburg VA 24061, USA

***Corresponding author: agsonol@posgrado.upv.es**

Abstract

Polyesters based on polyols and sebacic acid, known as poly(polyol sebacate)s (PPS) are good candidates to develop degradable materials, due to their combination of flexibility and degradability, which are both useful properties in the context of soft-tissue engineering.[1-4] However, PPS generally display poor mechanical properties, in particular low modulus, that limit the true potential of these materials in the biomedical field. Here, we introduce an approach to obtain nanocomposites based in poly(mannitol sebacate) (PMS) matrices reinforced with cellulose nanocrystals (CNCs) in order to improve the application range of these materials. Different strategies were used based on varying the feed ratios between mannitol:sebacic acid (1:1 and 1:2), crosslinking conditions and CNCs content, resulting in different degrees of crosslinking and, therefore, mechanical and degradation behavior. All of the developed nanocomposites displayed the expected mass loss during the degradation studies in simulated body fluid (SBF) similar to the neat matrix, however, doubling the sebacic acid feed ratio or extending the curing temperature and time, resulted in higher mechanical properties, structural integrity, and shape stability during degradation time lessening mass loss rate. Changing

mannitol:sebacic acid reaction ratios from 1:1 to 1:2 and for low crosslinking degree neat samples, the Young´s modulus increases four-fold, while mass loss after 150 days of incubation is reduced by half. The Young´s modulus range obtained with this process cover the range of human elastic soft tissues to tough tissues (0.7-200 MPa).

Keywords: Poly(polyol sebacate), cellulose nanocrystals, nanocomposites, mechanical properties, mass loss.

1. INTRODUCTION

In the past few years, there has been steady progress in the development of biodegradable polymers for application in the medical field because these materials provide new opportunities to design less invasive and resorbable implants, tissue scaffolds, and medical devices that are able to avoid second revision surgeries, that limit the risk of infection and results in less trauma for the patient.[5-8] Moreover, biodegradable polymeric systems which offer the possibility to tailor their mechanical properties from soft to stiffer as well as the biodegradability ratio by varying the processing conditions also have additional advantages. Medical devices based on different classes of biodegradable polymers such as polyesters, polyanhydrides and polyurethanes have been widely investigated and some of them are commercially available as resorbable sutures, drug delivery systems, vascular grafts, wafers and orthopaedic fixation devices based, among others, on polylactic acid (PLA), polyglycolic acid (PGA), poly(lactic-*co*-glycolic acid) (PLGA), poly(*ε*-caprolactone) (PCL), poly(*p*-dioxanone) (PDO), or poly(trimethylene carbonate) (PTMC).[9, 10] However, most of these polymeric systems have degradation rates that are not optimal for short-medium term applications. For example, it takes more than 24 months for poly(caprolactones) and poly(L-lactic acid) to degrade in a biological environment, and from 2 to 24 months, depending on the ratio, for copolymers of polylactic acid (PLA) and polyglicolic acid (PGA). Also, the degradation rate for polyanhydrides is slow, around 12 months.[6, 9, 11] Moreover, these polymers have a lack of flexibility and elasticity at body temperature due to their high glass transition temperature and too high elastic modulus (400 MPa for PCL and 1200-3000 MPa for PLA)[12] that fail to mimic the elastic nature of many soft tissues such as blood vessels, cartilage, tendons or ligaments causing irritation, and sometimes damage, to the surrounding tissues.[13-15] To overcome these shortcomings, the development of novel biodegradable polyester elastomers, which are able to control their elastic

properties and flexibility to better match with the elastic nature, biocompatibility and degradation profile of soft tissues, has increased considerably.[16, 17] Several researchers have synthesized polyester elastomers based on polyols such as 1,8-octanediol, ethylene glycol, butylene glycol, castor oil or glycerol, and carboxylic acids such as citric acid, ricinoleic acid, and sebacic acid,[18-25] which find application in soft-tissue engineering as nerve-guidance, drug delivery, tissue adhesives and scaffolds to repair or replace body tissues.[1-4, 19, 26, 27] Poly(glycerol sebacate) (PGS) represents the most studied member of the poly-polyol sebacate (PPS) family, all of which are attractive because they are inexpensive and endogenous monomers found in human metabolism.[27-29] PGS is a randomly crosslinked polyester elastomer, whose design was motivated by the need to find biodegradable materials with tough mechanical properties.[26] Since PGS was firstly reported, several other polyols have been polymerized with sebacic acid to cover a wide range of mechanical properties and expand the spectrum of biomedical applications for these materials.[16, 27, 30] The most attractive synthetic feature of PPS is that through altering the stoichiometry of the diacid and polyol as well as varying the polycondensation conditions, the mechanical properties and degradation rates can be easily tuned. Moreover, PPS have biodegradability under physiological conditions and acceptable biocompatibility comparable to PLGA,[16, 31] and they have been reported as non-toxic based on *in vitro*[32] and *in vivo* studies.[33] These results indicate that these materials will be successful biomaterials with many biomedical applications. These thermoset elastomers have been reported to degrade *via* hydrolysis by surface erosion into metabolizable products, that maintain their structural integrity and geometric stability, and they are able to provide mechanical support during *in vivo* degradation.[30, 33, 34] The mechanical properties of PPS (tensile strength and elastic modulus) can be enhanced within a modest range by modifying the crosslink densities or in a much wider range by adjusting the stoichiometry. Nevertheless, to ensure an elongation at break higher than 10% (required for most tissue engineering applications), the range of Young´s modulus for these materials

(0.05-13 MPa) does not entirely cover that of living tissues such as skin (0.7-16 MPa), ligaments (1.5-54.5 MPa), tendons (1.5 GPa), or mandibular trabecular bone (6.9-200 MPa).[14, 35, 36] This fact restricts their usefulness in applications where high strength and flexibility are required, such as ligating rubber bands for blood vessels or bones, elastomeric sutures, flexible coatings for stents, surgical devices, vascular grafts, surgical wound dressings, or catheters and small diameter tubes for drainage.[37] In this regard, we have reported in a previous work[38] that the addition of cellulose nanocrystals (CNCs) as a reinforcing filler in a poly(mannitol sebacate) (PMS) matrix with mannitol:sebacic acid ratio 1:1, is an effective approach to increase the strength and stiffness without compromising the elongation at break due to a strong affinity between matrix and filler, and the superior specific properties of the CNC (specific Young´s modulus ~100 GPa/cm^3/g)[39, 40] compared with other nanofillers such as clays or bioceramics (Bioglass®). In that work, we developed 1:1 PMS nanocomposites with 1, 5 and 10 wt% of CNCs using the solution casting method followed by two different thermal crosslinking profiles, under low and high temperature-time conditions, to achieve samples with high and low degree of crosslinking. Mechanical, thermal, thermomechanical, and shape-memory properties of the samples were then evaluated, and the results indicated that at least in a certain extent CNCs interact with the matrix either, physically and chemically.[41, 42] However, as was mentioned above, different ratio of mannitol and sebacic acid in PMS will hardly influence the properties of the matrix as well as the interactions with the filler. Therefore, to complete our previous study,[38] the aim of the present work is to develop PMS/CNC nanocomposites with mannitol:sebacic acid 1:2 stoichiometry, using the same CNCs loading and crosslinking profiles than for previously reported 1:1 PMS stoichiometry, to compare how mechanical, thermal and degradation properties are affected. For PMS matrix with mannitol:sebacic acid 1:2 stoichiometry, we have also demonstrated that the residual alcohol groups of PMS matrix serve as ideal scaffolds for covalent tethering of chromophores with potential applications as bio-based up-converting rubbery

systems for drug-delivery, bio-imaging, solar harvesting or displays.[43] This previous experience demonstrates the possibility to covalently attach chromophores to a PMS matrix. In this regard, PMS/CNC nanocomposites with 1:2 ratio were developed and final properties were tuned and evaluated taking into account the possibility to be influenced either by physical and chemical CNC/PMS interactions, but in a different way than for 1:1 PMS system, due to the stark differences of the matrices. Here we reported an approach build upon previous work, showing a study of PMS/CNC nanocomposites from mannitol:sebacic acid 1:1 and 1:2 reaction ratios with low and high crosslinking degrees that were able to cover a wide range of mechanical properties and degradation rates for potential biomedical applications.

2. EXPERIMENTAL SECTION

2.1. MATERIALS

Deuterated dimethylsulfoxide (DMSO-d_6), dimethylformamide (DMF), sulfuric acid, sebacic acid (SA) (99% purity), and D-mannitol (MA) (99% purity), were purchased from Sigma Aldrich. Hydrochloric acid (HCl, 37% reagent grade) and sodium hydroxide (NaOH, 98% reagent grade) were purchased from Scharlau. Ultrapure water was directly taken from a Sartorius Stedim Arium 611 VF® water purification system (ρ = 18.2 mΩ·cm). Cellulose nanocrystals were isolated from cotton (Whatman No.1 filter paper) by controlled hydrolysis with sulfuric acid according to a protocol that is a modification of the method originally described by Dong et al.[44] This protocol introduces a small concentration of sulfate ester groups on the surface of the CNCs, which help to form stable suspensions in polar solvents.[45] Protocols followed to analyse dimensions, apparent crystallinity, crystal structure as well as the concentration of sulfate groups in the surface of the obtained CNCs

were previously reported,[38] and main results are collected in **Supporting Information Table S3.2**.

2.2. SYNTHESIS OF POLY(MANNITOL SEBACATE) (PMS) PRE-POLYMER

Sebacic acid (SA) and mannitol (MA) were reacted in a manner described previously.[16] Two poly(mannitol sebacate) pre-polymers were first synthesized to obtain 1:1 and 1:2 mannitol:sebacic acid ratios. Poly(mannitol sebacate) pre-polymer with a mannitol:sebacic acid 1:1 ratio was prepared following a previously described procedure.[38] To obtain the pre-polymer with a mannitol:sebacic acid 1:2 ratio,[43] appropriated molar amounts (0.034:0.068) of MA (6.21 g) and SA (13.79 g) were charged into a 250 mL three-necked round-bottom flask equipped with a stirrer and a condenser, which was placed in an oil heating bath and purged for 0.5 h with nitrogen. The temperature was slowly increased to 150 °C under continuous stirring and nitrogen flow to produce approximately 20 g of pre-polymer (**Scheme 3.1**).

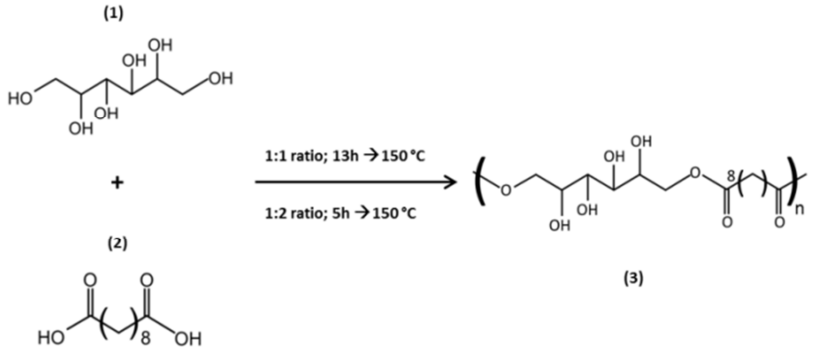

Scheme 3.1. Schematic representation of the general synthetic scheme of poly(mannitol sebacate) pre-polymer. Mannitol (1) was polymerized with sebacic acid (2) in different stoichiometries, yielding poly(mannitol sebacate) (PMS) (3) ratio 1:1 and 1:2. Note that simplified representations of the monomers and pre-polymers are shown.

The reaction was stopped after 5 h (1 h before gelation occurs), and the pre-polymer was dissolved in DMF (150 mg/mL), filtered and purified by dropwise

precipitation into a four-fold excess of cold ultrapure water under continuous stirring. The precipited pre-polymer was collected and dried under vacuum until no more solvent was detected in the infrared spectra. The yield of the reaction for 1:1 ratio was ~82%, while for 1:2 ratio was ~88%, as calculated from the weight of the monomers before reaction and the weight of each obtained pre-polymer after reaction.

2.3. CHARACTERIZATION OF PMS PRE-POLYMERS

The ^{1}H-NMR spectrum of 1:1 and 1:2 MA:SA ratio PMS pre-polymers were acquired in DMSO-d_6 on a Varian Mercury VX-300 MHz NMR spectrometer (**Supporting Information Fig. S3.1**). The compositions were determined from the ratio of the integrals of the signals associated with the mannitol and sebacic acid peaks[16] which reveal an incorporation of stoichiometric ratios mannitol:sebacic acid approximately of 1:1 and 1:2 (**Supporting Information Table S3.1**).

2.4. PREPARATION OF PMS/CNC NANOCOMPOSITES

The pre-polymers (1:1 and 1:2 MA:SA ratio) were first dissolved in DMF (100 mg/mL) by stirring at room temperature for 4 h. Suspensions of CNCs at concentration of 10 mg/mL were prepared at appropriate ratio in DMF (designed to combine with 1.5 g of dry pre-polymers and form 1 wt%, 5 wt% and 10 wt% of PMS/CNC nanocomposites) by 40 min of ultrasonic treatment in a horn sonicator (Q500 sonicator, QSonica) with 1 sec on/off pulse conditions at a 20% amplitude. CNCs suspensions were stirred with a PMS pre-polymer/DMF solution for 30 min and cast into aluminium Petri dishes (93 x 7 mm) and allowed to dry in an oven at 70 °C. Films consisting of the neat pre-polymers were prepared for reference purposes under the same conditions. The resulting pre-polymer/nanocomposites and the neat pre-polymer films were placed in a vacuum oven for further reaction. Two different curing profiles were applied to both pre-polymer/nanocomposites

series (1:1 and 1:2 MA:SA reaction ratios), in which temperature and duration of the thermal treatment were varied to obtain samples with low and high degree of crosslinking and reaction ratios 1:1 and 1:2. Samples with low degree of crosslinking were maintained at 120 °C for 72 hours under vacuum (60 cm Hg). Samples with high degree of crosslinking were obtained by using the same protocol and subsequently increasing the temperature to 170 °C while maintaining the vacuum (60 cm Hg) for a further 24 hours. Both procedures afforded films of ~150-200 μm of thickness.

2.5. TRANSMISSION ELECTRON MICROSCOPY (TEM)

CNCs TEM micrographs were recorded in a Phillips CM10 microscope with an accelerating voltage of 80kV. Samples were prepared by drying a drop of dilute CNCs suspension in distilled H_2O (0.1 mg/mL) onto a carbon-coated copper grid (Electron Microscopy Sciences) and subsequently dried under a lamp for 1 h.

2.6. DIFFERENTIAL SCANNING CALORIMETRY (DSC)

Thermal behavior of neat 1:1 and 1:2 PMS and their CNC nanocomposites was studied in a Mettler-Toledo DSC 800. Samples were heated from -60 to 180 °C, cooled down to -60 °C and heated again to 180 °C at a heating/cooling rate of 10 °C/min under an N_2 atmosphere. The glass transition temperatures (T_g) were calculated as the midpoint of the transition in the second heating run for all samples.

2.7. THERMO GRAVIMETRIC ANALYSIS (TGA)

Thermal stability of all obtained samples and CNCs was recorded in a Mettler-Toledo TGA/SDTA 851 modulus analyser. The samples (5-10 mg) were weighted in zircona crucibles and were heated in air at a rate of 10 °C/min from ambient

temperature to 700 °C. Thermal stability temperatures were determined as onset temperatures obtained by a tangential intercept method onto the TG curves.

2.8. SWELLING AND DEGRADATION STUDIES IN SBF

The swelling degree and degradation studies of all obtained samples (*n=4*, 5x5 mm, 150-200 µm thickness) were studied under physiological conditions, in phosphate buffered saline solution (SBF) of 7.4 ± 0.5 at 37 °C, prepared following a previously reported protocol.[46] For swelling studies, samples were collected after a 24 hour hydration period in SBF, blotted with a filter paper to remove excess surface water, and weighed (swelled weight; W_s). The swelling percentage of the networks after 24 h was determined comparing the swelled weight (W_s) with the initial weight (W_o) using equation (3.1).

$$Swelling\ degree(\%) = \frac{W_S - W_O}{W_o}\ x\ 100 \tag{3.1}$$

The degradation behavior was determined by monitoring the weight loss at different times. Samples were weighed, immersed in 15 mL of SBF and incubated at 37 °C in an oven for various periods of time. Polymer samples were removed from SBF at different time intervals (14 days, 28 days, 42 days, 56 days and 150 days), thoroughly washed with distilled H_2O and dried under vacuum at 37 °C until constant weight was reached. The degradation degree of the polymers in SBF was calculated averaging the values of three samples by comparing the mass at each time interval (M_t) with the initial mass (M_o) using equation (3.2).

$$Mass\ Loss\ (\%) = \frac{M_o - M_t}{M_o} \tag{3.2}$$

2.9. FOURIER TRANSFORM INFRARED SPECTROSCOPY (FTIR)

FTIR transmission spectra were recorded for all neat 1:1 and 1:2 PMS and their CNC nanocomposites, using a Thermo Nicolet 5700 spectrometer, between 500-4500 cm^{-1} with a 4 cm^{-1} resolution and an Attenuated Total Reflectance (ATR) cell. Backgrounds were acquired before every 3rd sample. All samples were vacuum-dried before measurement. FTIR spectra of neat 1:1 and 1:2 PMS with low and high crosslinking degree samples after 150 days of immersion in SBF were also recorded.

2.10. MECHANICAL MICRO-TESTING

Tensile tests were carried out on a DEBEN microtester equipped with a 150 N load cell and operated at a crosshead speed of 0.4 mm/min at room temperature. Specimen dimensions were typically 15 x 4 mm x 150-200 µm. The elongation to break, Young´s modulus, toughness and ultimate tensile strength were analysed for samples at initial stage (day 0 of degradation). Young´s modulus of degraded samples was analysed at different degradation stages (immersion in SBF at 37 °C for 1, 28 and 150 days). Degraded samples were taken out from SBF and immediately tested. The Young´s modulus (E) was determined from the initial slope of the stress-strain curves in the strain range of 0-10% for samples with low degree of crosslinking and 0-5% for samples with high degree of crosslinking. For each sample, a minimum of 5 rectangular samples were tested and the mechanical data were averaged.

3. RESULTS AND DISCUSSION

3.1. CHARACTERIZATION OF INITIAL SAMPLES

3.1.1. SYNTHESIS OF PMS PRE-POLYMERS AND ITS NANOCOMPOSITES WITH CNCs

The preparation of the PMS/CNC nanocomposites (1:1 and 1:2 MA:SA reaction ratios) were achieved in a two-step process. Soluble poly(mannitol sebacate) pre-

polymers with stoichiometric ratios of mannitol:sebacic acid 1:1 and 1:2 were formed *via* the polycondensation reaction between the appropriated molar amounts of sebacic acid and D-mannitol (**Scheme 3.1**). In this first stage, the esterification is preferentially dominated by the reaction of the primary hydroxyl groups from D-mannitol (situated at both ends) with the carboxylic acid groups from sebacic acid.[47, 48] The reactions were stopped before gelation occurred, thus affording two polyesters with approximately the initial molar amounts incorporated during synthesis as was revealed by ^{1}H NMR spectra (**Supporting Information Fig. S3.1**). Nanocomposites with 1 wt%, 5 wt%, and 10 wt% of CNCs were subsequently prepared by solution-casting mixtures of the PMS1:1 and PMS1:2 pre-polymers and the CNCs were cured in a second step under vacuum using two different curing profiles designed to prepare materials with low and high degree of crosslinking of each stoichiometric ratio, referred to in this paper as L and H, respectively. **Figure 3.1** and **Supporting Information Table S3.2** show TEM micrographs and the key properties of isolated CNCs used to develop the nanocomposites.

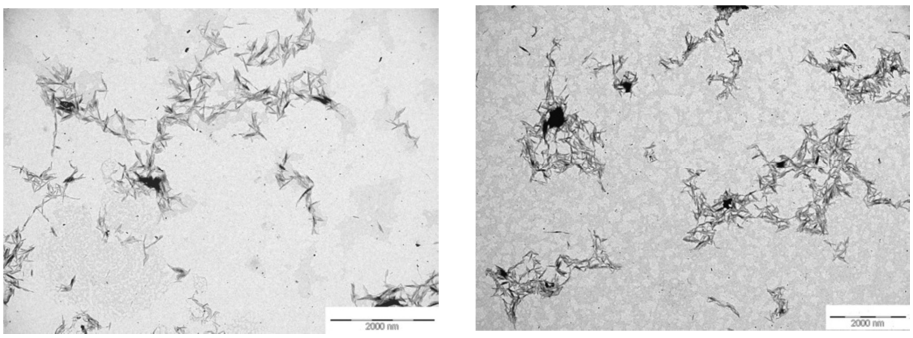

Figure 3.1. Transmission electron micrographs (TEM) of CNCs isolated by hydrolysis with sulfuric acid.

3.1.2. FTIR STUDY

In order to confirm the ester formation and the presence of CNCs, the ATR-FTIR spectra of the neat PMS matrix and the PMS/CNC nanocomposites of 1:1 and 1:2

stoichiometric ratios prepared under a low and high degree of crosslinking conditions were recorded. **Figures 3.2a** and **3.2b** show the most relevance bands for the neat PMS and PMS/CNC nanocomposites with stoichiometric ratio 1:1 and 1:2 respectively.

The neat PMS samples show the characteristic absorption bands for hydrogen-bonded hydroxyl groups (3500-3200 cm^{-1}) and for carbonyl-stretching vibrations of the ester groups (1800-1600 cm^{-1}) in the polymer backbone, thus confirming the formation of polyesters. The bands around 2924 cm^{-1} and 2852 cm^{-1} are assigned to methylene (-CH_2-) groups for the diacid residue and are observed in all spectra. A peak close to 1150 cm^{-1} is assigned to the –CO stretch associated with the ester groups (**Supporting Information Figure S3.2**).[49]

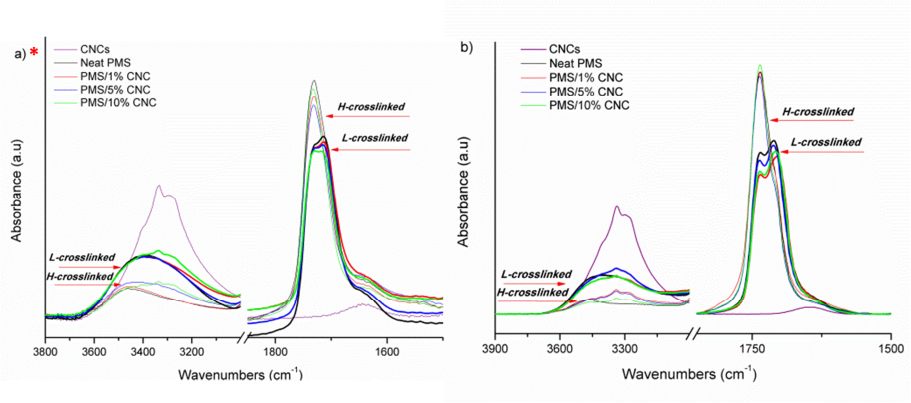

Figure 3.2. FTIR spectra detail of -OH band (3500-3200 cm^{-1}) and C=O region (1800-1600 cm^{-1}). Thick lines in the graphs correspond to low crosslinking degree samples, and thin lines correspond to high crosslinking degree samples. For 1:1 low crosslinked (L) and high crosslinked (H) neat PMS and PMS/CNC nanocomposites **(a)** and for 1:2 low crosslinked (L) and high crosslinked (H) neat PMS and PMS/CNC nanocomposites **(b)**. The presence of these both bands confirms the formation of polyesters with the highest esterification degree for the 1:2 high crosslinked samples. *Figure 3.2 is included in the present thesis chapter for reference purposes, and has been included in the article with changes as Figure 3.2a was published in a previous work.[38]

Samples prepared under a low degree of crosslinking conditions (L-crosslinked) for both stoichiometric ratios showed a broad and intense -OH stretch peak at 3350

cm^{-1}, an acid peak at 1705 cm^{-1}, and an ester peak at 1740 cm^{-1}, thus revealing a substantial fraction of unreacted hydroxyl and acid groups.[38] The –OH band intensity was lower for the 1:2 stoichiometric ratio while the acid peak (1705 cm^{-1}) was more evident in accordance with the higher sebacic acid content and lower mannitol presence compared with the 1:1 ratio. All samples prepared under a high degree of crosslinking conditions (H-crosslinked) showed a reduction absorption spectra related to the hydroxyls groups at 3350 cm^{-1} a more distinct 1:2 ratio, and a more pronounced –CO stretch associated with the ester groups, thus indicating a higher degree of esterification between acid and hydroxyl groups. The FTIR spectra of the nanocomposites revealed a similar pattern; it was able to discerned peaks associated with the CNC–OH close to 3338 cm^{-1} in the samples with 5 and 10 wt% of CNCs.

3.1.3. MECHANICAL TESTING

To relate the incorporation of CNCs and the different PMS ratios and crosslinking conditions to the mechanical properties of the PMS matrix, micro-tensile tests were carried out. The average tensile Young´s modulus, ultimate tensile strength, and elongation at break and toughness for all samples are summarized in **Table 3.1**.

Comparing the neat PMS matrices, as was expected, the average ultimate tensile strength (UTS) and Young´s modulus increased with the feed ratio of the sebacic acid monomer and to a greater extent for samples with a high crosslinking degree. The PMS 1:1 with a low degree of crosslinking had average UTS of 1.2±0.7 MPa and a Young´s modulus of 1.8 ±0.3 MPa, while for the high crosslinking degree these values increase to 7.0±0.6 MPa and 54.4±3.3 MPa, respectively. While doubling the feed ratio of the sebacic acid monomer, the crosslink density increased[30] and for low degree of crosslinking samples a four-fold enhancement in UTS (4.5±0.7 MPa) and Young´s modulus (7.2±0.1 MPa) values were obtained compared with 1:1 stoichiometry. Elongation at break of these samples (low crosslinking degree) is

also hardly affected by changing stoichiometry to 1:2 ratio being reduced by half. In contrast, high degree of crosslinking 1:2 PMS samples are the stiffer and stronger showing a higher Young´s modulus for a comparable elongation to their 1:1 PMS counterpart, however, the enhancement in the mechanical properties comparing neat matrices with this crosslinking profile for both stoichiometric ratios, is not as marked as occurs for low degree of crosslinking samples. Thus altering monomer-feed ratio of sebacic acid (increasing it) in PMS elastomers resulted in a wide range of mechanical properties, whilst for high degree of crosslinking samples similar elongation at break is maintained with a slightly increase in the mechanical properties.

Regarding nanocomposites, the improvement of the Young´s modulus and tensile strength by increasing the CNCs content (**Table 3.1**, **Figure 3.3**) was appreciated for both stoichiometric ratios and crosslinking profiles. As was happened in previously reported 1:1 PMS nanocomposites system, by applying the high crosslinking degree profile to 1:2 PMS nanocomposites results in much stiffer and stronger samples than their low crosslinking degree counterparts, reaching the highest Young´s modulus close to 170 MPa for 5 and 10 wt% of CNC loads. Same CNCs content, produce in all 1:2 PMS nanocomposites a five-fold and nearly two-fold increase in Young´s modulus, for low and high degree of crosslinking nanocomposites respectively, compared with the analogous samples of 1:1 PMS nanocomposites. Thus, at equal CNCs load, the PMS 1:2 nanocomposites showed higher enhancement in mechanical properties than the PMS 1:1 nanocomposites due to a higher crosslink density from the matrix. Surprisingly, for this stoichiometric ratio (1:2), the addition of a small amount of CNCs (only 1 wt%) results in a noticeable increase in the Young´s modulus of 54% and 109% for low and high crosslinking degree samples, respectively, over the neat matrix. However, the addition of 1 wt% of CNCs in the 1:1 ratio does not produce as high reinforcement as in the 1:2 PMS matrix, thus having similar Young´s modulus to the neat polymer.

Table 3.1. Main mechanical properties of neat PMS and PMS/CNC composites (1, 5 and 10 wt% of CNCs), obtained under different curing conditions (low and high crosslinked materials).

Curing conditions and mechanical properties of PMS and nanocomposites with low degree of crosslinking (L); 120°C, 60cm Hg, 3 days					
Sample	MA:SA ratio	Young´s modulus (MPa)[a]	Ultimate tensile strength (MPa)[a]	Elongation at break (%)[a]	Toughness (MJ/m^3)[a]
Neat PMS	Ratio 1:1	1.8±0.3	1.2±0.7	80.0±29.0	63.6±50.0
PMS/1% CNC		2.1±0.5	2.3±0.02	147.0±31.1	187.4±46.3
PMS/5% CNC		3.0±0.3	4.6±0.6	166.0±20.5	393.5±5.2
PMS/10%CNC		6.0±0.7	5.6±0.4	119.5±18.3	389.0±86.4
Neat PMS	Ratio 1:2	7.2±0.1	4.5±0.7	35.8±3.5	81.8±5.4
PMS/1% CNC		11.1±0.6	4.6±1.2	25.6±2.5	72.5±22.6
PMS/5% CNC		14.8±1.2	6.2±1.3	25.4±2.4	94.6±23.5
PMS/10%CNC		32.3±2.6	8.5±2.0	23.4±0.04	89.3±39.1

Curing conditions and mechanical properties of PMS and nanocomposites with high degree of crosslinking (H); L + 170°C, 60cm Hg, 1day					
Sample	MA:SA ratio	Young´s modulus (MPa)[a]	Ultimate tensile strength (MPa)[a]	Elongation at break (%)[a]	Toughness (MJ/m^3)[a]
Neat PMS	Ratio 1:1	54.4±3.3	7.0±0.6	40.5±7.0	204.4±6.3
PMS/1% CNC		54.5±1.6	13.2±2.2	94.1±14.0	757.4±238.0
PMS/5% CNC		132.5±20.6	20.1±3.4	77.0±12.6	1047.0±310.0
PMS/10%CNC		103.0±12.2	19.4±2.4	37.4±6.0	470.0±102.2
Neat PMS	Ratio 1:2	69.8±0.6	13.3±1.6	55.1±4.9	482.0±13.3
PMS/1% CNC		146.4±5.5	14.8±3.3	35.4±9.4	325.3±9.9
*PMS/5% CNC		166.5±4.0	--	--	--
*PMS/10%CNC		167.5±5.0	--	--	--

[a]Young´s modulus was calculated from the initial slope between 0-10% of strain for low crosslinked samples and between 0-5% strain for high crosslinked samples. All the values are an average of 2-5 specimens and are determined from stress strain curves.
***** These samples break in the clamp due to the high stiffness.

Another remarkable effect reported in the previous work,[38] and in what differs the behavior of nanocomposites with different stoichiometry, was that increasing the CNCs content in the PMS 1:1 samples provided higher stiffness without significantly compromising the elongation at break of the composites for both crosslinking profiles. This was related to a molecular level reinforcement induced by reactions between the nanoparticles with high hydroxyl functionality and the matrix during

the second polycondensation step, which also occur for previously reported clays and CNC-reinforced polyurethane nanocomposites.[50-52] In contrast increasing the CNCs content in PMS 1:2 matrix for both crosslinking profiles, results in higher stiffness whereas the elongation at break decreases, but not significantly.

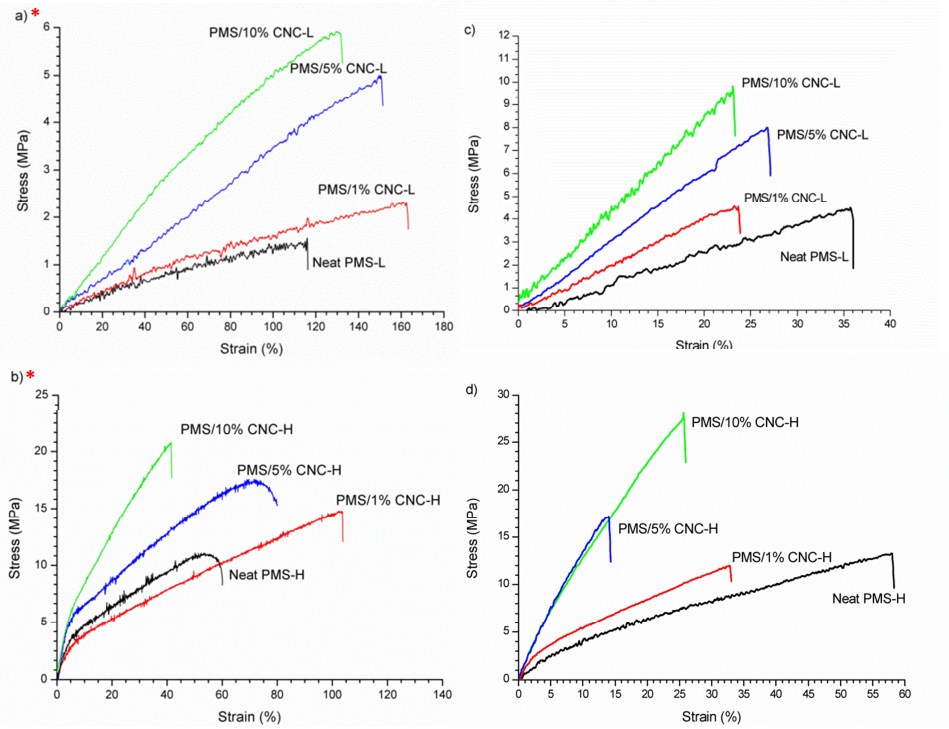

Figure 3.3. Typical tensile stress *versus* strain curves registered at room temperature of low Young´s modulus PMS and PMS/CNC nanocomposites cured under low crosslinking conditions (L) from mannitol/sebacic acid ratio 1:1 **(a)**, and mannitol/sebacic acid ratio 1:2 **(c)**. Typical tensile stress versus strain curves registered at room temperature of high Young´s modulus PMS and PMS/CNC nanocomposites cured under high crosslinking conditions (H) from mannitol/sebacic acid ratio 1:1 **(b)**, and mannitol/sebacic acid ratio 1:2 **(d)**. *Figures 3.3a and 3.3b are included in the present thesis chapter for reference purposes, and have been not be included in the article as were published in a previous work.[38]

Therefore, the increase in mechanical properties without compromising the elongation at break in the 1:1 system are due to the presence of CNC nanoparticles in the matrix and from polymer molecules interacting physically and chemically

with CNC surfaces; however, for the 1:2 system, the higher improvement in the mechanical properties, even for lower CNC contents, and the slight decrease in elongation at break, seem to be influenced by the higher crosslink density, together with the presence of well-dispersed stiff nanoparticles and CNC/CNC interactions, more than from polymer/CNC interactions.

The different behaviors observed in terms of stiffness, strength, and elongation at break between the 1:2 and 1:1 neat matrices with the CNCs presence can be associated to the differences in the OH:COOH ratio. One must consider that CNC is highly –OH functional and capable to interact with the residual hydroxyl or acid groups from PMS. As was already reported, as the value of average functionality (f_{av}) increases, the degree of polymerization also increases.[47, 53] For the 1:1 PMS, and 1:2 PMS, the f_{av} calculated using Pinner´s equation[53, 54] was 1.3 and 2.6, respectively. This implies that for the 1:2 pre-polymer, the free reactive sites available after the first polycondensation step are probably lower than in the 1:1 pre-polymer due to the higher density of crosslinking that results in fewer possibilities to form PMS/CNC interactions during the extent of the second polycondensation step. In the same way, the high offset in stoichiometry between available carboxylic acid and hydroxyl groups, is also responsible of losing the positive effect in the mechanical properties and elongation at break (tends to decrease) for the PMS 1:1 and 10 wt% of CNCs nanocomposite with a high degree of crosslinking, as produce a loss of the polymer-filler synergistic effect.[38, 55]

3.1.4. SWELLING STUDIES

The crosslinking density of the neat PMS and PMS/CNC nanocomposites was determined by evaluating the swelling degree after the 24 h immersion of the samples in SBF at 37 °C. **Table 3.2** shows the swelling degree for the neat and nanocomposites samples and the 1:1 and 1:2 reaction ratios. Samples with a higher sebacic acid ratio have a lower swelling degree that reveals an increase of the

crosslink density of the networks for the same curing conditions in agreement with the mechanical property results.[30] For example, the neat PMS 1:1 obtained with low crosslinking curing conditions, swells to 17.7±1.0 % and to 8.7±0.5 % cured with high crosslinking conditions, whereas changing the reaction ratio to 1:2 reduces the swelling degree to 14.4±1.0 % and to 5.1±0.8% for the low and high crosslinking degree of the neat PMS, respectively. Moreover, it seems that there are two clearly differentiated effects with the addition of CNCs to the 1:1 and 1:2 neat PMS networks. In the case of the 1:1 ratio, the addition of CNCs does not seem to significantly modify the swelling behavior of the neat matrix for low crosslinking degree nanocomposites, while it tends to slightly decrease for 1 and 5 wt% of CNCs for high crosslinking degree samples.

High crosslinking degree samples with 10 wt% of CNCs have the highest swelling degree; this fact is in concordance with the observed mechanical behavior and could be ascribed to the loss of polymer-filler interactions due to the high offset in the stoichiometry. For 1:2 stoichiometry it is more evident that the addition of CNCs results in a lower swelling degree for both curing conditions. The addition of 10 wt% of CNCs reduces the swelling degree to 10.4±0.8% and 2.1±0.5% for low and high crosslinking degree samples respectively. These results indicate that for the 1:1 ratio samples, the crosslinking degree of 1 and 5 wt% of CNC content nanocomposites, is mainly governed by the PMS matrix and CNC interactions, probably due to the excess of hydroxyl groups in the polymer backbone and the new introduced by the fillers, while higher CNC contents (10 wt%) offer an excess of hydroxyl groups that would favour the CNC/CNC interactions, thus reducing the polymer/polymer interactions and, hence, the crosslinking degree. In the case of samples with a higher sebacic acid feed ratio, the excess acid groups, instead of hydroxyl groups in the polymer backbone, are expected to provide additional esterification sites that, together with the hydroxyl groups available in the CNCs, seem to be the responsible for the reduction in the swelling degree with the

increase of the CNCs content; that is, at least in a certain extent, CNC can act as a chemical crosslinker to enhance the crosslinking between CNC and PMS chains.[56]

Table 3.2. Main thermal and swelling properties of neat PMS and PMS/CNC composites (1, 5 and 10wt% of CNCs), obtained under different curing conditions, (low and high crosslinked materials).

Curing conditions, swelling and thermal properties of PMS and nanocomposites with low degree of crosslinking (L); 120°C, 60cm Hg, 3 days				
Sample	MA:SA ratio	T_g by DSC (°C)[a]	Degradation onset temperature (°C)[b]	Hydration by mass (%)
Neat PMS	Ratio 1:1	18	227	19.6±1.5
PMS/1% CNC		18	237	20.2±0.2
PMS/5% CNC		18	228	19.3±1.1
PMS/10%CNC		17	215	21.5±0.3
Neat PMS	Ratio 1:2	16	236	14.4±1.0
PMS/1% CNC		16	239	12.0±0.3
PMS/5% CNC		10	238	11.4±0.3
PMS/10%CNC		8	233	10.4±0.8

Curing conditions, swelling and thermal properties of PMS and nanocomposites with high degree of crosslinking (H); L + 170°C, 60cm Hg, 1day				
Sample	MA:SA ratio	T_g by DSC (°C)[a]	Degradation onset temperature (°C)[b]	Hydration by mass (%)
Neat PMS	Ratio 1:1	26	263	9.0±0.2
PMS/1% CNC		24	274	8.7±0.1
PMS/5% CNC		21	280	8.0±0.3
PMS/10%CNC		20	268	11.2±0.5
Neat PMS	Ratio 1:2	32	272	5.1±0.8
PMS/1% CNC		30	277	4.7±0.4
PMS/5% CNC		23	278	2.2±1.0
PMS/10%CNC		21	279	2.1±0.5

[a] DSC glass transition temperatures were calculated as the midpoint of the transition in the 2nd heating run from differential scanning calorimetry traces (**Supporting Information Fig. S3.3**)

[b] Determined from thermogravimetric analysis traces as onset temperatures obtained by a tangential intercept method.

3.1.5. THERMAL CHARACTERIZATION (DSC AND TGA)

The effect of the CNCs addition and crosslinking profiles over the thermal stability of the samples and glass transition (T_g) were investigated using DSC and TGA. **Table 3.2** shows the glass transition and the onset of degradation values obtained for each sample. **Supporting Information Figure S3.3** shows the second heating run

thermograms for all the 1:1 and 1:2 PMS and PMS/CNC samples. In the case of thermal stability, the neat PMS and nanocomposites with a high degree of crosslinking revealed an increase of thermal stability for these curing conditions compared with their low crosslinking counterparts. Yet no marked differences in the thermal stability behavior were evidenced by comparing both reaction ratios (1:1 and 1:2). Some of the nanocomposites containing 5–10 wt% of CNCs showed a slightly lower degradation onset temperature than the neat PMS or 1 wt% CNC samples, most likely due to the lower onset degradation temperature associated with the CNC glycosyl units degradation starting at 220 °C.[57] Regarding the DSC results, there are two factors in the nanocomposites that could influence T_g in opposite directions. First, for the same curing profile, all the high crosslinking degree samples had a T_g higher than the low crosslinking degree samples; that is, longer curing times and higher temperature result in a higher degree of crosslinking, probably due to that hydrogen bonding and/or chemical crosslink was gradually intensified during thermal curing, which hinders the mobility of polymeric chains and increases the T_g. Moreover, T_g tends to decrease by slightly increasing the CNCs content for the 1:1 low crosslinking degree samples, thus becoming more prominent for high crosslinking and 1:2 ratio samples due to the disruption of polymeric network.[49, 58] This second phenomenon could be explained as follows: in the first step of the condensation there occurs an esterification dominated by the reaction of the primary hydroxyl groups founded at both ends of mannitol with carboxylic acid groups from sebacic acid, thus leaving a large amount of secondary –OH groups in the pre-polymer backbone and also an excess of free carboxylic acid groups for 1:2 ratio. For both systems, CNCs were added into the PMS pre-polymers at this point and were subject to low and high crosslinking conditions, which considerably changed the OH/COOH ratio. These variations in the initial stoichiometry reaction of the 1:1 and 1:2 ratios not only seemed to be responsible for CNCs not increasing the T_g as was expected, but also shifting it to lower temperatures for nanocomposites.[57] Similar behavior was observed for

polyurethanes reinforced with CNCs and poly(glycerol sebacate) bioglass nanocomposites due to strong associations between the filler and matrix.[50, 58] The new interactions between polymer chains and CNCs which seem to be favoured by higher sebacic acid feed ratios, higher crosslinking conditions, and raising the filler contents, all of which could reduce the polymer/polymer interactions and, therefore, be responsible for lowering the T_g.

3.2. CHARACTERIZATION OF DEGRADED SAMPLES

3.2.1. DEGRADATION IN SBF

The degradation of nanocomposites was investigated under physiological conditions (SBF, 37 °C) over the period of 150 days, showing the well-known scission of ester bonds occurring in the polyester network.[34, 59] **Figure 3.4** shows the obtained degradation rates that seem to be loosely correlated to the swelling and mechanical properties. Taking these results into account, roughly, the highest degradation rates correspond to samples with the lowest mechanical properties and highest swelling degrees; thus, to the 1:1 low crosslinking degree samples and nanocomposites. Continuing with the observed trend, the 1:1 reaction ratio samples with a high crosslinking degree have slightly slower degradation behavior than the 1:2 low crosslinking degree samples, while the slowest degradation rate was obtained for the high crosslinking degree 1:2 samples. Comparing both reaction ratios, an increase in sebacic acid content increases the time required for degradation due to an extent in the crosslink density that can effectively reduce the degradation rate for the same curing profile. Interestingly, the presence of CNCs does not seem to have a great influence on the degradation rate of the neat polymer matrices.

As was observed in previously reported systems,[60] the differences in mass loss between the two studied systems (1:1 and 1:2) could also be related to the higher presence of mannitol, which is more noticeable in the 1:1 low crosslinking degree

samples, that increases the hydrolytic degradation rate and enhances water penetration into the polymer matrix. An increase in the crosslink density achieved by changing the mannitol:sebacic acid ratio from 1:1 to 1:2 (corresponding to more equal numbers of alcohol and carboxylic groups) was also reported to be an important factor to significantly decrease the mass loss.[61] The results indicate considerable impact of the network structure on the degradation rates, which can be tuned or slowed by changing the stoichiometric ratio or crosslinking conditions without being affected by CNCs presence.

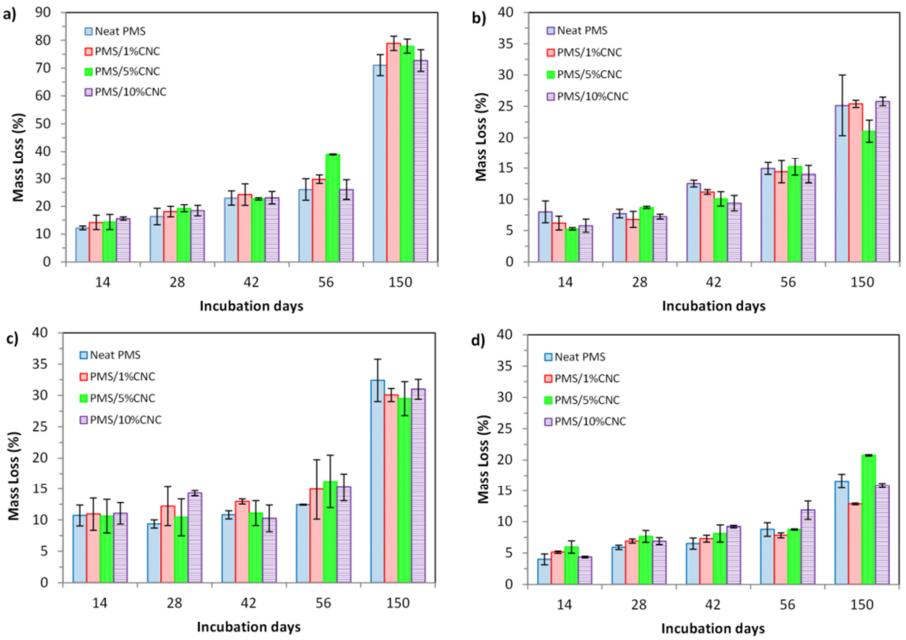

Figure 3.4. Degradation of neat PMS and PMS/CNC nanocomposites under physiological conditions (SBF at 37 °C) monitored over 150 days. Weight loss of 1:1 neat PMS and PMS/CNC nanocomposites with low crosslinking degree **(a)**. Weight loss of 1:1 neat PMS and PMS/CNC nanocomposites with high crosslinking degree **(b)**. Weight loss of 1:2 neat PMS and PMS/CNC nanocomposites with low crosslinking degree **(c)**. Weight loss of 1:2 neat PMS and PMS/CNC nanocomposites with high crosslinking degree **(d)**.

To confirm the degradation of the samples, **Figure 3.5** shows FTIR spectra's main bands of films immersed in SBF after 150 days. All the samples developed a new

peak centred around 1560 cm^{-1}, which is not present in the spectra of dry samples. This peak is characteristic of the stretch of carboxylate groups, indicating that some salts of carboxylic acid have been formed due to the hydrolysed ester bonds.[62, 63]

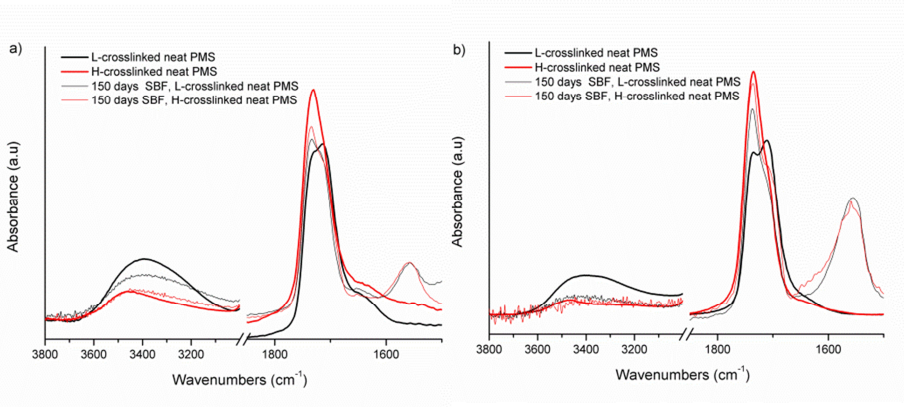

Figure 3.5. FTIR spectra detail of -OH band (3500-3200 cm-1) and C=O region (1800-1600 cm-1). Comparison between low crosslinked (L) and high crosslinked (H) 1:1 neat PMS as prepared (dry state) and after 150 days immersion in SBF **(a)**. Comparison between low crosslinked (L) and high crosslinked (H) 1:1 neat PMS as prepared (dry state) and after 150 days immersion in SBF **(b)**. New peaks centered around 1570 cm-1 not present in the spectra of dry samples indicates the formation of salts of carboxylic acids in the SBF immersed samples during the catalysed reaction of ester groups.

3.2.2. MECHANICAL PROPERTIES OF PMS/CNC IN SBF MEDIUM

In order to evaluate the effect of physiological conditions over the tensile properties of the developed materials, we allowed the samples to hydrate/degrade in SBF at 37 °C for 1, 28 and 150 days and then subjected them to a micro-tensile test. The changes in Young´s modulus over the degradation time for all the samples are shown in **Figure 3.6**. After 150 days of immersion, the 1:1 low crosslinking degree samples still mostly retained their shape but had completely lost their mechanical compliance and their testing and manipulation became impractical.

The mechanical behavior under hydrated conditions of biomaterials is an important factor in determining their possible biomedical and biological applications[59] since a drastic reduction in the mechanical properties of conventional polyesters between

dry and wet conditions, may induce an inflammatory response that enhances fibrous capsule formation.[49] Regarding to the developed materials, it was observed that all the samples had a similar Young´s modulus after one day hydration under physiological conditions that demonstrated low differences between dry and wet conditions. As expected, for the low and high crosslinking degree of neat PMS 1:1 and its CNC nanocomposites, a prolonged incubation time of up to 30 days produced a significant drop in the Young´s modulus compared with the 1:2 ratio samples due to the higher presence of the hydrophilic nature mannitol unit.[59] In contrast, Young´s modulus for the low and high crosslinking degree of 1:2 PMS samples and CNC nanocomposites is less deteriorated over time in culture media.

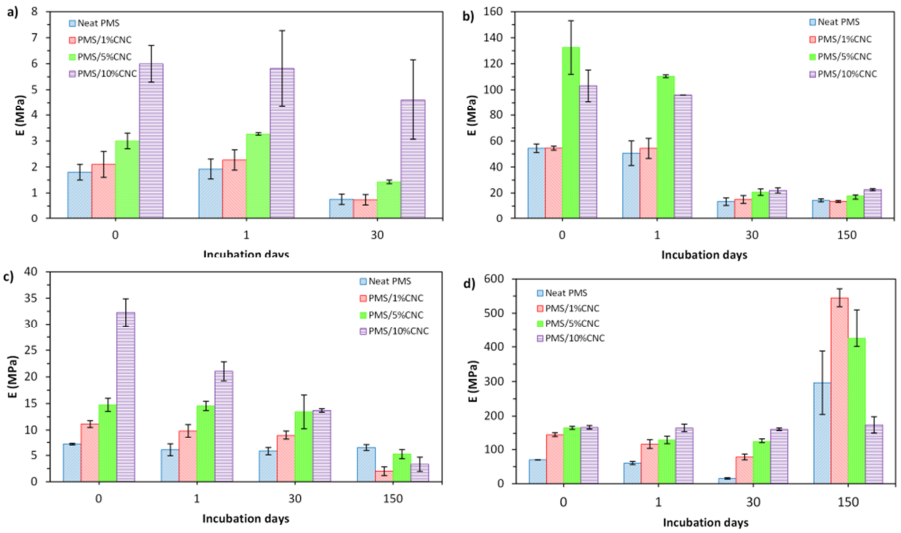

Figure 3.6. Young´s modulus changes between dry state (as prepared) and after immersion in SBF for different periods of time. Young´s modulus of 1:1 neat PMS and PMS/CNC nanocomposites with low crosslinking degree as prepared and after 1 and 30 days of immersion in SBF **(a)**. Young´s modulus of 1:1 neat PMS and PMS/CNC nanocomposites with high crosslinking degree as prepared and after 1 and 30 days of immersion in SBF **(b)**. Young´s modulus of 1:2 neat PMS and PMS/CNC nanocomposites with low crosslinking degree as prepared and after 1, 30 and 150 days of immersion in SBF **(c)**. Young´s modulus of 1:2 neat PMS and PMS/CNC nanocomposites with high crosslinking degree as prepared and after 1, 30 and 150 days of immersion in SBF **(d)**.

Similar behaviors have been reported for the poly(xylitol sebacate) 1:1 and 1:2 ratios elastomers.[34]

The dependence of Young´s modulus on the immersion time in culture medium revealed marked differences between 1:1 and 1:2 ratios without a clear dependence with CNC content, except for the high crosslinking degree of 1:2 PMS and nanocomposites. These samples are able to retain the initial stiffness by increasing the CNC content over the degradation time, probably due to less deterioration of the network and motivated by a higher crosslink density.

In general, mechanical properties are expected to decrease with time for these systems; however, after long periods of incubation (150 days), the 1:2 neat PMS and nanocomposites with a high degree of crosslinking had an increased Young´s modulus, yet the other samples tended to decrease or remain unchanged after 30 days of incubation. Similar phenomena was observed in poly(propylene fumarate) composites and were initially ascribed to the complexation of the carboxylic groups formed during degradation.[64, 65] In our case, it could probably be related to the generation of new crosslinking/interaction points in the network due to the scission of ester linkages that increase free carboxylic acid salts (**Figure 3.5**). The fact that it is only occurring for these samples poses the question of whether these new crosslinking/interaction points can be favoured for the higher network density, and within that, whether all the new available functional groups are closer and can easily interact.

There are a couple of important features that can be concluded from this degradation study: On the one hand, the synthesized materials cover a wide range of mechanical properties and, hence, may be used for biomedical and tissue engineering. For example, tough living tissues such as tendon (E=143-2310 MPa), human ligament (E=65-541 MPa), or cancellous bone (E=20-500 MPa)[66] have a Young´s modulus comparable to the high crosslinking degree samples. In applications where the involved tissue is softer and more elastic, the low crosslinking degree samples could be offered similar mechanical compliance for some human elastic soft tissues such as knee articular cartilage (2.1-11.8 MPa),[67, 68]

cerebral vein (6.85 MPa) and artery (15.6 MPa), aortic valve leaflet (15±6 MPa)[59] or pericardium (20.4±1.9 MPa).[69] On the other hand, in the context of biomaterials applications, the design of mechanically stable materials over an extended period is of importance for tissue remodelling at the wound site.[70, 71] Regarding this highly desirable mechanical stability following implantation, the 1:2 reaction ratio nanocomposites have the highest mechanical stability over a one month period, and could be good candidates for mechanical support to damaged tissues during the lag phase of the healing process. Finally, it should be pointed out that for long-term biomedical applications, one major requirement of any material is that must be biocompatible. Thus, it has to be able to stay in contact with living tissues without causing any cytotoxic or other derived side effects. Previous studies have investigated approaches to create PPS composites based on the introduction of inorganic components such as halloysite nanotubes (clays) or multi-walled carbon nanotubes (MWCNTs) with improved mechanical properties.[70, 72, 73] However, the main drawback derived from the use of these inorganic nanoparticles *in vivo* is their potential toxicity as well as the uncertain (or non-existent) mechanism of removal from the body.[74] By using organic based fillers these drawbacks could be lessen. In this regards, although CNC is known as non-biodegradable material for a long time, it has recently gained attention because exhibit low cytotoxicity with a range of animal and human cell types and no cytotoxicity at concentration ranges of ~50 μg/mL of CNC.[74-79] Mahmoud et al.[80] reported that any noticeable cytotoxic effect on two different cell lines occurred during in vitro cellular studies of two differently charged CNCs (positively and negatively) suggesting possible applications in both drug delivery and bioimaging. Jia et al.[81] reported potential application of microcrystal cellulose (MCC) and CNC as a filler of electrospun cellulose acetate vascular tissue scaffolds to improve biocompatibility. Thus, although the present work should be biocompatible, given that both components have been previously tested separately, future investigations are needed to characterize the toxicology of these cellulose nanocomposites materials thorough

in vitro and *in vivo* testing, to confirm the potential biomedical application. The *in vitro* studies reported until now highlight that CNCs hold great promise in a wide variety of biotechnological and biomedical applications especially in tissue engineering.[82]

4. CONCLUSIONS

Several strategies have been employed to prepare biodegradable poly(mannitol sebacate) based materials having a broad range of mechanical properties and degradation characteristics. These strategies are based on varying feed reaction ratios, crosslinking conditions or the addition of CNC as reinforcing fillers to alter the degradation rates as well as to tailor the mechanical stiffness of the poly(mannitol sebacate) from 1.8±0.3 MPa to 167.5±5.0 MPa. Compared to similar reported systems based in poly(glycerol sebacate), addition of high contents of nano-clays or Bioglass® (10-20 wt%) are necessary to achieve Young´s modulus close to 2 MPa. In this regard, the addition of CNCs in poly(mannitol sebacate) matrices combined with different stoichiometry and crosslinking profiles, results in a more efficient and remarkable improvement in mechanical properties well above of the enhancement obtained for other fillers. Reported systems containing Bioglass® tends to experiment a sudden drop in mechanical properties after one day of immersion in SBF medium almost getting back to the strength level of neat materials. In comparison PMS/CNC nanocomposites, provides more reliable mechanical support materials without immediately loss of mechanical stability. The amorphous nature of materials prepared provides the retention of mechanical properties and shape stability during long periods of incubation which are beneficial as could allow the load to be transferred to the surrounding tissues considering the development of a possible biomedical device. Moreover, acceleration (or deceleration) of the mass loss in similar nanocomposites, have been typically achieved through varying the filler content, or crosslinking degree of

the neat matrix, but to our knowledge, no studies about the affection of both variables together for the same nano-filler composition over the degradation behavior have been reported. Mass lose rate was primary determined by the degree of the crosslink density of materials that demonstrate slower degradation with the increasing feed ratio of sebacic acid or thermal curing time and temperature. However, the presence of CNCs does not slow or accelerate the mass loss of the matrix, that makes easy to predict the behavior of the material over the degradation period. In summary, the large number of variables to be applied during the synthesis of these nanocomposites provides a wide range of possible mechanical properties, which could be broadly employed in many biomedical applications that approximate those of soft and tough tissues. Moreover, *in vivo* experiments will also provide the indications of biocompatibility, and finally determine the real utility of these materials.

ACKNOWLEDGEMENTS

The authors gratefully acknowledge financial support received from Spanish Ministry of Economy and Competitiveness (Project MAT2010/21494-C03), as well as the support of FPU grant from MED (MED-FPU; AP2009-2482) and the Adolphe Merkle Foundation.

5. REFERENCES

1. Z. Sun, C. Chen, M. Sun, C. Ai, X. Lu, Y. Zheng, B. Yang and D. Dong, *Biomaterials,* 2009, **30**, 5209-5214.
2. C. Sundback, J. Shyu, Y. Wang, W. Faquin, R. Langer, J. Vacanti and T. Hadlock, *Biomaterials,* 2005, **26**, 5454-5464.
3. D. Motlagh, J. Yang, K. Lui, A. Webb and G. Ameer, *Biomaterials,* 2006, **27**, 4315-4324.

4. A. Mahdavi, L. Ferreira, C. Sundback, J. W. Nichol, E. P. Chan, D. J. D. Carter, C. J. Bettinger, S. Patanavanich, L. Chignozha, E. Ben-Joseph, A. Galakatos, H. Pryor, I. Pomerantseva, P. T. Masiakos, W. Faquin, A. Zumbuehl, S. Hong, J. Borenstein, J. Vacanti, R. Langer and J. M. Karp, *Proceedings of the National Academi of Sciences U. S. A.,* 2008, **105**, 2307-2312.
5. I. Vroman and L. Tighzert, *Materials,* 2009, **2**, 307-344.
6. B. D. Ulery, L. S. Nair and C. T. Laurencin, *Journal of Polymer Science Part B: Polymer Physics,* 2011, **49**, 832-864.
7. L. Xue and H. P. Greisler, *Journal of Vascular Surgery,* 2003, **37**, 472-480.
8. L. S. Nair and C. T. Laurencin, *Progress in Polymer Science,* 2007, **32**, 762-798.
9. P. A. Gunatillake and R. Adhikari, *European Cells & Materials,* 2003, **5**, 1-16.
10. J. C. Middleton and A. J. Tipton, *Biomaterials,* 2000, **21**, 2335-2346.
11. K. Athanasiou, C. Agrawal, F. Barber and S. Burkhart, *Arthroscopy: The Journal of Arthroscopic & Related Surgery,* 1998, **14**, 726-737.
12. I. Engelberg and J. Kohn, *Biomaterials,* 1991, **12**, 292-304.
13. Q. Chen, A. Bismarck, U. Hansen, S. Junaid, M. Q. Tran, S. E. Harding, N. N. Ali and A. R. Boccaccini, *Biomaterials,* 2008, **29**, 47-57.
14. S. Liang, W. D. Cook, G. A. Thouas and Q. Chen, *Biomaterials,* 2010, **31**, 8516-8529.
15. M. A. Meyers, P. Chen, A. Y. Lin and Y. Seki, *Progress in Materials Science,* 2008, **53**, 1-206.
16. J. P. Bruggeman, B. de Bruin, C. J. Bettinger and R. Langer, *Biomaterials,* 2008, **29**, 4726-4735.
17. Y. Li, G. A. Thouas and Q. Chen, *RSC Advances*, 2012, **22**, 8229-8242.
18. J. Yang, A. Webb, S. Pickerill, G. Hageman and G. Ameer, *Biomaterials,* 2006, **27**, 1889-1898.
19. J. Yang, A. Webb and G. Ameer, *Advanced Materials* 2004, **16**, 511-516.
20. H. Park, J. Seo, H. Lee, H. Kim, I. B. Wall, M. Gong and J. C. Knowles, *Acta Biomaterialia,* 2012, **8**, 2911-2918.

21. Z. Sun, L. Wu, X. Lu, Z. Meng, Y. Zheng and D. Dong, *Applied Surface Science,* 2008, **255**, 350-352.
22. Q. Liu, T. Tan, J. Weng and L. Zhang, *Biomedical Materials,* 2009, **4**, 025015.
23. M. Y. Krasko, A. Shikanov, A. Ezra and A. J. Domb, *Journal of Polymer Science Part A: Polymer Chemistry,* 2003, **41**, 1059-1069.
24. P. S. Sathiskumar and G. Madras, *Polymer Degradation and Stability,* 2011, **96**, 1695-1704.
25. I. Djordjevic, N. R. Choudhury, N. K. Dutta and S. Kumar, *Polymer,* 2009, **50**, 1682-1691.
26. Y. Wang, G. Ameer, B. Sheppard and R. Langer, *Nature Biotechnology,* 2002, **20**, 602-606.
27. D. G. Barrett and M. N. Yousaf, *Molecules,* 2009, **14**, 4022-4050.
28. K. Ellwood, *The American Journal of Clinical Nutrition,* 1995, **62**, 1169-1174.
29. S. Natah, K. Hussien, J. Tuominen and V. Koivisto, *The American Journal of Clinical Nutrition,* 1997, **65**, 947-950.
30. J. P. Bruggeman, C. J. Bettinger, C. L. E. Nijst, D. S. Kohane and R. Langer, *Advanced Materials,* 2008, **20**, 1922-1927.
31. S. Liang, W. D. Cook, G. A. Thouas and Q. Chen, *Biomaterials,* 2010, **31**, 8516-8529.
32. C. Bettinger, E. Weinberg, K. Kulig, J. Vacanti, Y. Wang, J. Borenstein and R. Langer, *Advanced Materials,* 2006, **18**, 165-169.
33. Y. Wang, Y. Kim and R. Langer, *Journal of Biomedical Materials Research Part A,* 2003, **66A**, 192-197.
34. J. P. Bruggeman, C. J. Bettinger and R. Langer, *Journal of Biomedical Materials Research Part A,* 2010, **95A**, 92-104.
35. K. Firoozbakhsh, I. Yi, M. Moneim and Y. Umada, *Clinical Orthopaedics and Related Research,* 2002,**403**, 240-247.
36. S. K. Ha, *Medical Engineering & Physics,* 2006, **28**, 534-541.

37. V. R. Sastri, *Plastics in Medical Devices, properties, requirements, and applications*, ed. V.R. Sastri, William Andrew Publishing, Boston, 2010, pp. 217-262.
38. A. Sonseca, S. Camarero-Espinosa, L. Peponi, C. Weder, E. J. Foster, J. M. Kenny and E. Gimenez, *Journal of Polymer Science Part A: Polymer Chemistry,* 2014, **52**, 3123-3133.
39. R. Rusli and S. J. Eichhorn, *Applied Physics Letters,* 2008, **93**, 033111.
40. C. C. Sun, *Journal of Pharmaceutical Sciences,* 2005, **94**, 2132-2134.
41. J. S. Haghpanah, R. Tu, S. Da Silva, D. Yan, S. Mueller, C. Weder, E. J. Foster, I. Sacui, J. W. Gilman and J. K. Montclare, *Biomacromolecules,* 2013, **14**, 4360-4367.
42. M. Jorfi, M. N. Roberts, E. J. Foster and C. Weder, *ACS Applied Materials & Interfaces,* 2013, **5**, 1517-1526.
43. S. Lee, A. Sonseca, R. Vadrucci, E. Giménez, E. J. Foster and Y. Simon, *Journal of Inorganic and Organometallic Polymers and Materials,* 2014, **24**, 898-903.
44. X. Dong, T. Kimura, J. Revol and D. Gray, *Langmuir,* 1996, **12**, 2076-2082.
45. B. Braun and J. R. Dorgan, *Biomacromolecules,* 2009, **10**, 334-341.
46. T. Kokubo, H. Kushitani, S. Sakka, T. Kitsugi and T. Yamamuro, *Journal of Biomedical Materials Research Part A,* 1990, **24**, 721-734.
47. R. Maliger, P. J. Halley and J. J. Cooper-White, *Journal of Applied Polymer Science,* 2013, **127**, 3980-3986.
48. Q. Chen, *Biomedical Materials and Diagnostic Devices*, ed. A. Tiwari, M. Ramalingam, H. Kobayashi and A. P. F. Turner, John Wiley & Sons, Inc., MA, USA, 2012, pp. 529-560.
49. A. Patel, A. K. Gaharwar, G. Iviglia, H. Zhang, S. Mukundan, S. M. Mihaila, D. Demarchi and A. Khademhosseini, *Biomaterials,* 2013, **34**, 3970-3983.
50. A. Pei, J. Malho, J. Ruokolainen, Q. Zhou and L. A. Berglund, *Macromolecules,* 2011, **44**, 4422-4427.
51. Y. Tien and K. Wei, *Macromolecules,* 2001, **34**, 9045-9052.

52. Q. Wu, M. Henriksson, X. Liu and L. A. Berglund, *Biomacromolecules,* 2007, **8**, 3687-3692.
53. G. Odian, *Principles of Polymerization*, ed. G. Odian, John Wiley & Sons, Inc., New Jersey, 2004, pp. 39-197.
54. S. H. Pinner, *Journal of Polymer Science,* 1956, **21**, 153-157.
55. M. A. Hood, C. S. Gold, F. L. Beyer, J. M. Sands and C. Y. Li, *Polymer,* 2013, **54**, 6510-6515.
56. A. K. Gaharwar, A. Patel, A. Dolatshahi-Pirouz, H. Zhang, K. Rangarajan, G. Iviglia, S. Shin, M. A. Hussain and A. Khademhosseini, *Biomaterials Science,* 2015, **3**, 46-58.
57. Y. Li and J. A. Ragauskas, *Advances in diverse industrial applications of nanocomposites*, ed. B. Reddy, InTech, 2011, pp. 18-36.
58. S. Liang, W. D. Cook and Q. Chen, *Polymer International,* 2012, **61**, 17-22.
59. B. Amsden, *Soft Matter,* 2007, **3**, 1335-1348.
60. Y. Chandorkar, G. Madras and B. Basu, *Journal of Materials Chemistry B,*2013, **1**, 865-875.
61. S. Liang, X. Yang, X. Fang, W. D. Cook, G. A. Thouas and Q. Chen, *Biomaterials,* 2011, **32**, 8486-8496.
62. M. Partini and R. Pantani, *Polymer Degradation and Stability,* 2007, **92**, 1491-1497.
63. X. Gu, D. Raghavan, T. Nguyen, M. R. VanLandingham and D. Yebassa, *Polymer Degradation and Stability,* 2001, **74**, 139-149.
64. M. J. Yaszemski, R. G. Payne, W. C. Hayes, R. Langer and A. G. Mikos, *Biomaterials,* 1996, **17**, 2127-2130.
65. Z. Ge, J. C. H. GoH, L. Wang, E. P. S. Tan and E. H. Lee, *Journal of Biomaterials Science-Polymer Edition,* 2005, **16**, 1179-1192.
66. M. Sabir, X. Xu and L. Li, *J. Journal of Materials Science,* 2009, **44**, 5713-5724.
67. D. E. T. Shepherd and B. B. Seedhom, *Rheumatology,* 1999, **38**, 124-132.

68. A. Thambyah, A. Nather and J. Goh, *Osteoarthritis and Cartilage,* 2006, **14**, 580-588.
69. J. Lee and D. Boughner, *Circulation Research,* 1985, **57**, 475-481.
70. Q. Chen, S. Liang, J. Wang and G. P. Simon, *Journal of the Mechanical Behavior of Biomedical Materials,* 2011, **4**, 1805-1818.
71. T. Schepull, J. Kvist, C. Andersson and P. Aspenberg, *BMC Musculoskeletal Disorders,* 2007, **8**, 116-116.
72. Q. Liu, J. Wu, T. Tan, L. Zhang, D. Chen and W. Tian, *Polymer Degradation and Stability,* 2009, **94**, 1427-1435.
73. Q. Chen, L. Jin, W. D. Cook, D. Mohn, E. L. Lagerqvist, D. A. Elliott, J. M. Haynes, N. Boyd, W. J. Stark, C. W. Pouton, E. G. Stanley and A. G. Elefanty, *Soft Matter,* 2010, **6**, 4715-4726.
74. X. Yang, E. Bakaic, T. Hoare and E. D. Cranston, *Biomacromolecules,* 2013, **14**, 4447-4455.
75. T. Kovacs, V. Naish, B. O'Connor, C. Blaise, F. Gagné, L. Hall, V. Trudeau and P. Martel, *Nanotoxicology,* 2010, **4**, 255-270.
76. S. Dong, A. A. Hirani, K. R. Colacino, Y. W. Lee and M. Roman, *Nano Life,* 2012, **02**, 1241006.
77. M. J. D. Clift, E. J. Foster, D. Vanhecke, D. Studer, P. Wick, P. Gehr, B. Rothen-Rutishauser and C. Weder, *Biomacromolecules,* 2011, **12**, 3666-3673.
78. M. M. Pereira and N R B Raposo and R Brayner and E M Teixeira and V Oliveira and C C R Quintäo and L S A Camargo and L H C Mattoso and,H.M.Brand, *Nanotechnology,* 2013, **24**, 075103.
79. M. Jorfi and E. J. Foster, *J Appl Polym Sci,* 2015, **132**, 41719.
80. K. A. Mahmoud, J. A. Mena, K. B. Male, S. Hrapovic, A. Kamen and J. H. T. Luong, *ACS Applied Materials & Interfaces,* 2010, **2**, 2924-2932.
81. B. Jia, Y. Li, B. Yang, D. Xiao, S. Zhang, A. V. Rajulu, T. Kondo, L. Zhang and J. Zhou, *Cellulose,* 2013, **20**, 1911-1923.

82. J. M. Dugan, J. E. Gough and S. J. Eichhorn, *Biomacromolecules,* 2010, **11**, 2498-2504.

S.I. Chapter 3

Supporting Information: Mechanical and degradation studies of Poly(mannitol sebacate)/Cellulose Nanocrystal nanocomposites

Águeda Sonseca, Oscar Sahuquillo, E. Johan Foster, Enrique Giménez

RSC Advances 5 (2015) 55879-55891

DOI: 10.1039/C5RA06768E

GRAPHICAL ABSTRACT

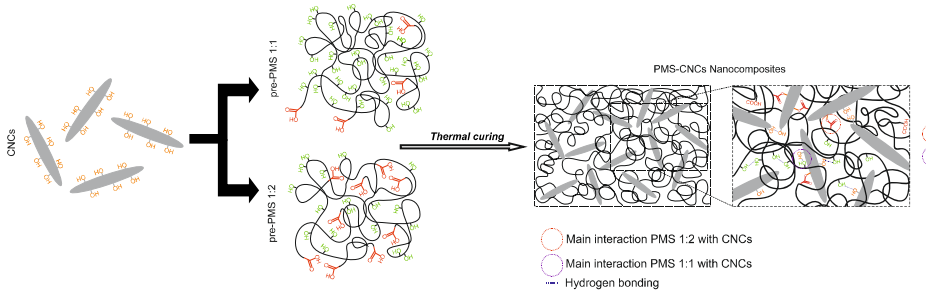

Two different low-molecular-weight pre-polymers with a D-mannitol:sebacic acid feed ratio 1:1 and 1:2 respectively were combined with cellulose nanocrystals (CNCs) and crosslinked applying different time-temperature profiles under vacuum to obtain PMS/CNC nanocomposites. Higher free –OH presence in pre-PMS 1:1 matrix could promote higher interaction with the filler through hydrogen bonding, while one can surmise that at least in a some extent, larger amount of free -COOH groups in pre-PMS 1:2 matrix increases the probability to obtain polymer/filler interactions through the formation of ester groups. These differences between the two studied systems affects to crosslinking degree, mechanical properties and degradation rates obtained.

1. ^{1}H-NMR STUDIES

^{1}H-NMR spectra of PMS 1:1 and PMS 1:2 pre-polymers were obtained in deuterated dimethylsulfoxide (DMSO-d_6), on a Varian Mercury VX-300 MHz NMR spectrometer. Samples were prepared dissolving the pre-polymers into 750 µL of DMSO-d_6 in a glass tube. The peaks from the mannitol appeared at 3.5-5.5 ppm due to central and terminal methylene units. The protons from methylene units of sebacic acid showed peaks at 1.3, 1.6 and 2.3 ppm. The peak at 3.3 was due to residual water.[1]

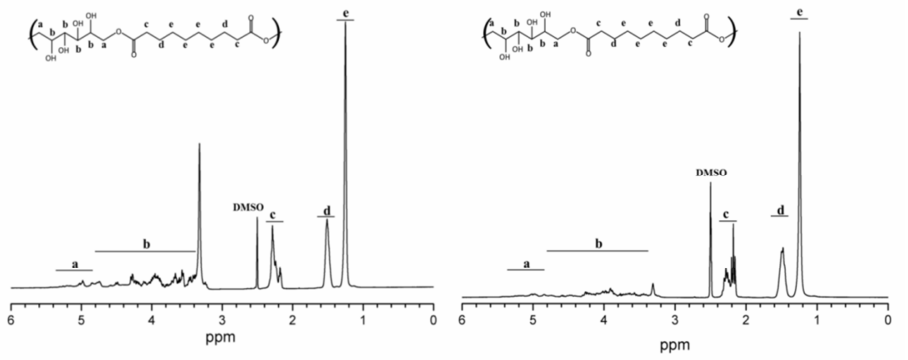

Figure S3.1. ^{1}H-NMR spectra of **(left)** 1:1 pre-poly(mannitol sebacate), and **(right)** 1:2 pre-poly(mannitol sebactate) were recorded in DMSO-d_6. Signal intensities of the polyol were identified at 3.5-5.5 ppm, and for sebacic acid at 1.3, 1.6 and 2.4 ppm by hydrogens on the carbons "a" and "b" and "c", "d" and "e" respectively. Simplified representations of the pre-polymers are shown.

Table S3.1. Composition by ^{1}H NMR of PMS pre-polymer 1:1 (pre-PMS 1.1) and PMS pre-polymer 1:2 (pre-PMS 1:2) stoichimetric ratios after purification step.

^{1}H NMR composition	
Sample	Composition by ^{1}H NMR
Pre-PMS 1:1	1:0.93
Pre-PMS 1:2	0.83:2

2. CNC PROPERTIES

Charge concentration was determined by conductometric titration as described previously.[2, 3] The concentration of sulphate groups on CNCs was calculated from the titration results according to a reported protocol.[4] Dimensions and aspect ratio of CNCs were calculated as an average of randomly measures in TEM images at different magnifications (2950x, 3900x and 5200x). CNCs TEM micrographs were recorded in a Phillips CM10 microscope with an accelerating voltage of 80kV. Samples were prepared by drying a drop of dilute whiskers suspension in H_2OD (0.1 mg/mL) onto a carbon-coated copper grid (Electron Microscopy Sciences) and subsequently dried under a lamp for 1 h. ImageJ software (National Institute of Health in USA) was used to evaluate the length and width of the CNCs. The crystalline structure of the CNCs was investigated with an RXSiemens D5000 equipped with a Cu Kα radiation source (λ = 1540 A) operating at 40kV. A CNC sample was dispersed in water and dried in oven at 100°C for 0.5h. After drying the compact powder obtained was regrounded and transferred to scan. The scanning range was 2°-40°, step-size and count time per step were 0.02° and 8 seconds, respectively. Apparent crystallinity was calculated from X-ray diffraction pattern using www.magicplot.com software.[5]

Table S3.2. Main CNCs properties analysed through conductometric titration, TEM images and X-ray diffraction pattern.

Main CNC Properties	
Charge concentration ($mM/kg_{cellulose}$)[a]	104.3±4
Length (nm)	199±14
Width (nm)	18±2
Aspect ratio (nm)	11±1
Apparent crystallinity (%)	68

[a] Determined by conductimetric titration

3. FOURIER TRANSFORM INFRARED SPECTROSCOPY (FTIR)

Transmission spectra were recorded using a Thermo Nicolet 5700 spectrometer, in the 500 to 4500 cm^{-1} region, with a 4 cm^{-1} resolution with an Attenuated Total Reflectance (ATR) cell. Backgrounds were acquired before every 3rd sample. All samples were vacuum-dried before measurement.

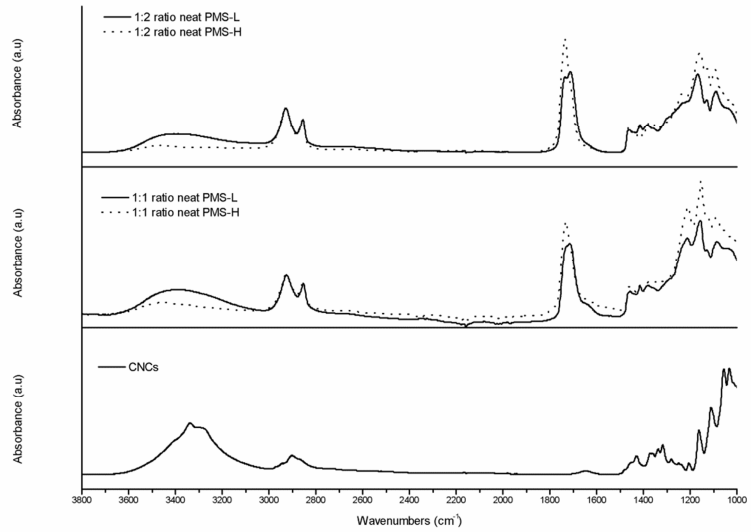

Figure S3.2. FTIR spectra from top to bottom, low crosslinked (L) and high crosslinked (H) PMS 1:2 stoichiometric ratio, low crosslinked (L) and high crosslinked (H) PMS 1:1 stoichiometric ratio, and CNCs.

4. DIFFERENTIAL SCANNING CALORIMETRY (DSC)

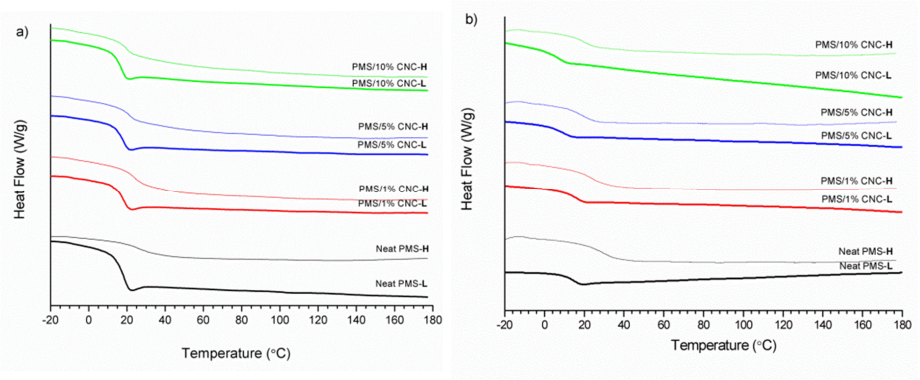

Figure S3.3. DSC second heating run thermograms of 1:1 low (L), and high (H) crosslinked neat PMS and PMS/CNC nanocomposites **(a)**, and for 1:2 low (L) and high (H) crosslinked neat PMS and PMS/CNC nanocomposites **(b)**.

5. REFERENCES

1. H. Gottlieb, V. Kotlyar and A. Nudelman, *The Journal of Organic Chemistry,* 1997, **62**, 7512-7515.
2. M. Jorfi, M. N. Roberts, E. J. Foster and C. Weder, *ACS Applied Materials & Interfaces,* 2013, **5**, 1517-1526.
3. A. C. Correa, E. d. M. Teixeira, L. A. Pessan and L. H. Capparelli Mattoso, *Cellulose,* 2010, **17**, 1183-1192.
4. S. Camarero Espinosa, T. Kuhnt, E. J. Foster and C. Weder, *Biomacromolecules,* 2013, **14**, 1223-1230.
5. A. Sonseca, S. Camarero-Espinosa, L. Peponi, C. Weder, E. J. Foster, J. M. Kenny and E. Giménez, *Journal of Polymer Science Part A: Polymer Chemistry,* 2014, **52**, 3123-3133.

Chapter 4

Electrospinning of Biodegradable Polylactide/Hydroxyapatite Nanofibers: Study on the Morphology, Crystalline Structure and Thermal Stability

Águeda Sonseca, Laura Peponi, Oscar Sahuquillo, José M. Kenny, Enrique Giménez

Polymer Degradation and Stability 97 (2012) 2052-2059

DOI: 10.1016/j.polymerdegradstab.2012.05.009

ELECTROSPINNING OF BIODEGRADABLE POLYLACTIDE/HYDROXYAPATITE NANOFIBERS: STUDY ON THE MORPHOLOGY, CRYSTALLINE STRUCTURE AND THERMAL STABILITY

Águeda Sonseca[1]*, Laura Peponi[2], Oscar Sahuquillo[1], José M. Kenny[2], Enrique Giménez[1]

[1]Instituto de Tecnología de Materiales, Universitat Politècnica de València (UPV), Camino de Vera s/nº, 46022 Valencia (Spain)

[2]Instituto de Ciencia y Tecnología de Polímeros (ICTP - CSIC), 28006 Madrid, (Spain)

***Corresponding author: agsonol@posgrado.upv.es**

Abstract

Aligned mats of poly(lactic acid) (PLA) nanofibers containing nano-sized hydroxyapatite filler have been obtained via electrospinning onto a rotating mandrel. Their structure and morphology have been characterized as a function of the production parameters, by SEM, DSC, DMA and WAXS, with emphasis in the effects of the take-up velocity**.** SEM, DSC and X-ray diffraction studies confirmed a reduction in fiber diameter, an increase of fiber orientation and a highly crystalline structure of the mats collected at higher speed due to the stretching produced during the process. Double melting behavior was observed, suggesting the presence of two crystalline forms. Moreover the higher storage modulus (*E´* modulus), and glass transition temperatures of the higher speed collected mats were correlated with an enhanced in the thermal stability and nanofiller distribution.

Keywords: Polylactide, Hydroxyapatite, Electrospinning, Morphology, Crystallinity, Thermal Stability.

1. INTRODUCTION

Aliphatic polyesters as poly(lactic acid) (PLA), poly(glycolides) (PGA) and poly(ε-caprolactone) (PCL) have attracted wide attention for their biodegradability and biocompatibility in the human body. In order to obtain new biomaterials with enhanced properties, there is a trend towards the introduction of organic and inorganic nanofillers into biodegradable polymers to produce materials containing hydroxyapatite, metal nanoparticles or carbon nanotubes.[1]

Electrospinning is a straightforward technique to produce non-woven micro or nanofibrous mats, based on the application of high voltage to a polymeric solution, in order to create an electrically charged jet randomly collected onto a grounded target.[2] The current interest on nano and micro fibers has produced a particular relevance for developing this process. This technique has been recognized as an efficient, simple and versatile method for the fabrication of ultrathin fibers with diameters between 50 and 500 nm and has been successfully used with a wide range of polymers, some of them biodegradable.[3] Because biodegradable materials are often easy to dissolve, they are suitable for the formation of mats by electrospinning, so until date, this process has been widely used in the field of biomedical engineering for the fabrication of nanofibrous scaffolds for tissue engineering, cardiac grafts, wound dressings, blood vessel substitutes, carriers for delivery of drugs and other therapeutic agents from numerous biodegradable polymers such as poly(ε-caprolactone) (PCL), poly(lactic acid) (PLA), poly(glycolic acid) (PGA), some polyurethanes (PU) and their copolymers.[4-6]

The morphology of obtained nanofibers can be controlled to a certain extent changing the voltage, feed rate, collector shape and distance values, but basic electrospinning can only yield randomly aligned nanofibers. This will limit the areas which electrospun fiber mesh can be used in. Thus, to fully explore the potential of

electrospinning, it is necessary to have some control on the deposition of the fibers.[3] Is well known that solution parameters as viscosity, surface tension, concentration and dielectric properties, and process parameters such as the feed rate and the acceleration voltage have a great influence on the nanofibers morphology. Recently it was determined that the nature of the collector plays a significantly role in the morphological and the physical characteristics of the spun fibers.[7, 8] In fact, it has been seen that nanofibers can be aligned introducing a specially designed collectors, among them a cylinder collector capable of rotating at high speeds and taking up the fibers on the surface of the cylinder tightly in a circumferential manner.[9, 10] At rotational speeds slower or higher than the optimum fiber take-up speed, randomly or non-continuous fibers are collected respectively. Ideally, the linear rate of the rotating drum should match the evaporation rate of the solvent, such that solvent free fibers are deposited and engaged on the surface of the drum.[11] However, precise control of the alignment of spun fibers remains a challenge.

The electrospun fibers have large surface area to volume ratio and should also have good mechanical properties combining mechanical strength with flexibility and lightness.[12] Incorporating determinate fillers is a way to increase these mechanical properties, as well as diversifying and exploring potential fields of application offering new electrical,[13-16] magnetic,[17-22] optical[23-26] and biological[27-30] functionalities. Nowadays the use of nanofillers instead of microfillers inside of a polymer matrix, has raised a huge interest in the scientific community. In the biomedical field, the nanocomposites based on biodegradable polymers filled with hydroxyapatite (HA) particles have received special attention due to their good osteoconductivity, osteointegration, biodegradability and enhanced mechanical properties.[1] Due to its biodegradability and biocompatibility, poly(lactic acid) (PLA) is one of the polymers where micro/nanocrystals of HA have been dispersed. Despite numerous reports on the effect of processing conditions on the PLA/HA

fibers morphology, degradation properties and biological efficacy of these bioresorbable polymer mats, limited studies have been devoted to investigate the influence of this nanofiller on the morphology and structure of electrospun PLA fibers.[31-33] In this work, the morphology, thermal behaviour and crystalline structure of PLA/HA nanofibers obtained by electrospinning process under both low and high take-up velocities have been investigated. Special emphasis on crystal modifications and orientations has been made, and their effect on mechanical properties and the dimensional stability has been determined. Moreover the work involves the use of a cylindrical rotating collector as a key component because it is generally used to produce high collecting areas, as well as a scalable-up process potentially suitable for future mass production combined with other processing strategies as multiple needle nozzles.[34]

2. EXPERIMENTAL

2.1. MATERIALS

Biodegradable Poly(lactic acid) was supply by NatureWorks® (USA) under the trade name PLA3051D, with 3% of D-lactic acid monomer. Its molecular weight (M_n) was ca.142x10^4 g/mol, and its density was 1.24 g/cm^3. Dichloromethane (DCM) and N,N-dimethylformamide (DMF) from Sigma Aldrich were used as solvents. Hydroxyapatite nanofiller (HA) was a non-commercial grade synthesized by chemical precipitation method employing calcium and phosphorus precursors in solutions and 30 g/L concentration of commercial gelatine (Dr Otker). To avoid the formation of hydroxyapatite aggregates in the polymer solution, sodium dodecyl sulphate was used as an anionic surfactant.

2.2. SYNTHESIS OF HYDROXYAPATITE

For the nanosized hydroxyapatite synthesis, the gelatin was dissolved in 250 mL of deionized water at 40 °C, calcium hydroxide ($Ca(OH)_2$) (2.0 mol/L) was then added to this solution and the mixture was appended drop by drop to 250 mL of an aqueous suspension of ortho-phosphoric acid (H_3PO_4, 85%) (1.2 mol/L) in order to obtain a stoichiometric hydroxyapatite with a ratio of calcium (Ca) and phosphorous (P) moles of 1.67 (Ca/P). Ammonium hydroxide was added to obtain a final pH of 10. The precipitate was left to age for 24 h. The resulting particle size and surface area measuring by BET (Brunauer, Emmett and Teller) were 35.74 nm and 54.2038 m^2/g respectively, and crystallite size measured by WAXD was 47.98.

2.3. PREPARATION OF ELECTROSPUN NANOFIBERS

Non-woven and aligned PLA/HA nanofibers were prepared by electrospinning method. In our case, we worked with a standard horizontal electrospinning setup with a rotating mandrel as a collector, connected directly to a high voltage power supply, and a syringe infusion pump. Viscous polymer solutions with a concentration of 7 %wt were prepared by dissolving PLA3051D in dichloromethane:N,N-dimethylformamide (70:30). Different contents of nano-hydroxyapatite (HA) were added to the polymer solutions and thoroughly mixed by sonication. Each solution was loaded into the syringe and an electrode was clipped onto the needle. The whole apparatus was enclosed with a methacrylate cover in order to reduce the effect of air currents on the trajectory of the electrospun jet. All air bubbles were purged prior to electrospinning and the solutions were electrospun at 14kV and a flow rate of 0.6 ml/h. The ground mandrel was at a distance of 13 cm from the charged capillary tip and electrospun mats were collected at two different take-up velocities; randomly oriented fibers were produced on a stationary shaft (low collecting rate fibers; LCR), whereas highly oriented fibers were produced when rotation speed was increased around 1100

rpm (high collecting rate fibers; HCR). Series of samples were made from pure polymer and different weight ratios polymer/HA (9:1, 5:1 and 3:1) and all of them were obtained from 10 mL of solution.

2.4. CHARACTERIZATION TECHNIQUES

The morphology of the electrospun fibers was examined using scanning and transmission electron microscopy (SEM, JEOL JSM6030 and TEM, PHILIPS CM10). Samples were gold-coated to minimize the charging effect during SEM observation, an accelerating voltage of 10 kV and a working distance of 10-15 mm were used for viewing the samples. For TEM, a few fibers were collected on carbon covered mesh copper grids and observed at 100 kV. SEM images at 5000x magnifications and the ImageJ software (National Institute of Health in USA) were used to evaluate the diameters and the alignment of the nanofibers. Diameters and fiber orientation angle were calculated as an average of 30 randomly measures. The angle was measured between the long axes of the fibers and the vertical axis of the image.

The thermal behavior was studied by using a differential scanning calorimetry (DSC, Mettler-Toledo DSC 800). Samples were heated from 30 to 220 °C at a heating rate of 10 °C/min under a nitrogen atmosphere. The calibration of the DSC was carried out with a standard sample of indium. The glass transition temperature (T_g), cold-crystallization temperature (T_{cc}), melting temperature (T_m), cold-crystallization enthalpy (ΔH_c), melting enthalpy (ΔH_m) and degree of crystallinity (X_c%) of the electrospun fibers mats were evaluated from first heating curves. The glass transition was calculated as the midpoint of the jump in heat capacity (ISO 11357-2). The crystallization (exothermal) and melting (endothermal) were characterized by the onset and peak temperatures, as well as by the area under the corresponding peaks. The crystallinity content (X_c%) was evaluated according to the following equation:

$$X_c(\%) = \frac{100(\Delta H_m - \Delta H_c)}{\Delta H_m^0} \quad (4.1)$$

, where ΔH_m and ΔH_c are the melting and the crystallization enthalpies respectively, and ΔH_m^0 is the reference ΔH_m (93.6 J/g) of 100% crystalline PLA.

The thermal gravimetric analysis (TGA) was conducted on a TA Instrument Q50 under N_2 flow from 25 to 650 °C at 10 °C/min. Dynamic mechanical analysis (DMA) was carried out on a Mettler-Toledo DMA/SDT A 861 at the frequency of 1 Hz and at the heating rate of 3 °C/min from 30 to 130 °C at which the sample lost its dimensional stability.

The crystalline structure of the samples was monitored by wide-angle X-ray diffraction (WAXS, RX Siemens D5000) with a Cu Kα source. The scanning range was 2°-40°, step-size and count time per step were 0.02° and 8 seconds respectively. The percentages of crystallinity were calculated by a fitting process using a deconvolution method of the peaks. A peak fitting program (PeakFit; www.systat.com) was used. In all cases, samples were cut from the middle regions of electrospun mats, with a thickness about 80-150 μm.

3. RESULTS AND DISCUSSION

3.1. NANOFIBERS MORPHOLOGY

Figure 4.1 shows SEM images of the microstructure of pure PLA and PLA/HA nanofibers mats produced on a stationary shaft (LCR) and at rotation speed nearly 1100 rpm (HCR) with neat polymer and different polymer/HA weight ratios: 9:1, 5:1 and 3:1. It is possible to note that through optimized solvent system and electrospinning parameters, uniform PLA and PLA/HA fibers mats with a random or more directional distribution were obtained. The surface of PLA/HA nanofibers was much coarser than the neat PLA fibers due to the dispersion of HA particles.

Agglomerates gradually appeared on the fiber surface along with increase of the nano-hydroxyapatite concentration and the deformation of the fiber. For the same electrospinning conditions and the stationary collector, the neat PLA fiber average diameter was nearly to 400nm, as shown in **Table 4.1**. Increasing collector rotating speed to 1100 rpm, the neat PLA fiber diameter was reduced by nearly 20%. For all mats, the fiber average diameter collected at higher speed was smaller than those of collected at lower speed. Likewise, the fiber diameter increased with filler content. It was found that the dynamic fluctuations of Taylor cone, electric field strength and charge density are the main important process variation factors which determine the resulting fiber diameter distributions.[35-37]

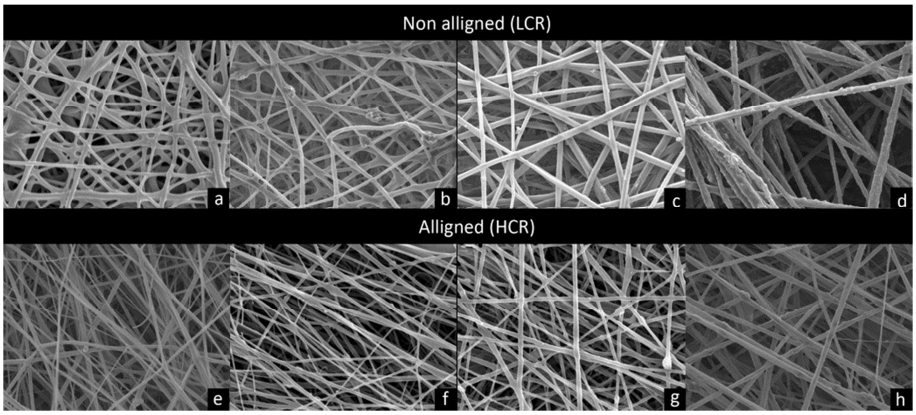

Figure 4.1. SEM images of electrospun PLA/HA mats obtained with different hydroxyapatite (HA) content at low and high collecting speeds (LCR and HCR). All the images are 5000x magnifications: neat PLA **(a,b)**, PLA/HA 9:1 **(c,d)**, PLA/HA 5:1 **(e,f)**, PLA/HA 3:1 **(g,h).**

According to the related literature, most obtained electrospinning mats with diameters in the nanometer range, showed Gaussian even Bimodal diameter distributions with standard deviations between 20% and 60% [36, 38, 39] depending on the material and processing conditions. In this regard, the standard deviation values showed in **Table 1** were within the normal range due to the instabilities in the jet during the electrospinning process.

Figure 4.2 shows the frequency distribution of the fiber orientation angle based on SEM images. When the speed increased to 1100 rpm, the fiber angle decreased and the amount of fiber in the same direction increased to approach to collector rotating direction, which implied that nanofiber orientation was improved. So the alignment degree of the electrospun nanofibers was increased with higher rotation speed of the collector.

Table 4.1. Electrospinning conditions for PLA and PLA/HA nanofibers mats and their corresponding average fiber diameter**.**

Electrospinning conditions							
Sample code	PLA/HA[a]	Rotation speed	Collector distance	Flow rate	Voltage	mL/mat	Diameter (nm)[b]
HCR PLA/HA (3:1)	3:1	1100	130	0.6	14	10	439±147
HCR PLA/HA (5:1)	5:1						357±92
HCR PLA/HA (9:1)	9:1						308±88
HCR PLA	1:0						323±117
LCR PLA/HA (3:1)	3:1	300					600±148
LCR PLA/HA (5:1)	5:1						523±120
LCR PLA/HA (9:1)	9:1						335±124
LCR PLA	1:0						409±163

Experimental results are expressed as mean ± standard deviation.
[a] Concentration of 7 wt% PLA solutions in DCM/ DMF (70/30).
[b] Average diameter was calculated by measuring the size of 30 fibers from SEM images at 5000x magnifications.

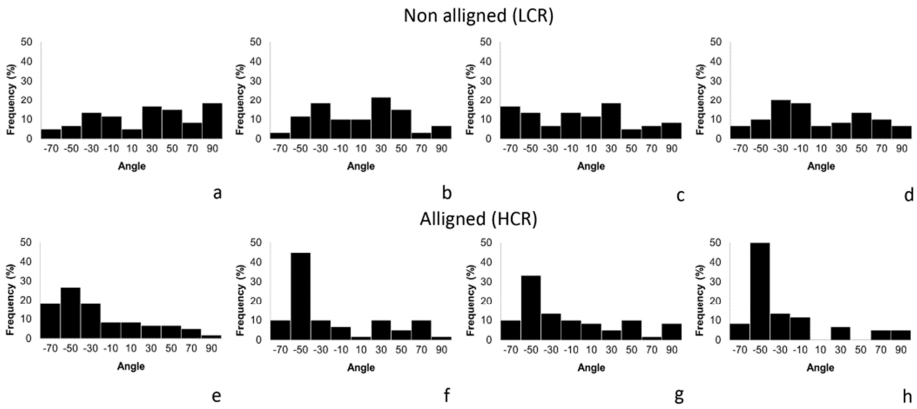

Figure 4.2. Fiber aligned angle distributions of PLA/HA mats obtained with different hydroxyapatite (HA) content at low and high collecting speeds (LCR and HCR): neat PLA **(a,b)**, PLA/HA 9:1 **(c,d)**, PLA/HA 5:1 **(e,f)**, PLA/HA 3:1 **(g,h)**.

Furthermore, the morphology of the hydroxyapatite embedded in the nanofibers was analyzed using TEM. As shown in the **Figure 4.3**, HA nanoparticles were dispersed in the matrix of PLA for low and high collecting rates. The fiber collected with the highest speed, seems to have low amount of aggregates for the same content of filler. In this regard, the smaller diameter, smoother surface and lower deformation of the fiber can be observed specially in the 3:1 sample collected at high speed, probably due to the high stretching force over the electrospinning jet induced by the faster rotation of the collector, which avoids the formation of the agglomerates and improves the dispersion of the filler inside the fiber.

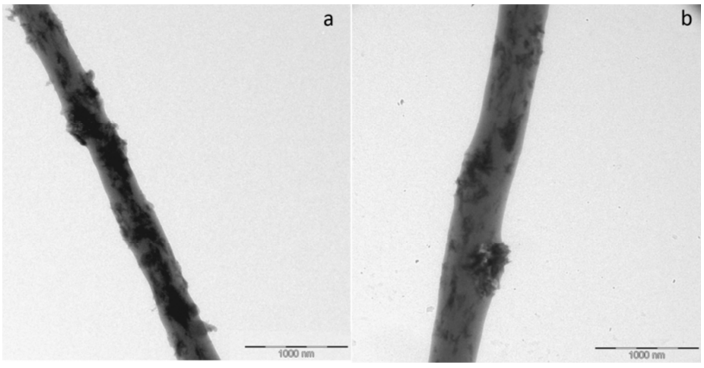

Figure 4.3. TEM images of electrospun fiber prepared with PLA/HA (3:1) at low and high collecting speeds (LCR and HCR): LCR **(a)** and HCR **(b)**.

3.2. THERMAL AND CRYSTALLINE BEHAVIOUR OF NANOFIBERS

The thermal behavior of PLA/HA nanofibers mats was characterized by means of DSC and the data were summarized in **Table 4.2**. **Figure 4.4** shows thermograms obtained from 1st heating run curves of pure PLA and PLA/HA (3:1) mats at high and low collecting rates (HCR and LCR). This heating run is characterized by a change in the heat capacity of the mats associated with the glass transition of PLA (between 55 °C and 60 °C), followed by an exothermic peak resulting from a partial crystallization of the material, attributed to the rearrange in amorphous molecular chains into a more ordered crystalline phase. The observed T_g for the casting PLA

was 54.79 °C and it showed a single melting peak at 152.31 °C. As can be seen, DSC curves of mats collected at high and low rates, experiment the glass transition and cold crystallization process.

Table 4.2. The melting and crystallization behaviors of PLA/HA nanofibers mats.

Sample	DSC 1st heating								DSC 2nd heating	Crystallinity (*Xc%*)	
	T_g (°C)	ΔC_p J/(g°C)	T_{cc} (°C)	ΔH_c (J/g)	T_{m1} (°C)	ΔH_{m1} (J/g)	T_{m2} (°C)	ΔH_{m2} (J/g)	T_{g2} (°C)	DSC 1st h.	WAXS
HCR PLA/HA (3:1)	60.9	0.5	89	10.0	166.7	24.7	195.6	1.7	60.9	17.5	17.2
HCR PLA/HA (5:1)	58.2	0.5	85	11.4	151.4	24.7	195.6	2.3	55.1	16.7	13.5
HCR PLA/HA (9:1)	57.1	0.6	84.5	11.8	152.1	32.0	195.6	3.4	54.9	25.3	16.3
HCR PLA	60.3	0.7	86.8	15.4	150.9	27.1	195.6	4.3	51.4	17.2	14.2
LCR PLA/HA (3:1)	63.5	0.2	96.7	15.5	164.3	23.1	--	--	60.6	8.1	9.3
LCR PLA/HA (5:1)	62.3	0.6	90.5	14.1	150.2	26.6	--	--	60.1	13.3	11.8
LCR PLA/HA (9:1)	61.3	0.8	87.4	15.9	153.3	35.1	--	--	60.4	20.5	11.5
LCR PLA	61.2	0.7	89.9	17.3	152.6	32.7	--	--	59.7	16.4	4.7
BULK PLA	54.8	0.4	--	--	152.3	1.1	--	--	61.0	1.2	0

*Glass transition temperature (T_g), cold crystallization temperature (T_{cc}) melting temperatures (T_{m1} and T_{m2}), crystallization and melting enthalpies (ΔH_c and ΔH_m) calculated from the first DSC heating run. T_{g2} was calculated from the second DSC heating run. DSC crystallinity values for LCR mats were calculated from Eq. (4.1), note that for HCR the ΔH_m value results are the sum of $\Delta H_{m1} + \Delta H_{m2}$.

After the rapid crystallization process, two well differentiate melting peaks (at about 150-166 °C and 195 °C respectively) appear only for PLA/HA samples collected at higher speeds, instead of the typical single melting peak that occurs on stationary mats. These melting peaks are separated by several degrees (28 °C for the PLA/HA (3:1) mat, and about 44 °C for the rest of mats). The double melting phenomenon is generally ascribed to several factors as reorganization processes of imperfect crystals leading to melt-recrystallization that occurs during the DSC

heating scan, and that may result from different crystal morphologies formed during electrospinning.[40-42]

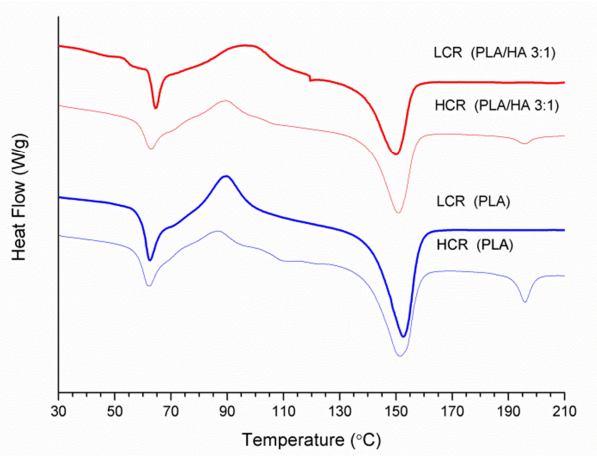

Figure 4.4. First heating run DSC thermograms of electrospun mats prepared from neat polylactic acid and PLA/HA (3:1) obtained at low and high collecting speeds (**LCR** and **HCR**).

Poly(lactic acid) can exhibit up to three possible crystal modifications (α, β and γ), depending upon the crystallization conditions.[43] The crystal structure of α and β forms have been widely investigated by several research groups, the first one was studied by De Santis and Kovacs[44] while the second one was reported by Eling.[45] Hoogsteen,[46] who found that the β structure melts at temperature about 10 °C below the melting temperature of the α structure. From this observation they concluded that the PLA β structure is some-what less stable than the α structure. In our case, the LCR and HCR electrospinning mats conserved the single melting peak that occurs in the casting PLA, but the second melting peak developed in the high collecting mats occurs about 40 °C above the first, that is, it has a higher thermal stability than the first one. So, the double melting peak phenomenon can be attributed here to the cold crystallization during the heating scan probably due to orientated crystals formed at a higher collection speed. As can be seen in **Table 4.2** a faster speed of the rotating collector not only produced two melting peaks in DSC

results, but also a slightly increase in the degree of crystallinity comparing the results of LCR with HCR mats.

Figure 4.5a shows the wide-angle diffraction pattern for neat hydroxyapatite and PLA/HA (3:1) mat obtained at high collecting speed. All peaks observed in the WAXS pattern of hydroxyapatite (HA) correspond to the hexagonal crystal system and are identified according to ICDD (International Centre for Diffraction Data) standard (PDF Card no. 9-432).[32, 47] These peaks appears for all PLA/HA mats around 2θ=25°, revealing the presence of the filler as can be previously seen in SEM images (**Fig.4.1**). The peaks intensity increases with the filler concentration.

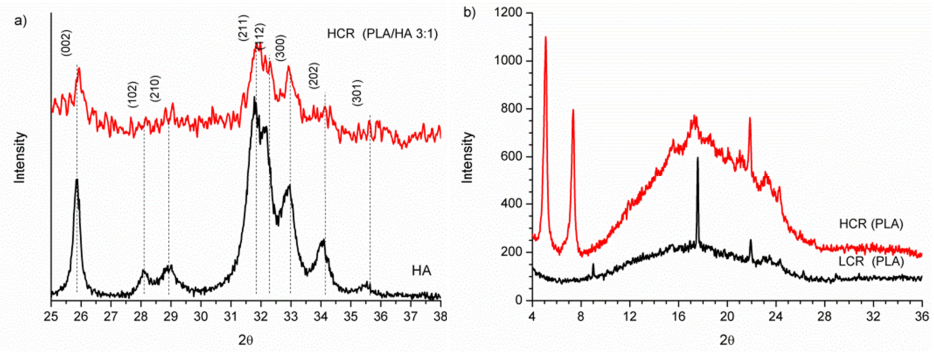

Figure 4.5. WAXS patterns for neat hydroxyapatite (HA) and PLA/HA (3:1) mat obtained at high collecting speed (HCR) **(a)**, WAXS patterns for neat poly-lactic acid (PLA) mats at low and high collecting speeds (LCR and HCR) **(b)**.

Figure 4.5b shows the diffraction patterns of low and high collecting rates for neat PLA mats, which exhibited notable differences in the crystalline peaks between them. LCR diffraction pattern exhibited six diffraction peaks with different intensities; two strong at 2θ = 17.1° and 21.4°, and four weaker peaks at 2θ = 8.5°, 22.6°, 23° and 28°. The HCR diffraction pattern shows at least eight peaks; three strong at 2θ =4.57°, 6.83° and 21.4° and five weaker at 2θ = 14.9°, 16.8°, 20.6°, 22.8° and 23.8°. **Figure 4.6** shows the resulting WAXS pattern for neat PLA mat after the fitting process.

Generally, authors have identified four PLA representative crystalline peaks in samples obtained by precipitations methods (casting) around 2θ =15°, 16°, 18.5° and 22.5° which are associated with the pure PLA crystallizing in a pseudo-orthorhombic α-form crystal with a 10_3 helical chain conformation and unit cell dimensions of a=1.07 nm, b=0.595 nm, and c=2.78 nm.[48] In the scientific literature regarding PLA electrospun mats, the diffraction peaks are partly or totally detected in many cases for annealed samples, depending on the treatment conditions. Zong and Fundador produced PLA electrospinning mats, and only after annealing processes the as-spun material showed at least the two main PLA diffraction peaks at around 16° and 18.5° [49, 50] which were in agreement with the values indexed as 110 and 131 reflections by Ikada for the α form of the PLA crystal. Fundador reported two other PLA characteristic peaks at 21.8° and 28.38°.[50] With respect to electrospun of poly(lactic acid)/Hydroxyapatite mats, Jeong and Sui,[51] reported peaks at around 2θ=26° and 32° which correspond to the typical diffraction angles of crystalline hydroxyapatite, indexed as 002 and 211 respectively.[52]

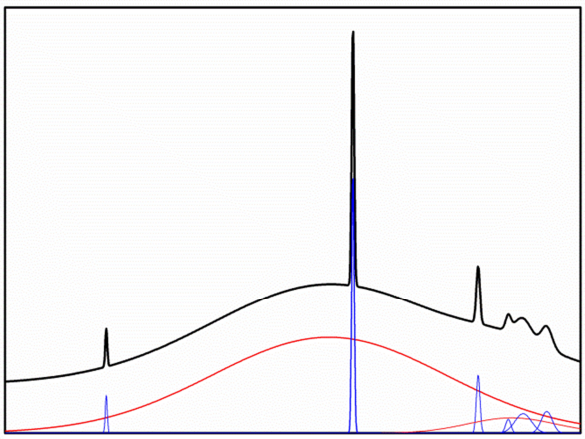

Figure 4.6. Gaussian peak fitting for neat PLA mat at low collecting speed (LCR PLA).

Liao et al.[53] used an additional centrifugal field to introduce a stronger stretching force in the preparation of aligned polylactic acid nanofibers. The diffraction

patterns of their material exhibited nine diffraction peaks, demonstrating than this additional centrifugal field induces crystalline features in the spun nanofibers. In our case, the LCR mats present the main peaks at about 17° and 21° which are in agreement with previous reports as characteristic peaks for the pseudo-orthorhombic α -form crystal with a 10_3 helical chain conformation form of the PLA crystal. The development of new peaks in the case of HCR mats demonstrate that an increase in collector speed not only increases the degree of alignment of the nanofibers, but can also induce crystalline features in PLA nanofibers, which is supported by WAXS and DSC crystallinity results (**Table 4.2**). Both methods show different values but the same general trend. The differences in the results between both crystallinity measuring methods is habitual in the published literature, and may be explained because of the X-ray diffraction measures the intramolecular order as a result of chain packaging and DSC measures the "meltable" crystalline portion which numerical values are not as exactly (real) as X-ray measurements. If we focus the attention on the X-ray crystallinity measurements, the results show evidence of the possible nucleating effect of the hydroxyapatite on the PLA as a consequence of the linear increase in crystallinity in the low volume fraction region. This effect decreased for high filler contents probably due to the formation of agglomerates, being more prominent in randomly oriented mats, as can be seen in the SEM images (**Fig.4.1**).

The T_g values obtained in second DSC heating scans are shown in **Table 4.2**. The T_g of neat PLA and PLA/HA at a weight ratio of 9:1, 5:1, 3:1 were in case of LCR mats: 59.7 °C, 60.4 °C , 60.1 °C and 60.6 °C and in case of HCR mats: 51.4 °C , 54.9 °C, 55.1 °C and 60.9 °C respectively. So, as expected, glass transition temperatures slightly increased with the addition of HA with an evident higher effect in the case of stretched HCR nanofibers.

Finally, regarding the thermal properties, **Figure 4.7** shows the TGA curves for PLA and PLA/HA nanofibers mats with different hydroxyapatite content. The % of filler

was found to be reasonably close to the values used in the initial formulations. HCR mats start their thermal decomposition at temperatures slightly higher than LCR mats, and the higher alignment produced less difference in the drop between neat and filled mats; but in all cases, an increase in the thermal stability of the filled samples confirms the stiffening effect of the nanoparticles. Moreover, thermal results measured as a maximum in a derivative curve, demonstrated a loss weight at about 230 °C in HCR samples probably due to the solvent remaining because of the high collecting speed which prevents its full evaporation.

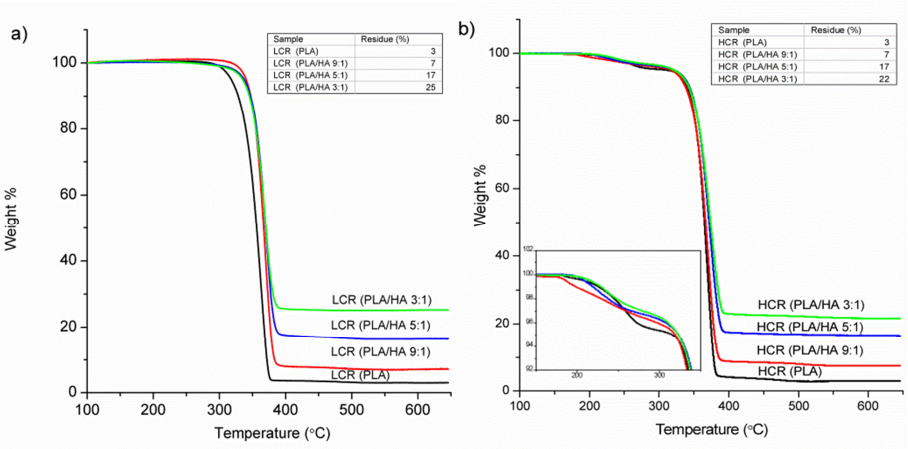

Figure 4.7. TGA curves of electrospun PLA and PLA/HA nanofibers mats. Low collecting speed mats (LCR) **(a)** and high collecting speed mats (HCR) **(b)**.

3.3. DYNAMIC MECHANICAL PROPERTIES

DMA thermograms of neat PLA and PLA/HA (3:1) nanofibers mats for LCR and HCR are reported in **Figure 4.8**. The storage modulus (E´) of HCR mats was higher than LCR probably due to a high degree of alignment and more packing structure. Moreover the E´ values of the electrospun nanofibers mats of PLA/HA were slightly higher, and the drops were more gradual than that of the unfilled samples. Also in this case, the higher alignment of the mats produced less difference in the drop between neat and filled mat. So it can be concluded that while the main effect of

the filler in the LCR mats is the stiffness increase produced, in case of HCR mats, the synergic effect of the alignment with the filler content is more noticeable.

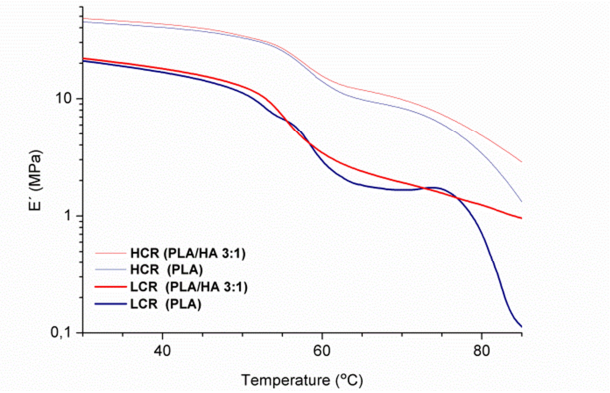

Figure 4.8. DMA thermograms of neat PLA and PLA/HA (3:1) nanofibers mats obtained at low and high collecting speeds (LCR and HCR).

4. CONCLUSIONS

Nanofibers mats of PLA/HA have been obtained via electrospinning onto a rotating mandrel, and their morphology has been characterized as a function of the production parameters. Electrospun mats were collected at two take-up velocities; randomly oriented fibers were produced on a stationary shaft, whereas highly oriented fibers were produced when rotation speed was increased to 1100 rpm. On one hand, the added HA particles into the nanofibers produced an efficient nucleating effect, and as a result of it, an enhanced in thermal and mechanical properties was observed. On the other hand, thanks to the high collection speed, the HCR resulting mats showed higher alignment and crystallinity degree until a certain value above which, the properties of the mats did not further improve probably due to the formation of filler aggregates. Crystallinity behavior was studied by DSC and supported by WAXS, both methods showed different numerical values as they measured different kinds of crystallinity, but the general trend was

the same. Finally, TGA results confirmed a higher thermal stability for aligned mats, as well as for mats with higher filler content.

ACKNOWLEDGEMENTS

This project has been supported by Project MAT2010/21494-C03 of Spanish Ministry for Science and Innovation (MICINN). AS acknowledges the support of FPU grant from MED (MED-FPU; AP2009-2482).

5. REFERENCES

1. I. Armentano, M. Dottori, E. Fortunati, S. Mattioli and J. M. Kenny, *Polymer Degradation and Stability*, 2010, **95**, 2126-2146.
2. A. Frenot and I. Chronakis, *Current Opinion in Colloid & Interface Science*, 2003, **8**, 64-75.
3. S. Ramakrishna, K. Fujihara, W. E. Teo, T. C. Lim and Z. Ma, *An Introduction to Electrospinning and Nanofibers*, World Scientific, Singapur, 2005.
4. P. P. Quynh, S. Upma and G. M. Dr. Antonios, *Tissue Engineering*, 2006, **12**, 1197-1211.
5. Z. Jing, X. Xu, X. Chen, Q. Liang, X. Bian, L. Yang and X. Jing, *Journal of Controlled Release*, 2003, **92**, 227-231.
6. S. Agarwal, J. H. Wendorff and A. Greiner, *Polymer,* 2008, **49**, 5603-5621.
7. H. Liu and Y. Hsieh, *Journal of Polymer Science Part B: Polymer Physics*, 2002, **40**, 2119-2129.
8. H. S. Kim, K. Kim, H. J. Jin and I. Chin, *Macromolecular Symposia*, 2005, **224**, 145-154.
9. S. F. Fennessey and R. J. Farris, *Polymer*, 2004, **45**, 4217-4225.
10. Z. M. Huang, Y. Z. Zhang, M. Kotaki and S. Ramakrishna, *Composites Science and Technology,* 2003, **63**, 2223-2253.

11. B. Sundaray, V. Subramanian, T. Natarajan, R. Xiang, C. Chang and W. Fann, *Applied Physics Letters*, 2004, **84**, 1222-1224.
12. D. H. Reneker and A. L. Yarin, *Polymer,* 2008, **49**, 2387-2425.
13. G. Lu, H. Tang, Qu. Y, L. Li and X. Yang, *Macromolecules*, 2007, **40**, 6579-6584.
14. N. Liu, M.M. Shi, X.W. Pan, W.M. Qiu, J.H. Zhu and H.P. He, *The Journal of Physical Chemistry C,* 2008, **112**, 15865-1869.
15. Q. Chen, L. Zhao, C. Li and G.Shi, *The Journal of Physical Chemistry C*, 2007, **111**, 18392-18396.
16. R. Gangopadhyay and A. De, *Chemistry of materials*, 2000, **12**, 608-622.
17. Y. Yang, M.C. Gupta, K.L. Dudley and R.W. Lawrence, *Nano letters*, 2005, **5**, 2131-2134.
18. G. Liu, H. Wang and X. Yang, *Polymer*, 2009, **50**, 2578-2586.
19. F. F. Fang, J. H. Kim and H. J. Choi, *Polymer*, 2009, **50**, 2290-2293.
20. F. Guo, Q. Zhang, B. Zhang, H. Zhang and L. Zhang, *Polymer*, 2009, **50**, 1887-1894.
21. H. Ding, X.M. Liu, M. Wanm and S.Y. Fu, *The Journal of Physical Chemistry B*, 2008, **112**, 9289-9294.
22. N.S. Kommareddi, M. Tata, V.T. John, G.L. McPherson, M.F. Herman and Y.S. Lee, *Chemistry of Materials*, 1996, **8**, 801-809.
23. L.L. Beecroft and C.K. Ober, *Chemistry of Materials*, 1997, **9**, 1302-1317.
24. L. Dennany, E.J. O´Reilly, P.C. Innns, G.G. Wallace and R.J. Foster, *The Journal of Physical Chemistry B*, 2009, **113**, 7443-7448.
25. R. Sainz, W.R. Small, N.A. Young, C. Vallés, A.M. Benito and W.K. Maser, *Macromolecules*, 2006, **39**, 7324-7332.
26. R. Ravindranath, P.K. Ajikumar, N.B. Hanafiah, W. Knoll and S. Valiyaveettil, *Chemistry of Materials*, 2006, **18**, 1213-1218.
27. U. Costantino, V. Bugatti, G. Gorrasi, F. Montanari, M. Nocchetti and L. Tammaro, *ACS Applied Materials & Interfaces*, 2009, **1**, 668-677.

28. E. Chiellini, P. Cinelli, V.I. Ilieva and M. Martera, *Biomacromolecules*, 2008, **9**, 1007-1013.
29. D. Zhang, M.A. Kandadai, J. Cech, S. Roth and S.A. Curran, *The Journal of Physical Chemistry B*, 2006, **110**, 12910-12915.
30. M.C. Urbina, S. Zinoveva, T. Miller, C.M. Sabliov, W.T. Monroe and C.S.S.R. Kumar, *The journal of physical chemistry C*, 2008, **112**, 11102-11108.
31. H. Kim, H. Lee and J. C. Knowles, *Journal of Biomedical Materials Research Part A*, 2006, **79A**, 643-649.
32. A. Bigi, B. Bracci and S. Panzavolta, *Biomaterials*, 2004, **25**, 2893-2899.
33. X. Xu, X. Chen, A. Liu, Z. Hong and X. Jing, *European Polymer Journal,* 2007, **43**, 3187-3196.
34. R. Dersch, T. Liu, A. K. Schaper and A. Greiner, J. H. Wendorff, *Journal of Polymer Science Part A: Polymer Chemistry*, 2003, **41**, 545-553.
35. A. Greiner, J. H. Wendorff, S. Ramakrishna and S. Agarwal, *Electrospinning: Materials, Processing, and Applications*, John Wiley & Sons, Germany, 2012.
36. K. Chang and H. Lin, *Journal of Polymer Research,* 2009, **16**, 611-622.
37. J. M. Deitzel, J. Kleinmeyer, D. Harris and N. C. Beck Tan, *Polymer,* 2001, **42**, 261-272.
38. X. Yan and M. Gevelber, *Journal of Electrostatics*, 2010, **68**, 458-464.
39. Z. Jun, H. Q. Hou, A. Schaper, J. H. Wendorff and A. Greiner, *e-Polymers*, 2003, **9**, 001- 009.
40. X. Hu, H. Xu and Z. Li, *Macromolecular Materials and Engineering*, 2007, **292**, 646-654.
41. M. L. Di Lorenzo, *Journal of Applied Polymer Science*, 2006, **100**, 3145-3151.
42. C. Wang, H. Chien, K. Yan, C. Hung, K. Hung, S. Tsai and H. Jhang, *Polymer*, 2009, **50**, 6100-6110.
43. R. Auras, L.T. Lim, S.EM: Selke and H. Tsuji, *Poly(Lactic Acid): Synthesis, Structures, Properties, Processing, and Applications*, John Wiley & Sons, Inc., New Jersey, 2010.

44. P. De Santis and A. J. Kovacs, *Biopolymers,* 1968, **6**, 299-306.
45. B. Eling, S. Gogolewski and A. J. Pennings, *Polymer*, 1982, **23**, 1587-1593.
46. W. Hoogsteen, A.R. Postema, A.J. Pennings, G.T. Brinke and P. Zugenmaier, *Macromolecules*, 1990, **23**, 634-642.
47. M. Sadat-Shojai, *Journal of the Iranian Chemical Society*, 2009, **6**, 386-392.
48. Y. Ikada, K. Jamshidi, H. Tsuji and S. Hyu Hyon, *Macromolecules* 1987, **20**, 904-906.
49. X. H. Zong, K. Kim, D. F. Fang, S. F. Ran, B. S. Hsiao and B. Chu, *Polymer* 2002, **43**, 4403-4412.
50. N. G. V. Fundador, A. Takemura and T. Iwata, *Macromolecular Materials and Engineering*, 2010, **295**, 865-871.
51. S. I. Jeong, E. K. Ko, J. Yum, C. H. Jung, Y. M. Lee and H. Shin, *Macromolecular Bioscience*, 2008, **8**, 328-338.
52. G. Sui, X. Yang, F. Mei, X. Hu, G. Chen, X. Deng and S. Ryu, *Journal of Biomedical Materials Research Part A*, 2007, **82A**, 445-454.
53. C. Liao, C. Wang, C. Chen, *Polymer*, 2011, **52**, 4303-4318.

Chapter 5

Mechanical and shape-memory properties of Poly(mannitol sebacate)/Cellulose Nanocrystal nanocomposites

Águeda Sonseca, Sandra Camarero-Espinosa, Laura Peponi, Christoph Weder, E. Johan Foster, José M. Kenny, Enrique Giménez

Journal of Polymer Science Part A; Polymer Chemistry 52 (2014) 3123-3133

DOI: 10.1002/pola.27367

MECHANICAL AND SHAPE-MEMORY PROPERTIES OF POLY(MANNITOL SEBACATE) /CELLULOSE NANOCRYSTAL NANOCOMPOSITES

Águeda Sonseca[1]*, Sandra Camarero-Espinosa[2], Laura Peponi3, Christoph Weder[2], E. Johan Foster[2], José M. Kenny[3], and Enrique Giménez[1]

[1]Instituto de Tecnología de Materiales, Universidad Politécnica de Valencia (UPV), Camino de Vera s/nº, 46022 Valencia (Spain)

[2]Adolphe Merkle Institute, University of Fribourg, Rte de l´Ancienne Papeterie, CH-1723 Marly (Switzerland)

[3]Instituto de Ciencia y Tecnología de Polímeros (ICTP-CSIC), Juan de la Cierva 3, 28006 Madrid (Spain)

***Corresponding author: agsonol@posgrado.upv.es**

Abstract

Polyesters based on polyols and sebacic acid, known as poly(polyol sebacate)s (PPS), are attracting considerable attention, as their properties are potentially useful in the context of soft-tissue engineering applications. To overcome the drawback that PPS generally display rather low strength and stiffness, we have pursued the preparation of nanocomposites based poly(mannitol sebacate) (PMS), a prominent example of this materials family, with cellulose nanocrystals (CNCs). Nanocomposites were achieved in a two-step process. A soluble, low-molecular-weight PMS pre-polymer was formed via the polycondensation reaction between sebacic acid and D-mannitol. Nanocomposites with different CNCs content were prepared by solution-casting and curing under vacuum using two different profiles designed to prepare materials with low and high degree of crosslinking. The as-prepared nanocomposites have higher stiffness and toughness than the neat PMS

matrix while maintaining a high elongation at break. A highly crosslinked nanocomposite with a CNCs content of 5 wt% displays a 6-fold increase in Young´s modulus and a 5-fold improvement in toughness. Nanocomposites also exhibit a shape-memory effect with a switch temperature in the range of 15-45 °C; in particular the materials with a thermal transition in the upper part of this range are potentially useful for biomedical applications.

Keywords: Poly(polyol sebacate), cellulose nanocrystals, nanocomposites, nanoparticles, mechanical properties, shape-memory.

1. INTRODUCTION

Synthetic polyester elastomers have received extensive attention in the past few years because of their stable network structure, elastic properties, biodegradability under physiological conditions and biocompatibility with response of the host tissue similar to PLA and PLGA resulting in formation of thinner fibrous capsules as well as lower inflammatory response.[1, 2] Several polyester elastomers based on polyols such as 1,8-octanediol, ethylene glycol, butylene glycol or glycerol, and carboxylic acids such as citric and sebacic acid,[3-7] have been considered for soft tissue engineering applications such a nerve-guidance, drug delivery, tissue adhesives and scaffolds to repair or replace body tissues.[8-11] After Wang et al.[12] first reported crosslinked poly(glycerol sebacate) (PGS) elastomers, several other polyols have been used instead of glycerol to expand the properties of the family of poly(polyol sebacate)s (PPS).[1] Attractive features of PPS are that they are based on inexpensive, non-toxic monomers and that their mechanical properties can be readily tuned through the choice of the polyol, the monomer ratio, and the polycondensation conditions. Nevertheless, the spectrum of mechanical properties (tensile strength and elastic modulus) that can be achieved without compromising their elasticity is limited.[1, 13] This limits their use even in some soft tissue engineering applications in which the tissue involved is at the same time stiffer (Young's modulus = 0.7-250 MPa) and more elastic (elongation at break > 10%) than representatives of the PPS family, such skin, nerves, cartilage, heart valves, and tendons.[14-16] Their usefulness is thus limited in applications where high strength and high flexibility are required, such as ligating rubber bands for blood vessels, elastomeric sutures, flexible coatings for stents, surgical devices, vascular grafts, surgical wound dressings, or catheters and small diameter tubes for drainage.[17] The addition of reinforcing fillers has proven to be an effective approach to increase the strength and stiffness of a given polymer, but normally these improvements come at the expense of a reduction of the elasticity. Most of

the approaches to create PPS composites are based on the introduction of inorganic components such halloysiste nanotubes (clays) or multi-walled carbon nanotubes (MWCNTs).[18-20] In the last decade, composite materials based on nanocellulose have been the base of research efforts because the fact that natural cellulosic materials are abundant, inexpensive, renewable, biodegradable under certain conditions, and exhibit generally low toxicity.[21, 22] Cellulose nanocrystals (CNCs)[23-26] might be a particularly interesting filler to reinforce low-modulus PPS matrices, as they exhibit high stiffness (elastic modulus ~143 GPa) and high aspect ratio (with diameters of ~5 to 50 nm and lengths of 100 to 3000 nm depending on the source).[27-29] Compared with other nanofillers such as clays or bioceramics (Bioglass®), CNCs have superior specific properties.[27, 30] The specific Young´s modulus of commercial Bioglass® is ~13 GPa cm^3/g and for clays ~55 GPa cm^3/g while the value for CNC, is ~100 GPa cm^3/g due to its low density.[31-34] Multi-walled carbon nanotubes MWCNTs have a higher specific modulus than CNCs, but the latter have an established manufacturing process and likely lower cost apart from significantly lower toxicity.[22, 35, 36] In addition, the presence of abundant hydroxyl groups on the CNC surface is expected to promote a uniform dispersion of the filler in the PMS matrix investigated through a strong affinity or reaction with the hydroxyl and carboxyl functional groups in the polymer backbone.[37] Here we show that the PMS/CNCs nanocomposites exhibit a higher stiffness and toughness than the neat PMS matrix while a high elongation at break is maintained. We further demonstrate that their property matrix makes the new nanocomposites useful as biomedical shape-memory polymers (SMPs); in particular the increased mechanical energy that can be stored in the temporary shape is useful,[38] as it permits to exert force enabling better shape recovery in complicated or restricted environments where displacement of the surrounding tissue is required. Based on this enhancement of the rubbery modulus region observed, we also investigated the thermal induced shape-memory properties of these materials.

2. EXPERIMENTAL SECTION

2.1. MATERIALS

Deuterated dimethylsulfoxide (DMSO- d_6), dimethylformamide (DMF), sulfuric acid, sebacic acid (SA) (99% purity), and D-mannitol (MA) (99% purity), were purchased from Sigma Aldrich. Hydrochloric acid (HCl, 37% reagent grade) and sodium hydroxide (NaOH, 98% reagent grade) were purchased from Scharlau. Ultrapure water was directly taken from a Sartorius Stedim Arium 611 VF® water purification system (ρ = 18.2 mΩ·cm). Cellulose nanocrystals were isolated from cotton (Whatman No. 1 filter paper) by controlled hydrolysis with sulfuric acid according to a protocol[39] that is a modification of the method originally described by Dong et al.[40] The protocol introduces a small concentration of sulfate ester groups on the surface of the CNCs, which help to form stable suspensions in polar solvents.[41]

2.2. ISOLATION AND PROPERTIES OF CNCs

CNCs were isolated from cotton using a previously reported protocol.[39] TEM analysis of the CNC suspension after sulfuric acid hydrolysis revealed a needle-like structure. Dimensions and aspect ratio (length:width) of the CNCs were determined by analysis of several TEM images (**Supporting Information Figures S5.1 and S5.2**) resulting in an average width of 18±2 nm, an average length of 199±14 nm, and an average aspect ratio of 11±1 (**Supporting Information Table S5.2**). The apparent crystallinity of the CNCs was calculated from X-ray diffraction (XRD) patterns. The crystal structure of the CNCs is cellulose I, and the apparent crystallinity was determined to be 69% (**Supporting Information Figure S5.3**). The concentration of the surface charges present as sulfate groups on the surface of the CNCs was determined by conductometric titration. This experiment revealed a sulfate content of 91±4 mM/$kg_{cellulose}$ (**Supporting Information Figure S5.4**), which is in accordance with previously reported values.[42]

2.3. SYNTHESIS OF POLY(MANNITOL SEBACATE) (PMS) PRE-POLYMER

Sebacic acid (SA) and mannitol (MA) were reacted as described previously.[1] Equimolar amounts (0.068 mol) of SA (13.79 g) and MA (12.42 g) were charged into a 250 mL three-necked round-bottom flask equipped with a stirrer and a condenser, which was placed in an oil heating bath and purged during 0.5 h with nitrogen. The temperature was slowly increased to 150 °C under continuous stirring and nitrogen flow to produce approximately 20 g of the pre-polymer (**Scheme 5.1**). The reaction was stopped after 13 h (1 h before gelation occurs), and the pre-polymer was dissolved in DMF (150 mg/mL), filtered and purified by dropwise precipitation into a 4-fold excess of cold ultrapure water under continuous stirring. The precipited pre-polymer was collected and dried under vacuum until no more solvent was detected in the infrared spectra. The yield of the reaction was ~82%, as calculated from the weight of the monomers before reaction and the weight of the obtained pre-polymer after reaction.

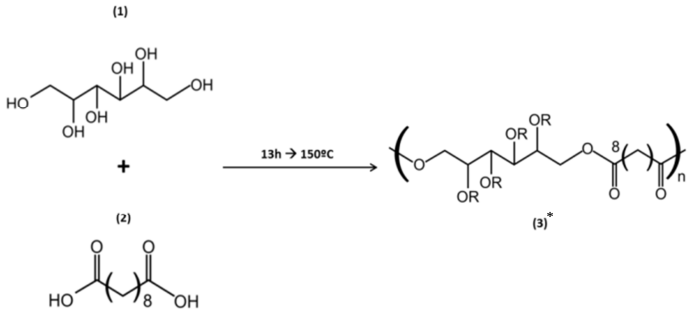

Scheme 5.1. Schematic representation of the general synthesis of the poly(mannitol sebacate) pre-polymer. Mannitol (1) was polymerized with sebacic acid (2) into poly(mannitol sebacate) (PMS) (3). *****Some degree of branching taking place at late stages of polymerization cannot be excluded.

2.4. CHARACTERIZATION OF PMS PRE-POLYMER

The number-average molecular weight (M_n), weight-average molecular weight (M_w), and polydispersity index (PDI) of the PMS pre-polymer were determined by gel permeation chromatography (GPC). The experiment was conducted on a series

1200 HPLC system (Agilent Technologies) equipped with a Polymer Laboratories PLgel 5 μm mixed-C column and two detection systems: a multi-angle laser light scattering (MALLS, miniDAWN^{TM} TREOS) (λ = 658 nm, 25 °C) and a refractive index (RI, Optilab REX) (λ = 658 nm, 40 °C) detector. The sample concentration was ~2 mg/mL and THF was used as eluent at 40 °C (flow rate, 1.0 mL/min). The chromatogram was processed with Wyatt Technology software (ASTRA). The incremental refractive index (*dn/dc*) was estimated by a single-injection method that assumed 100% mass recovery from the columns. The GPC analysis resulted a M_n = 6180 g/mol and M_w = 7501 g/mol (**Supporting Information Table S5.1**). The ^{1}H-NMR spectrum of the PMS pre-polymer was acquired in DMSO-d_6 on a Varian Mercury VX-300 MHz NMR spectrometer (**Supporting Information Figure S5.5**). The composition was determined from the ratio of the integrals of the signals associated with the mannitol and sebacic acid peaks[1] revealing an incorporation of approximately equimolar amounts of the monomers into the pre-polymer.

2.5. PREPARATION OF PMS/CNC NANOCOMPOSITES

The pre-polymer was first dissolved in DMF (100 mg/mL) by stirring for 4 h. Suspensions of CNCs at concentration of 10 mg/mL were prepared at appropriate ratio in DMF (designed to combine with 1.5 g of dry pre-polymer and form 1 wt%, 5 wt% and 10 wt% of PMS/CNC nanocomposites) by 40 min of ultrasonic treatment in a horn sonicator (Q500 sonicator, QSonica, 20kHz/500Watts, fitted with a ¼" microtip probe) with 1 sec on/off pulse conditions at a 20% of amplitude. CNC suspensions were stirred with PMS pre-polymer/DMF solution for 30 min and cast into aluminium Petri dishes (93 x 7 mm) and allowed to dry in an oven at 70 °C. Films consisting of the neat pre-polymer only, were prepared for reference purposes under the same conditions. The resulting pre-polymer/nanocomposite and the neat pre-polymer films were placed in a vacuum oven for further reaction. Two different curing profiles were applied, in which temperature and duration of the thermal treatment were varied to obtain samples with low and high degree of

crosslinking. Samples with low degree of crosslinking were maintained at 120 °C for 72 hours under vacuum (60 cm Hg). Samples with high degree of crosslinking were obtained by using the same protocol and subsequently increasing the temperature to 170 °C while maintaining the vacuum (60 cm Hg) for a further 24 hours. Both procedures afforded films of ~150-200 μm of thickness.

2.6. FOURIER TRANSFORM INFRARED SPECTROSCOPY (FTIR)

FTIR transmission spectra were recorded for all samples using a Thermo Nicolet 5700 spectrometer between 500-4500 cm^{-1} with a 4 cm^{-1} resolution and an Attenuated Total Reflectance (ATR) cell. Backgrounds were acquired before every 3rd sample. All samples were vacuum-dried before measurement.

2.7. TRANSMISSION ELECTRON MICROSCOPY (TEM)

A Phillips CM10 microscope with an accelerating voltage of 80 kV was used to record TEM micrographs of thin cross sections of the composites. Thin cross sections (thickness 3-10 μm) were cut under cryogenic conditions using a Leica CM1950 cryostat; they were stained with 2% aqueous uranyl acetate on carbon-coated copper grids.[43]

2.8. MECHANICAL MICROTESTING

The elongation at break, Young´s modulus and ultimate tensile strength were analyzed by mechanical tensile tests carried out on a DEBEN microtester equipped with a 150 N load cell and operated at a crosshead speed of 0.4 mm/min at room temperature. Specimen dimensions were typically 15 x 4 mm x 150 to 200 μm. The Young´s modulus (E) was determined from the initial slope of the stress-strain curves in the strain range of 0 to 10% for samples with low degree of crosslinking and 0 to 5% for samples with high degree of crosslinking. For each sample, a

minimum of 5 rectangular samples were tested and the mechanical data were averaged.

2.9. DYNAMIC MECHANICAL THERMAL ANALYSIS (DMTA) AND THERMALLY ACTIVATED SHAPE-MEMORY PROPERTIES

The mechanical behavior as a function of temperature was characterized by DMTA measurements on a TA Q800 instrument (TA instruments). Samples were cut into 30 x 4 mm x 150 to 200 µm rectangular shapes and tested in tensile mode with a temperature ramp method from -50 to 150 °C at a heating rate of 3 °C/min. Frequency and strain amplitude were kept constant at 1 Hz and 15 µm, respectively. Glass transition temperatures were calculated as the maximum in tangent delta peak. Shape-memory characteristics of the samples were quantified by cyclic, thermomechanical tensile tests in the DMTA. The experiment involved the creation of a temporary shape in a programming mode and a free stress recovery step of the permanent shape. The programming mode was performed under strain-controlled conditions in three steps: (1) the sample was equilibrated at 45 °C for 10 min before a force ramp of 3 N/min was applied until a strain of 30% was reached. (2) While the stress was kept constant, the sample was subsequently cooled to 15 °C. (3) The sample was unloaded to zero stress and the temperature was maintained at 15 °C for 5 min to ensure the fixation of the temporary shape. At this point, the recovery step was initiated by increasing the temperature to 45 °C, which was then maintained for 20 min. All samples were tested for 3 or 4 cycles. The ability to fix the temporary shape at 15 °C (shape fixity ratio, R_f) and the ability to recover the permanent shape at 45 °C (shape recovery ratio, R_r) were quantified using the following equations:[44-46]

$$R_f(N) = \frac{\varepsilon_u(N)}{\varepsilon_m(N)} \times 100\% \quad (5.1)$$

$$R_r(N) = \frac{\varepsilon_m(N) - \varepsilon_f(N)}{\varepsilon_m(N) - \varepsilon_f(N-1)} \times 100\% \quad (5.2)$$

, where ε_m is the maximum strain achieved in the N^{th} cycle after cooling and before unloading, ε_u is the fixed strain after unloading the sample at 15 °C in the same cycle, and ε_f is the residual strain of the sample after the recovery step. Samples with high degree of crosslinking conditions were also tested using a programming temperature of 60 °C. Should be pointed out that the shape-memory temperature profiles where selected taking in account the results obtained in the DMTA analysis and to fulfil the requirements for future biomedical applications in terms to facilitate the manipulation, storage and implantation of a possible device. Shape-memory biomedical devices are recommended to be activated in the range of 36-55 °C, being also desirable the possibility to avoid premature activation retaining the shape at room temperature.[47]

3. RESULTS AND DISCUSSION

3.1. SYNTHESIS OF THE PMS PRE-POLYMER AND ITS NANOCOMPOSITES WITH CNCs

The preparation of the PMS/CNC nanocomposites was achieved in a two-step process. First, a soluble, low-molecular-weight PMS pre-polymer was formed via the polycondensation reaction between sebacic acid and D-mannitol (**Scheme 5.1**). In this first stage, the esterification is preferentially dominated by the reaction of the primary hydroxyl groups from D-mannitol (situated at two ends) with carboxylic acid groups from sebacic acid.[48, 49] The reaction was stopped before gelation occurred, affording a polyester with a number-average molecular weight, M_n of 6180 g/mol and a weight-average molecular weight, M_w of 7501 g/mol. Nanocomposites with 1 wt%, 5 wt% and 10 wt% CNCs were subsequently prepared by solution-casting mixtures of the PMS pre-polymer and the CNCs, and curing in a second step under vacuum using two different curing profiles designed to prepare materials with low and high degree of crosslinking. At this point, there is a lack of primary hydroxyl groups in the pre-polymer backbone resulting in a second stage dominated by the reaction of the secondary hydroxyl groups from D-mannitol with

residual carboxylic acids from sebacic acid crosslinking the system. However, the addition of CNCs to the system, introduces new hydroxyl groups that can offset the initial stoichiometry of OH/COOH groups. Given the surface chemistry of the CNC along with the presence of unreacted hydroxyl and carboxyl groups in the pre-polymer, when the system is heated, the new hydroxyl groups from the filler can participate and compete in ester formation and hydrogen bonding interactions with the pre-polymer chains becoming part of the network. To have an idea of how much the stoichiometry of the system can be modified, **Table 5.1** shows an estimation of how the presence of CNCs affects the concentration of –OH groups introduced in each composite with the CNC addition (**Supporting Information Calculation Method M5.1**) increased from 6, 30 and 60 % for 1, 5 and 10 wt% of CNC respectively.

Table 5.1. Amount of –OH groups introduced by CNCs in the Pre-PMS samples.

Pre-PMS -OH available (mol)[a]	CNC (wt%)	Cellulose -OH available (mol)[b]	Total –OH available in the sample (mol)	Increase amount of -OH in the sample (%)	ρ (g/cm3)[c]	-OH Molarity (mol/cm^3)[d]
5.3e^{-4}	0	0	5.3e^{-4}	0	0.70±0.08	0.37
	1	3.3e^{-5}	5.6 e^{-4}	6	0.96±0.04	0.54
	5	1.6e^{-4}	6.9 e^{-4}	31	1.15±0.03	0.80
	10	3.2e^{-4}	8.6 e^{-4}	62	1.16±0.03	1.00

The total amount of –OHs available on 1g of PMS matrix was estimated assuming an ideal linear pre-polymer with four available –OHs per mannitol molecule taking into account the molecular weight value obtained from GPC experiments. The total amount of –OHs available on the CNC introduced in each sample (1, 5, and 10 wt %) was estimated taking in account the molecular weight of native cellulose with 20% of the total –OHs as reactive sites. As the addition of CNCs slightly changes the volume of the nanocomposites, the amount of moles, were adjusted to molarity taking in account the mass density of the materials obtained using a pycnometer (50 cm^3). Mass densities were obtained from dried pre-PMS and pre-PMS/CNC (1, 5, and 10 wt % of CNC) nanocomposites, previously treated at 120°C and 60 cmHg for 1 day to achieve a minimum stiffness and the same treatment for all the samples.

[a] Determined from GPC Pre-PMS M_w, considering four reactive –OH per molecule

[b] Determined considering 180.1 g/mol as a M_w of cellulose and 20% of reactive –OHs

[c] Samples were maintained 1 day at 120 °C under 60 cmHg before measuring the density with a pycnometer (50 cm^3)

[d] Determined taking into account the mass densities of the samples

The total amount of –OHs available on 1g of PMS matrix was estimated supposing an ideal linear pre-polymer with four available –OHs per mannitol molecule taking into account the molecular weight value obtained from GPC test. The total amount of –OHs available on the CNC introduced in each sample (1, 5 and 10 wt%) was estimated taking in account the molecular weight of native cellulose with 20% of the total –OHs as reactive sites.[50]

The morphology of the nanocomposites was investigated by transmission electron microscopy of cryo-microtomed samples. The micrograph shown in **Figure 5.1** corresponds to the highest filler ratio nanocomposite with high degree of crosslinking, and reveals well-dispersed CNCs in the PMS matrix. This sample is representative of the filler distribution along all the samples, since lower CNC contents are easy to disperse as they have lower trend to form aggregates, and in addition, the differences in the crosslinking profile are not expected to produce high differences in the dispersion of the filler as no solvent was present when the curing profiles were initiated.

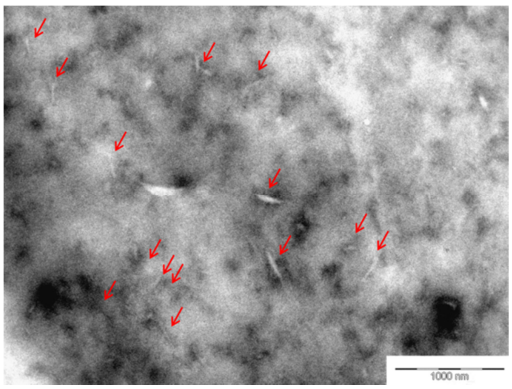

Figure 5.1. Transmission electron micrograph (TEM) of the PMS nanocomposite containing 10 wt% CNC and with a high degree of crosslinking, stained with 2% aqueous uranyl acetate solution. Note individualized CNCs indicated by the red arrows.

Furthermore, in order to confirm the ester formation and the presence of CNCs, ATR-FTIR spectra of the neat PMS matrix and the PMS/CNC nanocomposites

prepared under low and high degree of crosslinking conditions were recorded. **Figure 5.2** shows parts of the spectra in which the most relevance bands are observable; the full IR-spectra are shown in **Supporting Figure S5.6**. For both curing conditions, the spectra of the neat PMS show the characteristic absorption bands for hydrogen-bonded hydroxyl groups (3500-3200 cm^{-1}) and for carbonyl stretching vibrations of the ester groups (1800-1600 cm^{-1}) in the polymer backbone, confirming the formation of polyesters. The bands around 2924 cm^{-1} and 2852 cm^{-1} are assigned to methylene (-CH_2-) groups for the diacid residue and are observed in all spectra.

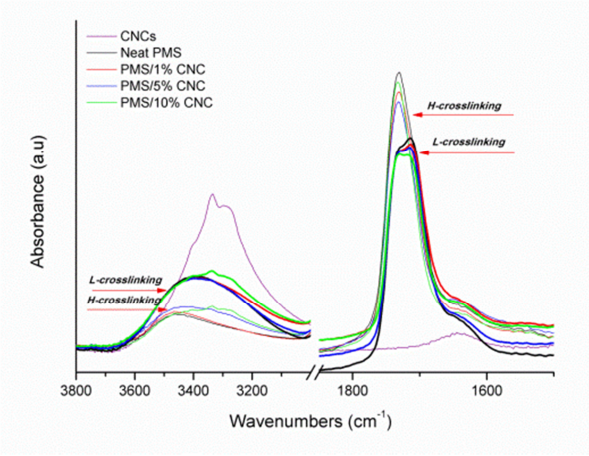

Figure 5.2. FTIR spectra detail of the -OH region (3500-3200 cm^{-1}) and C=O region (1800-1600 cm^{-1}) for low degree of crosslinking **(L)** and high degree of crosslinking **(H)** neat PMS and PMS/CNC nanocomposites.

A peak close to 1150 cm^{-1} was assigned to the –CO stretch associated with the ester groups.[51] Samples prepared under low degree of crosslinking conditions show a broad and intense -OH stretch peak at 3350 cm^{-1}, an acid peak at 1705 cm^{-1}, and an ester peak at 1740 cm^{-1}, revealing a substantial fraction of unreacted hydroxyl and acid groups. Samples prepared under high degree of crosslinking conditions show a smaller absorption related to the hydroxyl groups at 3350 cm^{-1} and a more pronounced –CO stretch associated with the ester groups, indicating a higher degree of esterification. Inspection of the spectra of the nanocomposites reveal a

similar picture; in the case of nanocomposites with 5 and 10 wt% CNCs, peaks associated with the CNC–OH close to 3338 cm^{-1} can also be discerned.

3.2. MECHANICAL TESTING

To relate the incorporation of CNCs and the different curing conditions to the mechanical properties of the PMS matrix, micro-tensile tests were carried out. In both systems (samples with low and high degree of crosslinking), the introduction of CNCs led to an improvement of the Young´s modulus and tensile strength, which increase with the CNC content (**Table 5.2**, **Figure 5.3**). Also the elongation at break and toughness increased up to a CNC content of 5 wt%, whereas a higher CNC content seems to decrease these properties.

Table 5.2. Curing conditions, physical and mechanical properties of PMS and nanocomposites.

Sample	Crosslinking conditions	Young´s modulus (MPa)[c]	Ultimate tensile strength (MPa)[c]	Elongation at break (%)[c]	Tg by DSC (°C)[d]	Tg by DMTA (°C)[e]	Toughness (MJ/m^3)[c]
Neat PMS	[a] Low degree of crosslinking **(L)**	1.8±0.3	1.2±0.7	80.0±29.0	18	21	63.6±50.0
PMS/1% CNC		2.1±0.5	2.3±0.02	147.0±31.1	18	22	187.4±46.3
PMS/5% CNC		3.0±0.3	4.6±0.6	166.0±20.5	18	23	393.5±5.2
PMS/10%CNC		6.0±0.7	5.6±0.4	119.5±18.3	17	14	389.0±86.4
Neat PMS	[b] High degree of crosslinking **(H)**	54.4±3.3	7.0±0.6	40.5±7.0	26	34	204.4±6.3
PMS/1% CNC		54.5±1.6	13.2±2.2	94.1±14.0	24	42	757.4±238.0
PMS/5% CNC		132.5±20.6	20.1±3.4	77.0±12.6	21	34	1047.0±310.0
PMS/10%CNC		103.0±12.2	19.4±2.4	37.4±6.0	20	32	470.0±102.2

[a] 120 °C, 60 cm Hg, 3days
[b] **L** + 170 °C, 60 cm Hg, 1day
[c] Determined from stress strain curves
[d] Determined from differential scanning calorimetry traces *(**Supporting Information Figure S5.9**)*
[e] Determined from the delta tangent peak of dynamic mechanical analysis curves

For the nanocomposites with low degree of crosslinking the Young´s modulus increases from 1.8±0.3 MPa for the neat PMS to 6±0.7 MPa for the PMS/10% CNC nanocomposite while the tensile strength grow from 1.2±0.7 to 5.6±0.4 MPa. The nanocomposites with high degree of crosslinking are much stiffer and stronger (up to 20-fold increase). The best balance of mechanical properties is observed for the 5 wt% CNC sample with a Young´s modulus of 132.5±20.6 MPa, a tensile strength of 20.1±3.4 MPa, and elongation at break of 77±12.6%, and a toughness of1047±310 MJ/m^3.

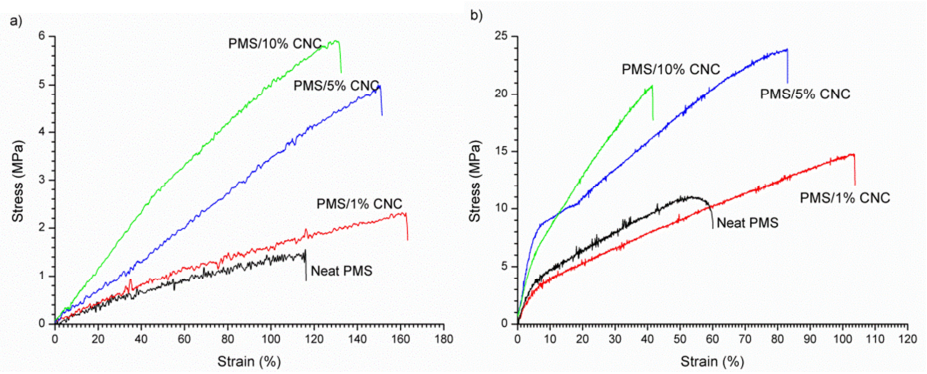

Figure 5.3. Typical tensile stress versus strain curves measured at room temperature of neat PMS and PMS/CNC nanocomposites with low degree of crosslinking **(a)** and with high degree of crosslinking **(b)**.

Interestingly, as can be seen in **Table 5.2**, the behavior of low content CNCs (1 wt%) nanocomposites for both crosslinking profiles is mainly governed by the PMS matrix, resulting in Young´s modulus and tensile strength values for these nanocomposites close to that of the pure PMS. Moreover, the highly crosslinked nanocomposite with 10 wt% CNCs shows a slightly lower Young´s modulus and a substantially lower elongation at break and toughness that the sample with only 5 wt% CNCs. Given the high hydroxyl functionality of CNCs, which offer an abundance of hydroxyl groups, and considering that the PMS network is established through the formation of ester groups between D-mannitol and sebacic acid, one can surmise that the CNC filler, at least to a certain extent, participates in this reaction through physical and chemical interactions. As a consequence, the CNCs become

part of the PMS network giving more network points through polymer/nanoparticle interactions. This provides higher stiffness without significantly compromising the elongation at break of the composites, which is related to the reinforcement induced by crosslinking reactions between the nanoparticles with high hydroxyl functionality and the matrix, as occur for previously reported polyurethane systems.[52, 53] One must, however, also consider the offset of the stoichiometry between available carboxylic acid and hydroxyl groups. As was mentioned before, the concentration of –OH groups increased from 6, 32 and 62% for 1, 5 and 10 wt% CNC addition respectively (**Table 5.1, Supporting Calculation Method M5.1**). The contribution to the mechanical properties and matrix extensibility of the CNC in the present study could be related to the high –OH groups in the surface of CNC that could strongly interact with the matrix, having a positive effect in the mechanical properties and strain except for high degree of crosslinking nanocomposite and 10 wt% of CNC content. The lowering on the mechanical properties for this sample can probably be ascribed to the high offset in stoichiometry due to the high –OH introduction, also the opposite effect occurs for samples with 1 wt% of CNCs in both crosslinking profiles, the –OH increase is not enough to produce a high enhancement of these properties being the behavior of these two samples closer than expected to the neat PMS. A high CNC content can presumably induce a shortening of the distance between crosslinking points and thus reducing the flexibility. This would favour the CNC/CNC interactions, reducing the polymer/CNC or polymer/polymer interactions. This situation can hinder the deformation of the system and lower the load transfer between the matrix and the filler because of the loss of polymer/filler synergistic effect.[54] In summary, the higher toughness, the reinforcement effect on mechanical properties, and higher elongation at break for the nanocomposites compared with neat samples, could be related to the combination of PMS crosslinks and PMS/CNC interactions that attaches the filler to the polymer chains.

3.3. DMTA TESTING

The mechanical properties were further probed as a function of temperature by dynamic mechanical thermal analyses (DMTA). **Figure 5.4a**, which shows the DMTA traces of samples with a low degree of crosslinking, reveals that in the glassy state the storage modulus (E´) is around 2 to 3 GPa and is not affected by the introduction of CNCs. Irrespectively of the CNCs content, all the materials with low crosslink density exhibit a glass transition temperature (T_g) of around 18 °C (as determined with DSC), above which E´ drops to ca. 2-4 MPa; all samples exhibit a rubbery plateau above ca. 40 °C. The increase in E´ resulting from the introduction of the CNCs is rather modest and is consistent with the observations in other studies based on glassy matrices reinforced with CNCs.[55] For some samples, E´ increases at temperatures between 60 and 80 °C, perhaps due to a loss of water or uncured small molecules. **Figure 5.4b** shows the DMTA traces of the corresponding samples with a high degree of crosslinking. Qualitatively, the curves mirror those of the materials cured under low crosslinking conditions. In the glassy state, the storage moduli are virtually identical to those of the materials described above.

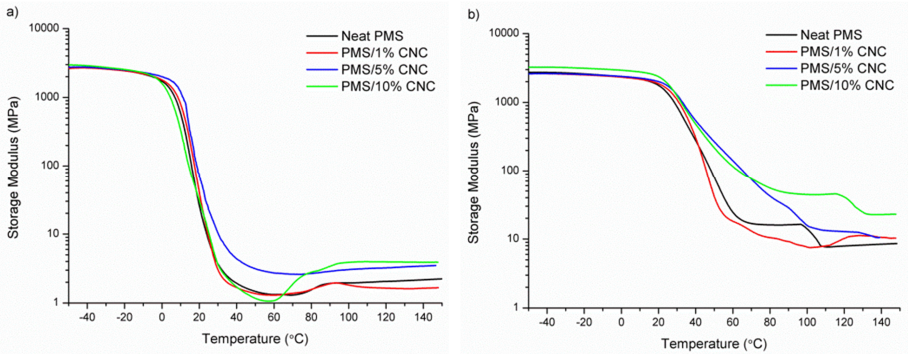

Figure 5.4. DMTA curves showing the storage modulus E´ as a function of temperature of neat PMS and PMS/CNC nanocomposites reacted under low degree of crosslinking conditions **(a)** and high degree of crosslinking conditions **(b)**.

The glass transition temperature, as determined by DSC, is slightly increased to 20-26 °C and the decrease of E' as the temperature is increased to the rubbery plateau

is less pronounced. Furthermore, the reinforcing effect induced by the CNCs appears to be more significant. For example at 90 °C E´ is increased from 13 MPa for the neat PMS matrix to 40 MPa for the nanocomposite with 10 wt% CNCs. **Supporting Figure S5.7** evidences the presence of two maxima in the tangent delta curves, located between 30 and 40 °C and 50 and 70 °C, respectively. The temperature of the first maximum coincides with the T_g established by DSC and is assigned to the glass transition. The second tangent delta peak at higher temperatures could be associated with a restriction in the thermal relaxation of a specific part of the polymeric matrix, indicating the presence of different regions inside of the network. These different domains seem to be induced with high content of CNCs or by combination of CNCs and higher crosslinking density, and can be caused by reactions between CNCs and PMS matrix. As was suggested in mechanical test results, is well known that CNC is highly –OH functional and then, capable to interact with the matrix taking profit of the residual hydroxyl or acid groups from PMS. Thus, it results logical that CNC can have affinity with D-mannitol and sebacic acid, generating a substantial part of the matrix that is forming new physical or chemical interactions with the CNC surfaces, increasing the effective filler-matrix and filler-filler interactions and generating differences in the thermo-mechanical behavior of these domains not accompanied by a step-wise reduction of E´.

3.4. THERMALLY ACTIVATED SHAPE-MEMORY PROPERTIES

The shape-memory properties of the new materials were quantified by cyclic thermomechanical tests conducted in a DMTA, quantifying shape recovery (R_r) and shape fixity (R_f) ratios for each cycle. Initially, a temporary shape was programmed at 45 °C ($T_{high}>T_g$) determined from the maximum of the tangent delta curves recorded by DMTA) where a stress was applied to elongate the samples to a strain of 30% (Step 1). The samples were subsequently cooled to 15 °C ($T_{low}<T_g$), tangent delta peak) under a constant stress to fix the programmed temporary shape (Step

2). The load was subsequently removed, the fixity of the temporary shape was quantified at this stress free state (Step 3) and the samples were heated again to 45 °C (T_{high}) to trigger the thermal recovery of the initial shape (Step 4). As was detailed in the experimental section, samples with high degree of crosslinking were also cycled between 15 °C (T_{low}) and 60 °C (T_{high}) as at this temperature all of these nanocomposites are above the upper end of the glass transition (tangent delta peak). **Figure 5.5** shows exemplarily the shape-memory cycles thus measured for nanocomposites with low (**Figure 5.5a**) and high (**Figure 5.5b**) degree of crosslinking with a CNCs content of 5 wt% at programming temperatures of 45 °C and 60 °C respectively.

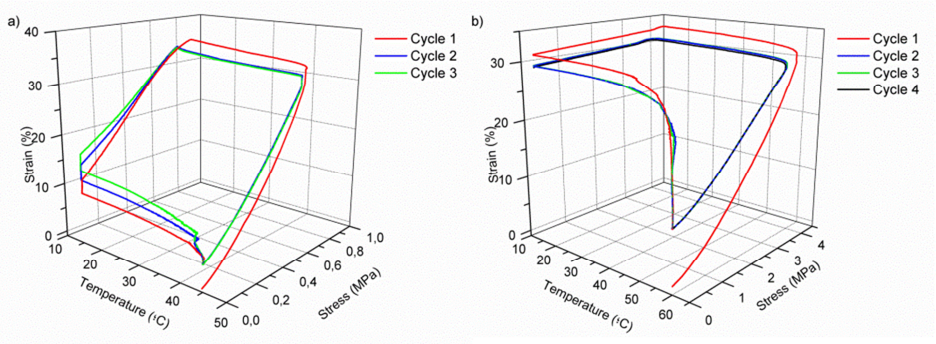

Figure 5.5. Shape-memory stress-strain-temperature curves of 3 consecutive cycles for low degree of crosslinking PMS/5 wt% CNC nanocomposite **(a)**. Shape-memory stress-strain-temperature curves of 4 consecutive cycles for high degree of crosslinking PMS/5 wt% CNC **(b)**.

Figure 5.5a shows a lack of shape-memory behavior for 5 wt% CNC nanocomposite with low degree of crosslinking as these sample is not able to fix the deformed shape at T_{low} after unloading. Under the conditions chosen for the shape-memory test, all the samples with low degree of crosslinking have an incomplete shape fixation (R_f<50%) of the programmed shape after cooling and releasing the applied stress, presumably due to the proximity of the fixing temperature (T_{low}) to the T_g (15-23 °C) as was evidenced in the previous DMTA analysis. By contrast, all samples prepared under high degree of crosslinking conditions showed a shape-memory effect with shape fixity R_f >90% after unloading at T_{low}, on account of their higher T_g

(**Figure 5.5b, Supporting Figure S5.8**). **Figures 5.6a** and 5.**6b** summarize the shape fixity (R_f) and shape recovery (R_r) values for nanocomposites prepared under high degree of crosslinking conditions tested at recovery temperature of 45 °C. For these samples, the shape fixity remained constant and was close to unity (R_f = 93-96%) without appreciable influence of the CNC content or the number of cycles (**Figure 5.6a**). In case of the shape recovery for the first cycle (**Figure 5.6b**) there is a loss in R_r% with increasing CNC content. Neat PMS and 1 wt % CNC sample achieve a R_r of 78% while for 5 and 10 wt % CNC nanocomposites the R_r% decrease to 62%. According to DMTA results, these lower R_r values for the first cycle in nanocomposites with high CNC load can probably be ascribed to the limited movement of the polymer chains due to interactions with CNCs.[56]

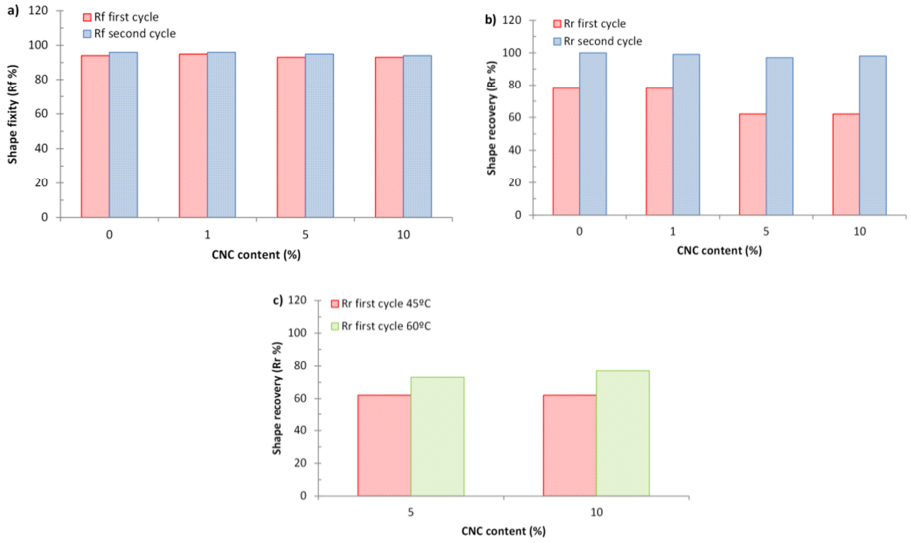

Figure 5.6. Shape fixity **(a)** and shape recovery **(b)** characteristic values for the first and second cycles of neat PMS and PMS/CNC nanocomposites with high degree of crosslinking obtained at recovery temperature of 45 °C. Comparative of the first cycle shape recovery values obtained at two different recovery temperatures (45 °C and 60 °C) for 5 and 10 wt% of CNC nanocomposites with high degree of crosslinking **(c)**.

An increased CNC content strongly decreases the magnitude of the transition associated with first delta tangent peak indicating that less mobile units at the

recovery temperature of 45 °C were participating in the relaxation processes resulting in higher non-reversible deformation for 5 and 10 wt% CNC samples during the first cycle (hysteresis). However, in the second cycle the R_r% becomes significantly higher and stabilizes at values of 99% in the 3rd and 4th cycles. Nevertheless, **Figure 5.6c** shows how increasing the temperature of the test to 60 °C allows the samples with 5 and 10 wt% of CNC to achieve R_r% values for the first cycle close to the neat PMS being 100% after the first cycle. At this higher temperature part of the chains associated with the second delta transition have higher mobility evidencing a temperature dependant shape recovery process.[57] However, neat PMS and nanocomposite with 1 wt% of CNC were not able to be cycled at 60 °C, apparently, due to the lower stiffness of these samples at this temperature that produces premature break (**Supporting Figure S5.8).** As was explained before, for biomedical uses is of special interest the recovery force that is related with the ability of the material to ensure good shape stability and a complete recovery under restricted environments. **Figure 5.7** shows that the maximum stress achieved in the shape-memory test increased with increasing CNC content.

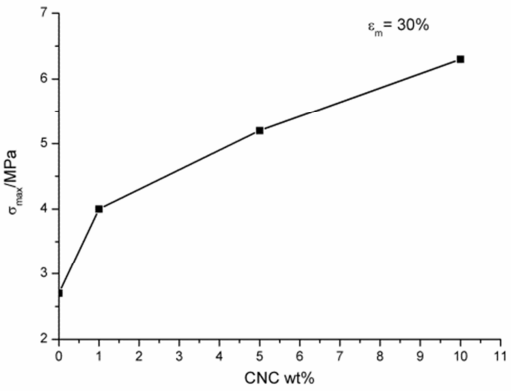

Figure 5.7. Dependence of maximum stress (σ_{max}) with CNC content for PMS/CNC nanocomposites with high crosslinking degree during the first shape-memory test for 30% of elongation (ε_m).

These indicate that the 5 and 10 wt% CNC nanocomposites are able to support a much higher stress, which is concomitant with a higher shape recovery force.[58] This is in agreement with the increase in the Young´s Modulus and rubbery modulus (E´) observed in the mechanical and DMTA tests respectively for these samples. Finally, shape-memory effect was obtained for all the highly crosslinked samples at programming temperature of 45 °C with R_r and R_f close to 100% after the first thermomechanical cycle and no deterioration over the rest of the cycles performed was observed, suggesting good cyclic behavior. Samples with 5 and 10 wt% CNC also have good shape-memory abilities at 60 °C demonstrating the temperature dependence of the recovery process.

4. CONCLUSIONS

Poly(mannitol sebacate) pre-polymers with different CNCs wt% were prepared using the solution-casting method followed by a thermal crosslinking procedure under low and high temperature-time conditions to obtain PMS/CNC nanocomposites with low and high stiffness. For the neat matrix, experimental results demonstrated the possibility to tailor the mechanical properties conform to specific soft or stiff applications depending on the time-temperature curing profiles. In nanocomposites, CNCs introduced high quantity of new hydroxyl groups that could efficiently interact with the matrix increasing the modulus and enhancing the strain and toughness of nanocomposites as compared to the neat polymer matrix probably due to the high filler-matrix compatibility. Nanocomposites with thermally actuated shape-memory properties could be achieve for all the samples with high degree of crosslinking at temperatures between 15-45 °C with R_r and R_f values close to 100% for the second thermo-mechanical cycle. Additionally reduced hysteresis between the first and second cycle could be achieved in highly crosslinked nanocomposites with 5 and 10 wt% of CNC when the temperature of deformation and recovery is 60 °C without

compromising the R_f values having a behavior similar to the neat matrix. The higher mechanical properties and elongation at break together with the possibility of achieving shape-memory properties in the range of physiological temperatures for the nanocomposites with high degree of crosslinking will allow the application of these materials in the biomedical field.

ACKNOWLEDGEMENTS

The authors gratefully acknowledge financial support received from Spanish Ministry of Economy and Competitiveness (Project MAT2010/21494-C03), as well as the support of FPU grant from MED (MED-FPU; AP2009-2482), Swiss National Science foundation (National Research Programme 64, Project #406440_131264/1) and the Adolphe Merkle Foundation.

5. REFERENCES

1. J. P. Bruggeman, B. de Bruin, C. J. Bettinger and R. Langer, *Biomaterials,* 2008, **29**, 4726-4735.
2. Y. Li, G. A. Thouas and Q. Chen, *RSC Advances*, 2012, **2**, 8229-8242.
3. J. Yang, A. Webb, S. Pickerill, G. Hageman and G. Ameer, *Biomaterials,* 2006, **27**, 1889-1898.
4. J. Yang, A. Webb and G. Ameer, *Advanced Materials*, 2004, **16**, 511-516.
5. H. Park, J. Seo, H. Lee, H. Kim, I. B. Wall, M. Gong and J. C. Knowles, *Acta Biomaterialia,* 2012, **8**, 2911-2918.
6. Z. Sun, L. Wu, X. Lu, Z. Meng, Y. Zheng and D. Dong, *Applied Surface Science*, 2008, **255**, 350-352.
7. Q. Liu, T. Tan, J. Weng and L. Zhang, *Biomedical Materials,* 2009, **4**, 025015.
8. C. Sundback, J. Shyu, Y. Wang, W. Faquin, R. Langer, J. Vacanti and T. Hadlock, *Biomaterials,* 2005, **26**, 5454-5464.

9. Z. Sun, C. Chen, M. Sun, C. Ai, X. Lu, Y. Zheng, B. Yang and D. Dong, *Biomaterials*, 2009, **30**, 5209-5214.
10. A. Mahdavi, L. Ferreira, C. Sundback, J. W. Nichol, E. P. Chan, D. J. D. Carter, C. J. Bettinger, S. Patanavanich, L. Chignozha, E. Ben-Joseph, A. Galakatos, H. Pryor, I. Pomerantseva, P. T. Masiakos, W. Faquin, A. Zumbuehl, S. Hong, J. Borenstein, J. Vacanti, R. Langer and J. M. Karp, *Proceedings of the National Academy of Sciences U.S.A.*, 2008, **105**, 2307-2312.
11. D. Motlagh, J. Yang, K. Lui, A. Webb and G. Ameer, *Biomaterials,* 2006, **27**, 4315-4324.
12. Y. Wang, G. Ameer, B. Sheppard and R. Langer, *Nature Biotechnology*, 2002, **20**, 602-606.
13. I. H. Jaafar, M. M. Ammar, S. S. Jedlicka, R. A. Pearson and J. P. Coulter, *Journal of Materials Science*, 2010, **45**, 2525-2529.
14. Q. Chen, A. Bismarck, U. Hansen, S. Junaid, M. Q. Tran, S. E. Harding, N. N. Ali and A. R. Boccaccini, *Biomaterials,* 2008, **29**, 47-57.
15. S. Liang, W. D. Cook, G. A. Thouas and Q. Chen, *Biomaterials*, 2010, **31**, 8516-8529.
16. M. A. Meyers, P.Y. Chen, A. Y.M. Lin and Y. Seki, *Progress in Materials Science*, 2008, **53**, 1-206.
17. V. R. Sastri, *Plastics in Medical Devices, properties, requirements, and applications*, ed. V.R. Sastri, William Andrew Publishing, Boston, 2010, pp. 217-262.
18. Q. Chen, S. Liang, J. Wang and G. P. Simon*, Journal of the Mechanical Behavior of Biomedical Materials*, 2011, **4**, 1805-1818.
19. Q. Liu, J. Wu, T. Tan, L. Zhang, D. Chen and W. Tian, *Polymer Degradation and Stability*, 2009, **94**, 1427-1435.
20. Q. Chen, L. Jin, W. D. Cook, D. Mohn, E. L. Lagerqvist, D. A. Elliott, J. M. Haynes, N. Boyd, W. J. Stark, C. W. Pouton, E. G. Stanley and A. G. Elefanty, *Soft Matter*, 2010, **6**, 4715-4726.

21. S. J. Eichhorn, A. Dufresne, M. Aranguren, N. E. Marcovich, J. R. Capadona, S. J. Rowan, C. Weder, W. Thielemans, M. Roman, S. Renneckar, W. Gindl, S. Veigel, J. Keckes, H. Yano, K. Abe, M. Nogi, A. N. Nakagaito, A. Mangalam, J. Simonsen, A. S. Benight, A. Bismarck, L. A. Berglund and T. Peijs, *Journal of Materials Science*, 2010, **45**, 1-33.
22. M. J. D. Clift, E. J. Foster, D. Vanhecke, D. Studer, P. Wick, P. Gehr, B. Rothen-Rutishauser and C. Weder, *Biomacromolecules,* 2011, **12**, 3666-3673.
23. J. Mendez, P. K. Annamalai, S. J. Eichhorn, R. Rusli, S. J. Rowan, E. J. Foster and C. Weder, *Macromolecules,* 2011, **44**, 6827-6835.
24. L. Hsu, C. Weder and S. J. Rowan, *Journal of materials Chemistry*, 2011, **21**, 2812-2822.
25. M. Samir, F. Alloin, J. Sanchez and A. Dufresne, *Macromolecules,* 2004, **37**, 4839-4844.
26. L. Goetz, M. Foston, A. P. Mathew, K. Oksman and A. J. Ragauskas, *Biomacromolecules*, 2010, **11**, 2660-2666.
27. R. Rusli and S. J. Eichhorn, *Applied Physics Letters*, 2008, **93**, 033111.
28. A. Sturcova, G. Davies and S. Eichhorn, *Biomacromolecules,* 2005, **6**, 1055-1061.
29. A. Lima, J. Wong, M. Paillet, R. Borsali and R. Pecora, *Langmuir*, 2003, **19**, 24-29.
30. C. C. Sun, J. Pharm. Sci. 2005, **94**, 2132-2134.
31. T. Kokubo, H. Kim and M. Kawashita, *Biomaterials,* 2003, **24**, 2161-2175.
32. M. Bellantone, H. Williams and L. Hench, *Antimicrobial Agents and Chemotherapy*, 2002, **46**, 1940-1945.
33. B. Lecouvet, J. Horion, C. D'Haese, C. Bailly and B. Nysten, *Nanotechnology*, 2013, **24**, 105704.
34. K. Prashantha, M. F. Lacrampe and P. Krawczak, *Express Polymer Letters*, 2011, **5**, 295-307.
35. B. Yakobson and P. Avouris, *Carbon Nanotubes,* 2001, **80**, 287-327.
36. Q. Lu, G. Keskar, R. Ciocan, R. Rao, R. B. Mathur, A. M. R. Rao and L. L. Larcom, *The Journal of Physical Chemistry B*, 2006, **110**, 24371-24376.

37. D. J. Gardner, G. S. Oporto, R. Mills and M. A. S. A. Samir, *Journal of Adhesion Science and Technology*, 2008, **22**, 545-567.
38. H. Koerner, G. Price, N. Pearce, M. Alexander and R. Vaia, *Nature Materials*, 2004, **3**, 115-120.
39. J. R. Capadona, O. Van Den Berg, L. A. Capadona, M. Schroeter, S. J. Rowan, D. J. Tyler and C. Weder, *Nature Nanotechnology*, 2007, **2**, 765-769.
40. X. Dong, T. Kimura, J. Revol and D. Gray, *Langmuir,* 1996, **12**, 2076-2082.
41. B. Braun and J. R. Dorgan, *Biomacromolecules,* 2009, **10**, 334-341.
42. S. Camarero Espinosa, T. Kuhnt, E. J. Foster and C. Weder*, Biomacromolecules,* 2013, **14**, 1223-1230.
43. E. Lecam, D. Frechon, M. Barray, A. Fourcade and E. Delain, *Proceedings of the National Academy of Sciences U.S.A.*, 1994, **91**, 11816-11820.
44. M. Behl and A. Lendlein, *Materials Today*, 2007, **10**, 20-28.
45. W. Wagermaier, K. Kratz, M. Heuchel and A. Lendlein, *Advances in Polymer Science*, 2010, **226**, 97-145.
46. D. Ratna and J. Karger-Kocsis, *Journal of Materials Science*, 2008, **43**, 254-269.
47. C. M. Yakacki and K. Gall, *Shape-Memory Polymers*, ed. A. Lendlein, Springer-Verlag, Berlin, 2010, pp.147-175.
48. R. Maliger, P. J. Halley and J. J. Cooper-White, *Journal of Applied Polymer Science*, 2013, **127**, 3980-3986.
49. Q. Chen, *Biomedical Materials and Diagnostic Devices*, ed. A. Tiwari, M. Ramalingam, H. Kobayashi and A.P.F. Turner, Scrivener-Wiley, Beverly, MA, USA, 2012, pp 529-560.
50. I. Filpponen and D. S. Argyropoulos, *Industrial & Engineering Chemistry Research*, 2008, **47**, 8906-8910.
51. A. Patel, A. K. Gaharwar, G. Iviglia, H. Zhang, S. Mukundan, S. M. Mihaila, D. Demarchi and A. Khademhosseini, Biomaterials, 2013, **34**, 3970-3983.
52. A. Pei, J. Malho, J. Ruokolainen, Q. Zhou and L. A. Berglund, *Macromolecules,* 2011, **44**, 4422-4427.

53. Y. Tien and K. Wei, *Macromolecules,* 2001, **34**, 9045-9052.
54. M. A. Hood, C. S. Gold, F. L. Beyer, J. M. Sands and C. Y. Li, *Polymer,* 2013, **54**, 6510-6515.
55. K. Shanmuganathan, J. R. Capadona, S. J. Rowan and C. Weder, *Journal of Materials Chemistry*, 2010, **20**, 180-186.
56. S. A. Abdullah, A. Jumahat, N. R. Abdullah and L. Frormann, *Procedia Engineering*, 2012, **41**, 1641-1646.
57. B. A. Nelson, W. P. King and K. Gall, *Applied Physics Letters*, 2005, **86**, 103108
58. Q. Meng, J. Hu and Y. Zhu, *Journal of Applied Polymer Science*, 2007, **106**, 837-848.

S.I. Chapter 5

<u>Supporting Information</u>: Mechanical and shape-memory properties of Poly(mannitol sebacate)/Cellulose Nanocrystal nanocomposites

Águeda Sonseca, Sandra Camarero-Espinosa, Laura Peponi, Christoph Weder, E. Johan Foster, José M. Kenny, Enrique Giménez

Journal of Polymer Science Part A; Polymer Chemistry 52 (2014) 3123-3133

DOI: 10.1002/pola.27367

GRAPHICAL ABSTRACT

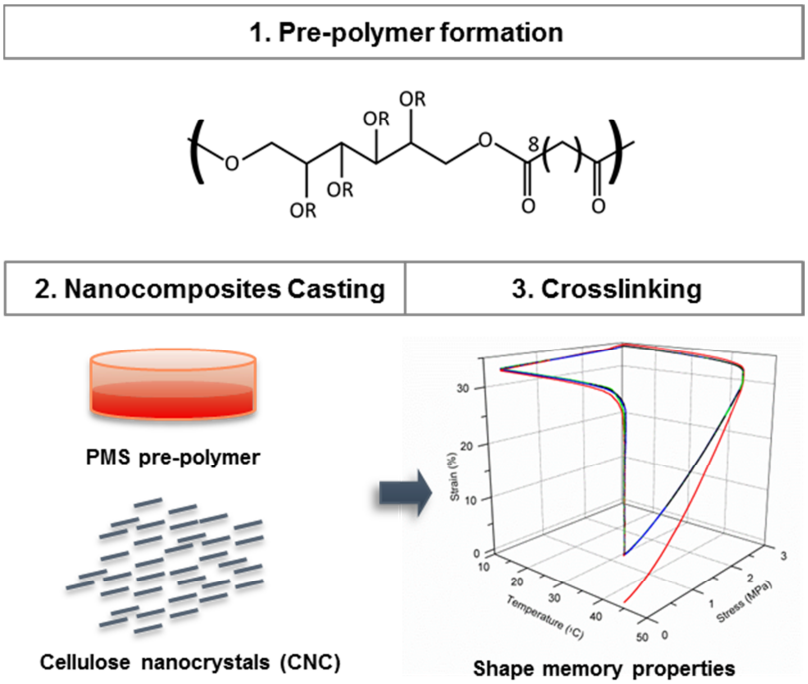

The synthesis of nanocomposites of Poly(mannitol sebacate) (PMS) and cellulose nanocrystals (CNCs) was achieved in two steps. A low-molecular-weight pre-polymer that was soluble in common solvents was first formed via the polycondensation reaction between sebacic acid and D-mannitol. Nanocomposites with different CNC contents were subsequently prepared by solution-casting and curing under vacuum. The new materials display a shape-memory effect.

1. PRE-PMS PROPERTIES

Table S5.1. Composition and molecular weight distribution of PMS pre-polymer after 13 h of polycondensation reaction of sebacic acid and mannitol monomers under continuous stirring and nitrogen flow at 150 °C.

Table S5.1. Main PMS Pre-Polymer Properties	
Composition by ^{1}H NMR	1:0.93
M_w (g/mol)[a]	7501
M_n (g/mol)[b]	6180

[a] M_w: weight average molecular weight. [b] M_n: number average molecular weight.

2. CNC PROPERTIES

Charge concentration was determined by conductometric titration (**Figure S5.4**). Dimensions and aspect ratio of CNCs were calculated as an average of randomly measures in TEM images at different magnifications (2950x, 3900x and 5200x). ImageJ software (National Institute of Health in USA) was used to evaluate the length and width of the CNCs. Apparent crystallinity was calculated from X-ray diffraction pattern (**Figure S5.3**).

3. TRANSMISSION ELECTRON MICROSCOPY OF CNCs

CNCs TEM micrographs were recorded in a Phillips CM10 microscope with an accelerating voltage of 80kV. Samples were prepared by drying a drop of dilute whiskers suspension in H_2OD (0.1 mg/mL) onto a carbon-coated copper grid (Electron Microscopy Sciences) and subsequently dried under a lamp for 1 h.

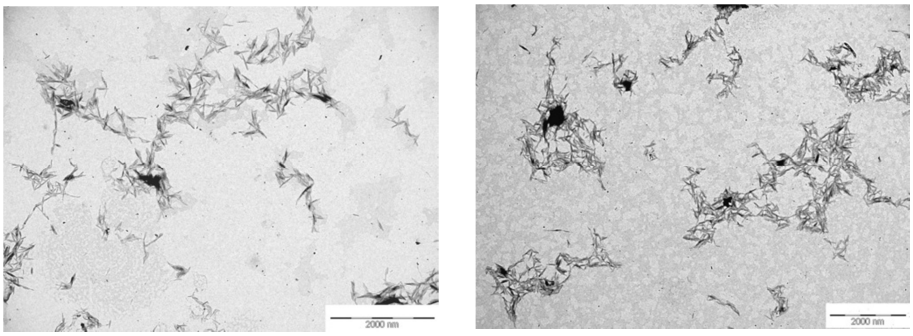

Figure S5.1. Transmission electron micrographs (TEM) of CNC isolated by hydrolysis with sulfuric acid.

Table S5.2. Main CNCs properties analysed through conductometric titration, TEM images and X-ray diffraction pattern.

Table S5.2. Main CNCs Properties

charge concentration (mM/$kg_{cellulose}$)[a]	91 ± 4
length (nm)	199 ± 14
width (nm)	18 ± 2
aspect ratio	11 ± 1
apparent crystallinity (%)	68

[a] Determined by conductimetric titration

4. X-RAY DIFFRACTION (XRD)

The crystalline structure of the CNCs was investigated with an RXSiemens D5000 equipped with a Cu Kα radiation source (λ = 1540 A) operating at 40 kV. A CNC sample was dispersed in water and dried in oven at 100 °C for 0.5 h. After drying the compact powder obtained was regrounded and transferred to scan. The scanning range was 2°-40°, step-size and count time per step were 0.02° and 8 seconds, respectively. To calculate the apparent crystallinity, difractogram was fitted using www.magicplot.com software. Gaussian shaped peaks were assumed and let free for intensity, position and FWMH after background subtraction, and

non-crystalline peak was fixed at position. Data was deconvoluted taking into account only cellulose type I.[1, 2]

(101):14.8°, (10I): 16.7°, (021): 21.7°, (002):22.8° and (040): 34.7°

The percentage of apparent crystallinity was estimated from the ratio of the crystalline area peaks to the total area including the non-crystalline peak (equation 1) to be ~68%.

Equation (S.5.1)

$$A.C = 100\ \frac{I_{(101)} + I_{(10I)} + I_{(021)} + I_{(002)} + I_{(040)}}{I_{(101)} + I_{(10I)} + I_{(021)} + I_{(002)} + I_{(non\ crystalline)}}\ [\%] \qquad (S.5.1)$$

,where A.C means apparent crystalinity and $I_{(xxx)}$ is the area under the peak.

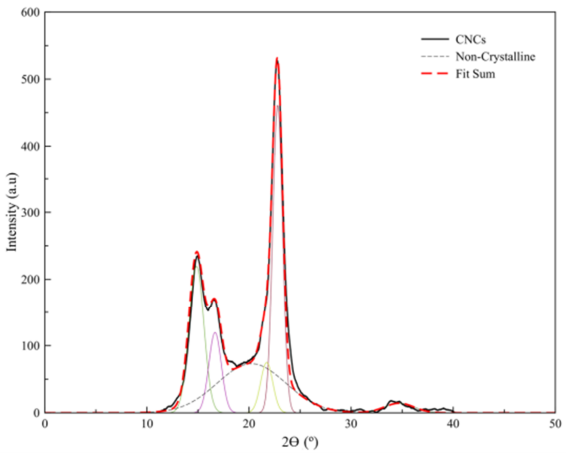

Figure S5.2. X-Ray diffractogram of CNCs. Data was fitted taking into account crystalline peaks of cellulose type I.

5. CONDUCTOMETRIC TITRATION OF CNCS

To determine the surface charge density, CNCs were conductometric titrated as described previously.[3, 4] Briefly ≈ 50 mg of CNCs were dispersed via sonication in a mixture of 10 mL of 10 mM aqueous hydrochloric acid and 25 mL of ultrapure H_2O. The sample was titrated with aliquots of 10 mM aqueous NaOH recording the

conductivity after the addition of each aliquot. The concentration of sulphate groups on CNCs was calculated from the titration results according to a reported protocol.[5]

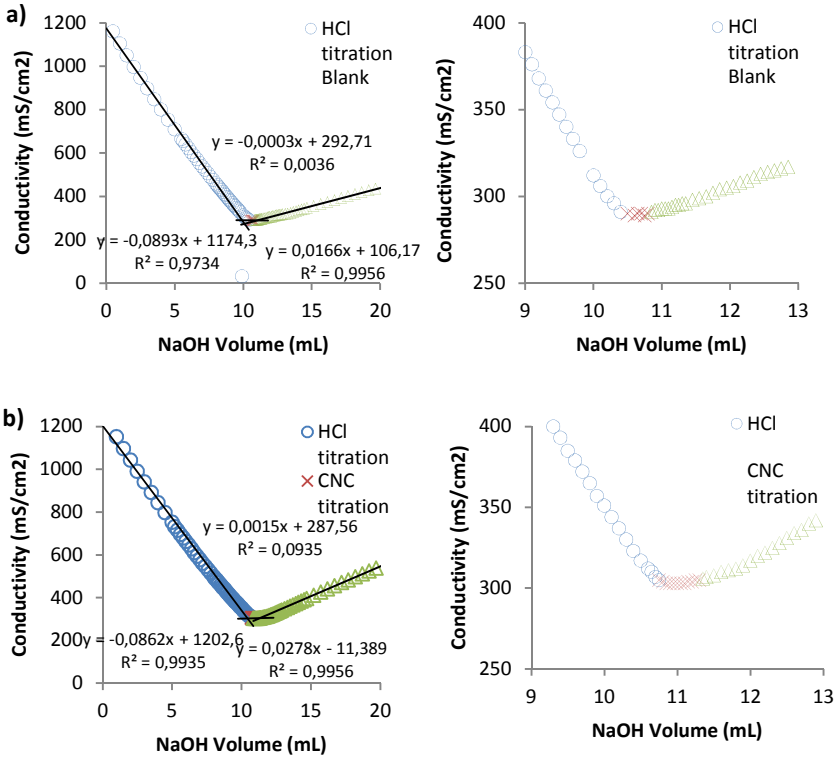

Figure S5.3. Conductometric titration curves of a) neat medium and b) CNCs

6. CALCULATION METHOD M5.1

Percentage of OH groups introduced with the CNC addition in the PMS matrix

The total amount of –OHs available on 1g of PMS matrix was estimated supposing an ideal linear pre-polymer with 4 available OHs per mannitol molecule taking into account the molecular weight value obtained from GPC (7501 g/mol) test.

The quantity of –OHs available in 1g of pre-PMS was calculated following the equation:

$$\left(\frac{W_{pre-PMS}}{Mw_{pre-PMS}}\right) x\ 4 = mol_{available-OH} \qquad (S.5.2)$$

, obtaining a value of ***5.3 e^{-4}*** mol of available -OH in 1g of pre-PMS matrix.

The total amount of –OHs on the CNC was estimated taking in account the molecular weight of native cellulose (180.1 g/mol) and supposing 3 available OHs per cellulose unit. Only the 20% of the total –OHs was considered as reactive sites [6]

The total amount of –OHs available on the CNC introduced in each sample (0.01, 0.05 and 0.1 g for 1, 5 and 10 wt% of CNC samples respectively) was calculated following the equation:

$$\left(\left(\frac{W_{CNC}}{Mw_{CNC}}\right) x\ 3\right) x\ 0.2 = mol_{available-OH} \qquad (S.5.3)$$

, obtaining values of ***3.3 e^{-5}***, ***1.6 e^{-4}***, ***3.3 e^{-4}*** for 1, 5 and 10 wt% of CNC addition in 1g of pre-polymer.

The increase % of –OH per sample was calculated relative to the available OH in the pre-polymer matrix with the following equation:

$$\left(\frac{mol_{available-OH\ in\ CNC}}{mol_{available-OH\ in\ pre-PMS}}\right) x100 = increase\ \%\ of\ -OH\ in\ each\ sample \qquad (S.5.4)$$

, obtaining an approximate increase of 6, 30 and 60 % of –OHs with 1, 5 and 10 wt% of CNC addition.

7. ^{1}H-NMR STUDIES

A ^{1}H-NMR spectrum of the PMS pre-polymer was obtained in deuterated dimethylsulfoxide (DMSO- d_6) on a Varian Mercury VX-300 MHz NMR spectrometer. The sample was prepared dissolving the pre-polymer in 750 μL of d_6DMSO in a glass tube. The peaks from the mannitol appeared at 3.5-5.5 ppm due to central and terminal methylene units identified by hydrogens on the carbons "a" and "b".

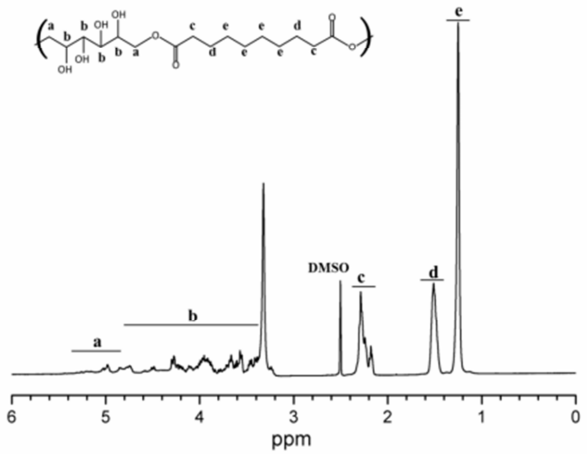

Figure S5.4. ^{1}H-NMR spectrum of the PMS pre-polymer, recorded in DMSO- d_6.

The protons from the methylene units of sebacic acid showed peaks at 1.3, 1.6 and 2.3 ppm identified by hydrogens on the carbons "c", "d" and "e" respectively. The peak at 3.3 was due to residual water.[7] Note that as the monomers are multifunctional, at late stages of polymerization some degree of branching can take place and cannot be excluded completely.

8. FOURIER TRANSFORM INFRARED SPECTROSCOPY (FTIR)

Transmission spectra were recorded using a Thermo Nicolet 5700 spectrometer, in the 500 to 4500 cm^{-1} region, with a 4 cm^{-1} resolution with an Attenuated Total Reflectance (ATR) cell. Backgrounds were acquired before every 3rd sample. All samples were vacuum-dried before measurement.

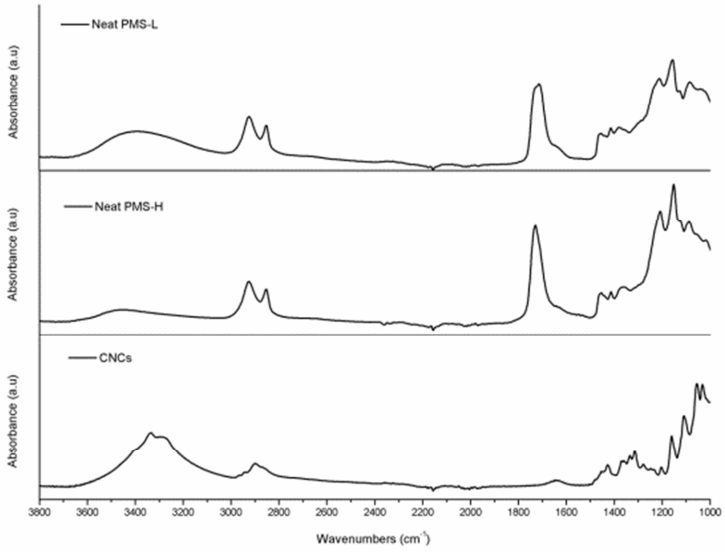

Figure S5.5. FTIR spectra from top to bottom, neat PMS with low degree of crosslinking **(L)**, high degree of crosslinking **(H)** and CNCs.

9. DYNAMIC MECHANICAL THERMAL ANALYSIS (DMTA)

The mechanical behavior as a function of the temperature was characterized by DMTA measurements in a TA Q800 instrument (TA instruments) in tensile mode with a temperature ramp method from -50 to 150 ºC at a heating rate of 3 ºC/min. Frequency and strain amplitude were kept constant at 1 Hz and 15 µm, respectively.

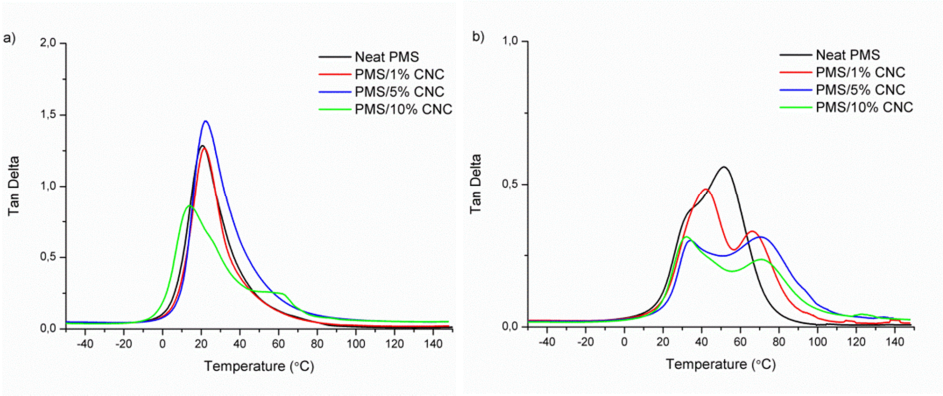

Figure S5.6. DMTA delta tangent curves as a function of temperature of neat PMS and PMS/CNC nanocomposites reacted under low degree of crosslinking **(a)** and high degree of crosslinking conditions **(b)**.

10. THERMALLY ACTIVATED SHAPE-MEMORY PROPERTIES

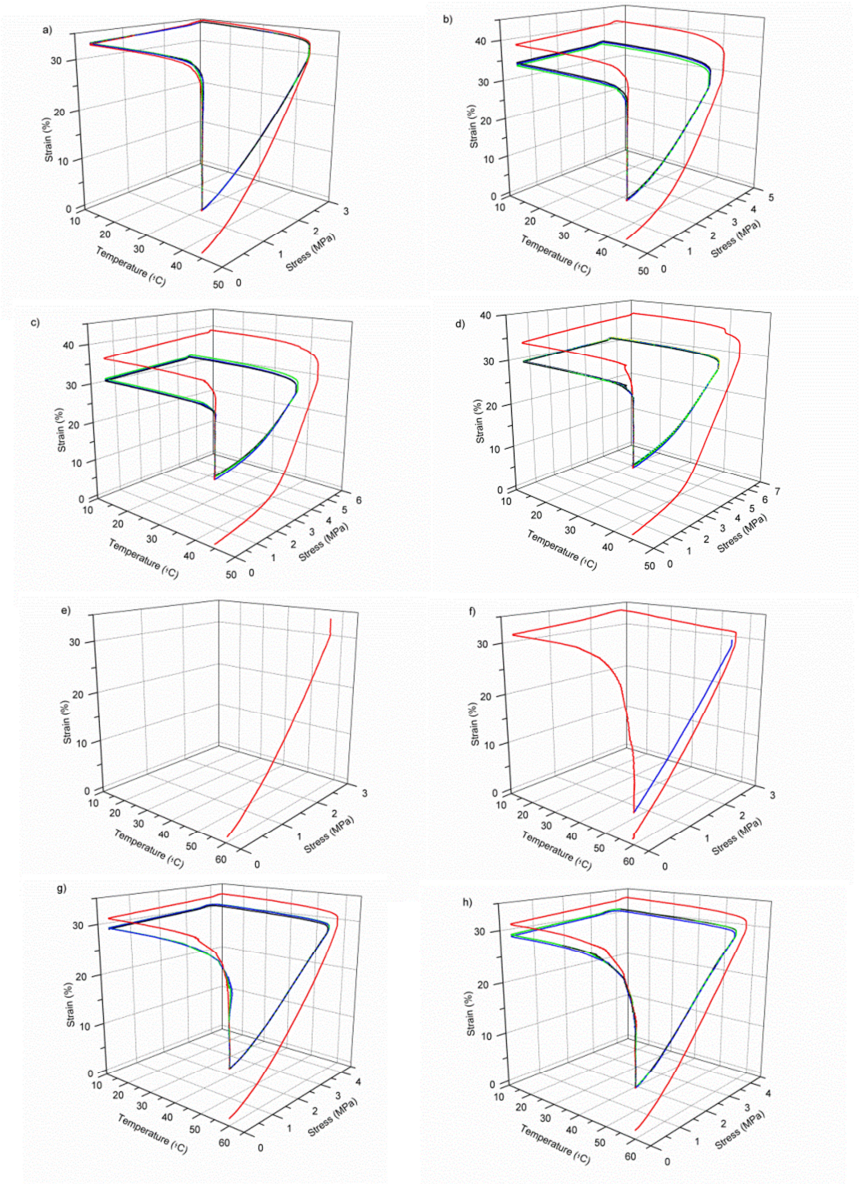

Figure S5.7. Shape-memory stress-strain-temperature curves of consecutive cycles for high degree of crosslinking PMS and PMS/CNC nanocomposites. Neat PMS **(a)**, 1wt% CNC **(b)**, 5wt% CNC **(c)** and 10 wt% CNC **(d)** with programming-recovery temperature of 45ºC. Neat PMS **(e)**, 1wt% CNC **(f)**, 5wt% CNC **(g)** and 10 wt% CNC **(h)** with programming-recovery temperature of 60 °C.

11. THERMOGRAVIMETRIC ANALYSIS (TGA)

Thermal stability of all the obtained samples and the CNCs was recorded in a Mettler-Toledo TGA/SDTA 851^{e} modulus analyser. The samples (5-10 mg) were weighted in zircona crucibles and were heated in air at a rate of 10 ºC/min from ambient to 700 ºC. **Figure S5.8** shows the thermogravimetric profile for all the composites and for CNC. Typically, H_2SO_4-CNC, showed two well separated degradation processes, one started from 220 to 280 °C (attributed to depolymerisation, dehydration, and decomposition of glycosyl units followed by the formation of a char) and the other was between 330 to 500 °C (attributed to the oxidation and breakdown of the char to lower molecular weight gaseous products).[8]

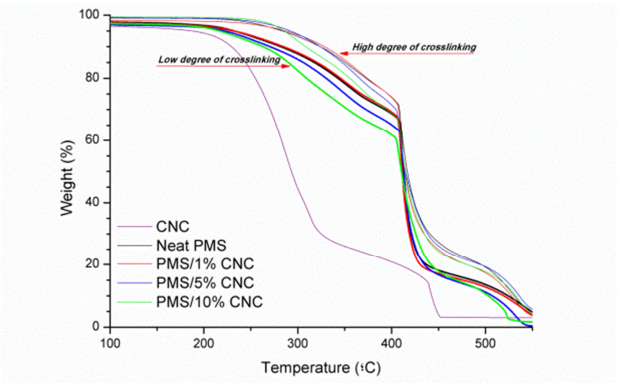

Figure S5.8. TGA curves of CNC, neat PMS and PMS/CNC nanocomposites with low and high degree of crosslinking.

In case of thermal stability of the films, TGA curves of neat PMS and CNC load samples with high degree of crosslinking revealed an increase of thermal stability for these curing conditions compared with the low degree of crosslinking samples, that is, the initial drop in the slop occurred at higher temperature for samples with high degree of crosslinking. PMS/CNC nanocomposites containing 5-10 wt% of CNC showed slightly lower onset degradation temperature than neat PMS due to the lower onset degradation temperature of CNC than the matrix.

12. DIFFERENTIAL SCANNING CALORIMETRY (DSC)

Thermal behavior was studied in a Mettler-Toledo DSC 800 under N_2 atmosphere. Samples were heated from -60 to 180 °C, cooled down from to -60 °C and heated up again to 180 °C at a heating/cooling rate of 10 °C/min under a nitrogen atmosphere. The glass transition temperatures (Tg) were calculated as the midpoint of the transition in the 2^{nd} heating run for all the samples. **Figure S9** shows the differential scanning calorimeter (DSC) second heating run for all the samples. All the high crosslinked samples had a T_g higher than the low crosslinked ones, that is, longer curing times and temperatures derivate in a higher degree of crosslinking. It could be due to the fact that hydrogen bonding and/or chemical crosslink was gradually intensified during thermal curing limitating the mobility of polymeric chains increasing the T_g and also the thermal stability. Generally, nanofillers are expected to increase considerably the T_g of materials difficulting chain motions of the matrices, however, we observed no significant influence of CNC content in the T_g of the low degree of crosslinking samples, and in samples with high degree of crosslinking the T_g tended to decrease while increasing the CNC content. This all phenomena could be explained as follows; in the first step of the condensation, a 1:1 molar ratio of the reactants produced an esterification dominated by the reaction of the primary hydroxyl groups founded at both ends of mannitol with carboxylic acid groups from sebacic acid, leaving a large amount of secondary –OH groups in the pre-polymer. CNCs were added into the PMS pre-polymer at this point and were sommeted to a curing under vacuum and temperature. CNC changed considerably the OH/COOH ratio due to the higher -OH groups content in the surface of the filler, varying the stoichiometry reaction of the neat PMS samples, increasing ratio of –OH groups and favouring the interactions between CNC and matrix and CNC-CNC being more notable under high crosslinking profile and higher filler loads. These changes in the initial OH/COOH ratio of the monomers seemed to be responsible for CNC was not producing a notable increase

in the T_g as was expected or even shifted to lower temperature for nanocomposites.[9]

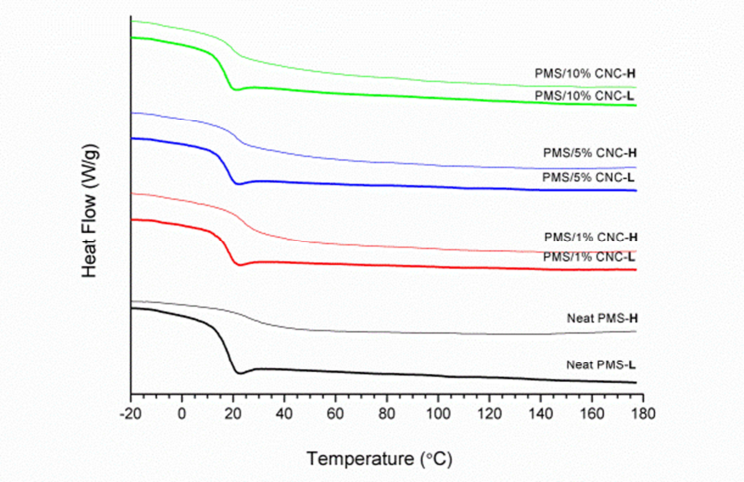

Figure S5.9. DSC second heating run thermograms of neat and nanocomposite samples with low **(L),** and high **(H)** degree of crosslinking.

13. REFERENCES

1. E. N. J. Ford, S. K. Mendon, S. F. Thames and J. W. Rawlins, *Journal of Engineered Fibers and Fabrics,* 2010*,* **5**, 10-20.
2. N. Terinte, R. Ibbett and C. K. Schuster, *Lenzinger Berichte*, 2011, **89**, 118-131.
3. M. Jorfi, M. N. Roberts, E. J. Foster and C. Weder, *ACS Applied Materials & Interfaces,* 2013*,* **5**, 1517-1526.
4. A. C. Correa, E. d. M. Teixeira, L. A. Pessan and L. H. Capparelli Mattoso, *Cellulose*, 2010*,* **17**, 1183-1192.
5. S. Camarero Espinosa, T. Kuhnt, E. J. Foster and C. Weder, *Biomacromolecules*, 2013*,* **14**, 1223-1230.
6. I. Filpponen, D. S. Argyropoulos, *Industrial & Engineering Chemistry Research,* 2008*,* **47**, 8906-8910.

7. H. Gottlieb, V. Kotlyar and A. Nudelman, *The Journal of Organic Chemistry,* 1997*,* **62**, 7512-7515.
8. Y. Li and J. A. Ragauskas, *Advances in Diverse Industrial Applications of Nanocomposites*, ed. B. Reddy, InTech, 2011, pp 18-36.
9. M. Samir, F. Alloin, J. Sanchez and A. Dufresne, *Polymer,* 2004*,* **45**, 4149-4157.

Chapter 6.I

A comparative study of the mechanical, shape-memory, and degradation properties of fiber- and particulate- reinforced Poly(mannitol sebacate) nanocomposites

Águeda Sonseca, Olivia Menes, Oscar Sahuquillo, Enrique Giménez

Manuscript

A COMPARATIVE STUDY OF THE MECHANICAL, SHAPE-MEMORY, AND DEGRADATION PROPERTIES OF FIBER- AND PARTICULATE- REINFORCED POLY(MANNITOL SEBACATE) NANOCOMPOSITES

Águeda Sonseca[1*], Olivia Menes[2], Oscar Sahuquillo[1] and Enrique Giménez[1]

[1]Instituto de Tecnología de Materiales, Universitat Politècnica de València (UPV), Camino de Vera s/nº, 46022 Valencia (Spain)

[2]Instituto Tecnológico del Plástico (AIMPLAS), Parque Tecnológico, Calle Gustave Eiffel 4, 46980, Paterna, Valencia (Spain)

***Corresponding author: agsonol@posgrado.upv.es**

Abstract

Nanocomposites based on a poly(mannitol sebacate) (PMS) matrix - a member of the poly(polyol sebacate) (PPS) polyesters family- reinforced either with cellulose nanocrystals (CNCs) or electrospun poly(lactic acid) nanofibers (NF-PLA) have been developed in order to evaluate the reinforcing filler morphology for achieving useful adaptive materials with shape-memory functionality. All the as-prepared nanocomposites have higher mechanical properties than the neat PMS matrices, allowing for a wider range of mechanical and degradation properties. However, superior balance of properties was observed after the introduction of nanofibers into the low-modulus PMS matrix. In particular, enhanced shape-memory properties are imparted to the PMS matrix by using nanofibers as reinforcing filler, specifically in a temperature range (15-45 °C) of interest for possible medical applications. In addition, two well-separated thermal glass transitions due to matrices and nanofibers could enable the future design of triple-shape-memory systems. Mechanical properties are markedly enhanced with a 4-fold increase when a 4 wt% of PLA nanofibers are infiltrated. When increasing the filler content

to 10 and 15 wt%, 20-fold and 53-fold enhancements in the Young´s modulus were achieved, respectively. These better mechanical properties are accompanied by higher toughness than the neat matrix without lessening the elongation at break. In addition, the shape stability during degradation and the obtained mass loss rates implies that these nanocomposites as useful materials for long-term implants.

Keywords: Poly(polyol sebacate), cellulose nanocrystals, electrospinning, poly(lactic acid), nanocomposites, shape-memory.

1. INTRODUCTION

Soft biodegradable polyesters have been gaining attention as potentially useful polymers in the biomedical field due to the possibility to tuning their mechanical properties and degradation profiles by adjusting the processing conditions or the composition ratio.[1-14] Typically, all the reported systems are easily prepared through melt polycondensation reactions, and by using non-toxic monomers that incorporate ester bonds in the polymer chains, which allows the hydrolytic degradation and the enzymatic activity.[1, 15] A wide range of monomers have been used for the synthesis of crosslinked polyester elastomers: nevertheless, the most common materials are based on the reaction of glycerol, 1,10-didecanediol or low molecular weight poly(ethylene glycol) with either adipic acid, sebacic acid, 1,10-didecanoic acid, 1,12-didodecanoic acid or citric acid.[4, 16-18] Recently, poly(glycerol sebacate) (PGS), the most studied member of poly(polyol sebacate) (PPS) polyesters family, has been considered a good candidate for cardiovascular, cartilage and nerve tissue applications, among others. In order to enhance the range of potential biomedical and clinical applications, many efforts have been made in the development of other members of this family by polycondensation reactions of sebacic acid with other polyols such as mannitol, sorbitol, xylitol and maltiol.[1, 3, 6, 11, 19-22] Despite the wider range of Young´s modulus (0.05-13 MPa) and UTS (0.6-3.3 MPa) among the members of the PPS family and the elongation at break of greater than 10% (as required for tissue engineering),[1] these materials have still not proven useful for many applications in which high strength and flexibility are required. For example, these materials have not been shown to work as ligating rubber bands for blood vessels or arteries, elastomeric sutures, flexible coatings for stents, surgical devices and wound dressings, vascular grafts, catheters or small-diameter tubes for drainage and cartilage tissue engineering.[23] That is, the current applications do not involve elastic and stiff tissues (E 0.7-250 MPa; UTS 0.3-54 MPa) such as skin, nerves, cartilage, heart valves, tendons and trabecular bones,

among others.[24-27] In this instance, the most appropriated strategy involves nanocomposites materials designed to achieve a higher modulus without significantly lowering or compromising the elongation at break of the elastomeric matrix. Typically, this has been reported in the literature through the introduction of nanosized inorganic components in the matrices, such as halloysite nanotubes (clays), multi-walled carbon nanotubes (MWCNTs) and bioceramics.[28-30] In this regard, we have previously reported[31, 32] that the addition of cellulose nanocrystals (CNCs) in poly(mannitol sebacate) (PMS) matrices results in efficient and highly compatible filler that is able to interact with the matrix both physically and chemically,[33, 34] positively affecting the systems properties. We have demonstrated that the presence of CNCs in PMS matrices, combined with different crosslinking profiles (thermal curing under low- and high-temperature/time conditions) and stoichiometry between mannitol and sebacic acid (1:1 and 1:2), results in an improvement in mechanical properties well above that of the enhancement obtained by other fillers, without highly compromising the elongation at break of the neat matrices. In addition, this method provides more reliable mechanical support without an immediate loss of mechanical stability during immersion in simulated body fluid tests (SBF).

In addition, from a medical point of view, biodegradability and thermal-induced shape-memory properties at physiological temperature are both highly desirable for surgical implantation and minimally invasive applications. This combination is especially advantageous, as a device could be inserted in a smaller shape into the body to pass through narrow places, and once in its final position, be deployed to adopt its final functional shape; it can then be reabsorbed when its objective is fulfilled.[35-39] To cover these needs for shape-memory polymers (SMPs) with biomedical applications, apart from achieving a thermal transition (T_{trans}) close to the body ´s temperature, it is essential to improve the mechanical properties of polymers, including the strength and the rubbery modulus of the polymer

networks, to avoid device failure when working in restricted environments (surrounded by tissues) inside the body.[40] In this respect, to get SMPs with excellent shape-memory properties, particulate and layered nanofillers have typically been used to modify the thermal and mechanical properties of soft biodegradable matrices to ensure high strength and minimum flexibility and elasticity at implantation temperatures. Moreover, there has been steady progress in the development of new polymeric fibers processed by electrospinning,[41] with nanometer architecture and unique features (high aspect ratio, flexibility and surface area along with light weight) to be used in a wide variety of applications including, tissue engineering for wound healing and tissue regeneration, drug delivery, filtration devices and biosensors, among others.[42, 43] These facts imply that electrospun nanofibers are promising fillers[44-46] to achieve high strength and long-term implantable shape-memory devices. Recent literature has included only a couple of stimuli-responsive polymer composites. These were fabricated with electrospun mats as fillers of non-degradable matrices, in which shape-memory was achieved through melting semicrystalline poly(ε-caprolactone) (PCL) nanofibers at 60 °C.[47, 48] However, the use of PCL nanofiber mats as a switching phase has some drawbacks. The shape fixity depends on the PCL melt-crystallization process, and it is a time-consuming process due to the slow crystallization kinetics of this material. In addition, as the system works above T_m of the PCL, changes in the morphology due to partial melting of the nanofibers can take place. Therefore, with this background and the benefit of our previous experience in the development of PMS nanocomposites with potential applications in the biomedical field, here we report in this paper a new type of SMP based on the use of poly(lactic acid) (PLA) nanofibers obtained through the electrospinning process as a fixing phase in a PMS matrix, with 1:2 mannitol:sebacic acid (MA:SA) ratio, to conform a glass transition temperature (T_g) based recovery. The enhanced mechanical stiffness of PLA nanofibers mats and their flexibility compared to that of bulk polymer are expected to provide an advantage over the individual polymer

in terms of physical, mechanical and shape-memory properties, especially in the shape fixity ratio.

In this study, to complete our previous research about nanocomposites based on PMS (1:2 MA:SA ratio) reinforced with CNCs,[32] we further evaluate the thermal induced shape-memory properties of this system to provide a comparative study between nanoparticulate- and nanofiber- reinforced PMS matrices. This comparison, allowed us to better understand how different filler geometries affect matrix properties as well as to evaluate the usefulness of each kind of filler in developing nanocomposite materials as shape-memory polymers (SMPs). In summary, the main interest of the present work is to determine the mechanical and functional properties, through the use of nanofillers, of low modulus PMS (MA:SA 1:2 ratio). Our goal is to customize these materials for use in long-term and high-strength biomedical implantation shape-memory devices.

2. EXPERIMENTAL SECTION

2.1. MATERIALS

Deuterated dimethylsulfoxide (DMSO-d_6), dichloromethane (DCM), dimethylformamide (DMF), sulfuric acid, sebacic acid (SA) (99% purity), and D-mannitol (MA) (99% purity), were purchased from Sigma Aldrich. Poly(lactic acid) (PLA) with 3% of D-lactic acid monomer was supplied by NatureWorks® (USA) under the trade name PLA3051D (M_n ca. 142 x 10^4 g/mol, density 1.24 g/cm^3). Hydrochloric acid (HCl, 37% reagent grade) and sodium hydroxide (NaOH, 98% reagent grade) were purchased from Scharlau. Ultrapure water was directly taken from a Sartorius Stedim Arium 611 VF® water purification system (ρ = 18.2 mΩ·cm). Cellulose nanocrystals (CNCs) were isolated from cotton (Whatman No. 1 filter paper) by controlled hydrolysis with sulphuric acid according to a protocol that is a modification of the method originally described by Dong et al.[49] This protocol

introduces a small concentration of sulfate ester groups on the surface of the CNCs, which help to form stable suspensions in polar solvents.[50] In our previous work[31, 32] we presented data on the synthesized cellulose nanocrystals (CNCs) in terms of particle morphology, crystal structure, concentration of sulfate groups in the surface and properties.

2.2. SYNTHESIS OF PMS PRE-POLYMER

Sebacic acid (SA) and mannitol (MA) were reacted in a manner described previously.[1] PMS pre-polymer (pre-PMS) was synthesized to obtain 1:2 mannitol:sebacic acid ratio.[32] Briefly, appropriated molar amounts (0.034:0.068) of MA (6.21 g) and SA (13.79 g) were charged into a 250 mL three-necked round-bottom flask equipped with a stirrer and a condenser, which was placed in an oil heating bath and purged for 0.5 h with nitrogen. The temperature was slowly increased to 150 °C under continuous stirring and nitrogen flow to produce approximately 20 g of pre-polymer. The reaction was stopped after 5 h (1 h before gelation occurs), and the pre-polymer was dissolved in DMF (150 mg/mL), filtered and purified by dropwise precipitation into a four-fold excess of cold ultrapure water under continuous stirring. The precipited pre-polymer was collected and dried under vacuum until no more solvent was detected in the infrared spectra. The yield of the reaction was ~88%, as calculated from the weight of the monomers before reaction and the weight of obtained pre-polymer after reaction. A composition of mannitol:sebacic acid of 0.83:2 determined by ^{1}H-NMR was achieved.[32]

2.3. PRODUCTION OF NANOFIBERS MATS

Poly(lactic acid) (PLA) was electrospun into a nanofiber mat (NF-PLA) through electrospinning method following a previously reported protocol[51] to obtain average fiber diameters nearly to 300-400 nm and electrospun mat thickness

around 100 μm. Briefly, 10 mL of viscous polymer solution with a concentration of 7 wt% was prepared by dissolving PLA (3051D) in a mixture solvent system with dichloromethane and N,N-dimethyl-formamide (DCM:DMF 70:30). The solution was injected using a 10 mL disposable syringe with a 22-G needle connected to the positive terminal of the high voltage supply. All air bubbles were purged prior to electrospinning and the applied voltage was kept at 14kV, the distance between the charged capillary tip and the collector mandrel was 13 cm, and the flow rate of the solution was always kept at 0.6 mL/h, controlled by a syringe infusion pump. The collector mandrel was covered with aluminium foil, and a take-up velocity (rotation speed of the mandrel) of 1100 r.p.m. was used.

2.4. PREPARATION OF PMS/CNC NANOCOMPOSITES

Previously reported protocol was followed to prepare films of neat PMS (1:2 MA:SA ratio) and poly(mannitol sebacate)/cellulose nanocrystals (PMS/CNC) nanocomposites with 1, 5 and 10% of filler content (**Scheme 6.1**).[32] The resulting pre-polymer/nanocomposites and the neat pre-polymer films obtained by applying this protocol (after step **3** in **Scheme 6.1**), were placed in a vacuum oven for further reaction at 120 °C for 72 hours under vacuum (60 cm Hg) to afford films of ~150-200 μm of thickness of neat PMS and PMS/CNC final samples (step **4** in **Scheme 6.1**).

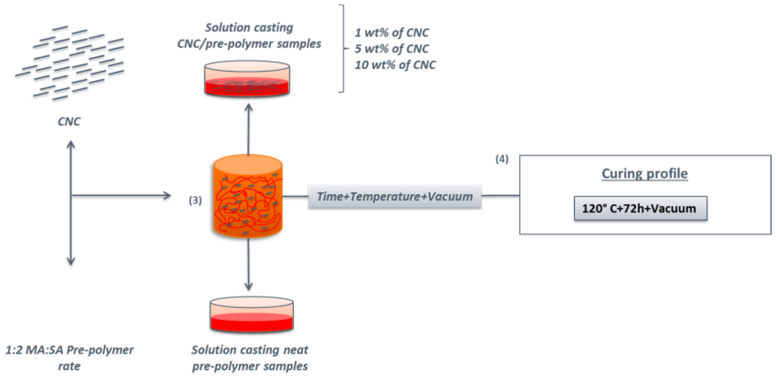

Scheme 6.1. Schematic representation of the methodology followed to obtain all the PMS/CNC nanocomposites. Solutions of pre-polymer in DMF **(1)** were mixed with CNC suspensions also in DMF **(2)**. Mixtures obtained and neat pre-polymer solutions were casted **(3)** and after evaporation of the solvent, samples were crosslinked through further polycondensation step **(4)**.

2.5. PREPARATION OF PMS/CNC NANOCOMPOSITES

The methodology schematically shown in **Scheme 6.2** was used to prepare poly(mannitol sebacate)/nanofiber nanocomposites (PMS/NF-PLA), from previously obtained pre-PMS (1:2 MA:SA ratio)[32] and electrospun PLA mats (NF-PLA). Samples with different amount of layered mats of NF-PLA (according to the number of layers used: 1, 2 and 3 mats) were obtained by cutting a rectangular area of dimensions 4 x 8 cm from the electrospun mat and infiltrating them into the pre-PMS. Briefly, nanocomposites with different matrix/nanofibers weight percentage ratio were produced using a stratification technique by means of which 0.6 g of pre-polymer were combined with 1, 2 and 3 layers of electrospun NF-PLA mats. The pre-polymer was heated at 40 °C (as starts to be a viscous clear liquid at this temperature losing the waxy aspect) and spread into a Teflon® surface, appropriate amounts of previously cut NF-PLA mat fragments were then immersed while vacuum (30 cm Hg) was applied for 20 min to ensure complete infiltration of pre-PMS into the NF-PLA mats (steps **1-3** in **Scheme 6.2**). Afterward, the pre-PMS/NF-PLA nanocomposites were placed in a vacuum oven (at the same conditions that pre-PMS/CNC nanocomposites) (step **4** in **Scheme 6.2**) for further reaction of the

matrix to obtain final crosslinked PMS/NF-PLA samples. Previously to infiltration, the NF-PLA mats and the amount of pre-PMS used in each sample were weighed, as well as the obtained nanocomposites after curing. Final weight ratio between nanofibers and matrix were then calculated to be 4, 10 and 15 wt% with the addition of 1, 2 and 3 layers of electrospun NF-PLA mats respectively.

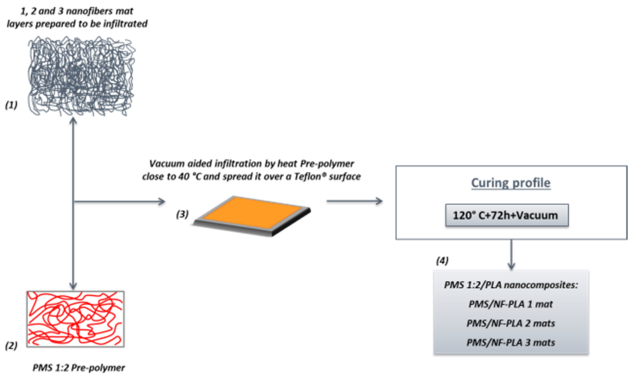

Scheme 6.2. Schematic representation of the methodology followed to obtain all the PMS/PLA nanocomposites. Electrospun PLA mats **(1)** were infiltrated into spread pre-polymer PMS 1:2 **(2)** over a Teflon® surface **(3)** with the help of vacuum and temperature. After infiltration, further polycondensation step under low curing designed profile was carried out **(4)**.

2.6. SWELLING AND DEGRADATION STUDIES IN SBF

The swelling degree and degradation studies of all obtained samples (*n=4*, 5x5 mm, 150-200 µm thickness) were studied under physiological conditions, in phosphate buffered saline solution (SBF) of 7.4 ± 0.5 at 37 °C, prepared following a previously reported protocol.[52] For swelling studies, samples were collected after a 24 hour hydration period in SBF, blotted with a filter paper to remove excess surface water, and weighed (swelled weight; W_s). The swelling percentage of the networks after 24 h was determined comparing the swelled weight (W_s) with the initial weight (W_o) using equation (6.1).

$$Swelling\ degree(\%) = \frac{W_S - W_O}{W_o}\ x\ 100 \tag{6.1}$$

The degradation behavior was determined by monitoring the weight loss at different times. Samples were weighed, immersed in 15 mL of SBF and incubated at 37 °C in an oven for various periods of time. Nanocomposite samples were removed from SBF at different time intervals (14 days, 28 days, 42 days, 56 days and 150 days), thoroughly washed with distilled H_2O and dried under vacuum at 37 °C until constant weight was reached. To the degradation study of neat PMS and PMS/NF-PLA nanocomposites two longer degradation time intervals at 210 days (7 months) and 240 days (8 months) were incorporated. The degradation degree of the polymers in SBF was calculated averaging the values of three samples by comparing the mass at each time interval (M_t) with the initial mass (M_o) using equation (6.2).

$$Mass\ Loss\ (\%) = \frac{M_o - M_t}{M_o} \tag{6.2}$$

2.7. SCANNING ELECTRON MICROSCOPY (SEM)

Morphological investigation of PLA electrospun nanofibers mat and cross-section of the PMS/NF-PLA nanocomposites were carried out by means of a JEOL JSM6030 scanning electron microscope. Nanofibers mats samples were prepared by cutting square pieces from randomly chosen parts of the processed specimen, while nanocomposites were cryo-fractured under liquid nitrogen. Specimens were gold-coated to minimize the charging effect during SEM observation as well as give enough conductivity to the sample. Operating conditions were set at 10 kV of accelerating voltage and a working distance of 10-15 mm.

2.8. MECHANICAL MICROTESTING

Tensile tests were carried out on a DEBEN microtester equipped with a 150 N load cell and operated at a crosshead speed of 0.4 mm/min at room temperature. Specimen dimensions were typically 15 x 4 mm. The elongation to break, Young´s modulus, toughness and ultimate tensile strength were analysed for samples at initial stage (day 0 of degradation). Young´s modulus of degraded samples was analysed at different degradation stages (immersion in SBF at 37 °C for 1, 28 and 150 days). Degraded samples were taken out from SBF and immediately tested. For each sample, a minimum of 5 rectangular samples were tested and the mechanical data were averaged.

2.9. THERMOGRAVIMETRIC ANALYSIS (TGA)

Thermal stability of all obtained samples was recorded in a Mettler-Toledo TGA/SDTA 851 modulus analyser. The samples (5-10 mg) were weighted in zircona crucibles and were heated in air at a rate of 10 °C/min from ambient temperature to 700 °C. Thermal stability temperatures were obtained as onset temperatures (T_o), obtained by a tangential intercept method onto the TG curve. The electrospun NF-PLA mats were also analysed for reference purposes.

2.10. DYNAMIC MECHANICAL THERMAL ANALYSIS (DMTA) AND THERMALLY ACTIVATED SHAPE-MEMORY PROPERTIES

The mechanical behavior as a function of temperature was characterized by DMTA measurements on a TA Q800 instrument (TA instruments). Samples were cut into 30 x 4 mm rectangular shapes and tested in tensile mode with a temperature ramp method from -50 to 150 °C at a heating rate of 3 °C/min. Frequency and strain amplitude were kept constant at 1 Hz and 15 μm, respectively. Glass transition temperatures were calculated as the maximum in tangent delta peak. Shape-

memory characteristics of the samples were quantified by cyclic, thermomechanical tensile tests in the DMTA. The experiment involved the creation of a temporary shape in a programming mode and a free stress recovery step of the permanent shape. The programming mode was performed under strain-controlled conditions in three steps: (1) the sample was equilibrated at 45 °C for 10 min, before a force ramp of 3 N/min was applied until a strain of 30% was reached. (2) While the stress was kept constant, the sample was subsequently cooled to 15 °C. (3) The sample was unloaded to zero stress and the temperature was maintained at 15 °C for 5 min to ensure the fixation of the temporary shape. At this point, the recovery step was initiated by increasing the temperature to 45 °C, which was then maintained for 20 min. All samples were tested for 3 or 4 cycles. The ability to fix the temporary shape at 15 °C (shape fixity ratio, R_f) and the ability to recover the permanent shape at 45 °C (shape recovery ratio, R_r) were quantified using the following equations[53-55]

$$R_f\,(N) = \frac{\varepsilon_u\,(N)}{\varepsilon_m\,(N)} x100\% \tag{6.3}$$

$$R_r\,(N) = \frac{\varepsilon_m\,(N) - \varepsilon_f\,(N)}{\varepsilon_m\,(N) - \varepsilon_f\,(N-1)} x100\% \tag{6.4}$$

, where ε_m is the maximum strain achieved in the N^{th} cycle after cooling and before unloading, ε_u is the fixed strain after unloading the sample at 15 °C in the same cycle, and ε_f is the residual strain of the sample after the recovery step. Should be pointed out that the shape-memory temperature profiles where selected taking in account the results obtained in the DMTA analysis and to fulfil the requirements for potential biomedical applications in terms to facilitate the manipulation, storage and implantation of a possible device. Shape-memory biomedical devices are recommended to be activated in the range of 36-55 °C, being also desirable the

possibility to avoid premature activation retaining the shape at room temperature.[56]

3. RESULTS AND DISCUSSION

3.1. PROPERTIES OF REINFORCING FILLERS

The most important properties of the isolated CNCs (by hydrolysis of cotton with sulfuric acid) used in the present work, were characterized and reported in our previous work.[31, 32] The morphology of PMS/NFPLA nanocomposites was studied by scanning electron microscopy (SEM). **Figure 6.1a** and **Figure 6.1b** show a representative SEM image and a histogram of PLA fiber diameters (obtained by image analysis), respectively. This images show a uniform and bead-free fiber morphology produced by electrospinning with an average diameter of 365±101 nm.

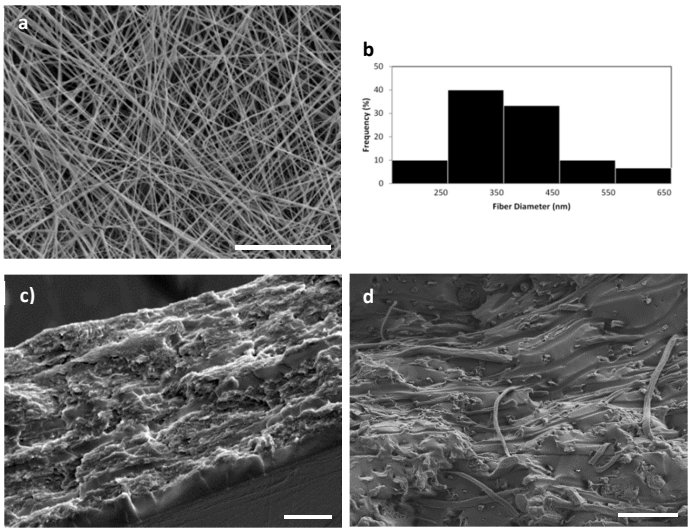

Figure 6.1. SEM image of the surface morphology of the electrospun nanofiber PLA mat (scale bar 20 μm) **(a)**, fiber diameter distribution histogram **(b)**, cross-sectional SEM of PMS/NFPLA 15 wt% nanocomposite (scale bars 20 and 2 μm respectively) **(c-d)**.

For all PMS/NF-PLA nanocomposites, cross-sectional SEM revealed a sandwich-type structure, showing that the infiltration was complete with all the original voids occupied by the PMS matrix (**Figure 6.1c and Supporting Information Figure S6.1**). The PMS matrix seems to be well-interfaced with the electrospun mats without an evident delamination. In this regard, a rough surface area is shown, which indicates that electrospun PLA-reinforced nanocomposites require more energy to delaminate. In **Figure 6.1d** the fiber structure is preserved after applying the necessary processing conditions (vacuum and temperature). The electrospun nanofiber mat shows improved bonding with the PMS matrix. The nanofibers appear broken on the same plane with the matrix and do not exhibit a clear pull-out or debonding.

3.2. CHARACTERIZATION OF INITIAL SAMPLES

3.2.1. MECHANICAL TESTING

In order to evaluate the mechanical properties of the PMS nanocomposites with different contents of CNC and PLA nanofibers, micro-tensile tests were carried out. The average tensile Young´s modulus, ultimate tensile strength, and elongation at break and toughness for all samples are summarized in **Table 6.1**.

The effect of nanocellulose content on the mechanical properties of PMS was discussed in our previous work;[31, 32] however, the purpose of the present paper is the comparison between the different fillers used. The addition of CNCs to the PMS matrix was found to improve its mechanical properties. In particular, it led to a noticeable increase in the Young´s modulus, even for low contents of CNC. Only 1 wt% of CNC increased the Young´s modulus by 54%.

The reinforcement of the PMS matrix upon addition of 4, 10 and 15 wt% of PLA nanofibers was indicated by increases in elastic modulus, UTS and toughness as filler content increased. In addition, a similar elongation was observed for all

electrospun PLA nanofiber-reinforced nanocomposites, probably due to strong interactions and adhesion between the higher modulus nanofibers and the low modulus PMS matrix, resulting in a more effective stress transfer and enhancement of the overall strength of the material during stretching.

Table 6.1. Main mechanical properties of neat PMS, PMS/CNC and PMS/NF-PLA nanocomposites.

Sample	Young´s modulus (MPa) [a]	Ultimate tensile strength (MPa)	Elongation at break (%)	Toughness (MJ/m^3)
NF-PLA	125.6±6.5	3.7±1	48.5±5.7	196.4±23.4
PMS/4% NF-PLA	30.8±0.5	4.1±1.0	45.7±2.8	105.4±25.7
PMS/10% NF-PLA	142.7±3.3	7.3±1.1	32.2±3.5	156.8±21.0
PMS/15% NF-PLA	380.3±5.5	14.0±1.4	37.0±5.6	427.0±54.1
Neat PMS	7.2±0.1	4.5±0.7	35.8±3.5	81.8±5.4
PMS/1% CNC	11.1±0.6	4.6±1.2	25.6±2.5	72.5±22.6
PMS/5% CNC	14.8±1.2	6.2±1.3	25.4±2.4	94.6±23.5
PMS/10%CNC	32.3±2.6	8.5±2.0	23.4±0.04	89.3±39.1

[a] Young´s modulus was calculated for PMS/CNC nanocomposites from the initial slope between 0-10%. For PMS/NF-PLA nanocomposites and NF-PLA was calculated between 0-1% of strain.

As seen in **Figure 6.2**, a low content of PLA nanofibers (4 wt%) results in better behavior than that of the neat matrix, but lower than that of the nanofibers alone; however, by increasing the PLA nanofiber content to over 10 wt%, a synergic effect between the filler and the matrix occurs, resulting in a marked enhancement in mechanical properties. In comparison with the results obtained in the PMS/CNC nanocomposites, the introduction of 4 wt% of PLA nanofibers results in a similar elastic modulus and a higher elongation at break than PMS/CNC nanocomposites with 10 wt% of CNCs. In contrast, nanocomposites with 15 wt% of PLA nanofiber content results in a much greater enhancement of the mechanical properties achieving a 50-fold enhancement of the Young´s modulus. UTS and toughness are also increased 3-fold and 5-fold, respectively, for this sample.

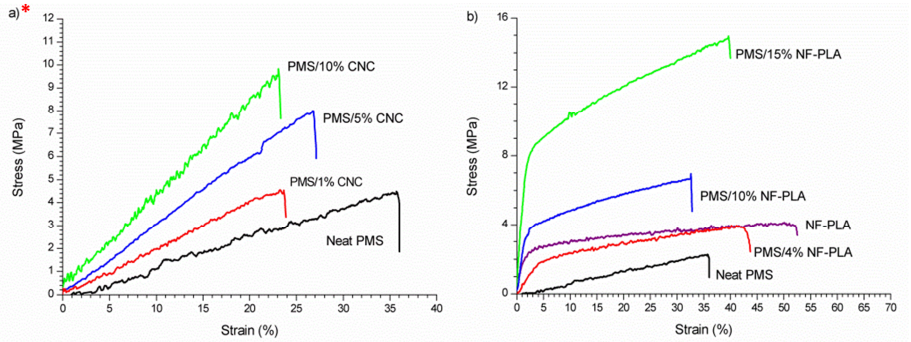

Figure 6.2. Typical tensile stress versus strain curves registered at room temperature for PMS/CNC nanocomposites **(a)** and PMS/NF-PLA nanocomposites **(b)**. *Figure 6.2a is included in the present thesis chapter for reference purposes, and will not be included in the article as was published in a previous work.[32]

The contribution to the mechanical properties of the PLA nanofibers over the PMS matrix was seen to be more efficient than that of CNCs. In this regard, the electrospun PLA nanofibers provide a significant increase in plastic deformation due to their polymeric nature and their good interfacial adhesion with the matrix, which results in nanocomposites with enhanced toughness and strength. Although both fillers have nanosized morphology, a higher aspect ratio (diameter to length relation) results in a much more effective reinforcing effect. In addition, the larger surface-area-to-volume ratio of electrospun nanofibers (compared to that of CNCs) considerably increases the interphase area (contact area) between the matrix and the reinforcing filler.

3.2.2. THERMOGRAVIMETRIC ANALYSIS

Table 6.2 shows the onset degradation temperature values for all developed samples. In regard to the thermal stability of PMS/CNC nanocomposites, these values revealed a slight increase in thermal stability for low CNC contents (1 wt%); this stability decreases with increasing filler content (5 and 10 wt% of CNC) probably due to CNC's lower onset degradation temperature relative to that of the

matrix. The first degradation CNC process typically starts close to 220 °C and is associated with the CNC glycosyl units degradation.[57]

However, the opposite phenomenon occurs in PMS/NF-PLA nanocomposites, as the degradation onset temperature increases with the NF-PLA content on account of the higher thermal stability of the nanofibers (352 °C) compared to that of the neat matrix (236 °C). The nanocomposite with 4 wt% of NF-PLA has similar degradation onset temperature to that of the neat matrix which represents most of the material. However, with 10 wt% of NF-PLA, thermal stability is improved by 8 °C; with 15 wt% of NF-PLA, the stability increases more considerably, by 25 °C.

3.2.3. DMTA TESTING

DMTA was used to determine the elastic modulus properties of all systems. **Figure 6.3a** and **Figure 6.3b** show the DMA curves of the storage modulus for PMS/CNC and PMS/NF-PLA nanocomposites, respectively. In the glassy state, all DMA curves follow the same general trend; thus, the storage modulus (E´) is only slightly increased by adding CNCs or NF-PLA contents lower than 10 wt%, which is consistent with the observations in both our previously reported system (based on a PMS 1:1 matrix) and those of other studies (based on glassy matrices reinforced with nanofillers).[31, 57] However, the introduction of high amounts of CNCs (10 wt%) and NF-PLA (10-15 wt%) fillers leads to a clear reinforcement in the glassy-state storage modulus. The storage modulus of neat PMS increases from 2600 MPa to 3500 MPa by adding 10 wt% of CNCs, and the addition of 10 and 15 wt% of NF-PLA storage modules values of 3000 and 4750 MPa are reached, respectively. The PMS/CNC nanocomposites exhibit a T_g between 18 and 23 °C (**Table 6.2 and Supporting Information Figure S6.3a**). These values are consistent with those previously reported from Differential Scanning Calorimetry (DSC) for these materials.[32] Thus, T_g slightly decreases with increasing the CNC content, probably

due to the disruption of the PMS polymeric network along with strong interactions between filler and matrix and decreasing the T_g of the global system.[58] Similar behavior was also observed in PGS bioglass nanocomposites and polyurethane systems reinforced with CNCs.[59, 60] Regarding to the PMS/NF-PLA nanocomposites (**Figure 6.3b**), as was expected, two different clear transitions appeared in the storage modulus; these can be attributed to the glass transition of PMS (21-26 °C) and the glass transition of NF-PLA (83-85 °C), as determined from the tangent delta peaks (**Supporting Information Figure S6.3b**). In contrast, both the PMS matrix and the PMS/CNC nanocomposites have only one transition, which is related to the glass transition of the neat matrix; however, the reinforcing effect induced by the fillers appears to be much more significant as the temperature increases to the rubbery plateau (above 40 °C).

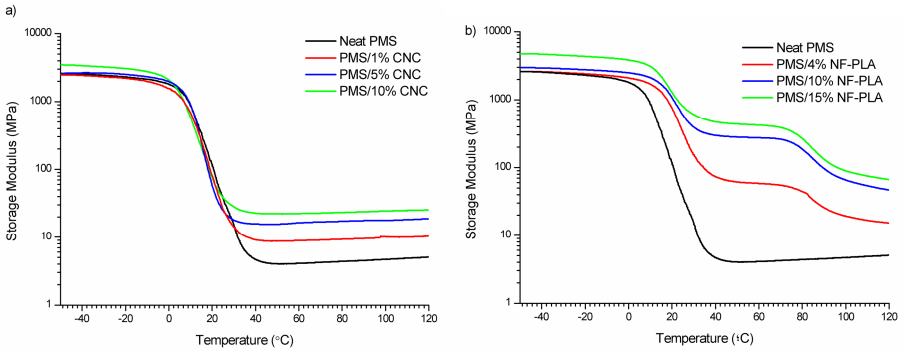

Figure 6.3. Storage modulus (E') as a function of temperature for PMS/CNC nanocomposites **(a)** and PMS/NF-PLA nanocomposites **(b)**.

In addition, the storage modulus in the rubbery plateau above glass transition of the neat PMS matrix also increases as the filler content increases for both types of nanocomposite systems (CNCs and NF-PLA reinforced). By introducing a 10 wt% of NF-PLA content, the storage modulus is increased to 280 MPa, more than 3 times higher than the value obtained for the same CNCs content sample. Thus, a pronounced reinforcing effect is achieved by introducing nanofibers, with storage modulus values as high as 445 MPa at 45 °C (after PMS glass transition) for 15 wt%

of NF-PLA content (**Figure 6.3b**). Finally, comparing all the developed materials at high temperatures (85-90 °C), the highest E´ values are also observed for the PMS/NF-PLA nanocomposites with values between 25 and 120 MPa. This reinforcement effect in the rubbery plateau observed for nanocomposite samples and is comparable with values reported in the literature that were obtained in materials with good shape-memory properties.[47, 61] This trend is in accordance with the results obtained in tensile tests at room temperature, in which the Young´s modulus increases markedly with the wt% of the NF-PLA addition.

Table 6.2. Hydration by mass and thermal properties of PMS and PMS nanocomposites.

Sample	$T_{g\text{-}PMS}$ [a]	$T_{g\text{-}NF\text{-}PLA}$ [a]	T_{ONSET} (°C) [b]	Hydration by mass (%)
PLA NF	-	83	352	20.7±1.6
PMS/4%NF-PLA	26	84	235	12.4±1.1
PMS/10%NF-PLA	23	85	244	6.3±1.1
PMS/15%NF-PLA	21	85	261	5.4±1.3
Neat PMS	23	-	236	14.4±1.0
PMS/1% CNC	23	-	239	12.0±0.3
PMS/5% CNC	19	-	238	11.4±0.3
PMS/10%CNC	18	-	233	10.4±0.8

[a] Glass transition temperatures were calculated as the delta tangent peak from DMTA curves (**Supporting Information Figure SI 6.4**)
[b] Determined from the onset of degradation from TGA curves .

3.2.4. THERMALLY ACTIVATED SHAPE-MEMORY PROPERTIES

The shape-memory properties were determined by cyclic thermomechanical tests conducted in a DMTA, quantifying shape recovery (R_r) and shape fixity (R_f) ratios for each cycle by applying the method detailed in the experimental section. **Figure 6.4** shows an example of the shape-memory cycles measured for PMS/CNC and PMS/NF-PLA nanocomposites with 10 wt% of CNC and NF-PLA respectively. Under the conditions chosen for the shape-memory test, all the samples reinforced with

CNCs have an incomplete shape fixation (R_f<50%) of the programmed shape after cooling and unloading the applied stress, probably due to the fact that the fixing temperature (T_{low}) is in the vicinity of the T_g (18-23 °C). This was observed in previously reported similar systems,[31] which also resulted in insufficient shape-memory behavior.

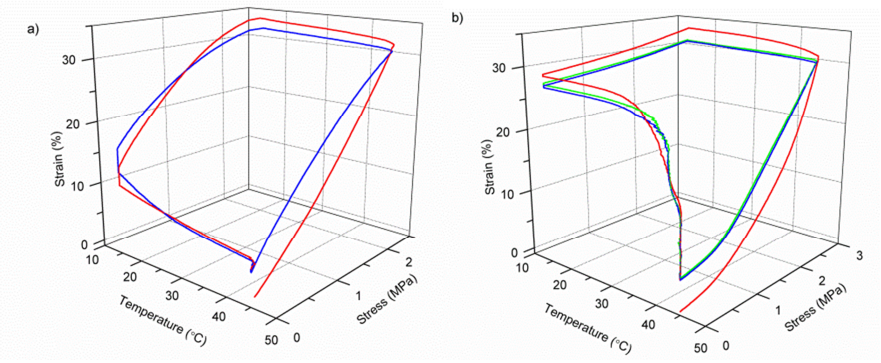

Figure 6.4. Shape-memory stress-strain-temperature curves of two and three consecutive cycles for PMS/CNC 10 wt% **(a)** and PMS/NF-PLA 10 wt% nanocomposite **(b)** respectively.

By contrast with the previously discussed PMS/CNC nanocomposites (employing NF-PLA as reinforcement fillers), enhanced shape-memory properties are imparted to the system. All PMS/NF-PLA nanocomposites showed a marked shape-memory effect, with an increase in shape fixity (**Figure 6.5a**) as the filler content increases after unloading at T_{low}. The nanofibers' presence helps constrain the premature recovery of the matrix, which occurs in PMS and PMS/CNC nanocomposites that are not able to fix the shape. Importantly, nanofibers played a significant role in maintaining the shape of the PMS matrix above its T_g. Shape fixity ratio values (R_f) were 72, 87 and 91% for PMS with 4, 10 and 15 wt% of PLA nanofibers respectively. In case of the shape recovery for the first cycle (**Figure 6.5b**) there is a loss in R_r% with increasing NF-PLA content, but the second cycle stabilizes at values of 99-100%. Thus, the fibers's possible plastic deformation (as they are above their glass transition during deformation and recovery) seems not to impede the system's

recovery, and the PMS matrix chains' mobility and rubber elasticity at 45 °C achieve a good global recovery. One can surmise that this phenomenon is the result of a complete infiltration of the mats inside the matrix, resulting in a synergic effect of both components. It should be pointed out that for a PMS/NF-PLA sample with 4 wt%, shape recovery starts at a temperature slightly higher than the neat PMS T_g (~30 °C); however, by increasing the nanofiber content to 10 and 15 wt%, the relaxation processes during the shape-memory test occur at temperatures in the range of 40-45 °C. This fact is of interest to avoid the premature recovery of a possible biomedical device during implantation.

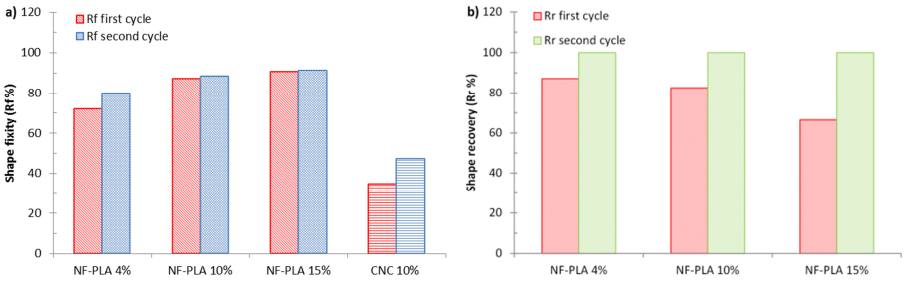

Figure 6.5. Shape fixity characteristic values for the first and second cycles of PMS/NF-PLA nanocomposites compared with PMS/CNC 10 wt% sample **(a)** and shape recovery characteristic values for the first and second cycles of PMS/NF-PLA nanocomposites **(b)**.

In general, the main goal of the concept introduced in this work is to achieve design flexibility by using nanofibers as a reinforcement phase to impart shape-memory properties that cannot be achieved by fillers with nanoparticulate morphology, such as CNCs. It should be pointed out that the temperatures at which the reinforcement effect occurs in the DMTA curves is a key factor in the usefulness of the PMS/NF-PLA nanocomposites as shape-memory materials for biomedical applications. In addition, a clear enhancement in the shape fixity (R_f%) ratios could be reached by increasing the wt% of NF-PLA content of the matrix. On the other hand, since the shape recovery process is thermally dependent,[63] the recovery ratios (R_r%) can be improved by increasing the recovery temperature to make it

closer to the nanofibers' T_g or by employing nanofibers with lower glass transitions to allow partial mobility of the chains at the temperature of interest. It is also remarkable that the higher stress during shape-memory cycles (~6MPa) is reached with PMS/NF-PLA 15 wt% nanocomposite, in agreement with the improvement in the Young´s modulus and storage modulus (*E´*) at the rubbery plateau observed for this sample. This fact is reported to be concomitant with a higher shape recovery force and is very useful in ensuring good shape stability and complete recovery during the application of a device.[64] The introduction of 10-15 wt% of nanofibers as a reinforcement phase into a low-modulus neat PMS imparts shape-memory properties with R_f close to 90% and R_r of 100% (after the first thermomechanical cycle) without deterioration over the rest of the cycles performed in these samples.

3.3. CHARACTERIZATION OF DEGRADED SAMPLES

3.3.1. SWELLING STUDIES

The swelling degree of the neat PMS, PMS/CNC and PMS/NF PLA nanocomposite samples was determined after 24h immersion in SBF at 37 °C, and the results are shown in **Table 6.2**. Regarding the PMS/CNC nanocomposites, there is a slight reduction in the swelling degree with increasing CNCs content, probably due to the higher crosslink density as a result of filler/matrix interactions.[32, 64] The trend of these results is in agreement with the mechanical properties' results. Neat PMS swells to 14.4±1.0 % and to 10.4±0.8 % for 10 wt% of CNCs. Unlike in the case of PMS/CNC nanocomposites, the swelling results obtained for PMS/NF-PLA nanocomposites seem to be related to the sample's wt% of NF-PLA, instead of to the reactions between the matrix and the filler. The initial swelling behavior of each component separately is 14.4±1.0 % for neat PMS and 21.5±0.3 % for NF-PLA. However, by combining them to obtain nanocomposites, swelling is reduced as nanofiller content increases, with swelling of 12.4±1.1 %, 6.3±1.1 % and 5.4±1.3 % for 4, 10 and 15 wt% of NF-PLA, respectively. The high initial swelling of nanofiber mats could be attributed to the nanoporous structures and amorphous fraction

presence.[65-67] For a 4 wt% PMS/NF-PLA nanocomposite, the swelling degree of the isolated PLA-NF decreases significantly as voids in the interconnected network are filled with the PMS polymer matrix. Moreover, as was expected, by increasing the nanofiber weight fraction in the nanocomposite, the swelling degree lowers even further due to a combination of less porous inner structures combined and a PMS matrix that restricts nanofiber swelling.[68]

3.3.2. DEGRADATION IN SBF

The degradation of nanocomposites was investigated under physiological conditions (SBF, 37 °C) over periods of 150 and 210 days for PMS/CNC and PMS/NF-PLA nanocomposites, respectively. **Figure 6.6** shows neat PMS, PMS/CNC and PMS/NF-PLA nanocomposites degradation rates, revealing that the highest degradation rate corresponds to the neat matrix, which also has the highest swelling degree. At least for the first stages (14 to 42 incubation days), increasing nanofiber content seems to slow down the degradation rate (**Figure 6.6b**). For these short degradation times, similar behavior is observed in the neat matrix and in the nanocomposite with 4 wt% of NF-PLA, as the major part of each material is PMS.

Although the nanocomposites with 10 and 15 wt% of NF-PLA content show a slower degradation process, in accordance with swelling results, their behavior at short immersion times is closer to that of the neat matrix than to that of the neat nanofiber mat. Interestingly, the presence of different weight ratios of nanofibers does not seem to have a great influence on the degradation rate of the nanocomposites at longer degradation times, as the nanocomposite degradation trend becomes more equal over time. This is probably due to the degradation of the neat matrix, which makes it easier for the nanofibers to contact the SBF. As a

result, degradation rates for all the PMS/NF-PLA nanocomposites at this stage are similar to the nanofibers mat's degradation profile.

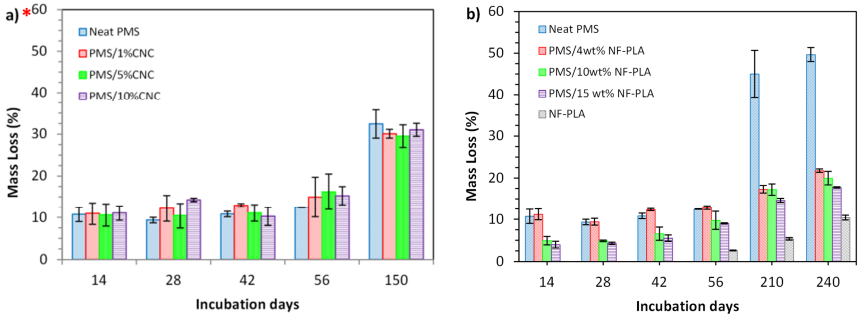

Figure 6.6. Degradation of PMS/CNC nanocomposites **(a)** and PMS/NF-PLA nanocomposites **(b)** under physiological conditions (SBF at 37 °C) monitored over immersion days. *Figure 6.6a is included in the present thesis chapter for reference purposes, and will not be included in the article as was published in a previous work.[32]

As could be seen in **Figure 6.6**, the mass loss of PMS/NF-PLA nanocomposites is comparable to that of PMS/CNC nanocomposites at short immersion times, with mass loss for both systems near 15% after 56 days. However, at longer immersion times, the mass loss rate of PMS/NF-PLA nanocomposites is markedly lower than that of PMS/CNC nanocomposites. Thus, this degradation behavior observed in PMS/NF-PLA nanocomposites can be explained as a combination of the matrix presence, which protects the nanocomposites from water penetration, and the nanofibers' lower hydrolytic degradation rate due to their more hydrophobic nature.[1, 69, 70] In summary, the degradation rate of PMS is reduced at long immersion times by the presence of PLA nanofibers. This fact, together with the diversity and stability of mechanical properties and enhanced shape-memory behavior of these nanofiber nanocomposites, could be beneficial in the development of active long-term implants for biomedical applications.

3.3.3. MECHANICAL PROPERTIES OF NANOCOMPOSITES IN SBF

In order to evaluate the effect of physiological conditions over the tensile properties of the developed materials, we allowed the samples to hydrate/degrade in SBF at 37 °C for 1, 28 and 150 days and then subjected them to a micro-tensile test. The changes in Young´s modulus over the degradation time for neat PMS, PMS/CNC and PMS/NF-PLA nanocomposites are shown in **Figure 6.7.** Regarding the developed materials, it was observed that, in general, all the samples had low differences between dry and wet conditions, as similar Young´s moduli were found in the dry state and after one day of hydration. As seen in **Figure 6.7**, a prolonged incubation time of up to 150 days produced a deterioration of mechanical properties for all PMS/CNC (**Figure 6.7a**) and for PMS/NF-PLA nanocomposites with 4 to 10 wt% of NF-PLA content (**Figure 6.7b**). However, the PMS/NF-PLA sample with 15 wt% of NF-PLA retained close to the 80% of its initial Young´s modulus. It is also remarkable that the PMS/NF-PLA nanocomposites' mechanical behavior over immersion time seems much more predictable that of the PMS/CNC nanocomposites. There is a clear trend in slower mass loss with increasing NF-PLA content that is not observed in their CNC counterparts.

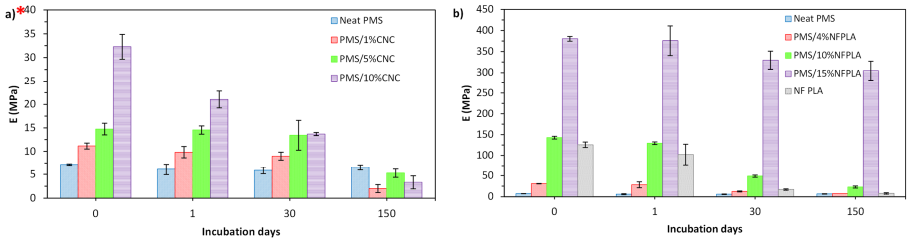

Figure 6.7. Young´s modulus values for the dry state (as prepared) and after 1, 30 and 150 days of immersion in SBF for neat PMS and PMS/CNC nanocomposites **(a)** and neat PMS, NF-PLA and PMS/NF-PLA nanocomposites **(b)**. *Figure 6.7a is included in the present thesis chapter for reference purposes, and will not be included in the article as was published in a previous work.[32]

Thus, main advantage of using nanofibers as PMS filler is that they provide high mechanical retention and stability that can be controlled by increasing the nanofibers' weight fraction. This high mechanical stability over an extended period of time makes could make these nanocomposites potential candidates to serve as mechanical support during tissue remodeling at a wound site.[28, 71] In addition, the use of nanofibers as a reinforcing material provides greater design flexibility, as one can separately modify the two functional components (matrix and fibers) to achieve optimum control of mechanical properties and degradation profiles.

Although it has been demonstrated that the easiest way to tune the properties of a PMS matrix is through combination with nanofibers, it should be pointed out that all developed PMS nanocomposites revealed mechanical properties that could be useful for a variety of medical applications, such as implantable medical devices, depending on the type of filler used. As an example, the mechanical properties of PMS/NF-PLA nanocomposites are comparable to those of human cartilage (E=130 MPa, UTS; 19 MPa, elongation at break= 20-120 %) and skin (E= 15-50 MPa, UTS= 5-30 MPa, elongation at break= 35-115 %)[73]. Other tough living tissues, such as tendon (E=143-2310 MPa), human ligament (E=65-541 MPa), trabecular bone (E=6.9-200 MPa) and cancellous bone (E=20-500 MPa) also a Young´s moduli comparable to those of these samples.[25, 27, 73, 74] The mechanical properties obtained for PMS/CNC nanocomposites are found in the range of several soft and elastic living tissues, such as veins, arteries and some articular cartilage.[75-78] Finally, despite the fact that this work is indicative of biodegradability, to accurately represent the biodegradation and the usefulness of the developed materials as biomedical devices, future in vivo studies should be developed.

4. CONCLUSIONS

In this study, two different approaches to the reinforcing filler morphology were proposed to obtain polymer nanocomposites with potential biomedical

applications. A PMS matrix is reinforced either with CNCs or electrospun PLA nanofibers to obtain, respectively, nanoparticulate- and nanofiber- reinforced nanocomposites. PMS pre-polymer was infiltrated into different amounts of NF-PLA followed by a thermal crosslinking procedure under vacuum to obtain PMS/NF-PLA nanocomposites. The mechanical, thermal, degradation and shape-memory properties of these materials were evaluated and compared with those of the PMS/CNC system. Results indicated that by employing different nanofillers, a considerable wide range of mechanical and degradation properties are accessible. In this regard, the addition of NF-PLA in PMS matrices results in a remarkable improvement in mechanical properties, with a 53-fold increase in Young´s modulus when a neat PMS matrix is combined with 15 wt% of PLA nanofibers, well above the enhancement obtained for the CNC-reinforced system. At the same time, this system offers the highest mechanical retention and stability over degradation time. At long degradation times, PMS/CNC samples retain Young´s modulus on the order of the modulus for the neat PMS matrix (4-6 MPa). The same behavior occurs in PMS/NF-PLA nanocomposites with low wt% of nanofibers (4 wt%); however, the addition of 10 or 15 wt% of NF-PLA allows for a Young´s modulus of 25 and 300MPa, respectively, a 3-fold and 46-fold increase over the values for the neat matrix and PMS/CNC nanocomposites. This mechanical behavior is directly related to the filler morphology, thus, a higher aspect ratio and contact area between the matrix and the reinforcing nanofibers results in effective load transference, even at long degradation times. In addition, the matrix probably protects the nanofibers from SBF penetration by lowering their hydrolytic degradation rate, which could help to the retention of these properties over time.

Regarding to shape-memory behavior, neat PMS and PMS/CNC nanocomposite samples presented poor shape-memory properties; nevertheless, the introduction of nanofibers as filler improved the shape-memory properties of neat PMS thanks to the marked enhancement achieved in the rubbery modulus (more than 100

times higher than that of the neat PMS matrix with the addition of 15 wt% of NF-PLA). The resulting material can fix a temporary shape and obtain shape recovery values of 100% for the second thermomechanical cycle. In addition, the presence of two well-separated thermal transitions (as shown in DMTA analysis) enables the design of a triple-shape-memory systems for target applications.[79] Thus, nanocomposites with good thermally activated shape-memory properties were obtained based on a PMS matrix reinforced with the NF-PLA with the best fixity ratios (R_f) and on filler contents of 10 and 15 wt%. The data analysed and discussed for each nanocomposite system provide insights for broadening applications of the PMS matrix, independently on the type of filler used. Owing to shape-memory properties and the high retention of mechanical properties over degradation time during immersion in SBF, the obtained PMS/NF-PLA nanocomposites seem to be good candidates for use as smart and responsive materials in long-term medical applications.

ACKNOWLEDGEMENTS

The authors gratefully acknowledge financial support received from Spanish Ministry of Economy and Competitiveness (Project MAT2010/21494-C03), as well as the support of FPU grant from MED (MED-FPU; AP2009-2482).

5. REFERENCES

1. J. P. Bruggeman, B. de Bruin, C. J. Bettinger and R. Langer, *Biomaterials,* 2008, **29**, 4726-4735.
2. Y. Li, G. A. Thouas and Q. Chen, *RSC Advances*, 2012, **2**, 8229-8242.
3. Y. Wang, G. Ameer, B. Sheppard and R. Langer, *Nature Biotechnology,* 2002, **20**, 602-606.
4. J. Yang, A. Webb and G. Ameer, *Advanced Materials,* 2004, **16**, 511-516.

5. J. Yang, A. Webb, S. Pickerill, G. Hageman and G. Ameer, *Biomaterials,* 2006, **27**, 1889-1898.
6. C. Sundback, J. Shyu, Y. Wang, W. Faquin, R. Langer, J. Vacanti and T. Hadlock, *Biomaterials,* 2005, **26**, 5454-5464.
7. J. B. Allen, S. Khan, K. A. Lapidos and G. A. Ameer, *Stem Cells,* 2010, **28**, 318-328.
8. Z. Sun, C. Chen, M. Sun, C. Ai, X. Lu, Y. Zheng, B. Yang and D. Dong, *Biomaterials,* 2009, **30**, 5209-5214.
9. A. Mahdavi, L. Ferreira, C. Sundback, J. W. Nichol, E. P. Chan, D. J. D. Carter, C. J. Bettinger, S. Patanavanich, L. Chignozha, E. Ben-Joseph, A. Galakatos, H. Pryor, I. Pomerantseva, P. T. Masiakos, W. Faquin, A. Zumbuehl, S. Hong, J. Borenstein, J. Vacanti, R. Langer and J. M. Karp, *Proceedings of the National Academy of Sciences U.S.A.,* 2008, **105**, 2307-2312.
10. D. G. Barrett and M. N. Yousaf, *Molecules,* 2009, **14**, 4022-4050.
11. Y. Kang, J. Yang, S. Khan, L. Anissian and G. Ameer, *Journal of Biomedical Materials Research Part A,* 2006, **77A**, 331-339.
12. A. K. Sharma, P. V. Hota, D. J. Matoka, N. J. Fuller, D. Jandali, H. Thaker, G. A. Ameer and E. Y. Cheng, *Biomaterials,* 2010, **31**, 6207-6217.
13. M. A. Hood, C. S. Gold, F. L. Beyer, J. M. Sands and C. Y. Li, *Polymer,* 2013, **54**, 6510-6515.
14. X. Zhang, H. Tang, R. Hoshi, L. De Laporte, H. Qiu, X. Xu, L. D. Shea and G. A. Ameer, *Biomaterials,* 2009, **30**, 2632-2641.
15. C. J. Bettinger, *Macromolecular Bioscience,* 2011, **11**, 467-482.
16. T. Kiyotsukuri, M. Kanaboshi and N. Tsutsumi, *Polymer International,* 1994, **33**, 1-8.
17. Y. Wang, G. Ameer, B. Sheppard and R. Langer, *Nature Biotechnology.,* 2002, **20**, 602-606.
18. T. Ding, Q. Liu, R. Shi, M. Tian, J. Yang and L. Zhang, *Polymer Degradation and Stability,* 2006, **91**, 733-739.

19. G. C. Engelmayr , M. Cheng, C. J. Bettinger, J. T. Borenstein, R. Langer and L. E. Freed, *Nature Materials,* 2008, **7**, 1003-1010.
20. D. Motlagh, J. Yang, K. Lui, A. Webb and G. Ameer, *Biomaterials,* 2006, **27**, 4315-4324.
21. M. Nagata, T. Machida, W. Sakai and N. Tsutsumi, *Journal of Polymer Science Part A: Polymer Chemistry,* 1999, **37**, 2005-2011.
22. C. J. Bettinger, B. Orrick, A. Misra, R. Langer and J. T. Borenstein, *Biomaterials,* 2006, **27**, 2558-2565.
23. 287.V. R. Sastri, *Plastics in Medical Devices, properties, requirements, and applications*, ed. V.R. Sastri, William Andrew Publishing, Boston, 2010, pp. 217-262.
24. Q. Chen, A. Bismarck, U. Hansen, S. Junaid, M. Q. Tran, S. E. Harding, N. N. Ali and A. R. Boccaccini, *Biomaterials,* 2008, **29**, 47-57.
25. S. Liang, W. D. Cook, G. A. Thouas and Q. Chen, *Biomaterials,* 2010, **31**, 8516-8529.
26. M. A. Meyers, P. Chen, A. Y. Lin and Y. Seki, *Progress in Materials Science,* 2008, **53**, 1-206.
27. K. Firoozbakhsh, I. Yi, M. Moneim and Y. Umada, *Clinical Orthopaedics and Related Research,* 2002, **403**, 240-247.
28. Q. Chen, S. Liang, J. Wang and G. P. Simon, *Journal of the Mechanical Behavior of Biomedical Materials,* 2011, **4**, 1805-1818.
29. Q. Liu, J. Wu, T. Tan, L. Zhang, D. Chen and W. Tian, *Polymer Degradation and Stability,* 2009, **94**, 1427-1435.
30. Q. Chen, L. Jin, W. D. Cook, D. Mohn, E. L. Lagerqvist, D. A. Elliott, J. M. Haynes, N. Boyd, W. J. Stark, C. W. Pouton, E. G. Stanley and A. G. Elefanty, *Soft Matter,* 2010, **6**, 4715-4726.
31. A. Sonseca, S. Camarero-Espinosa, L. Peponi, C. Weder, E. J. Foster, J. M. Kenny and E. Giménez, *Journal of Polymer Science Part A: Polymer Chemistry,* 2014, **52**, 3123-3133.

32. A. Sonseca, O. Sahuquillo, E. J. Foster and E. Gimenez, *RSC Advances,* 2015, **5**, 55879-5581.
33. J. S. Haghpanah, R. Tu, S. Da Silva, D. Yan, S. Mueller, C. Weder, E. J. Foster, I. Sacui, J. W. Gilman and J. K. Montclare, *Biomacromolecules,* 2013, **14**, 4360-4367.
34. M. Jorfi, M. N. Roberts, E. J. Foster and C. Weder, *ACS Applied Materials & Interfaces,* 2013, **5**, 1517-1526.
35. A. Lendlein, A. M. Schmidt and R. Langer, *Proceedings of the National Academy of Sciences of the U.S.A.,* 2001, **3**, 842-847.
36. A. Lendlein and R. Langer, *Science,* 2002, **296**, 1673-1676.
37. W. Small, T. Wilson, W. Benett, J. Loge and D. Maitland, *Optics Express,* 2005, **13**, 8204-8213.
38. W. Small, M. F. Metzger, T. S. Wilson and D. J. Maitland, *Journal of Selected Topics in Quantum Electronics,* 2005, **11**, 892-901.
39. D. J. Maitland, M. F. Metzger, D. Schumann, A. Lee and T. S. Wilson, *Lasers in Surgery and Medicine,* 2002, **30**, 1-11.
40. Y. Liu, K. Gall, M. L. Dunn and P. McCluskey, *Mechanics of Materials,* 2004, **36**, 929-940.
41. Darrell H Reneker and Iksoo Chun, *Nanotechnology,* 1996, **7**, 216.
42 A. Greiner, J. H. Wendorff, S. Ramakrishna and S. Agarwal, *Electrospinning: Materials, Processing, and Applications*, John Wiley & Sons, Germany, 2012.
43. N. Bhardwaj and S. C. Kundu, *Biotechnology Advances,* 2010, **28**, 325-347.
44. S. F. Fennessey and R. J. Farris, *Polymer,* 2004, **45**, 4217-4225.
45. I. S. Chronakis, *Journal of Materials Processing Technology,* 2005, **167**, 283-293.
46. Z. M. Huang, Y. Z. Zhang, M. Kotaki and S. Ramakrishna, *Composite Science and Technology,* 2003, **63**, 2223-2253.
47. X. Luo and P. T. Mather, *Macromolecules,* 2009, **42**, 7251-7253.
48. X. Luo and P. T. Mather, *Advanced Functional Materials,* 2010, **20**, 2649-2656.
49. X. Dong, T. Kimura, J. Revol and D. Gray, *Langmuir,* 1996, **12**, 2076-2082.

50. B. Braun and J. R. Dorgan, *Biomacromolecules,* 2009, **10**, 334-341.
51. A. Sonseca, L. Peponi, O. Sahuquillo, J. M. Kenny and E. Giménez, *Polymer Degradation and Stability,* 2012, **97**, 2052-2059.
52. T. Kokubo, H. Kushitani, S. Sakka, T. Kitsugi and T. Yamamuro, *Journal of Biomedical Materials Research,* 1990, **24**, 721-734.
53. M. Behl and A. Lendlein, *Materials Today,* 2007, **10**, 20-28.
54. W. Wagermaier, K. Kratz, M. Heuchel and A. Lendlein, *Advances in Polymer Science,* 2010, **226**, 97-145.
55. D. Ratna and J. Karger-Kocsis, *Journal of Materials Science.,* 2008, **43**, 254-269.
56. C. M. Yakacki and K. Gall, *Shape-Memory Polymers*, ed. A. Lendlein, Springer-Verlag, Berlin, 2010, pp.147-175.
57. K. Shanmuganathan, J. R. Capadona, S. J. Rowan and C. Weder, *Journal of Materials Chemistry*, 2010, **20**, 180-186.
58. Y. Li and J. A. Ragauskas, *Advances in diverse industrial applications of nanocomposites*, ed. B. Reddy, InTech, 2011, pp. 18-36.
59. A. Pei, J. Malho, J. Ruokolainen, Q. Zhou and L. A. Berglund, *Macromolecules,* 2011, **44**, 4422-4427.
60. S. Liang, W. D. Cook and Q. Chen, *Polymer International,* 2012, **61**, 17-22.
61. A. Saralegi, S. C. M. Fernandes, A. Alonso-Varona, T. Palomares, E. J. Foster, C. Weder, A. Eceiza and M. A. Corcuera, *Biomacromolecules,* 2013, **14**, 4475-4482.
62. B. A. Nelson, W. P. King and K. Gall, *Applied Physics Letters,* 2005, **86**, 103108-103108-3.
63. Q. Meng, J. Hu and Y. Zhu, *Journal of Applied Polymer Science,* 2007, **106**, 837-848.
64. A. K. Gaharwar, A. Patel, A. Dolatshahi-Pirouz, H. Zhang, K. Rangarajan, G. Iviglia, S. Shin, M. A. Hussain and A. Khademhosseini, *Biomaterials Science*, 2014, **3**, 46-58.
65. H. Ying Tang, D. Ishii, K. Sudesh, T. Yamaoka and T. Iwata, *Nanofibers*, ed. A. Kumar, Intech, 2010, Chapter 10.

66. W. Li, J. A. Cooper Jr., R. L. Mauck and R. S. Tuan, *Acta Biomaterialia,* 2006, **2**, 377-385.
67. K. Kim, Y. Akada, W. Kai, B. Kim and I. Kim, *Journal of Biomaterials and Nanobiotechnology,* 2011, **2**, 353-360.
68. J. Choi, K. M. Lee, R. Wycisk, P. N. Pintauro and P. T. Mather, *Macromolecules,* 2008, **41**, 4569-4572.
69. E. Hendrick and M. Frey, *Journal of Engineered Fibers and Fabrics,* 2014, **9**, 153-164.
70. D. P. Li, M. W. Frey and A. J. Baeumner, *Journal of Membrane Science,* 2006, **279**, 354-363.
71. T. Schepull, J. Kvist, C. Andersson and P. Aspenberg, *BMC Musculoskeletal Disorders,* 2007, **8**, 116-116.
72. W. Li, C. T. Laurencin, E. J. Caterson, R. S. Tuan and F. K. Ko, *Journal of Biomedical Materials Research,* 2002, **60**, 613-621.
73. S. K. Ha, *Med. Eng. Phys.,* 2006, **28**, 534-541.
74. M. Sabir, X. Xu and L. Li, *Journal of Materials Science,* 2009, **44**, 5713-5724.
75. A. Thambyah, A. Nather and J. Goh, *Osteoarthritis and Cartilage,* 2006, **14**, 580-588.
76. D. E. T. Shepherd and B. B. Seedhom, *Rheumatology,* 1999, **38**, 124-132.
77. B. Amsden, *Soft Matter*, 2007, **3**, 1335-1348.
78. J. Lee and D. Boughner, *Circulation Research,* 1985, **57**, 475-481.
79. S. Chatani, C. Wang, M. Podgórski and C. N. Bowman, *Macromolecules,* 2014, **47**.

S.I. Chapter 6

<u>Supporting Information</u>: A comparative study of the mechanical, shape-memory, and degradation properties of fiber- and particulate-reinforced Poly(mannitol sebacate) nanocomposites

Águeda Sonseca, Olivia Menes, Oscar Sahuquillo, Enrique Giménez

Manuscript

1. SCANNING ELECTRON MICROSCOPY

The morphology of PMS/NF-PLA nanocomposites was studied by scanning electron microscopy (SEM). **Figure S6.1** shows representative SEM images for the cross-section of PMS nanocomposites with 4 and 10 wt% of PLA nanofiber contents.

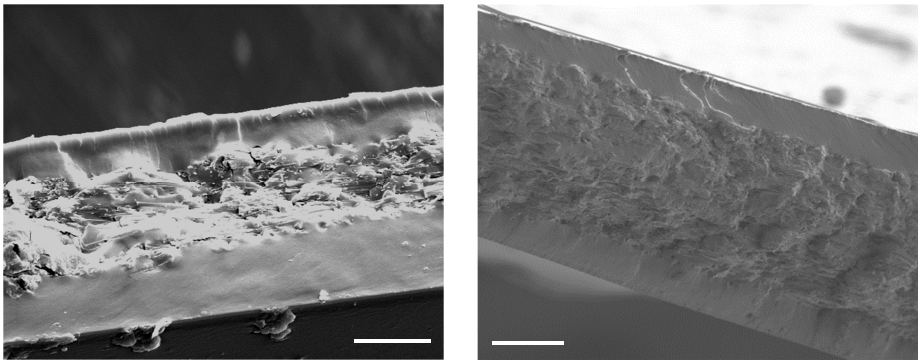

Figure S6.1. Left to right, cross-sectional SEM for PMS/NFPLA 4 wt% and 10 wt% nanocomposites (scale bars 20 μm).

2. DIFFERENTIAL SCANNING CALORIMETRY

The thermal behavior for PMS/NF-PLA nanocomposites was studied in a Mettler-Toledo DSC 800 under N_2 atmosphere. Samples were heated from -60 to 180 °C, cooled down to -60 °C and heated again to 180 °C at a heating/cooling rate of 10 °C/min under an N_2 atmosphere. **Figure S6.2a** evidences a melting peak in the PMS/NF-PLA samples due to the infiltration of the PLA mats. Glass transition temperature of the PLA at 65 °C is clearly evident for the nanocomposite with 15 wt% of nanofibers.

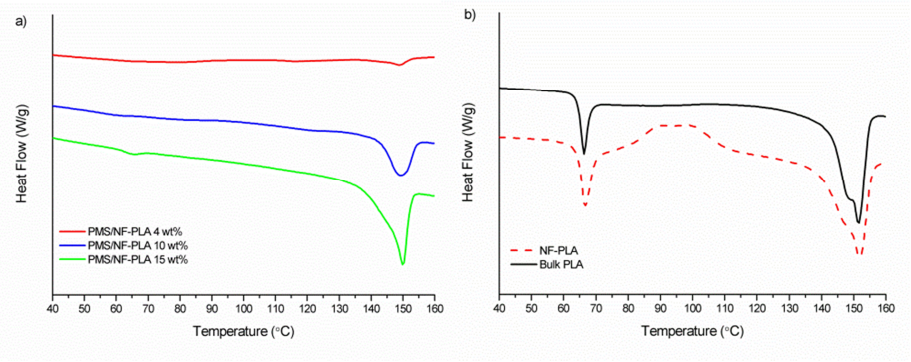

Figure S6.2. First heating run thermograms for PMS/NF-PLA nanocomposites **(a)**, and for electrospun PLA nanofibers and bulk PLA **(b).**

3. DINAMIC MECHANICAL THERMAL ANALYSIS (DMTA)

Figure S6.3 shows Tan Delta peaks for PMS/CNC and PMS/NF-PLA nanocomposites evidencing a second peak in the nanofiber nanocomposites due to the NF-PLA presence.

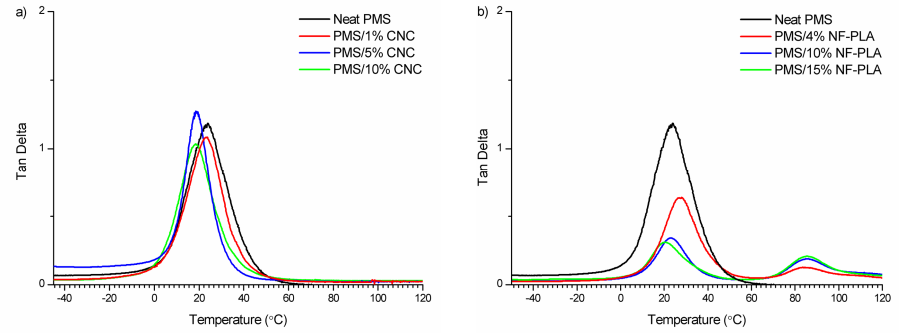

Figure S6.3. DMTA delta tangent curves as a function of temperature for neat PMS and PMS/CNC nanocomposites **(a)** and neat PMS and PMS/NF-PLA nanocomposites **(b)**.

4. THERMALLY ACTIVATED SHAPE-MEMORY PROPERTIES

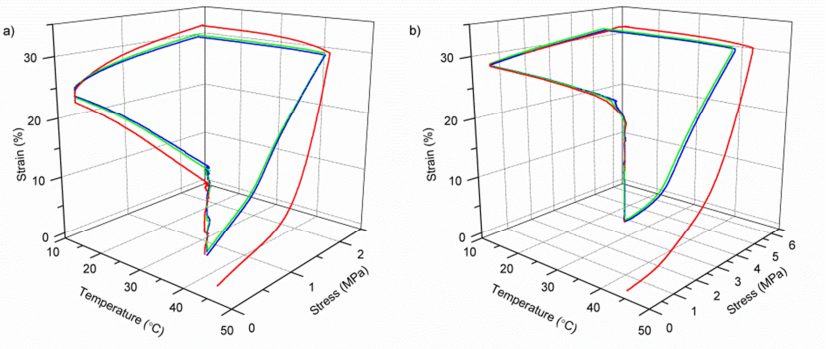

Figure S6.4. Shape-memory stress-strain-temperature curves of consecutive cycles for; PMS/NF-PLA 4 wt% nanocomposite **(a)** and PMS/NF-PLA 15 wt% nanocomposite **(b)**.

Chapter 6.II

Complementary shape-memory studies

Complementary shape-memory studies

In order to reinforce and complement the scientific contributions presented in this thesis, important additional results are provided in this chapter. A brief discussion about shape-memory properties of poly(mannitol sebacate) 1:2 mannitol:sebacic acid ratio system, reinforced with cellulose nanocrystals (CNCs) and crosslinked under high crosslinking degree profile are presented and shortly discussed here.

1. RESULTS AND DISCUSSION

1.1. DMTA TESTING

Figure 6.II.1 show the DMTA traces of PMS/CNC nanocomposites with high degree of crosslinking. In the glassy state, the storage modulus (E´) is not highly affected with increasing the CNCs, however, these set of samples have the highest values of E´ moduli (for all the CNC nanocomposites developed along this thesis) once the rubbery plateau is reached, and an enhanced reinforcing effect as CNCs load increases. At rubbery plateau (above 45 °C) E´ values are close to 20, 25, 30 and 40 MPa for neat PMS, and 1, 5 and 10 wt% of CNC nanocomposites respectively. **Figure 6.II.1b** evidenced a slightly decrease with increasing the CNCs content of the delta tangent peak. Both, the superior enhancement in the rubbery modulus as well as the lowering of T_g with the CNCs presence, are in accordance with results in **Chapter III,** where detailed evaluation of these samples is provided. Thus, the reported higher degree of crosslinking for this samples as well as the fact that interactions between filler and matrix are promoted lowering the T_g of the global system are confirmed by DMTA results presented here.

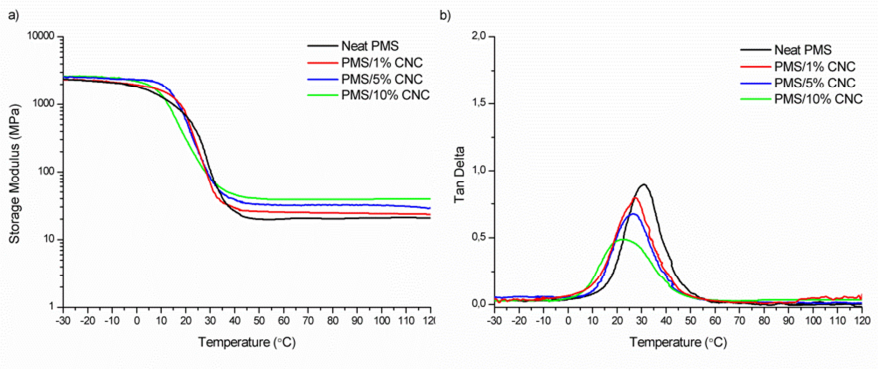

Figure 6.II.1. Storage modulus (E') as a function of temperature of neat PMS and PMS/CNC nanocomposites reacted under high degree of crosslinking conditions **(a)** Tan Delta as a function of temperature of neat PMS and PMS/CNC nanocomposites reacted under high degree of crosslinking conditions **(b)**.

1.2. THERMALLY ACTIVATED SHAPE-MEMORY PROPERTIES

Figure 6.II.2 shows the shape-memory cyclic behaviour of PMS/CNC nanocomposites with high degree of crosslinking. As could be seen, only the neat matrix and 1 wt% of CNC nanocomposite were able to be cycled. Apparently, due to the high stiffness and low elongation at break of the samples with 5 and 10 wt% of CNCs, at the temperature of the test, premature break takes place. **Figure 6.II.3** shows that for neat PMS and PMS/CNC 1 wt% good shape-memory ability is reached. The shape fixity remained constant at 96% and in case of the shape recovery for the first cycle, although there is a loss in R_r% by adding CNCs, the R_r% stabilizes at values of 99-100% in the second cycle.

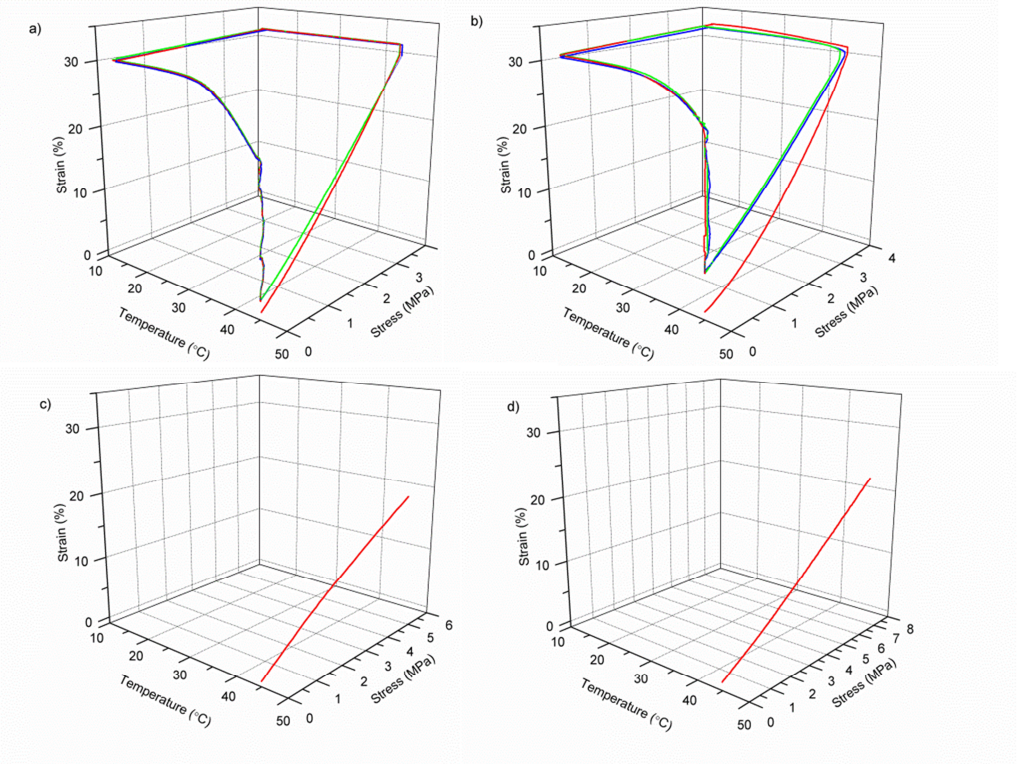

Figure 6.II.2. Shape-memory stress-strain-temperature curves for high crosslinking degree neat PMS sample **(a)**, PMS/CNC 1 wt% **(b),** PMS/CNC 5 wt% **(c),** and PMS/CNC 10 wt% **(d)** nanocomposites.

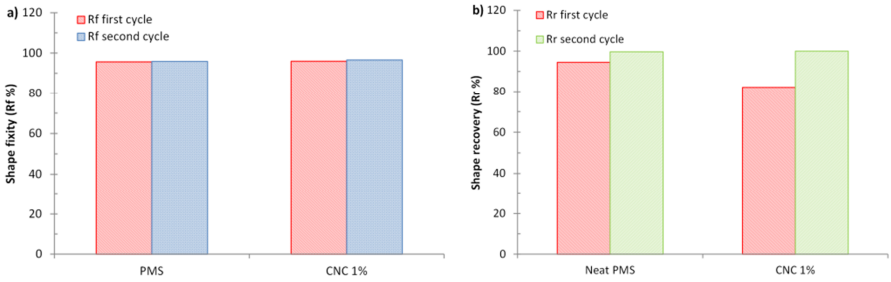

Figure 6.II.3. Shape fixity and shape recovery characteristic values for the first and second cycles. Shape fixity of neat PMS and PMS/CNC 1 wt% nanocomposite with high degree of crosslinking **(a)**, and shape recovery of neat PMS and PMS/CNC 1 wt% nanocomposite with high degree of crosslinking **(b)**.

Chapter 7

Conclusions and future research lines

1. CONCLUSIONS

The present PhD thesis has been focused on the development of novel nanocomposites based on the addition of nanofillers such as cellulose nanocrystals (CNCs) and electrospun poly(lactic acid) nanofibers (NF-PLA) into poly(mannitol sebacate) matrices.

Following are the main conclusions derived from this thesis work:

Regarding the polymeric matrix

A biodegradable polyester elastomer known as poly(mannitol sebacate) (PMS) was successfully synthesized from mannitol and sebacic acid through a two-step polycondensation reaction. Two different stoichiometric ratios between mannitol and sebacic acid (1:1 and 1:2) and two different curing profiles were applied in order to obtain elastomers with low and high degrees of crosslinking.

The experimental results demonstrated the possibility of tailoring the mechanical properties to conform to specific soft or stiff applications depending on the monomer (MA:SA) ratio and the time-temperature curing profiles. Increasing the mannitol/sebacic acid ratio from 1:1 to 1:2 and/or extending the curing temperature and time to achieve a high degree of crosslinking enhanced the mechanical properties.

Mass loss rate of the PMS polymers was primarily determined by the degree of crosslinking density which demonstrated a slower degradation with the increasing feed ratio of sebacic acid or the thermal curing time and temperature.

Soft elastomeric nanocomposites reinforced with CNCs

Cellulose nanocrystals (CNCs) were isolated from sulfuric acid hydrolysis of cotton, resulting in an average width of 18±2 nm, an average length of 199±14 nm and an average aspect ratio of 11±1. Crystal structure was determined to be cellulose I with apparent crystallinity of 69%, and sulfate content on the surface of CNC was calculated to be 91±4 mM/$kg_{cellulose}$.

Different CNC contents (1, 5 and 10 wt%) were added as reinforcing fillers to PMS matrices with 1:1 and 1:2 stoichiometries to alter the degradation rates as well as to tailor and broaden the mechanical stiffness of the neat matrices. Nanocomposites were prepared by solution-casting and cured under designated profiles for low and high degrees of crosslinking.

The appropriate combination of matrix stoichiometry and crosslinking profile with different amounts of CNCs was demonstrated to be an efficient strategy to achieve remarkable improvements in mechanical properties well above the enhancement obtained with other fillers in similar matrices such as Bioglass® or nanoclays. By adding a 5 wt% of CNCs in the 1:1 ratio PMS matrix and applying the high crosslinking degree curing profile, a 50-fold enhancement of the Young´s modulus was achieved in comparison with the neat PMS obtained by applying a low crosslinking degree profile.

The presence of CNCs did not slow or accelerate the mass loss of the neat matrices, making it easy to predict the behavior of the material over the degradation period. However, PMS/CNC nanocomposites provided more reliable mechanical support than matrices alone without immediate loss of mechanical stability during long periods of incubation in SBF, with the best mechanical stability over a one-month period achieved for 1:2 PMS matrix filled with CNCs.

The synthesis of these PMS/CNC nanocomposites provides a wide range of possible values for the mechanical properties (Young´s modulus from 1.8±0.3 MPa to 167.5±5.0 MPa), which allows coverage of a wide range of biomedical applications, in particular those associated with soft and tough tissues (0.7 to 200 MPa).

Nanocomposites with thermally activated shape-memory properties were preferentially achieved for all the neat PMS matrices (1:1 and 1:2 stoichiometric ratios) and most of the PMS/CNC nanocomposite samples with high degree of crosslinking at temperatures between 15 and 45 °C with R_r and R_f values close to 100% for the second thermo-mechanical cycle. Additionally, reduced hysteresis between the first and second cycle was achieved when the temperature of deformation and recovery was 60 °C.

Soft elastomeric nanocomposites reinforced with electrospun poly(lactic acid) nanofibers

Neat poly(lactic acid) nanofibers and poly(lactic acid) nanofibers containing nano-sized hydroxyapatite (HA) as a filler were prepared via electrospinning using a rotating mandrel as a collector in order to generate nanometric and uniform mats with high alignment.

The optimal conditions to fabricate nanofiber mats were determined by several experimental tests, and their structure and morphology were characterized as a function of the production parameters with emphasis on the effects of the take-up velocity. Final results showed randomly oriented fibers produced on a stationary shaft, whereas highly oriented fibers were obtained when rotation speed was increased to 1100 rpm. Collection at higher speeds resulted in a lower average fiber diameter (300-400 nm) at the same time that fiber orientation and crystallinity were enhanced due to the stretching produced during the process.

The added HA particles at 9:1, 5:1 and 3:1 polymer:filler ratios into PLA solutions produced an efficient nucleating effect, with improvement in thermal and dynamo-mechanical properties of the electrospun mats. Moreover, by combining the HA presence with high collection take-up speed, crystallinity of the mats was increased until a certain value above which the properties did not further improve, probably due to the formation of filler aggregates.

Electrospun PLA nanofiber mats were embedded in a PMS 1:2 pre-polymer to be further cured under low crosslinking conditions. Final samples contained 4, 10 and 15 wt% of nanofibers in the polymer matrix. The addition of NF-PLA in PMS matrices results in a remarkable improvement in mechanical properties, with a 53-fold increase in Young´s modulus when a neat PMS matrix is combined with 15 wt% of PLA nanofibers. At the same time, this system offers the highest mechanical retention and stability over degradation time.

Introduction of nanofibers as filler improved the shape-memory properties of neat 1:2 PMS matrix, cured under low crosslinking degree conditions, thanks to the marked enhancement achieved in the rubbery modulus (more than 100 times higher than that of the neat PMS matrix with the addition of 15 wt% of NF-PLA). The resulting material can fix a temporary shape and obtain shape recovery values of 100% for the second thermomechanical cycle. In addition, the presence of two well-separated thermal transitions (as shown in DMTA analysis) enables the design of a triple-shape-memory system for target applications. Thus, nanocomposites with good thermally activated shape-memory properties were obtained based on a PMS matrix reinforced with the NF-PLA with the best fixity ratios (R_f) and on filler contents of 10 and 15 wt%.

Importantly, nanofibers played a significant role in maintaining the fixed shape of the PMS/NF-PLA matrix at useful temperatures for clinical applications. By increasing the nanofiber content to 10 and 15 wt%, the activation of shape-

memory effect occurs at temperatures in the range of interest —40-45 °C— for the development of a possible biomedical device.

Of all the nanocomposites developed along this thesis, the nanofiber-reinforced PMS system offered the greater design flexibility in order to achieve the desired properties for tissue engineering applications. They also possess the best combination of mechanical and thermal properties as well as mechanical retention and stability over degradation time to be good candidates for use in long-term medical applications such as smart responsive materials.

2. FUTURE RESEARCH LINES

In order to promote and wide the studies performed in this thesis, the following future research lines can be addressed:

- In order to shorter the curing time of the polymer matrices, other techniques such as microwave-assisted polycondensation could be explored.
- In order to overcome the limitations associated with the application of high temperatures during the thermal curing process, which can affect on the stability of thermal sensitive fillers as well as on the method for manufacturing shape-memory nanocomposites, the study of other curing processes can be of great interest. In this regard, the introduction of functional groups into the polymer backbone such as acrylate moieties would allow achieve a feasible UV crosslinking at ambient temperature.
- In order to develop shape-memory nanocomposites with new functionalities, the study of how the nanofibers containing nanoparticles such as hydroxyapatite affect to the shape-memory behavior, especially to the shape recovery force of the global system, can result of interest for biomedical purposes.

Glossaries

LIST OF FIGURES

CHAPTER 1

CHAPTER 2

CHAPTER 3

CHAPTER 4

CHAPTER 5

CHAPTER 6.I

CHAPTER 6.II

LIST OF TABLES

CHAPTER 1

CHAPTER 2

CHAPTER 3

CHAPTER 4

CHAPTER 5

CHAPTER 6

EPILOGUE

AGRADECIMIENTOS Y DEDICATORIAS

Cuando llega el momento de cerrar una etapa tan intensa, una entiende la importancia de los agradecimientos y se emociona al pensar en toda la gente que ha formado parte vital a lo largo de toda la distancia recorrida y sin la que esta aventura no hubiese llegado a su fin. Intentaré resumir en unas líneas la gratitud a todas las personas que han hecho posible este sueño que se perfila ahora como una realidad.

En primer lugar, agradecer la labor de mi mentor profesional, el Dr. Enrique Giménez Torres, por haberme implicado en el mundo investigador ofreciéndome toda su confianza. Quique, mil gracias por tu estímulo, por transmitirme tu pasión por la investigación y tus ganas constantes de innovar, experimentar y emprender, pero sobre todo por la orientación y dedicación recibida a lo largo de toda esta "convivencia" en la que me has hecho sentir parte clave de un equipo, dándome fuerza para crecer en todos los aspectos de la vida. Ha sido todo un privilegio y una gran lección poder contar contigo.

Al Instituto de Tecnología de Materiales, al Departamento de Ingeniería Mecánica y de Materiales y al Servicio de Microscopía Electrónica de la UPV, por permitir el desarrollo de este trabajo en sus instalaciones. Es muy amplio el equipo humano ligado a estos centros, pero quiero hacer mención especial a Mª Dolores Salvador, Manolo, José Luis y a Amparo Ribes y su equipo, por toda la ayuda recibida al poner a mi disposición sus equipos. Gracias también a Laura, Alf, Jose, Marta, Soraya y Roberto, por recibirme como parte del grupo en cada visita a vuestro laboratorio, las risas entre muestra y muestra no tienen precio.

Al Prof. José María Kenny, y a Laura Peponi del ICTP-CSIC por su apoyo a lo largo del proyecto MAT2010/21494-C03, así como en el desarrollo de las publicaciones científicas.

A Adolfo Benedito y su grupo en AIMPLAS, porque vuestro apoyo ha sido vital para la consecución de este trabajo. Gracias por la confianza y la libertad que me habéis dado.

Al grupo de Ciencia y Tecnología de Polímeros de la Universitat Jaume I de Castelló por hacerme sentir como en casa. Gracias Luis, Jose, Jenny y Estefanía por las charlas científicas que al igual que iluminan resultados de tesis doctoral, ¡mejoran el mundo! Gracias Raquel y Pepe, porque no hay unos técnicos de laboratorio más comprometidos con las personas, que como yo, hemos tenido la suerte de contar con vuestra ayuda.

I would like to express my gratitude to Prof. Christoph Weder for welcoming me in the Adolphe Merkle Institute. Very special thanks to Dr. E. Johan Foster, for supporting me during the whole period of my stay in Switzerland. It was a pleasure to work with you and your group, thanks for your daily help in my professional development, it is fascinating all the things that you tough me, simply awesome. Of course, thanks for the beers, chats and for letting me win the poker game! ...you know… I hope that you still have tomato in that tablecloth. Christian, Tobias and Souleymane, thanks for your whole support, your smiles and friendship during my Swiss experience.

Sandra, tu mereces mención aparte, por los grandes momentos de diversión en nuestra lengua y mi "Spanglish". Aunque fue corto el tiempo que disfrutamos, que decir tiene que te tengo en un pedestal, no sólo en lo personal, sino también a nivel profesional.

Asimismo, quisiera dar las gracias a mis compañeros y amigos en el día a día, a los que todavía siguen y a los que ya no están. Gracias por haberme padecido todo este tiempo, por haber compartido mis logros como si fuesen vuestros, y darme alas en los momentos no tan buenos. Sin vosotros nada hubiese sido igual: Rut, Àngels, Juan, Óscar, Esther, Emilio, Irma, Maria-Do, Mutaz… y en

especial a mi primer compañero de laboratorio, Antonio, porque esos comienzos son inolvidables. Gracias también a Eva V., por su ayuda con todos los "papeleos" siempre entre una gran sonrisa.

Finalmente, gracias por su apoyo a Alfonso Cárcel. Alfonso, he tenido la suerte de compartir reuniones de proyecto contigo, así como algunas charlas importantes y otras del día a día más distendidas, que me han dado para admirar tu sabiduría, templanza y saber hacer.

En el terreno más personal, quiero dedicar esta tesis a todos los que bien saben que ocupan un lugar especial en mi vida y que tantas veces han recibido un "…hoy no puedo…pero mañana…" en estos últimos años, por disculpar mis ausencias y tener siempre la palabra justa de ánimo.

A la mejor cuerda de percusión que existe en Burriana y alrededores, por disfrutar y hacerme disfrutar haciendo música. "Al meu mestre", Guillamón, perquè sempre traus el millor de la meua musicalitat, per molts més "Blues for Gilbert", "l´histoire du soldat"o "memories of the seasore" junts.

A los amigos de siempre y para siempre, a ellos, Pedre, Diego, Alex, Ramón, Jesús, Chacón, Pablo, Víctor, Charly, Fidel… y a ellas, Marian, Anita, Gemi, Rose, Ari, Mamen, Blanca, Lledó, Luci, Lau, Cris, Elena, Trini, Clara… y en especial a ti Mire, por estar siempre justo a tiempo. A los que llegaron un poco más tarde a mi vida pero dejando una huella igual de profunda, gracias a "pollito la que s´ha liao" por amenizarme tantas noches de escritura, ¡¡soys las mejores chicas!! I com no, gràcies de tot cor Miquel, per brindar-me el teu recolzament tots aquestos anys, gràcies per tots els bons moments i el temps viscut. A todos os estoy eternamente agradecida pues con vosotros tengo una gran fortuna.

A mis grandes pilares en la aventura valenciana, a Jose, Marie-Pierre, Lissette, Alina, Jenny y en especial a ti Marga, te agradezco tu implicación conmigo, tu

alegría, positivismo y compromiso, en este tiempo te has hecho valer como una auténtica hermana, eres increíble. Gracias a todos por aportarme un gran crecimiento personal y estar tan cerca a pesar de la distancia que me separa de algunos de vosotros, gracias por todos los abrazos incondicionales, pues puede que sean gestos sencillos, pero cada uno ha sido un regalo capaz de recomponerme tras cada caída.

Finalmente, a mi familia, a mis padres, hermanos, cuñados y sobrinos, por enseñarme que la vida es para los valientes, por todo lo que me habéis inculcado mirando siempre al futuro de manera positiva, por apoyar mis pequeñas locuras, por ser únicos, por quererme tanto y por sacar siempre tiempo para que se mantengan las buenas costumbres familiares. Nunca os dejaré de admirar, gran parte de esta tesis es vuestra y por vosotros.

Antes de concluir todo este período tan intenso, quiero referir un pequeño diálogo que leí hace ya un tiempo y que me ha ayudado a reflexionar y valorar tantas veces la belleza de las relaciones humanas,

«No puedo vivir sin ti…

»*Sí que puedes…*

«Sí, pero no quiero»